Department of Theoretical Physics, Wrocław University
of Science and Technology
Department of Physics, University of Ottawa

Electronic and optical properties of two-dimensional transition metal dichalcogenide crystals

by
Maciej Bieniek

PhD thesis prepared under supervision of
Prof. Arkadiusz Wójs
Prof. Paweł Hawrylak
Dr Paweł Potasz

Wrocław, October 2020

Dedicated to my beloved wife Anna

Contents

Abstract

Over the last decade, two dimensional transition metal dichalcogenide crystals revolutionized physics of semiconductors thinned down to atomic limit. Understanding their electronic structure and optical response is vital for advancement of field towards practical devices and further discoveries of novel physical phenomena.

In the first part of the following thesis minimal, graphene like tight-biding model for MoS_2 and related transition metal dichalcogenides is derived and parametrized to reproduce low energy sector of *ab initio* electronic properties. In next step, effects of band nesting and related existence of additional valleys beyond those in K points is discussed. Different contributions to response to magnetic field are then analyzed, including valley Landé and Zeeman effects.

In second part, optical response of correlated electron-hole pairs is derived in configuration-interaction language, leading to analog of Bethe-Salpeter equation. The electron-hole direct and exchange interaction and microscopic electron and hole energies are computed using the tight-binding model. The exciton spectrum, including ground state, excited states, topology, K- and Q- valleys and screening are analyzed. Then, for specific case of MoS_2, fine structure of exciton spectrum is discussed quantitatively and it's implications on charged exciton fine structure are then discussed qualitatively.

In third part of the thesis, gate-defined quantum dots are studied. Multi-valley origin of states is first uncovered. Then special attention is paid to topology-related modification of Fock-Darwin states ladder resulting from parabolic confinement. Next, existence of SU(3) symmetric "quark" states resulting from additional valleys in conduction band is discussed. Finally, interplay of spin, valley and confinement on ordering of states inside quantum dots is presented.

Streszczenie

W ostatniej dekadzie dwuwymiarowe kryształy z rodziny dichalkogenków metali przejściowych zrewolucjonizowały fizykę półprzewodników o grubości rzędu kilku atomów. Zrozumienie ich właściwości elektronowych i optycznych jest podstawą dalszego rozwoju w dziedzinie zarówno praktycznych urządzeń, jak i odkrywania nowych efektów fizycznych.

W pierwszej części niniejszej rozprawy przedstawiony zostanie minimalny, grafeno - podobny model ciasnego wiązania półprzewodnika MoS_2, będącego przedstawicielem szerszej rodziny związków MX_2 (M=Mo, W, X = S, Se, Te). Następnie opisana zostanie parametryzacja modelu oddająca jak najlepiej niskoenergetyczną strukturę elektronową obliczoną metodami *ab initio*. W następnym kroku przedyskutowane zostaną efekty związane z równoległością pasm walencyjnego i przewodnictwa, powiązane z tym istnienie dolin w różnych częściach strefy Brillouina oraz odpowiedź elektronów na zewnętrzne pole magnetyczne.

W drugiej części pracy przedstawiona zostanie odpowiedź optyczna skorelowanych par elektron-dziura, wyprowadzona za pomocą metody oddziaływania konfiguracji, prowadząca do równania analogicznego do równania Bethe-Salpetera znanego z teorii pola. Równanie to zostanie następnie rozwiązane przy użyciu stworzonego w pierwszej części modelu ciasnego wiązania. Następnie przedyskutowane zostaną szczegóły struktury subtelnej ekscytonu w MoS_2 oraz jej wpływ na możliwe stany naładowanych ekscytonów.

W trzeciej części pracy opisane zostaną badania kropek kwantowych, definiowanych za pomocą metalicznych bramek nakładanych na dwuwymiarowe półprzewodniki. Główny nacisk położony zostanie na identyfikację wielodolinowej natury stanów zlokalizowanych w kropce. Następnie przedyskutowane zostaną efekty topologiczne modyfikujące drabinkę stanów dwuwymiarowego oscylatora harmonicznego. W dalszym kroku przeanalizowane zostanie istnienie tzw. stanów kwarkowych spełniających symetrię SU(3), wynikających z istnienia dodatkowych dolin w pasmie przewodnictwa. Rozdział zakończony zostanie dyskusją możliwych hierarchii spinowo- i dolinowo- rozszczepionych stanów w kropkach o różneym promieniu.

Acknowledgments

First, I would like to thank Prof. Paweł Hawrylak, Prof. Arkadiusz Wójs and Dr Paweł Potasz, my research supervisors, for allowing me to take part in challenging, international endeavor in theoretical physics. I thank them for exposing me to plethora of scientific topics, which combined and intertwined led to creation of this dissertation. Notably, I thank Prof. Paweł Hawrylak for his unprecedented hospitality in Ottawa and letting me being part of his Quantum Theory Group.

I thank all of my collaborators, especially Prof. Marek Korkusiński, Prof. Shun-Jen Cheng, Dr Alain Delgado Gran, Dr Moritz Cygorek, Dr Amintor Dusko, Dr Ping-yuan Lo, Dr Ludmiła Szulakowska and Yasser Saleem in Ottawa and Marta Brzezińska, Dr Wojciech Radosz, Dr Adam Mielnik-Pyszczorski and Tomasz Woźniak in Wrocław for fruitful work and countless discussions. I thank also many people I met along the way, especially Anna and Chris Hall for their warmth and help during my oscillation between Ottawa and Wrocław. I thank also our experimental collaborators, Prof. Joanna Jadczak, Prof. Leszek Bryja and Dr Joanna Kutrowska-Girzycka for allowing me to peek into experimental reality of optical properties of two dimensional crystals.

Last but not least, I would like to thank all of my family for their unconditional love, especially my wife Ania for her support in home and over the ocean.

List of Figures

List of Acronyms

2D - Two Dimensional
2DEG - Two Dimensional Electron Gas
3D - Three Dimensional
BSE - Bethe-Salpeter Equation
BZ - Brillouin Zone
CB - Conduction Band
CI - Configuration Interaction
DFT - Density Functional Theory
EMA - Effective Mass Approximation
FQHE - Fractional Quantum Hall Effect
GGA - Generalized Gradient Approximation
IQHE - Integer Quantum Hall Effect
mDF - massive Dirac Fermion
NN - Nearest Neighbor
NNN - Next-Nearest Neighbor
PBC - Periodic Boundary Conditions PL - Photo-Luminescence
QD - Quantum Dots
QSHE - Quantum Spin Hall Effect
R.-K. - Rytova - Keldysh
SK - Slater - Koster
SOC - Spin - Orbit Coupling
TDDFT - Time-Dependent Density Functional Theory
TMD - Transition Metal Dichalcogenides
VB - Valence Band

Purpose, Original Contribution and Plan of the Thesis

Purpose

In the following thesis I present results of theoretical investigation of electronic structure and optical properties of two dimensional transition metal dichalcogenide crystals. Broadly speaking, there are 3 major purposes of this work: building simplest possible, yet still correct, theory of electronic structure of 2D crystals and then applying this theory to understand physics of excitons and states confined inside gate-defined quantum dots.

More specifically, first purpose is to build *ab initio* based tight-binding model that will be minimal in number of orbitals and applicable to multi-million atom nanostructures. To do this it is necessary to understand first principles calculations in terms of orbitals contributing to bands around Fermi level. Next aim is to construct p^3d^3 orbital tight-binding model and parametrize it to reproduce *ab initio* electronic structure. Then we want to understand better how good such parametrization can be performed in terms of range of hopping on the lattice. Next goal is to understand how single-particle model can be useful in description of response of carriers to external magnetic fields.

Second purpose of the following thesis is to understand fine structure of excitonic response of TMD's. First objective is to build theory of exciton beyond one used usually in *ab initio* calculations, that in the future could be extended to describe all experimentally relevant excitations in TMD's, for example trions, biexcitons and charged biexcitons. Then such theory must be properly "discretized" to enable solving it on a computer with precision high enough to be able to obtain converged results. Next goal is to test if previously constructed tight-binding model is sufficient to understand experimental results.

Third objective of this work is to check how multi-valley structure and topological effects affect seemingly simple and well understood problem of carrier confinement in two dimensions by parabolic potential well, which is low energy approximation of realistic confinement induced by metallic gates. Purpose of this part of project is to understand spin- and valley- structure of states inside electrostatically defined quantum dots. Then, role of additional valleys in conduction band, resulting in quantized states possessing fascinating flavor SU(3) symmetry known from quark physics will be studied, especially from the point of view how many electrons are necessary inside quantum dot to probe physics of those states.

Original Contribution

My work described in Chapters 2 to 4 is scattered through several publications written in collaboration with many people. Main papers on thesis topic, in chronological order, are listed below:

1. M. Bieniek, M. Korkusiński, L. Szulakowska, P. Potasz, I. Ozfidan, and P. Hawrylak, "Band nesting, massive Dirac fermions, and valley Landé and Zeeman effects in transition metal dichalcogenides: A tight-binding model", Phys. Rev. B 97, 085153 (2018).[1]

2. J. Jadczak, L. Bryja, J. Kutrowska-Girzycka, P. Kapuściński, M. Bie-

niek, Y.-S. Huang and P. Hawrylak, "Room temperature multi-phonon upconversion photoluminescence in monolayer semiconductor WS_2", Nature Communications 10, 107 (2019)[2]

3. L. Szulakowska, M. Bieniek, P. Hawrylak, "Electronic structure, magnetoexcitons and valley polarized electron gas in 2D crystals", Solid State Electronics 155, 105 (2019)[3]

4. M. Bieniek, L. Szulakowska, and P. Hawrylak, "Effect of valley, spin, and band nesting on the electronic properties of gated quantum dots in a single layer of transition metal dichalcogenides", Phys. Rev. B 101, 035401 (2020)[4]

5. M. Bieniek, L. Szulakowska, and P. Hawrylak, "Band nesting and exciton spectrum in monolayer MoS_2", Phys. Rev. B 101, 125423 (2020)[5]

6. J. Jadczak, J. Kutrowska-Girzycka, M. Bieniek, T. Kazimierczuk, P. Kossacki, K. Watanabe, T. Taniguchi, C.-H. Ho, A. Wójs, P Hawrylak, and L. Bryja, "Fine structure of charged and neutral excitons in monolayer MoS_2", arXiv:2001.07929 (2020)[6]

7. L. Szulakowska, M. Cygorek, M. Bieniek, P. Hawrylak, "Valley and spin polarized broken symmetry states of interacting electrons in gated MoS_2 quantum dots", arXiv:2005.04467 (2020)[7]

I took part in discussing, testing and analyzing different theoretical and experimental aspects presented in those works. I also took part in writing, formatting and preparing figures of publications 1, 4, 5, 6 and I contributed to discussions and proofreading of all mentioned manuscripts. Due to highly collaborative nature of those works I would like to list aspects that I was directly responsible for. Tasks accomplished independently were:

- Re-derivation, parametrization and coding of p^3d^3 tight-binding model derived originally by prof. Marek Korkusiński and detailed study of orbital couplings and band nesting effect within it
- Derivation of Landé g-factors
- Derivation and numerical solution of Bethe-Salpeter-like equation for exciton using before-mentioned tight-binding model
- Detailed analysis of fine structure of valley excitons in MoS_2 and trends in other MX_2 materials (spin splitting, effective masses, polarizability), e.g. helping to understand differences in their excitonic properties
- Implementation of model of gate-defined quantum dot and single particle analysis of Fock-Darwin spectrum of K- and Q- valley derived states of gate-defined quantum dots in MoS_2
- Qualitative theoretical analysis of trion species in materials with small spin splitting in conduction band

I would like also to point to four papers that are not directly described in this thesis, however, they are related to topological properties of atomically thin crystals with significant spin-orbit coupling leading to their transition to topological insulator (quantum spin Hall insulator) state:

- M. Bieniek, T. Woźniak, P. Potasz, "Study of Spin-Orbit Coupling Effect on Bismuth (111) Bilayer", Acta Physica Polonica A 130, 609 (2016)
- M. Bieniek, T. Woźniak, P. Potasz, "Stability of topological properties of bismuth (111) bilayer", J. Phys.: Condens. Matter 29, 155501 (2017)
- M. Brzezińska, M. Bieniek, T. Woźniak, P. Potasz and A. Wójs, "Entanglement entropy and entanglement spectrum of $Bi_{1-x}Sb_x$ (111) bilayers", J. Phys.: Condens. Matter 30, 125501 (2018).
- N. Nouri, M. Bieniek, M. Brzezińska, M. Modarresi„ S. Zia-Borujeni, Gh. Rashedi, A. Wójs, P. Potasz, "Topological phases in Bi/Sb planar and buckled honeycomb monolayers", Physics Letters A 382, 2952 (2018)

Even though MoS_2 is topologically trivial, work leading to those four publications greatly improved my understanding of topological aspects of two dimensional semiconductors and quantum transport. Those papers are not described due to different material class studied in them and different methodology, namely Green's function- based methods for calculations of transport properties. To sum up, I hope those advances are sufficiently original and important in area of two dimensional semiconductors.

Plan

The following thesis is divided to introduction summarizing available literature and three large Chapters summarizing my original contribution. First I will describe current status of knowledge on both theoretical and experimental aspects of physics of two dimensional crystals. I will focus on semiconducting transition metal dichalcogenides and in principle largely omit enormous amount of works on graphene mono- and bi-layers and other two-dimensional crystals not included in transition metal dichalcogenide MX_2 (M=Mo,W, X=S, Se, Te) family. Even with this omissions number of works cited is large and reflects worldwide interest in atomically thin materials.

In the next part I describe electronic properties of molybdenum disulphide, focusing on construction of graphene-like tight-binding model capturing most important aspects of electronic structure close to the Fermi level. Then detailed analysis of origin of the band-gap within d-orbitals is discussed, along with explanation of process leading to additional secondary minima in conduction band at Q points. Chapter is finished with discussion of Landé and valley Zeeman response of MoS_2 (and more broadly MX_2 materials family) to external magnetic field.

In third chapter optical response defined by correlated electron-hole complexes, i.e. excitons, is described. First, I derive equation governing such correlated excitonic state following configuration-interaction methodology. Then I describe in details how this equation can be discretized and solved numerically using tight-

binding model derived in second Chapter of this thesis. Next I compare numerical approach with exact theoretical results and I asses issues related to convergence of such calculations. Then, by improving successively models of electron dispersion, wavefunctions and screening I show how MoS_2 excitonic spectrum evolves from simple "two-dimensional hydrogenic" exciton to rich spectrum that depends on topological properties of wavefunctions describing electron and hole components. I conclude with discussion on how this understanding helps to identify charged exciton fine structure.

In the last chapter of this thesis I describe single-particle properties of gate-defined quantum dots, modeled as parabolic potential confining electrons in conduction band. First, computational box with periodic boundary conditions avoiding problem with edge states is discussed. Then, confinement in such box is introduced. Modifications of Fock-Darwin spectrum of two-dimensional parabolic potential by existence of 2 K-valleys and additional 3-secondary Q-point "satellite" valleys are discussed. SU(3) symmetric nature of states from secondary minima in conduction band is elucidated. Then role of geometric field (Berry's curvature) on states with non-zero angular momentum is analyzed. In next step role of spin splitting between different MX_2 materials is discussed and possible experimental consequences on shell filling scheme are analyzed.

Chapter 1

Introduction

In the following chapter historical account of different physical phenomena related to reduced dimensionality, high energy physics and topology are described. Then, extensive review of experimental properties of transition metal dichalcogenides follows. Theoretical investigations into electronic and optical features of those crystals are then summarized. In the last part short summary of emerging field of quantum dots defined in 2D crystals is presented.

1.1 Overview of physics of low dimensional electron gas

First material platforms

Physics of two dimensional (2D) and quasi-2D electron systems is a large field of condensed matter physics, which flourished around 1970, after developing molecular beam epitaxy technique.[8] Electron systems that are "dynamically 2D[9]" means simply, that carriers are free to move in two dimensions and motion is quantized in the third one, situation that occurs e.g. in quantum well systems, on the surfaces/interfaces of crystals or on top of the liquid helium. One of the best quality samples exhibiting this physics were first obtained in GaAs/AlGaAs quantum well heterostructures, in which groundbreaking transport[10] and optical effects were observed.[11] Soon after, large new fields of low-dimensional physics were opened, e.g. physics of quantum wires[12] and quantum dots.[13–15]

Early theoretical approaches

First approaches to simulating electronic properties of nanostructures were based on free electron model (see[16] and reference therein), which assumed parabolic energy dispersion of carriers. Simultaneously, envelope function approximation was used. Later, $k \cdot p$ methods were extended, allowing to discuss more precisely effects of strain and band mixing effects.[17] For small systems, usually quantum dots and thin nanowires, it was possible to use tight-binding[18] and empirical pseudopotential[19–21] methods. Because application of *ab initio* techniques[22] was possible only for small systems, mixed techniques were developed, e.g. *ab initio* based tight-binding[23–25] and maximally localized Wannier orbital[26] approaches. Basis of electron wavefunctions is reduced in them and model parameters are

fitted to reproduce as good as possible bulk band structures. Then, theory is applied to nanostructures. All those approaches used single electron approximation, which provides in many cases reasonably good description of confined electrons.

Relativistic theory

Importance of Dirac equation for description of atoms and crystalline materials was understood from the very beginning of quantum mechanics,[27] especially due to importance of spin and spin-orbit coupling in atomic physics. This coupling, along with many other relativistic corrections, is crucial to understand how atoms behave when brought together to form crystalline material. On the other hand, notion of 2D relativistic physics applied to quasiparticles begun much later, with realization that there are physical systems described by low energy (2+1) relativistic gauge theories.[28–31] Later, massive Dirac fermion description of several materials have been proposed, e.g. for graphene on hBN[32,33] or MoS_2.[34] Low energy models corresponding to physics of Weyl[35] and Majorana fermions[36,37] have also been proposed. Currently, more and more materials with low-energy degrees of freedom described by theories beyond Standard Model are being proposed,[38] including type-II Weyl, hourglass and many other fermions,[39] some of them postulated in 2D materials.[40,41]

Topology of 2DEG in high B

Topological aspects of physics in 2D electron gas systems were first understood for non - relativistic and non-interacting electron gas systems in high magnetic fields. The most famous example is an integer quantum Hall effect (IQHE), discovered experimentally in 1980.[42] It was understood quickly that conductance in IQHE is related to topological invariant called Chern number.[43] Soon after, interacting counterpart of IQHE was discovered and dubbed fractional quantum Hall effect (FQHE).[44,45] This phenomenon was understood as IQHE of novel quasiparticles, called composite fermions.[46,47] Physics behind those concepts challenged Landau-Ginzburg classification of phases, leading to the idea of topological order of gapped phases of matter, breaking into two large classes of short- and long-range entangled electronic phases.[48,49]

Novel topological phenomena

In 1988 Haldane realized[50] that electron motion, similar to such as in quantum Hall effect, can be realized without magnetic field.[51] This idea led in 2005 to discovery[52] of novel type of semiconductor, called quantum spin Hall insulator (QSHE), later called also 2D topological insulator. Original proposal[53] to observe this effect in pristine graphene failed, due to vanishingly small SOC due to light carbon nucleus, however nowadays there are several known routes[54,55] to enhance SOC enough to observe this effect. In parallel, many other materials were predicted to and proved experimentally to exhibit QSHE.[56–61] Topological classification quickly burst into 3D systems, uncovering novel way to classify band structures of crystalline materials,[62–66] including both semi- and super-conductors. Rich physics related to electron-electron interactions,[67] magnetism[68,69] and interplay with crystalline symmetries[70–72] is still being vigorously studied.

Berry's curvature

Unifying concept in field of topology in crystals is Berry's curvature (geometric curvature) of the bands in the Brillouin zone.[73–75] Topologically, electron's Bloch wavefunctions on BZ torus are understood in terms of fiber bundles theory,[76] therefore properties of those wavefunctions define topological properties of

electron behavior. Interesting, even though in topology one usually talks about single invariants, e.g. Chern or Z_2 numbers, Berry's curvature is a k-space dependent quantity and can influence differently observables "feeling" different parts of reciprocal space, e.g. excitons localized in different parts of Brillouin zone.

Concepts of valley and pseudospin

The idea of valley was introduced in physics of silicon and germanium.[16] Later it become important for understanding graphene, which hexagonal structure implies hexagonal BZ with two non-equivalent valleys at it's corners. Valley index can be understood as a novel degree of freedom.[77–79] This quantity, just as electron's spin, can be controlled by various means, allowing for definition of valley qubit.[80] However, in graphene even for single valley one writes effective Dirac Hamiltonian, therefore one may wonder in what basis spinor in one valley is defined. The answer here is so-called sublattice pseudospin, which distinguishes between spinor wavefunction localized on two non-equivalent atoms in graphene unit cell.[81] Pseudospin may result from many other sources,[82] e.g. orbitals,[70] spin-orbit coupled orbitals,[56] energy bands[83,84] or Nambu pseudospin,[63] as well as be an emergent quantity.[85,86]

1.2 Renewed interest in atomically thin 2D crystals

Historical account

Fact that many crystals have layered form with strong intra-layer and weak inter-layer bonds was well-known for decades.[87–89] In 1962 it was confirmed, that single layer of graphite, called "graphene" later, can be thermodynamically stable. In 1970's many groups studied properties of few-lawyer graphite down to single layers, especially in relation to modification of properties of anisotropic crystals via intercalation.[90,91]

Mechanical exfoliation and transport

More widespread interest in graphene begun around 2005, mostly due to realization that high-quality few-layer crystals can be obtained via mechanical exfoliation[29] process, in which layers are peeled off using scotch tape and then are identified using optical microscope. Second important aspect was that advances in electron-beam lithography allowed for contacting those samples using gold electrodes and performing transport experiments.[30,31] Immediately it was realized that many other materials can be obtained using this technique,[92] i.e. isolators, semiconductors, metals and superconductors.

Zoo of 2D crystals

Since initial discovery that graphite, hexagonal boron nitride (hBN), many transition metal dichalcogenides (e.g. MoS_2) and "high-Tc oxides" (e.g. Bi2212) can be exfoliated, natural question arose how many 2D crystals exist in nature. Large scale data mining approaches, combined with high-throughput *ab initio* calculations established that from about 10^5 experimentally known crystals approximately 1800 should be exfoliable and thermodynamically stable.[93] They include 5 mono-atomic crystals occurring naturally in layered form (build from atoms C, P, As, Sb, Bi). Additionally, effort has been made to grow others (Si, Ge, Te, B)[94] synthetically. About 20% of them has chemical formula AB_2,[95]

and around 40 of them belong to family called transition metal dichalcogenides (TMD's). In this family, contrary to graphene, single layer is build from three planes of atoms: two of them build out of chalcogen X, surrounding symmetrically metal M plane (X-M-X structure). Usually, they have trigonal (1T), hexagonal (2H) or rhombohedral (3R) polymorphic structure.[96] Around half of them in bulk form is metallic, and other half is semiconducting.[97] All semiconducting materials from this family share common theme, that when thinned down from bulk to monolayer, the electronic band gap increases. In some cases, i.e. VS_2 or (W/Ti/Zr/Hf)Te_2, transition from metal to semiconductor is also predicted. Semiconducting TMD's that sparked largest attention due to promising optoelectronic properties[98] were compounds with formulas MoS_2, $MoSe_2$, $MoTe_2$, WS_2 and WSe_2. Interestingly, WTe_2 in 2H phase is predicted to be metastable and 1T phase is energetically more favorable, in which WTe_2 is rather semimetallic than semiconducting, possibly exhibiting topologically non-trivial characteristics.[99,100]

CVD/MBE growth

Even though monolayer TMD's samples obtained using mechanical exfoliation have excellent quality, for both transport[101] and optical studies,[102,103] scalable technology requires molecular beam epitaxy or chemical vapor deposition growth, the former having better quality with higher cost than the latter. Interestingly, even though first grown $MoSe_2$ films on bilayer graphene / highly oriented pyrolytic graphene on SiC substrate shown good optical quality,[104] they were still inferior to the exfoliated samples. Since then, many advances has been made.[105–107] For example, MoS_2 has been grown on many different substrates, including SiO_2,[108] hBN[109,110] or even highly mismatched in lattice constant graphene.[111] Despite that, exfoliated samples are still being used for optical studies requiring ultra-sharp transition lines.[112] Alternatively to those methods liquid phase exfoliation is possible as an cost-effective method, and was achieved for many TMD's[113] and nowadays is well understood e.g. for MoS_2 crystals.[114]

Role of substrate

Properties of monolayer crystals depend not only on their chemical composition and structural phase, but also on choice of the substrate on which they lie on. When first samples of TMD's were obtained, standard procedure after their exfoliation was to put them on properly prepared SiO_2 / Si substrate, which for certain thickness of SiO_2 layer enhanced contrast in optical microscopy.[115] It was also understood that optical quality depends heavily on surrounding dielectric environment,[116,117] which brought into question if SiO_2 is truly best substrate for optical studies. Nowadays it is clear that substrate on which subtle optical features of TMD's can be most easily observed is hBN,[118,119] for which e.g. exciton lines approach 2 meV widths.

1.3 Review of experimental properties of TMD's

Experimental techniques for TMD's

Optical and electrical measurements of crystals are primary tools in their studies.[120–122] Despite being well developed, even for nanostructures like quantum wells, atomically thin samples pose many challenges in performing "standard" experiments. Additionally, by mechanical exfoliation highly non-uniform sam-

ples are produced, resulting in spread of experimental results. Those depend also on history of the sample, e.g. oxidation.[123] Transport experiments are especially difficult due to limited possibility of attaching low resistance contacts, however many advances been made.[124] In general, standard procedure after deposing sample on a substrate is checking how many layers crystal actually has at a given position. To do that, optical contrast has been invaluable to quickly establish thickness of samples, which can be further confirmed by atomic force microscopy measurements[103] or Raman spectroscopy.[125,126] It is known also that, mostly due to strain, TMD's do not have homogenous band gaps, as shown by scanning tunneling microscopy experiments.[127,128] It should be therefore understood that optical methods, probing sample over some finite area, give rather averaged results. For bands filled with electrons it is possible to use high-energy photons to excite carriers so much that they leave the sample, and then can be detected keeping their angular information, reflecting their reciprocal space positions in the Brillouin zone, technique that is know as angle-resolved photoemission spectroscopy. This method was used to measure effective masses and band splittings of valence bands of TMD's,[129–135] however it requires metallic substrate that significantly screens interactions predicted in monolayers without substrate.

Optical probing

In order to study more subtle properties of TMD's, e.g. related to optical energy gap or dispersion of empty bands, absorption, reflection (RC) and photoluminescence (PL) experiments are preferred. In absorption usual problem is that for thin samples amount of absorbed light is small. Despite monolayer thickness, absorbance in TMD's for specific photon energies is exceptionally high (compared to 2.3 % in graphene),[136] promising novel solar cells and photodetectors with parameters already surpassing best Si and GaAs devices.[137–142] As for optical studies of quantum wells, one can study also reflection of light from the sample or excite carriers with photons with some energy and collects signal that is emitted back, which is essence of photoluminescence effect. Performing reflection and PL experiments at exactly the same spot and time is usually challenging, however it is possible.[2,143] Also, to study dynamical properties of samples, Raman effect measurements are routinely performed, which detect signal from vibrational degrees of freedom of the monolayers, e.g. different types of phonons helping to distinguish between samples with different numbers of layers.[144,145]

Giant PL enhancement

One of the results that sparked widespread attention around 2010 was establishing that MoS_2, when thinned down to a single monolayer, exhibits significantly stronger photoluminescence than two and more layer crystals.[103,146,147] Similar trend was then confirmed in $MoSe_2$,[148] WS_2,[149] WSe_2[148,149] and $MoTe_2$[150,151] semiconductors with varying magnitude of differences between samples with different number of layers. This phenomenon was related to indirect - direct band gap transition, caused by different renormalization of indirect (Γ-Q) band gap compared to much smaller renormalization of K-K direct gap when samples are thinned down. This trend was confirmed theoretically by *ab initio* calculations[152,153] and confirmed experimentally by photoemission spectroscopy for valence bands (valence band maximum change from Γ to K point between few and one monolayer).[129]

Valley excitons fine structure

First inkling that strong photoluminescence is dominated by excitonic (X) transition comes from comparison of PL peak energy position to known spectral positions of excitonic transitions in bulk MoS_2 at K point.[146,154] Two excitonic transitions, dubbed A and B, separated spectrally by approximately 140 meV in MoS_2 correspond to two bound states of electron-hole pairs with opposite spins arrangement, and their splitting reflects spin-orbit splitting of valence bands. Importantly, generation of excitons in a given valley is possible via specif selection rules, which couple circularly polarized light with excitation in a given valley (e.g. σ^+ generates excitons in $+K$ valley).[34,155–161] Valley coherence of such excitons has been probed in many experiments.[162–166] Spontaneous choice of valley after excitation with unpolarized light has also been observed,[167] pointing towards valley-polarized ground state.[168–170] Excited exciton states were measured in WSe_2,[171,172] WS_2[173] prior to molybdenum based TMD's due to larger separation between A and B excitons (0.4 eV), so that B exciton was not "masking" excited A exciton states. Alternative proposal, with 1s A, 1s B and then excited A series was also discussed.[174] Then, complementary PL excitation spectroscopy allowed to measure excited states in MoS_2, $MoSe_2$, WS_2 and WSe_2.[175–177] Excited B exciton series is more challenging to measure[172,176] due to overlap with wide PL signal from so-called C excitons, resulting from band nesting (parallel valence and conduction bands) around Q and Γ points of the BZ. All of those experiments confirmed that spectrum of s-like states deviates strongly from 2D hydrogen-like series. Further experiments in magnetic fields reached up to 5s excited states.[112,178–181] We note that exciton series consists not only of bright s-series, but also two types of so-called dark states, namely spin-forbidden and excited excitons states with different than s symmetry. The former one can be probed by PL dynamics,[182,183] different emission configurations,[184–189] different temperature dependence of emission[190] or by using tilted magnetic field.[185,191–194] The latter ones are usually probed using two photon spectroscopy.[195,196] Dark p-states can be also studied in pump-probe experiments,[197–203] where 1s excitons are generated and transition from 1s to 2p states can be measured by a probe terahertz beam.[204] Additionally, excitons with finite center-of-mass momentum, which require phonon-assisted excitation due to momentum conservation can also be probed, revealing complicated landscape of so-called momentum-indirect excitons.[205–208]

Trions

In addition to strongly bound excitons, TMD's exhibit another type of bound complex in their photoresponse, namely trion.[209–212] This complexes consists of 3 particles, i.e, 2 electrons + 1 hole (X^-) or 2 holes + 1 electron (X^+) for negatively and positively charged types, respectively. In GaAs quantum wells rule of thumb is that trion binding energy is order of magnitude smaller than for exciton, and same rule seems to work in TMD, in which, however, binding energy of exciton is in order of hundreds of meV, therefore trion binding energy is given in tens of meV.[143,213–221] Existence of such complexes depends heavily on excess carriers, which come from natural defect-induced,[222] chemical,[116,223] substrate[216,224,225] or gate doping.[162,226–232] Stability of those complexes has been shown to survive up to room temperatures.[143,213] For higher doping regimes, picture of exciton interacting with FErmi sea has been proposed.[169,233] Interest-

ingly, just as in exciton case, trions exhibit fine structure,[231,232,234–239] involving both dark-bright states and also excited trion states.[240] Moreover, strong electron-phonon interaction allows to couple trions and excitons, allowing for example so-called up-conversion process,[241] in which low energy photon excitation (exciting trion) via phonon coupling induces optical emission from higher energy state (exciton).

Large excitonic molecules

Due to exceptionally strong electron-electron interaction, manifesting itself in large binding energy of excitons and trions, it is natural to ask if optical complexes composed of more than 3 particles are possible. 2 electron + 2 hole bound state is called biexciton (XX). Several experimental fingerprints of those complexes have been detected.[228,234,242–246] Magnetic field measurements[247] revealed biexciton g-factors similar to excitonic ones. Biexcitonic thermoluminescence was proposed to dominate optical response of edge and grain boundaries for high excitation regime.[248] Stability of these complexes in room temperature has also been demonstrated.[249,250] Studies of tunability of XX with electrostatic gating[251–254] shed some light on relative positions of exciton - trion - biexciton lines, suggesting that biexciton lines are located between trion and exciton, and below trion line charged biexciton[255] (electron + trion bound complex) can be observed.

Other collective excitations

Interpretation of different lines in PL/ absorption spectrum is generally difficult, not only due to plethora of different optical complexes, but also due to possibility of coupling of those complexes to different quasiparticles, e.g. related to excess charge carriers.[211] For example, some of the lines interpreted as charged excitons / biexcitons, are also consistent with interpretation that exciton couples to plasmons, i.e. collective excitations of electron gas.[256,257] Coupling of excitons to so-called polarons[258] (polarization cloud) has also been used to explain effects of oscillator strength transfer between some features of PL spectrum in MoS2.[169] Novel mechanism of phonon - exciton interaction crating virtual trions has also been put forward.[259] Strong coupling to light in microcavities creating polaritons[260] has also been demonstrated.[261,262]

van der Waals heterostructures

Atomically thin crystals offer novel route to engineer material properties due to possibility of assembling them into different configurations.[263] Starting from proof-of-concept double layers of graphene with hBN layers between them,[264] subsequently it has been shown that graphene can act as atomically sharp contact to TMD's.[265] Recently, one of the greatest improvement of optical quality of semiconducting crystals was achieved by placing them in-between thin hBN crystals.[119,266] Different band gaps and band-edge positions allowed for creating analogues of type I and type II heterostructures.[267,268] Inter-layer excitons has been observed,[268–274] showing both PL and exciton energy electrical tunability and order of magnitude longer lifetimes than intra-layer exciton due to spatial separation of electron and hole.[269,275,276] Moreover, larger complexes with carriers residing in different layers has already been proposed and some evidence of such behaviour has been found.[277–280] Long inter-layer exciton lifetime naturally led to the proposal of exciton Bose condensates,[281,282] which first evidence of experimental realization emerged in $MoSe_2$-WSe_2 system.[283]

Straintronics

Another route to engineer material properties comes from strain engineering.

Atomic force microscope mechanical studies of MoS_2 has shown that samples can sustain large strain, between 6 and 11%[284] (13% for graphene) of lattice constant. Continuous tuning of optical band gap,[285] with changes reaching up to 400 meV for strains up to 3%[128] has been shown, along with direct to indirect band gap transition in MoS_2, occurring slightly above 1% of applied strain.[286] Optical strain mapping in TMD's has been demonstrated using Raman,[287] PL[288] and second harmonic generation[289] techniques. Interestingly, strained regions were shown to attract excitons and trions, enhancing exciton-to-trion conversion.[290] Strain can also induce confinement of carriers,[288] and can be used to deterministically arrange arrays of quantum dot-like emitters.[291,292] It is worth mentioning, that strain naturally occurs also inside so-called bubbles, which are ubiquitous in realistic atomically thin materials samples.[293]

Twistronics

Another alternative method to tune electronic properties, unique to 2D crystals, is related to modification of relative twist angle between two or more crystals or between crystal and the substrate. Starting from various studies of twisted graphene layers,[294–304] it was quickly realized that graphene on hBN substrate[33,86,305–312] exhibits so-called moiré pattern, opening unique avenue of superlattice engineering to study novel physical phenomena.[313–317] Tuning of electronic properties with respect to twisting for other crystals, e. g. two MoS_2 monolayers,[318–322] was also demonstrated. Additionally, novel type of exciton tuned by inter-layer twist was established.[323–327] Fascinating new line of research was opened by discovery of superconductivity in twisted bilayer graphene,[328–330] with potential of studying Hubbard physics in twisted TMD's platform already emerging in literature[331,332]

Superconductivity in TMD's

It has been long-known that metallic TMD's MX_2 (M=V, Nb, Ta, X=S, Se, Te) and $RhTe_2$ are superconducting,[89] with largest superconducting transition temperature in $NbSe_2$ at 7 K. Answer to question if superconducting state survives when crystals are thinned down to monolayer is positive. In metallic monolayers superconducting state was discovered for TaS_2[333] and $NbSe_2$.[334] Even though MoS_2 in bulk form is semiconductor with band gap approximately 1.0 eV, it has been shown experimentally that combination of liquid environment and crystal doping can induce superconducting state in thin films[335] with transition temperature up to 10.8 K. Interestingly, superconducting state in MoS2 can survive very high magnetic fields (up to 52 T at 1.5 K[336]) due to novel mechanism of protection of Cooper pairs against magnetic breakdown due to specific spin-valley structure of electron pockets (establishing so -called class of "Ising - superconductors").[337] Gate-tunable superconductivity in 2H-MoS_2 monolayer,[338] 2H- WS_2 monolayer[339] and 2H MoS_2 bilayer[340] samples has also been demonstrated. Experiments show,[338] that the explanation of pairing mechanism in MoS_2 has to go beyond conventional phonon-driven BCS s-like state,[341] with many proposals including topological nature of pairing.[342–346] Multi-valley nature component of superconducting state, associated with existence of Q points in which both spin orbit and electron - phonon couplings[152,347,348] are enhanced with respect to K valleys, has also been discussed experimentally.[349,350] Interestingly, recent experiments show also that monolayer 1T'-WTe2 topological insulator exhibits superconductivity with transition temperature around 1K,[351]

which can be enhanced by creating heterostructures with few-layer $NbSe_2$.[352]

1.4 Electronic structure of MX_2 semiconductors

Ab initio studies

Early *ab initio* calculations of MX_2 crystals[353–360] were motivated by many STM experiments of surfaces aimed at understanding structural properties of transition metal dichalcogenides.[361–364] Those studies confirmed long-known[89] fact that MX_2 crystals (then mainly TaS_2, $TaSe_2$, MoS_2, WS_2) have layered structure, with strong bonding inside "sandwich" of three layers of chalcogen-metal-chalcogen and weak van der Waals bonding between "sandwiches", which are nowadays called "monolayers". Plane wave calculations utilizing Vanderbilt's ultra-soft pseudopotentials[365] have shown differences between bulk and monolayer band structures.[355] Then many studies on, e.g., vacancies on surfaces,[366] fullerene-like structures,[367] nanotubes,[368,369] nanoclusters[370–372] and nanoribbons[373,374] appeared. Several pseudopotential calculations confirmed transition to direct electronic bandgap,[146,372,375] fact that was further verified by all-electron calculation.[152] Systematic study of TMD's family MX_2 (M=Mo, W, Nb, Ta, X= S, Se, Te) showed that Mo and W compounds are semiconducting while Nb and Ta are metallic.[376] Moreover, study of various approximate solutions to DFT band gap problem (Heyd-Scuseria-Ernzerhof (HSE) hybrid exchange - correlation functional,[377] GW correction[378]), showing large spread of estimated band gap, confirmed trend that bang gap lowers when changing from sulfides to selenides to tellurides.[376,379] Quasi-particle self-consistent GW method[380–385] calculations confirmed large increase of single-particle band-gap compared to LDA or GGA results.[386–389] Summary of many available LDA GGA, HSE, GW and experimental single particle properties are presented in Ref. 390. Further improvements over GW method including vertex corrections[391,392] are available for TMD materials, however different approaches like coupled-cluster theories[393–395] or many-body quantum Monte Carlo[396–399] known to improve over GW accuracy are yet to be calculated.

Nature of band gap problem

It well known that correct calculation of DFT band-gap is a challenging problem[400–402] even for 3D semiconductors. For 2D crystals, as can be deduced from many *ab initio* calculations (e.g. Ref.146,152), when thinning down MX_2 semiconductors band gap for bilayer systems is still indirect (in MoS_2 top of VB at Γ, bottom of CB at Q point, located half-way between K and Γ), while monolayer system becomes direct gap semiconductor with band gap at the corner of hexagonal Brillouin zone (at K-point). Interestingly, energy gap at K between bands changes much less at K point than in other points, therefore process of indirect to direct transition is mostly influenced by band structure change in VB at Γ and in CB at Q. Precise estimation of relative position of CB minima at K and Q at VB maxima at K and Γ is difficult and seems to be dependent on many details of calculations.[153,229,382,386,403–405] It is known also that substrate choice plays a role,[406,407] which is intertwined with dielectric environment.[408] Strikingly, hBN encapsulation was recently predicted to make MoS_2 indirect gap semiconductor.[409] Also, strain plays a pivotal role in bands renormalization.[286,382,410–417] Further complications arise when discussing few-layer

TMD's, e.g., GW theory of MX_2 homo-bilayers[418] suggest that band gap in all is direct, however not always between Γ and Q (case of MoS_2, $MoSe_2$ and WS_2), but may change to be indirect between K and Q (case for $MoTe_2$, WSe_2, WTe_2).

Spin-orbit splitting

Fully relativistic *ab initio* calculations uncovered large spin - orbit splitting of valence bands in MX_2 monolayers.[419] Spin texture in TMD's exhibits so-called spin-momentum locking,[34] which stems from combination of inversion symmetry breaking[420] and heavy atom nature of metal elements in MX_2. Magnitude of spin orbit splitting changes from around 140 meV in VB at K point in molybdenum-based materials to as much as 400 meV for tungsten based materials.[421] It is also well established that spin orbit-splitting in CB is at least order of magnitude smaller, however due to different mechanisms can be modified, e.g. enhanced spin-splitting by electron interactions,[422] dynamical effects[423] and inter-/ intra-valley phonon[424] and plasmon[257] contributions. By symmetry SOC vanishes at M and Γ points of the Brillouin zone, however it's value at Q point in CB is usually much larger than at K point, which stems from different orbital compositions of the bands.[421] Interestingly, strain tuning of spin-orbit splitting allows not only to modify spin-resolved band structures,[285,405,425–427] but also create on-demand, spatially localized emitters[288,428–433] which will be described later. Also, due to electric field, so-called Bychkov-Rashba SOC may be present in TMD's,[434] allowing for spin-valley qubits control.[80]

Carrier doping and study of defects

Additional problematic aspect of the band gap character in TMD's comes from renormalization effects from excess charge carriers in conduction band.[435–438] Density - dependent transition from direct (K-K) gap to indirect one (K-Q) in monolayer TMD's has been predicted.[439–441] Similarly to the case of strain modification of band structure, Q valleys energetic position is more sensitive to carrier doping concentration than K valleys in conduction band. This effect is important for efficiency of excitonic photoluminescence,[439] as well as for e.g. phonon-mediated superconductivity in doped MoS_2.[347] Complicated aspect of how doping may influence excitonic response is discussed further in text (in "Exciton interactions with Fermi sea"). It is worth mentioning also, that role of dopants, vacancy and defects has been studied heavily using density functional theory[442–446] and different experimental techniques,[447–457] pointing to importation role of defect states engineering as additional way of enhancing desired electronic properties.[458,459]

Tight-binding models

For more intuitive understanding of physical picture, tight-biding model of electronic structure is usually desired. Early tight-binding models approximating electronic structure of transition metal dichalcogenides were available as early as in 70's.[460,461] More recent tight-binding models tailored to reproduce DFT band structures of monolayers started with describing electron properties with d-orbitals localized only on metal atoms,[462] immediately followed by models including both d-orbitals on metals and p-orbitals on chalcogens.[463–473] All those models shed new light on several aspect of modeling of low-energy structure of TMD's, however many of them were either highly complicated,[464,465] or not describing conduction band of TMD's satisfactory enough while keeping desired short-range of hopping. Some of those models were able to describe also bi-layer and bulk TMD's.[464] One of the goals of this thesis is to construct TB model that

will describe correctly main features of bands around Fermi level with minimal number of orbitals used.

Massive Dirac fermion, $k \cdot p$ and parabolic dispersion models

Further simplification is possible by restricting only to part of the Brillouin zone (neighborhood of K points in TMD's) and modeling electronic structure there using so-called $k \cdot p$ theory.[17] In the case of MX_2 semiconductors, usual choice is massive Dirac fermion model[34] and it's extensions to either more terms in 2 band Hamiltonian[421,434,474,475] or adding more bands.[476] Even further simplification of two-band massive Dirac fermion model is possible, leading to parabolic model of bands, usually applied to empirical estimation of, e.g., g-factors of excitons[180] or effective mass of carriers in magneto-transport experiments.[477]

QSHE phase in TMD's

We note that from topological classification point of view[52] 2H MX_2 semiconductors have topological index $Z_2 = 0$ and are called topologically "trivial". However, other phase of those materials is possible (namely 1T' phase), for which there is an inversion of bands around Fermi level and consequently, change of topological properties is predicted.[478] Then material becomes quantum spin Hall insulator. This scenario has been experimentally demonstrated for 1T'-WTe_2.[99,100,479,480] Tight-binding models for TMD's in 1T' phase[481–483] point towards different main composition of orbitals, being rather $d_{x^2-y^2}$ and p_x instead of d-only in case of 2H phase. Intriguing proposal to realize topological phase transition via moire pattern in bilayer TMD's was proposed as well.[484,485] Also, in bulk materials other interesting novel phases has been predicted and measured, including Weyl semimetal in bulk WTe_2.[486]

QSHE 2D crystals with large spin-orbit coupling

QSHE phase in 2D materials were first predicted in graphene.[53] It quickly become clear that due to small spin orbit coupling[487,488] detection of topologically protected edge states is very challenging, however achievable.[489] Those problems sparked great interest in finding materials with similar properties as graphene, but with significantly larger spin orbit coupling. Many proposals have been put forward[61] and high-throughput scans of 2D materials databases suggest there there are many new materials to be discovered.[490–495] One of the most promising candidate for functional topological insulator devices are bismuth (111) monolayers,[59,496,497] exhibiting largest know band gap in topological materials. Interestingly, this material shares overall honeycomb structure with TMD's and large atomic number of atom corresponding to large value of atomic SOC, however due to different band composition (consisting mainly from p orbitals of Bi atoms) band inversion happens there naturally. Various proposals aimed at further control and modification of topological phase in bismuth-based 2D materials have been recently put forward,[60,498,499] including this thesis author's contribution.[500–502]

1.5 Theory of correlated optical excitations

DFT+GW+BSE framework

As discussed above, usual work flow of theoretical investigations into crystals, aimed for example at predicting band-gap of a given crystal, has to include approaches going beyond density functional theory, e.g. GW approximation. This correction does not, however, take into account that optically created elec-

tron - hole pair can interact strongly, forming so-called excitonic state.[503] Successful description of bound excitonic states requires analysis of two-particle correlations, which can be done by solving Bethe-Salpeter equation (BSE),[504] originally developed for bound states problems in high energy physics. Subsequently this method has been applied to Wannier exciton problem[505–507] and good agreement between theoretical[508–511] and experimental results was achieved for many different semiconductors. Nowadays several ab-initio codes implement DFT+GW+Bethe-Salpeter framework.[512–517]

Application to TMD's

First-principles Green's function theory of optical excitations, even though it was developed for 3D crystals, can also be applied to materials with different dimensionality. Many studies of excitons within DFT+GW+BSE emerged.[104,136,153,195,286,386,387,403,404,518–527] Those studies correctly identified that excitonic effects in TMD's should be large[153,386,518] due to reduced dimensionality and resulting much weaker electron-hole interaction screening compared to bulk crystals. Inclusion of spin-orbit coupling confirmed general double peak structure of optical response below band-gap, associated with existence of valence band split A and B excitons.[528] Existence of so-called C exciton associated with band nesting of states has also been established.[519] Even though there is large reduction of optical band gap when TMD's are strained, it has been uncovered that strain does not modify exciton binding energy significantly.[403] Superiority of TMD's for photovoltaic applications compared to Si and GaAs has also been proposed due to predicted enhancement of sunlight absorption.[136] Strain-tunable nature of bandgap has also been put forward.[286] Large differences between binding energies of excitons on substrate supported and suspended devices has been early realized.[520] Variation of exciton resonance with temperature has also been calculated.[521,524] Large renormalization of band gap and large exciton binding energies have also been studied for samples on top of graphene bilayers.[104] First *ab initio* calculations of excited states of exciton series predicted large deviations from non-hydrogenic series, and existence of 2p-2s splitting in first shell of excited exciton states.[195] Non-analytic (Dirac-like) dispersion of exciton excited branches due to inter-valley coupling has been shown.[387,522] Importance of corrections to linear dielectric function (Rytova-Keldysh theory) in hBN encapsulated monolayers has been shown.[523] Highly converged calculations uncovered common issues with numerical aspects of excitons in TMD's.[404] Exciton fine structure including spin dark states has been calculated in Ref. 529. Detailed studies in $MoTe_2$ uncovered small variation of 1s, 2s A exciton and 1s B-exciton binding energies between mono- and bi- layers.[525] Energetically higher transitions relevant for electron-energy-loss spectroscopy has been also studied.[526] Mixing of A- and B- excitons via inter-valley exchange interaction has shown that understanding them in terms of "Ising" excitons may not always be satisfactory.[527] Theory of mixing between photons inside cavities and excitons has been calculated in Ref. 530. Calculations including both spin- and momentum dark excitons in MoS_2 became available recently.[531] *Ab initio* calculated properties of topologically split 2p states in $MoSe_2$ have been presented.[203] Interestingly, DFT+GW+Bethe-Salpeter methodology has been recently extended to study charged exciton complexes.[240,532–534]

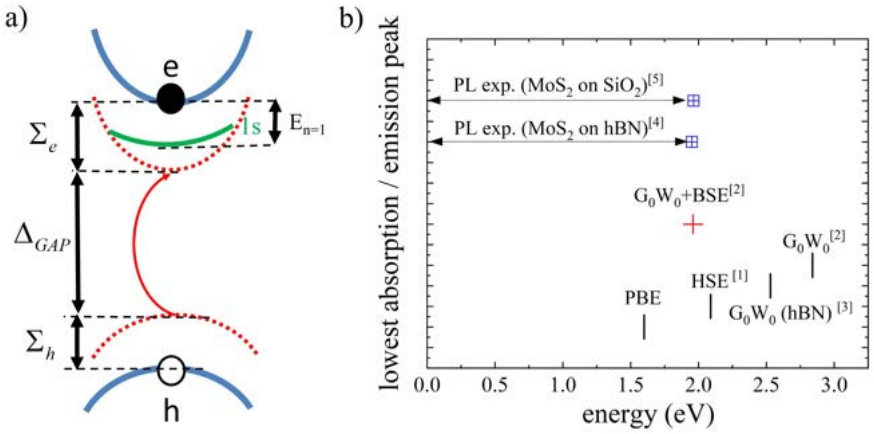

Figure 1.1: (a) Bound electron- hole pair energy states with respect to free particle bandgap. (b) Summary of free particle bandgaps (black vertical lines) obtained using different methodologies compared to experimental peak position for MoS_2 on SiO_2 and hBN (blue rectangles) and state-of-the-art calculation including excitonic effects (G_0W_0+BSE, red plus). PBE result is our own DFT calculation, other results are taken from: [1] - CMRDB database,[535] [2] - Ref. 519, [3] - Ref. 536, [4] - Ref. 6, [5] - Ref. 143. We note that theoretical calculations (except one for MoS_2 on hBN) are performed for systems surrounded by vacuum.

DFT+GW+BSE vs experimental optical bandgap

"Free particle" transitions, calculated form e.g. DFT energies, are well known to give incorrect optical band gaps in semiconductors. For both 3D and 2D crystals this effect is caused by interplay of two effects: renormalizations of energies of excited single-particle levels (known as electron and hole self-energies Σ) and existence of bound electron hole pairs, called excitons. First effect is schematically depicted in Fig. 1.1 (a), where red dotted bands symbolize DFT bands, e.g. at PBE level. Those bands, when carriers are excited and measured e.g. in ARPES type of experiments, do not describe their energies correctly, because electron in CB interacts differently with sea of electrons in VB. Also, missing electron in VB energy is renormalized. Those shifts in energies are usually called self-energy corrections and can be calculated by so - called GW method. GW renormalized bands are shown in Fig. 1.1 (a) as blue lines. Next effect is related to electron hole interaction, which creates bound state with negative binding energy, therefore exciton "band" lies below GW - corrected CB band (see green exciton band in Fig. 1.1 (a)). Because effect of band renormalization and negative binding energy of electron-hole pair have same order of magnitude, sometimes it might create confusion that DFT describes correctly absolute energy of optical gap. For MoS_2, experiments show that optical gap is located at $\approx$ 1.95 eV (position of 1s excitonic level), as shown in Fig. 3.3 (b). Interestingly, PBE result underestimates this energy. Only after calculation of GW correction one can obtain by solving Bethe-Salpeter equation correct estimate of absolute position of 1s excitonic state (red plus in Fig. 1.1), coinciding with experimental position of lowest PL excitonic peak.

Interestingly, MoS_2 put on two different, most popular substrates SiO_2 and hBN, has almost exactly the same energy of optical gap. This is surprising, because it is known that binding energies of excitons on those substrates should be significantly different. Another confusing result is that absolute peak position shown in Fig.1.1 (b) (G_0W_0 + BSE), almost identical as experimental, is calculated for MoS_2 in vacuum. Similarity of these values is coincidental and stems from before mentioned cancellation of self-energy and excitonic re-normalizations, which are true even when dielectric environment (vacuum, SiO_2, hBN) is vastly different. Recent GW calculation of MoS_2 on hBN[536] helps to rationalize this, showing actual position of GW-normalized "free particle" bandgap, showing that excitons in MoS2 in vacuum are bound much stronger that for hBN encapsulated samples. To best of our knowledge reliable *ab initio* calculations for same effect on SiO_2 are not available in literature yet.

Exciton calculation using approximate methods

Due to many computational challenges inside DFT+GW+Bethe-Salpeter theory, simplified approaches to excitonic problem have been studied, including various level of approximations, i.e., tight-binding,[204,205,207,208,430,537–543] $k \cdot p$ (massive Dirac fermion and beyond),[34,217,522,544–551] and effective mass approximations.[112,173,266,408,552–562] Those approximations routinely use DFT as a staring point, e.g. for calculation of effective mass of carriers and then simplify somehow their interaction, e.g. assuming only Rytova-Keldysh screening[563,564] without form factors coming from Bloch parts of electrons and holes. Those methods, being conceptually and numerically trackable allowed for many fascinating advances in understanding exciton properties in TMD's, as summarized briefly below.

TB exciton models

Tight-binding studies allowed to track exciton fine structure evolution dependence on electron doping,[537,538] exchange interaction,[544] magnetic[430] and electric fields.[542] Theoretical results on excitonic landscape have been show,[208,541] together with results confirming topological splitting of 2p states in exciton spectrum due to effect of Berry's curvature. Splitting of 2s and 2p states (and states with different symmetry in 3rd shell) have also been discovered.[204] Dynamics of excitons resulting in specific line-width broadening has been studied.[207] Possibility of constructing dark-states based sensor of molecules[205] has also been proposed.

$k \cdot p$ and mDF exciton models

Two-band $k \cdot p$ theory of edges of valence and conduction bands has been recognized as early as in 2012,[34] immediately relating physics of low-energy excitations in TMD's to massive Dirac fermion physics, known from study of graphene with increased SOC and other topological insulators. This model, used in exciton properties calculations, allowed for better understanding of spin and valley dynamics.[546] Important role of inter-valley exchange interaction on exciton with non-zero center-of-mass momentum[522] and excited exciton series[548] has been studied. Relevance of Berry's phase properties of single electron wavefunctions on excitonic spectrum has also been discussed,[545] leading to the idea of self-rotating excitons.[551] Influence od "Diracness" of low-energy Hamiltonian description on excitonic spectrum has been studied in Ref. 549. Exciton states with different symmetries (s- and p- like) mixing and resulting activity of both in single photon experiments has been predicted.[550] Also, ground state of doped

samples using variational approach has been studied in, e.g., Ref. 547.

Effective mass exciton models

Effective mass approximation (EMA), i.e. parabolic model of dispersion with different effective masses for electrons and holes, despite oversimplification of many features of band structure of TMD's, allows to obtain some results that are not easily available using more advanced methods. For example, studies have shown that by fine tuning of screening parameters of electron-hole interaction, results comparable to BSE can be obtained.[552] When EMA is employed together with electron - hole interaction with static screening, analytical solution for both 3D and 2D exciton are available. It has been noticed, however, that static screening is not enough to explain experimental results on excited exciton series (Rydberg series).[173] Combination of EMA with screening "averaged" over exction's radius allowed to obtain simple empirical formula for exciton binding energy for large class of 2D crystals, showing crucial role of polarizability.[556] Combination with so-called Kratzer form of electron - hole interaction[112] yielded good empirical model for excited states Rydberg series in several hBN encapsulated TMD's. Parametrization of different screening parameters and polarizability for various dielectric environments yield satisfactory method to explain experimental results on excited states series of s-like excitons.[408] Role of different dielectric surrounding,[559] especially hBN encapsulated MoS_2 samples has been measured and calculated also in Ref. 266. Dynamical effects, e.g., exciton formation, thermalization and PL evolution has been studied in Ref. 560. Stark shifts for excitons and trions has been studied under the assumption of parabolic dispersion of carriers.[558,561] Extending this description to more-than-two particle complexes, it is possible to obtain using variational methods not only trion, but also e.g. biexcitons, exciton-trion and exciton bound to charged defects energies.[553,557]

Configuration - interaction language

Alternatively to Bethe-Salpeter equation, exciton properties can be calculated from configuration-interaction approach to interacting electrons,[565,566] particularly useful in studies of nanostructures, e.g. quantum dots[81,567–582] or electron gas in quantum wells in strong magnetic field.[583,584] This approach is based on expansion of interacting wavefunction in basis of excitations with growing number of excited pairs (called singlets, doublets, triplets etc.) with specific rules for coupling between sub-spaces, connecting ground state only with doublet excitations, but every other subspace with two subspaces with one and two excitations more (e.g. singlets with doublets and triplets). This approach has only recently been utilized to study excitons in reciprocal space.[5,533] Configuration-interaction method, being long-known for theoretical simplicity and formidable computational challenge due to large Hilbert space, is therefore different theoretical route to study properties of excitons than GW+Bethe-Salpeter method based on Green's function perturbation theory. Although connection between consecutive steps and approximations in those two methods is known,[566,585,586] necessary truncations of expansions for configuration interaction, coupled cluster and "beyond-GW" methods[394,587–592] introduce errors in ground and excited states energies that are yet to be understood for TMD's. In this thesis, following methodology known for interacting electron problem in quantum dots[567] and Landau levels,[583] configuration-interaction method for exciton in TMD's will be constructed

Alternative approaches

One has to remember, that there exist different methods to calculate optical response of excitons, trions and systems with even more particles in both molecular and periodic systems. One class of methods stems from Heisenberg equation of motion and was dubbed "semiconductor Bloch equations".[436,548,593–598] Another approach is related to real space representation of kinetic energy of electrons and holes (usually parabolic dispersion of carriers is necessary) and utilizes variational approach.[552,557,599,600] When real-space kinetic energy is approximated by parabolic model, diffusion Quantum Monte Carlo methods have also been used to study optical response of TMD's.[554,601,602] Results for optical complexes with several particles hve also been obtained using path integral Monte Carlo method.[555] Most recently, combination of tensor networks and density matrix renormalization group-like methods has been used to study exciton and bi-exciton ground[603] and excited states.[604] Focusing on excitonic problem only, to lower computational complexity of Bethe-Salpeter equation, methods based on density functional theory which include electron-hole interaction in exchange correlation potential are also well-known,[605–608] and it's theoretical equivalence to Bethe - Salpeter theory was shown.[609] Successful calculations of weakly bound excitons in 3D solids was achieved,[610–614] despite several difficulties connected to e.g. lack of theorems relating unique density to energy of excited states[615] and problems constructing good exchange - correlation potentials.[503] Going beyond "continuum excitons" was also achieved e.g. by solving so-called "Casida equations".[616] Only very recently TDDFT solution for response function in hBN and MoS2 was possible,[617,618] reproducing A and B excitonic features, comparing favorably with GW+BSE method at the fraction of computational resources necessary. Focusing for a moment on trions, several methods for calculating their properties in ultra-low doping regime are available, including (beyond already mentioned) methods that utilize so-called Jacobi coordinates[619] leading to 1D problem in higher-dimensional space that can be solve numerically. Slightly different approach using hypershperical harmonic functions and leading to coupled equations parallel to so-called Fadeev equations for 3D trion problem[620] has also been used recently to study both positively and negatively charged trions in whole MX_2 (M=Mo,W, X=S,Se,Te) family of TMD's.

Exciton interactions with Fermi sea

As mentioned previously, calculation of exciton optical properties is even more difficult when finite density of electrons in conduction band is taken into account. Additionally to simple band renormalizations disused earlier, exciton binding energy also get's renormalized due to enhanced screening of electron-hole interactions.[621] However, it is known from physics of 2D electron gas in quantum wells, that for sufficiently high doping optical response is not coming mainly from excitons, but from so-called "Fermi edge singularity".[211,622] At low doping, trion formation and it's relative response compared to exciton is fairly well understood.[211,623–625] When density of excess carriers is in intermediate regime, picture of three interacting carriers has to be changed to picture of an exciton interacting with Fermi sea of excess carriers.[258,626,627] More precise calculations are necessary to resolve many conflicting results, especially when Fermi energy for n-doped samples reaches trion binding energy, as recently summarized in Ref. 628.

Topological effects in excitonic spectrum

In addition to unusual behavior of excited state exciton Rydberg series in TMD's due to Rytova-Keldysh screening of electron-hole interaction,[173] modification to whole spectrum resulting from topological properties of electron wavefunctions has to be taken into account.[551,629] Novel type of 2p-2p exciton splitting due to topological terms entering electron-hole direct interaction was recognized some time ago[204,430,541,545] and recently measured experimentally.[203] These advances paved the way for generalized optical selection rules in gapped fermion systems, where classification of optical transitions has to taken into account underlying topology of the system and consequently allows for additional means of control.[630–632] All selection rules for MoS_2 has recently been summarized in Ref. 633. We note that effect of Berry's curvature on optically addressable complexes is not restricted to excitons.[634] It is worth noting also that novel properties of excitonic spectrum due to different topology has been recognized first in area of topological insulators.[635–637]

1.6 Electronic properties of TMD's quantum dots

TMD's nanoribbons and finite clusters

When reducing dimensionality of 2D material by one (cutting finite width ribbon out of 2D plane), creation of so-called nanoribbon is possible, as pioneered by studies in graphene.[638–645] Usual scenario is that when nanoribbons get thinner, electronic band-gap should grow due to size quantization. In graphene, due to it's topological properties, situation is more complicated due to occurrence of edge-termination dependent edge states. In MoS_2 (and other TMD's from MX_2 family[646,647]) due to it's large semiconducting gap and trivial topology in 2H phase one could expect that there will be no in-gap states. This is, however, not true and metallic edge states in both armchair and zigzag type nanoribbons have been theoretically predicted and observed in transport experiments,[373,648–650] as well as novel optical response of the edges has been measured[651] and discussed theoretically in the context of "edge excitons".[652] These states can be understood as coming from specific topology associated with one of the two valleys of MoS_2. Properties of these edge states have been studied extensively[653] and many interesting phenomena have been predicted.[654–663] Further reduction of dimensionality to "0D", i.e., finite systems (usually called quantum dots, or for very small structures also (nano)clusters) has been focus of long interest for MoS_2 due to it's usefulness in catalysis.[370,664–666] Metallic edge states, similar to edge states in nanoribbons have been studied in nanoclusters.[372,667–669] MoS_2 2D clusters have been recently obtained using lithographic,[670] solution-based[671–674] techniques, which can be extended to other TMD's.[675–678]

Spin-valley mDF qubits

From the point of view of quantum computing, it has been early recognized that electrons (or holes) trapped inside quantum dots can serve as perfect quantum two-level information carrier, i.e. a qubit, utilizing either ground or excited states as 0 and 1 state[679,680] or carrier's spin.[681–694] Carriers confined in quantum dots with states derived from bottom of the conduction band in TMD's and described approximately by massive Dirac Fermion theory have been proposed as qubits, allowing novel schemes due to valley degree of freedom.[80,434,695–704]

Similarly to proposals in carbon nanotubes,[705] spin-valley coupled "Kramers qubit"[434] was proposed as realistic way of defining a qubit. Inter-valley interaction due to confinement potential has been studied in Ref. 695. Optical[696,699] and electrical[80,702] manipulation of spin-valley qubits have also been studied, together with magnetic means of control.[697] Due to challenging problem of inducing valley coupling between Kramers qubits[700] different scenario based on spin-only qubit has been studied.[698,704] Interactions between spin-valley qubit in two quantum dots and possible realization of quantum logic gates has been analyzed.[701] Additional degree of freedom coming from angular momentum of atomic orbitals[706] in valence band has also been proposed for spin-valley-orbital qubit.[703] Recent advances in the field of spin-valley qubits has been summarized in Ref. 707.

Defect-induced quantum dots in TMD's

As mentioned previously, spatially localized emitters[428–433] in TMD's can be formed due to strain. These emitters behave like quantum dots, efficiently confining photo-carriers in small regions. Spectrum of those dots resemble Fock-Darwin spectrum due to specific form of strain inside "bubbles".[708] Single photon emission from those sources has been achieved[709,710] and deterministic creation of such quantum emitters via strain engineering has been demonstrated.[292,433,711–714] Integration of such single-photon emitters with silicon photonic chip is possible,[715] along with coupling to plasmonic waveguides.[716,717] Recently, interactions between excitons trapped inside quantum dot emitters has been demonstrated.[718] Recent advances in this subject has been summarized in Ref. 719. Optical initialization of spin-valley hole state in WSe_2 in such quantum dots has been shown in Ref. 720, along with selective loading of such localized emitters in Coulomb blockage regime.[721] We note that exciton confinement can also be obtained by creation of moiré pattern,[324,722–724] allowing e.g. to engineer topologically non-trivial exciton bands.[725]

Experiments on TMD gate-defined quantum dots

Alternatively to finite clusters and strain-induced confinement, matured technology of gate-defined quantum dots exists.[14] By creating lateral confinement using metallic gates, trapping of electrons or holes can be achieved. This route to carrier confinement avoids necessary control of complicated edge physics and allows for electrical only fast qubit operations. Some demonstrations in bilayer graphene[726–730] and monolayer InSb exists[731,732] In TMD's, experimental demonstrations are scarce and this field is only at it's infancy. Up to now, relatively large, gate defined quantum dots have been reported.[733–738] Tunable size, single electron transport and tunable coupling have been achieved.[733,734] Further advances in fabrication methods increased mobility of electrons.[735] Zero-dimensional confinement of charged exciton has also been demonstrated in trilayer MoS_2.[736] Coulomb blockage and signatures of single-electron transport have also recently been reported.[738] One of the goals of the following work is to understand nature of confined states is such gate defined quantum dots.

Role of strong interactions

In addition to single particle aspects of tunability of gate-defined quantum dots (e.g. by shape, depth of confining potential, size), electronic states can be also greatly influenced by tunable interactions,[567,739,740] resulting in e.g. magnetic order,[573,741] entanglement[742] or electron - hole condensation[576] in quantum dots. In terms of ground state of electronic system, in TMD's situation is

even more complicated[743] due to possible symmetry breaking associated with spin[169,170] and valley polarized[167,168] ground states. Systematic study of effect of confinement and tunable interactions on spin-valley configurations of ground and excited states in TMD's quantum dots is, however, still largely unexplored and some results in this matter will be discussed in this thesis.

Chapter 2

Electronic properties of single layer MX_2 crystals

We begin this Chapter with presentation of *ab initio* calculations for monolayers of MX_2 semiconductors, focusing on orbital symmetry identification and role of spin-orbit coupling. Next, tight-binding model is constructed and parametrized, along with massive Dirac fermion and effective mass approximations. Then, mechanism of band gap opening and emergence of secondary minima in conduction band are studied. Chapter is concluded with discussion of Landé and valley Zeeman effects.

2.1 *Ab initio* band structure calculations

2.1.1 Structural properties of MX_2 single layer

We begin with general description of MX_2 single layer crystals in 2H phase. In those compounds atoms are arranged in trigonal prismatic structure (P-6m2 space group). Unit cell consists of three atoms, one metal (blue dots) and two chalcogens (red dots), as shown in Fig. 2.1. Looking from the top, arrangement of atoms reminds that of graphene (Fig. 2.1 (a)). Looking from the side, one can notice that atoms are actually organized in 3 planes, one (central) metal plane and two chalcogen planes shifted by $\pm d_\perp$. Distance between metal atom and central position between two chalcogens is denoted by $d_\parallel$. We define primitive vectors of real space lattice as $\vec{a}_1 = d_\parallel(0, \sqrt{3})$ and $\vec{a}_2 = d_\parallel(3/2, -\sqrt{3}/2)$. Lattice constant $a_0 = d_{M-M}$ can be written as $a_0 = d_\parallel\sqrt{3}$ and $d_\perp = d_{X-X}/2$, as shown in Fig. 2.1. Following commonly practiced *ab initio* procedure, we take lattice constants a_0 from experimentally known bulk structures[421] and relax geometry. All details of DFT calculations are summarized in Appendix 6.1. Lattice constants calculated using PBE exchange-correlation functional are collected in Table 2.1. They show noticeable increasing trend when changing from sulfur to selenium to tellurium. Much smaller change is observed when going from

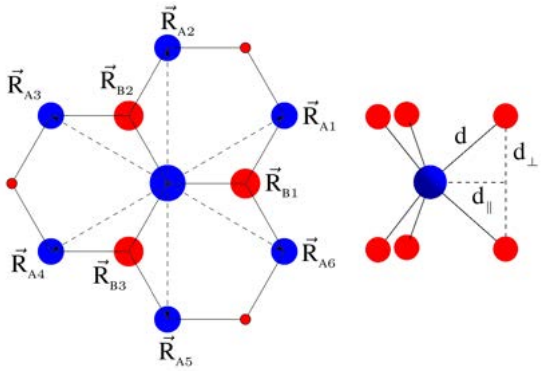

Figure 2.1: (a) Top view of the structure of MX_2 in 2H phase: metal atoms are denoted by blue dots, and chalcogen by red ones. (b) Side view of MX_2, showing that atoms are organized in 3 layers, central metal and two chalcogen, with structural constants parametrized by $d_\parallel$ and $d_\perp$.

	$d_\parallel$ in [Å]	$d_\perp$ in [Å]
MoS_2	1.8393 (1.8391 (PBE), 1.8247 (exp.))	1.5622 (1.5623,1.5850)
$MoSe_2$	1.9184 (1.9162, 1.8983)	1.6694 (1.7186, 1.6675)
$MoTe_2$	2.0605 (2.0536, 2.0317)	1.8112 (1.8098, 1.8020)
WS_2	1.8414 (1.8360, 1.8210)	1.5714 (1.5764, 1.5700)
WSe_2	1.9188 (1.9145, 1.8972)	1.6792 (1.7355, 1.6700)
WTe_2	2.0625 (2.0513, -)	1.8170 (1.8197, -)

Table 2.1: Structural constants obtained from our DFT (PBE) calculations for MX_2 materials. In brackets first PBE and then experimental values from literature[421] are given.

molybdenum to tungsten.

Having defined real space unit cell and primitive vectors, in next step we calculate reciprocal lattice vectors $\vec{b}$, which should satisfy relation $e^{i\vec{b}\cdot\vec{a}} = 1$. This gives in 2D set of four equations $\vec{b}_i \cdot \vec{a}_j = 2\pi\delta_{i,j}$ for $i, j \in 1, 2$ that has to be solved for $\vec{b}_{1,2}$. The solution yields $\vec{b}_1 = 2\pi/d_\parallel(1/3, 1/\sqrt{3})$ and $\vec{b}_2 = 2\pi/d_\parallel(2/3, 0)$. Those vectors define Brillouin zone, shown in Fig. 2.2. We note that such choice of real and reciprocal space primitive vectors gives the following position of hexagonal Brillouin zone corner at $K_1 = (0, 4\pi/(3\sqrt{3}d_\parallel))$ which is called K-point, just as in graphene. All other K points are obtained by successive application of C_6 rotation. We note, that in half of the distance between K - points and Γ point there are so called Q-points (alternatively Σ[439] or Λ[560] points). Halfway between two nearest K points lie so-called M points.

2.1.2 DFT band structures at GGA level

Now we describe general features of DFT bandstructure, choosing as an representative example MoS_2. In Fig. 2.3 (a) one can observe 11 bands around Fermi

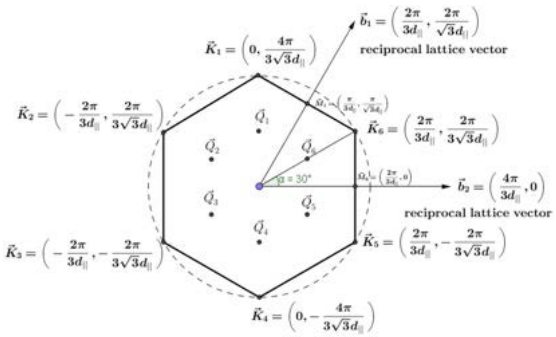

Figure 2.2: Brillouin zone defined by vectors $\vec{b}_1$ and $\vec{b}_2$. Positions of 6 K-points and corresponding 6 Q - points are also shown.

level (set to 0), with large gap to bands below them (7, 30 and 55 eV separation, those deep bands being almost non-dispersive) and significantly smaller, but still well resolved gap to bands above (2 eV at Γ point). Direct bandgap at

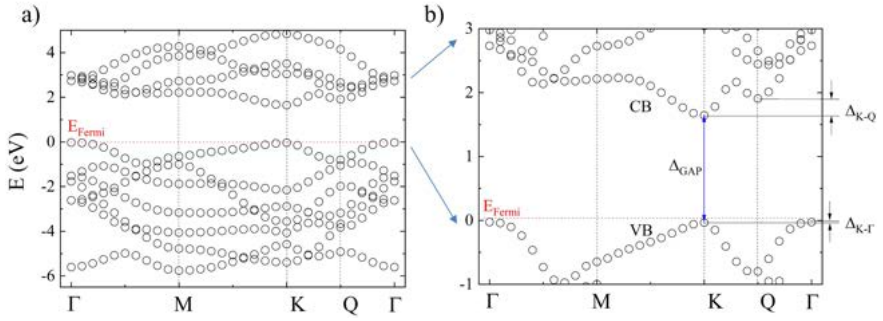

Figure 2.3: (a) Band structure of MoS_2 on Γ-M-K-Γ line, calculated using DFT (PBE) without spin-orbit coupling. Fermi level is shown as horizontal red line. (b) Zoom to valence and conduction bands with fundamental band gap at K point shown as Δ_{GAP}. Gaps to secondary maxima (minima) at Γ- (Q-) points in valence and conduction bands are denoted by $\Delta_{K-\Gamma}$ and Δ_{K-Q} , respectively.

K point without SOC is equal to $\Delta_{\mathrm{GAP}} = 1.67$ eV. We note that both valence band (VB) and conduction band (CB) have secondary extrema, at Γ point in VB and at Q - points in CB. In Fig. 2.3 (b) we denote energetic difference between primary and secondary minima as $\Delta_{K-\Gamma} = E(K) - E(\Gamma)$ in VB and Δ_{K-Q} in CB, which in MoS_2 have values -8.6 meV and -263.4 meV, respectively. It should be stressed that for calculation without spin - orbit interaction the smallest gap between VB and CB is actually located between Γ in VB and K point in CB. This is due to, general in MX_2 family, small negative splitting between energies in top of the valence band at K and Γ points ($\Delta_{K-\Gamma} \approx 10$ meV), which changes sign when spin - orbit interaction is included.

In next step we study general properties of DFT Kohn-Sham wavefunctions. First, we choose 3 spheres around one Mo and two S_2 atoms, as shown in Fig. 2.4 (a) and calculate how much of the wavefunction is localized inside

each sphere. We note that 11 bands around Fermi level have wavefunctions that are in general localized on both Mo and S_2 atoms, however there is clear trend that VB and bands above are mainly localized on Mo atoms, and VB-1 and lower bands on S_2 atoms. DFT wavefunctions inside spheres can be next projected onto Slater orbitals, as described in Appendix 6.2. We first confirm that largest overlap is achieved, in case of MoS_2, with localized Slater, single-zeta basis[744,745] consistent with orbitals with principal quantum number n = 4 on Mo and n=3 on S. For other compounds, eg. WSe_2, there is clear better numerical overlap with orbitals with quantum numbers n=5 for W and n=4 for Se, confirming that such projection is a reliable tool in studying symmetry and orbital composition properties of DFT wavefunctions. In next step, summarized in Fig. 2.4 (b) for each wavevector k and energy E DFT wavefunctions are projected onto symmetric and anti-symmetric orbitals with respect to the metal plane. One can observe, that VB and CB are symmetric across majority of the Brillouin zone, with exception of parts close to Γ point in CB, at which anti-symmetric states are lower than symmetric ones. This ordering of bands and their symmetry is general to all MX_2 family and is presented for another example of WSe_2 in Appendix 6.3.

2.1.3 Analysis of orbital composition

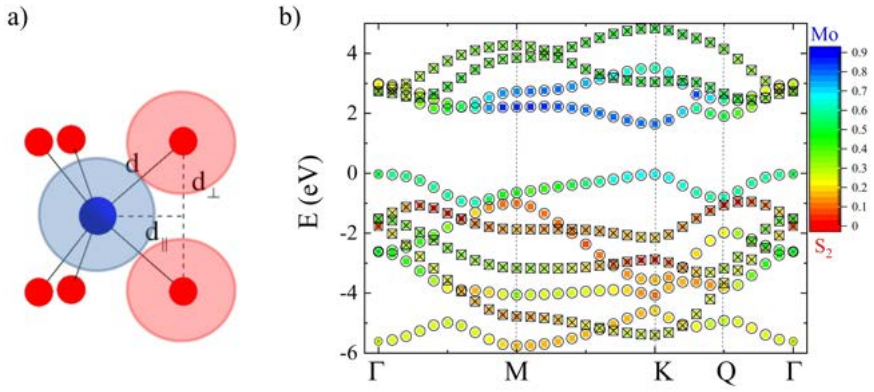

Figure 2.4: (a) Schematic representation of spheres around Mo atom and S_2 dimer which are used for DFT wavefunction analysis and orbital symmetry identification. (b) Color-mapped localization of a given k-resolved eigenenergy on Mo and S_2 spheres and symmetry of eigenvalues across Brillouin zone. Circles (crossed rectangles) denote symmetric (anti-symmetric) orbitals with respect to metal plane.

In next step orbital - resolved decomposition of wavefunctions is performed. As mentioned previously DFT wavefunctions are projected onto Slater orbitals with parameters describing isolated atoms,[744,745] see 6.2. In Fig. 2.5 each eigenvalue for each vector k is projected onto symmetric metal (4d $m = -2, 0, 2$) and sulfur dimer orbitals (proper combinations of upper and lower sulfurs, e.g. "$3p_0$" meaning $1/\sqrt{2}(|3p_0^{S-up}\rangle - |3p_0^{S-down}\rangle)$ and anti-symmetric ones. Both symmetric and anti-symmetric projections are normalized independently inside Mo and S spheres, therefore they show only information which quantum number con-

tributes to a given state and do not distinguish that e.g. $4d_{+2}$ orbitals on metal contribute to bottom of valence band at K point 2 orders of magnitude more than "$3p_{+1}$" sulfur states. In Fig. 2.5 one can immediately notice, that close to the K point in VB bands are combination of $4d_{+2}$ and $3p_{+1}$ orbitals. Contrary to VB, in CB $4d_0$ state coupled to $3p_{-1}$ state dominates. Higher symmetric conduction band (CB+1) ($4d_{-2}$) is coupled to $3p_0$ state. Coupling between anti-symmetric d and p states is also clear from right panel of Fig. 2.5, in which $4d_{-1}$ state is coupled to anti-symmetric $3p_{+1}$ and $4d_{+1}$ to both anti-symmetric $3p_{-1}$ and $3p_0$ states.

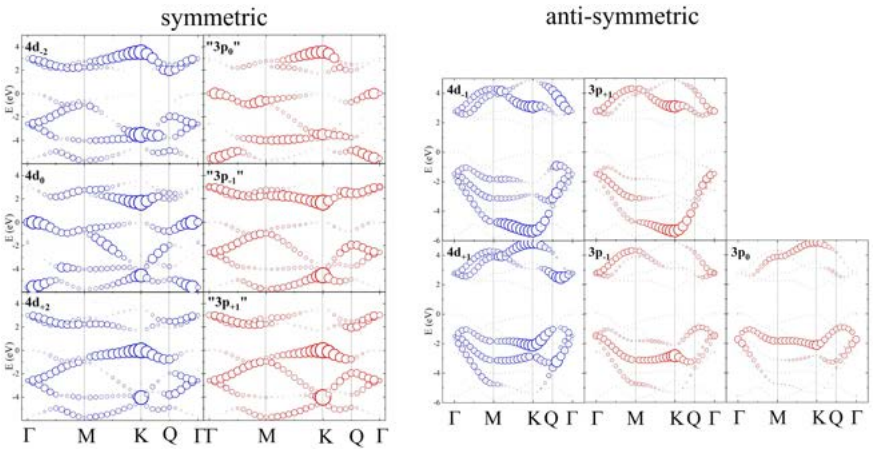

Figure 2.5: Collected symmetric and anti-symmetric orbital contributions to bands in MoS_2.

2.1.4 Spin-orbit splitting of bands

Due to heavy nature of atoms in MX_2 family (e.g. atomic number of Mo = 42, W = 74, Te = 52), one can expect that relativistic spin - orbit interaction may influence band structure heavily. Results of PBE + SOC calculation for MoS_2 are presented in Fig. 2.6. Major effect of SOC is visible in VB at K point, where bands are spin-split by $\Delta_{VB}^{SOC} = 148$ meV. It is worth mentioning that this is the smallest splitting in VB at K point in MX_2, which in WTe_2 reaches almost 500 meV. All values of gaps for different MX_2 combinations are summarized in Appendix 6.3. Significantly smaller splitting is observed in CB at K point in MoS2 ($\Delta_{CB}^{SOC} = 3$ meV), reaching up to 50 meV in WTe_2. This order of magnitude less pronounced effect comes from the fact that majority (80%) d-like orbital in CB has quantum number $m_d = 0$, therefore splitting must comes from admixture of p-orbitals (10%) from chalcogen atoms. What is also important, there is a significant spin splitting in second minimum of CB at Q point, which is larger than at K point, pushing the relative distance between CB minimum at K at Q point (Δ_{K-Q}^{SOC}) close to small values, making CB almost degenerate, e.g. in WSe_2. Let us note also that by symmetry there is no spin splitting along Γ-M line on BZ.

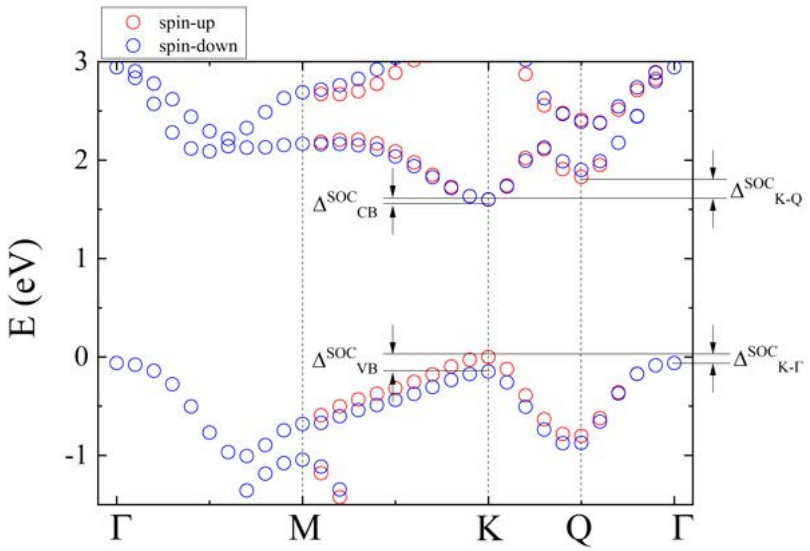

Figure 2.6: Spin splitting of even bands in MoS_2.

Let's now discuss spin arrangement of bands in VB and CB extrema. Fig. 2.7 summarizes spin orientation ($\hat{S}_z$ operator eigenvalues) in so-called "bright" (left panel, e.g. MoS_2) and "dark" (right panel, e.g. WSe_2) materials. In bright MX_2 (M=Mo) highest VB state at K point has the same spin arrangement as lowest CB at K- and Q-points. When analyzing states in opposite valley (-K, -Q), all spins are flipped, constituting spin-valley locked system. Interestingly, in dark materials the situation is different, where top of VB has opposite spin than bottom of CB at K point, but the same as bottom of CB at Q point. Let us note that spin splitting at Q - point is similar in VB and CB, because they are composed from $m_d = \pm 2$ orbitals.

2.2 Construction of low-energy effective theory

2.2.1 NN tunneling matrix element and orbital couplings

Building upon our analysis of DFT results (both presented in previous subsection and those done in collaboration with other co-authors of Ref. 1), we conclude that there are several common features in band structures of all MX_2 materials. Most notably, all show existence of direct band-gap at K-points, in opposite to their $N \geq 2$ layer form, which are indirect-gap semiconductors.[152] All materials exhibit also second minimum in conduction band, localized close to Q-points. Analyzing orbital compositions of the valence and conduction bands we conclude, that they are described by orbitals even with respect to metal plane. This result is consistent with several other works, therefore we can start

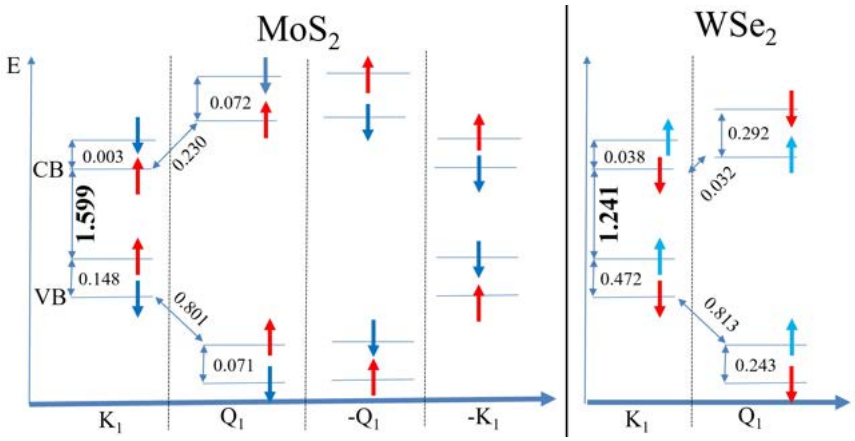

Figure 2.7: (Left) Comparison between spin splitting in bright material (here MoS_2) at K and Q points in both +K and -K valleys. (right) Spin arrangement in dark materials (here WSe_2), showing reversed order of states in CB at K point, but not at Q point. All states in the -K valley are opposite are not shown. All values are given in eV.

building tight-binding model of those materials from orbitals contributing most to the band structure around Fermi level.

Our conclusion is that minimal tight-binding model has to include orbitals that are even with respect to inversion symmetry about z plane of metal atoms ($z \to -z$). Motivated by *ab initio* results, at least $L = 0, \pm 2$ d - orbitals from metals and $L = 0, \pm 1$ symmetric symmetric p - orbital compositions from top and bottom sulfur atoms has to be taken into account. Those orbitals are discussed further in Appendix 6.2. We note only that for d orbitals of metals situation is clear, namely orbitals with given $L = 2$ and $m = -2, 0, +2$ are centered around M atoms. However, orbital construction for two chalcogens must be done with care. Because we define so-called dimer orbitals, that are centered around the same plane as metal atoms, we begin with upper (U, $\vec{R}^U = (0, 0, +d_\perp)$ with respect to dimer center) and lower (L, $\vec{R}^L = (0, 0, -d_\perp)$ p-orbitals with quantum numbers $L = 1$, $m = \pm 1$ ϕ and define dimer orbitals φ as proper combination of those two:

$$\varphi_{L=1,m_p=\pm 1}(\vec{r}) = \frac{1}{\sqrt{2}} \left[\varphi^U_{L=1,m_p=\pm 1}(\vec{r} - \vec{R}^U) + \varphi^L_{L=1,m_p=\pm 1}(\vec{r} - \vec{R}^L) \right] \quad (2.1)$$

For $L = 1$, $m = 0$, due to the nodal structure of p_z orbitals, dimer has to be constructed in such a way, that it needs to still to be symmetric with respect to z inversion. This can be achieved by changing sign of one of the orbitals (we choose to change sign of the bottom one):

$$\varphi_{L=1,m_p=\pm 0}(\vec{r}) = \frac{1}{\sqrt{2}} \left[\varphi^U_{L=1,m_p=0}(\vec{r} - \vec{R}^U) \underbrace{-}_{!} \varphi^L_{L=1,m_p=0}(\vec{r} - \vec{R}^L) \right]. \quad (2.2)$$

To conclude, our Hamiltonian in which tight-binding model will be constructed will be acting on spinor composed of metal orbitals $\varphi_{L=2,m_d}$ and dimer orbitals

$\varphi_{L=1,m_p}$ arranged in the following order:

$$\Psi = \left[\varphi_{2,-2}, \varphi_{2,0}, \varphi_{2,+2}, \varphi_{1,-1}, \varphi_{1,0}, \varphi_{1,-1}\right]^T. \tag{2.3}$$

In the next step, we construct linear combination of atomic orbitals for all orbitals discussed above. First, we note that thanks to our dimer orbital construction, it makes sense now to talk about A (metal positions, $\tau_1 = (0,0,0)$ inside unit cell) and B (chalcogen dimer centers, $\tau_2 = (d_\parallel, 0, 0)$) sublattices on real-space hexagonal lattice. Because we aim to understand fundamental properties of those materials in terms of graphene physics, we focus on sublattice A - sublattice B interaction. We write LCAO wavefunction for A and B sublattices separately:

$$\Psi^{\vec{k}}_{A,m_d}(\vec{r}) = \frac{1}{\sqrt{N_{UC}}} \sum_{i=1}^{N_{UC}} e^{i\vec{k}\cdot\vec{R}_{A,i}} \varphi_{L=2,m_d}\left(\vec{r} - \vec{R}_{A,i}\right) \tag{2.4}$$

$$\Psi^{\vec{k}}_{B,m_p}(\vec{r}) = \frac{1}{\sqrt{N_{UC}}} \sum_{i=1}^{N_{UC}} e^{i\vec{k}\cdot\vec{R}_{B,i}} \varphi_{L=1,m_p}\left(\vec{r} - \vec{R}_{B,i}\right) \tag{2.5}$$

and then the total electron wavefunction is given by

$$\Psi^{n,\vec{k}}(\vec{r}) = \sum_{m_d\in\{-2,0,+2\}} A^{n,\vec{k}}_{m_d} \Psi^{\vec{k}}_{A,m_d}(\vec{r}) + \sum_{m_p\in\{-1,0,+1\}} B^{n,\vec{k}}_{m_p} \Psi^{\vec{k}}_{B,m_p}(\vec{r}) \tag{2.6}$$

First, let us try to understand the physics of why considered MX_2 materials are semiconductors instead of semimetals such as graphene. To do that, let us analyze tunneling matrix element between central A atom from Fig. 2.8 with potential $V_A(\vec{r})$ and three nearest neighbor B atoms in positions $\vec{R}_{B_1}, \vec{R}_{B_2}, \vec{R}_{B_3}$:

$$\begin{aligned}\langle \Psi^{\vec{k}}_{A,m_d} | \hat{H} | \Psi^{\vec{k}}_{B,m_p} \rangle = \int d\vec{r} \varphi^*_{l=2,m_d}(\vec{r}) V_A(\vec{r}) \cdot \Big[& e^{i\vec{k}\cdot\vec{R}_{B1}} \varphi_{l=1,m_p}\left(\vec{r} - \vec{R}_{B1}\right) + \\ & e^{i\vec{k}\cdot\vec{R}_{B2}} \varphi_{l=1,m_p}\left(\vec{r} - \vec{R}_{B2}\right) + e^{i\vec{k}\cdot\vec{R}_{B3}} \varphi_{l=1,m_p}\left(\vec{r} - \vec{R}_{B3}\right) \Big].\end{aligned} \tag{2.7}$$

One can notice, that exactly at K point, this formula gives

$$\langle \Psi^{\vec{k}=K}_{A,m_d} | \hat{H} | \Psi^{\vec{k}=K}_{B,m_p} \rangle = \left(1 + e^{i(1-m_d+m_p)2\pi/3} + e^{i(1-m_d+m_p)4\pi/3}\right) V_{pd}, \tag{2.8}$$

where V_{pd} are standard Slater - Koster integrals. For such combinations of m_d and m_p quantum numbers, that $1 + m_p - m_d = 0, \pm 3$ tunneling matrix element is non-zero $\langle \Psi^{\vec{k}=K}_{A,m_d} | \hat{H} | \Psi^{\vec{k}=K}_{B,m_p} \rangle \neq 0$. This is different than same tunneling matrix element in graphene, in which only $L = 1$, $m_p = 0$ p_z orbitals play role and give $\langle \Psi^{\vec{k}=K}_{A,m_p} | \hat{H} | \Psi^{\vec{k}=K}_{B,m_p} \rangle = 0$. Non-vanishing tunneling will, therefore, open gap at K point, resulting in gapped, massive Dirac fermion dispersion instead of Dirac point at K, see Fig. 2.8. Non- zero interaction between different m_d and m_p orbitals at K point leads to the following pairs of orbitals that are coupled:

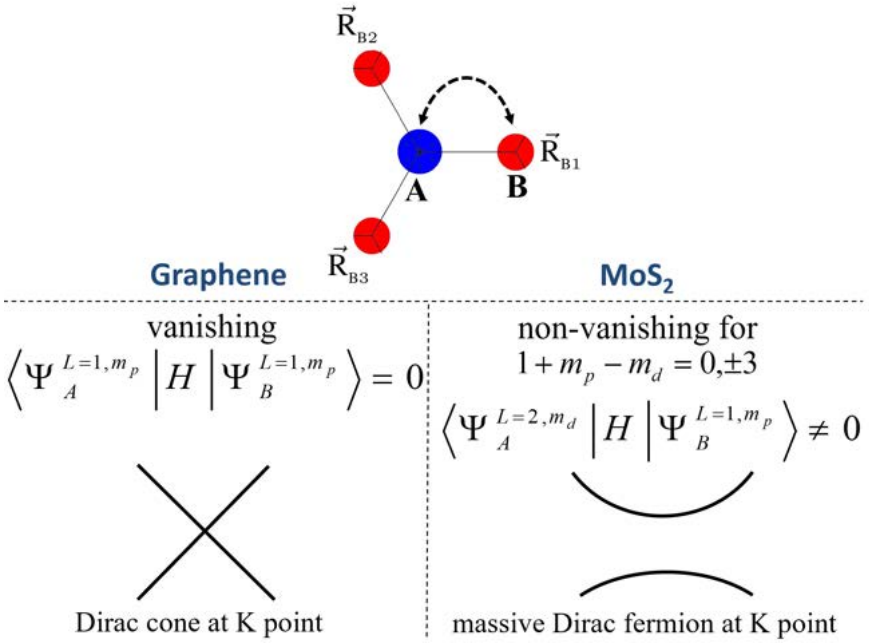

Figure 2.8: Comparison between A-B sublattice tunneling in graphene and MoS_2.

$[m_d = -2, m_p = 0]$, $[m_d = 0, m_p = -1]$, $[m_d = 2, m_p = 1]$. Similar analysis at -K point leads to selection rule

$$-1 + m_p - m_d = 0, \pm 3. \tag{2.9}$$

Resulting couplings are then $[m_d = -2, m_p = -1]$, $[m_d = 0, m_p = 1]$, $[m_d = 2, m_p = 0]$. Finally, at Γ point we obtain different scheme of couplings: $[m_d = 0, m_p = 0]$, $[m_d = 2, m_p = -1]$, $[m_d = -2, m_p = 1]$. We note that all those couplings explain couplings detected by analyzing even DFT wavefunction symmetries, as summarized in Fig. 2.5.

2.2.2 Nearest- and next-nearest TB Hamiltonian

In next step we move to discussion of nearest neighbor (NN) and next- nearest neighbor (NNN) tight-binding Hamiltonian. Standard procedure outlined by Slater and Koster (SK)[18] is used. All details of this straightforward but cumbersome calculation are moved to Appendix 6.4. We note only that because in our basis we are using complex orbitals, SK formulas cannot be used directly and we had to implement them into more complicated fashion, which is hidden in our notation behind functions V, depending on SK parameters. Full NN Hamiltonian can be written in block form as:

$$H\left(\vec{k}\right) = \begin{bmatrix} & H_{M-X_2} \\ H^{\dagger}_{M-X_2} & \end{bmatrix} \tag{2.10}$$

where NN tunneling between 3 metal and 3 dimer orbitals is given by a 3 by 3 matrix

$$H_{Mo-S_2} = \begin{bmatrix} V_1 f_{-1}(\vec{k}) & -V_2 f_0(\vec{k}) & V_3 f_1(\vec{k}) \\ -V_4 f_0(\vec{k}) & -V_5 f_1(\vec{k}) & V_4 f_{-1}(\vec{k}) \\ -V_3 f_1(\vec{k}) & -V_2 f_{-1}(\vec{k}) & -V_1 f_0(\vec{k}) \end{bmatrix} \tag{2.11}$$

inside which functions V depend on structural properties and SK parameters. For example, V_1 is given by

$$V_1 = \frac{1}{\sqrt{2}} \frac{d_\parallel}{d} \left[\frac{\sqrt{3}}{2} \left(\frac{d_\perp^2}{d^2} - 1 \right) V_{dp\sigma} - \left(\frac{d_\perp^2}{d^2} + 1 \right) V_{dp\pi} \right], \tag{2.12}$$

where $d_\parallel, d_\perp$ are given in Table 2.1 and $d = \sqrt{d_\parallel^2 + d_\perp^2}$. Functions f are proper combinations of exponents and depend on wave vectors $\vec{k} = (k_x, k_y)$, e.g.

$$f_{-1}\left(\vec{k}\right) = \left[e^{ik_x d_\parallel} + e^{-ik_x d_\parallel/2} e^{i\sqrt{3}k_y d_\parallel/2} e^{i2\pi/3} + e^{-ik_x d_\parallel/2} e^{i\sqrt{3}k_y d_\parallel/2} e^{i4\pi/3} \right]. \tag{2.13}$$

This Hamiltonian is a generalization of a Hamiltonian describing graphene, in which there are also two triangular sublattices of atoms, however in MX_2 we have to take into account three d-orbitals on one sublattice, and three dimer orbitals constructed out of three p-orbitals. Later we will discuss that due to specific symmetry of the lattice and orbital compositions in high symmetry points in BZ, in NN model it is not possible to open gap within group of d-orbitals across whole BZ, therefore NN model is not sufficient to describe MX_2 materials properly and hopping to NNN has to be included.

Details of the NNN model presented below are also discussed in Appendix 6.4. We note that each metal atom has 6 NNN and all possible hoppings between $m_d = \pm 2, 0$ orbitals are taken into account, adding 3 new SK parameters $V_{dd\sigma}, V_{dd\pi}, V_{dd\delta}$. For sulfur dimers, we neglect "crossed" interactions between upper and lower chalcogenides, e.g. top p_{-1} sulfur orbital is not interacting with NNN dimer lower sulfur orbital, consistent with idea it is not it's NNN. Taking into account NNN p-orbital interactions two new SK parameters have to be included, namely $V_{pp\sigma}$ and $V_{pp\pi}$. Full NNN Hamiltonian written again in block form is given by

$$H\left(\vec{k}\right) = \begin{bmatrix} H_{M-M} & H_{M-X_2} \\ H_{M-X_2}^\dagger & H_{X_2-X_2} \end{bmatrix} \tag{2.14}$$

where matrix describing metal-metal NNN interactions is given by

$$H_{M-M} = \begin{bmatrix} E_{m_d=-2} + W_1 g_0(\vec{k}) & W_3 g_2(\vec{k}) & W_4 g_4(\vec{k}) \\ & E_{m_d=0} + W_2 g_0(\vec{k}) & W_3 g_2(\vec{k}) \\ & & E_{m_d=2} + W_1 g_0(\vec{k}) \end{bmatrix} \tag{2.15}$$

and corresponding matrix describing $X_2 - X_2$ dimer interactions is given by

$$H_{X_2-X_2} = \begin{bmatrix} E_{m_p=-1} + W_5 g_0(\vec{k}) & 0 & -W_7 g_2(\vec{k}) \\ & E_{m_p=0} + W_6 g_0(\vec{k}) & 0 \\ & & E_{m_p=1} + W_5 g_0(\vec{k}) \end{bmatrix}. \tag{2.16}$$

As previously, complicated structure of SK parameters is hidden behind functions W, e.g. for W_1 we have

$$W_1 = \frac{1}{8}\left(3V_{dd\sigma} + 4V_{dd\pi} + V_{dd\delta}\right). \tag{2.17}$$

Functions g, depending on wave vector $\vec{k}$ combining proper summation of plane wave functions to six NNN are, for example for g_0, given by

$$g_0\left(\vec{k}\right) = 4\cos\left(\frac{3}{2}k_x d_{\parallel}\right)\cos\left(\frac{\sqrt{3}}{2}k_y d_{\parallel}\right) + 2\cos\left(\sqrt{3}k_y d_{\parallel}\right). \tag{2.18}$$

As discussed later, we find that Hamiltonian 2.14 presents a minimal model that describes correctly band gap across whole BZ and is able to quantitatively reproduce orbital compositions of VB and CB. We note that last column (except diagonal element) in full NNN Hamiltonian has sign opposite to the one used in Ref. 1 due to different convention of complex spherical harmonics (with Condon-Shortley phase) used in this Thesis. Here, complex and real orbitals are related by $\varphi_{m_{p=\pm1}} = \mp 1/\sqrt{2}(\varphi_{p_x} \pm i\varphi_{p_x})$, differently to Ref. 1 in which $\varphi_{m_{p=\pm1}} = 1/\sqrt{2}(\varphi_{p_x} \pm i\varphi_{p_x})$.

2.2.3 Slater-Koster parameters fitting procedure

After derivation of our tight-biding Hamiltonian, we turn to the problem of fitting SK parameters. Our goal is to obtain dispersion for even bands from TB as close as possible to even bands obtained and detected using *ab initio* method, as described above. We note that in principle it is possible to calculate SK parameters directly from first - principles calculation,[25] however resulting electronic dispersions are not satisfactory neither for graphene,[746] nor for MoS_2,[466] especially for unoccupied electronic states (CB and higher bands). Those parameters can be treated as a starting point for our analysis, however we do not reproduce those calculations and focus on available data to make our simplest TB model usable for excitonic and quantum dot properties simulations.

General problem with SK parameters is that even if we fix structural parameters $d_\perp$ and $d_\parallel$, we still end up with 10-dimensional, highly non-linear optimization problem, depending on energies $E_{m_d=0} = E_{m_d=\pm2}$, $E_{m_p=0}$, $E_{m_p=\pm1}$, $V_{dp\sigma}$, $V_{dp\pi}$, $V_{dd\sigma}$, $V_{dd\pi}$, $V_{dd\delta}$, $V_{pp\sigma}$, $V_{pp\pi}$. We have tested various schemes for choosing those parameters to fit dispersion of such model to DFT. One of the possible procedures that gives reasonable results is performed in the following way:

1. We choose some initial values for all parameters. This choice has to at least open gap in the whole BZ between CB and VB and should not give wrong (in sense of majority contribution) orbital compositions to bands. Our first choice, done by trial and error, was loosely based on parameters given in literature.[464,465] After finding good overall fit for one material (MoS_2) we choose this parametrization as a starting point for next materials (e.g. WSe_2).

2. Then, we choose direction in the Brillouin zone along which we will fit our model. We have chosen $\Gamma - M - K - \Gamma$ line in our procedure. Alternatively, it is possible to perform this procedure for all points in BZ at higher computational cost.

3. Then, we assign different weight to different bands and parts of directions in BZ (e.g. we want better fit in K point than in Γ, better representation of CB for quantum dot calculation, better VB-CB transition energy for excitonic calculations etc.).

4. Next we choose some range of values for which we will try to find better parametrization, e.g. we allow for E_d energy to change between $E_d \pm \Delta E_d/2$, where initial $\Delta E_d = 2$ eV.

5. We choose randomly for every SK parameter (e.g. ΔE_d) new update from given interval and calculate band structure.

6. In next step, we calculate energetic distance between bands obtained by TB and DFT as $\Delta E^{VB(CB)}_{TB-DFT}(\vec{k}) = |E^{VB(CB)}_{TB}(\vec{k}) - E^{VB(CB)}_{DFT}(\vec{k})|$, scaled by weighting factor w_{fit} depending on target bandstructure and sum over all $w_{fit} \cdot \Delta E$ to obtaining single parameter, showing overall quality of the fit.

7. We sample over large space of such random SK parameters (like in Monte Carlo integrals evaluation techniques) and choose the best fit respecting majority orbital contributions at Γ, K and Q point in VB, CB and CB+1 bands.

8. We repeat steps (4-7), choosing smaller (usually by 20% of the initial value) interval for extremal values, starting from best fit from previous iteration.

Usually in our procedure we first find model that best describes all bands, then we optimize for best VB, CB and CB+1 bands and then we perform further optimization focusing on purpose for which TB model will be used, e.g. for excitonic calculation we optimize model to reproduce at best possible way transition energies between VB and CB. All procedures are repeated 10 times, with usual space of 10^9 independent parameter choices and parameters spread starting from 2 eV and lowered by 0.4 eV after each 10^9 subspace search. We note that we tested simple linear sweep of 10 dimensional parameter space and results were significantly worse. It is also possible to code and test genetic algorithm or deep neural network to perform this optimization, however we leave performance analysis of such different methods for future work. We note also that such "Monte Carlo fitting" procedure is extremely easily parallelizable over different cores and nodes on high performance computing (HPC) clusters, which was one of the rationale for using this method. Parameters for this fit presented in Fig. 2.9 are shown in Table 2.2. We note that fit presented in the left of Fig. 2.9 was found by assuming equal weights for all k points and all even bands, therefore it is called "best all bands". Additionally to reproducing well overall energies of even bands, this parametrization reproduces very well VB. To obtain best transition energy (right panel of Fig. 2.9), much more complicated procedure was

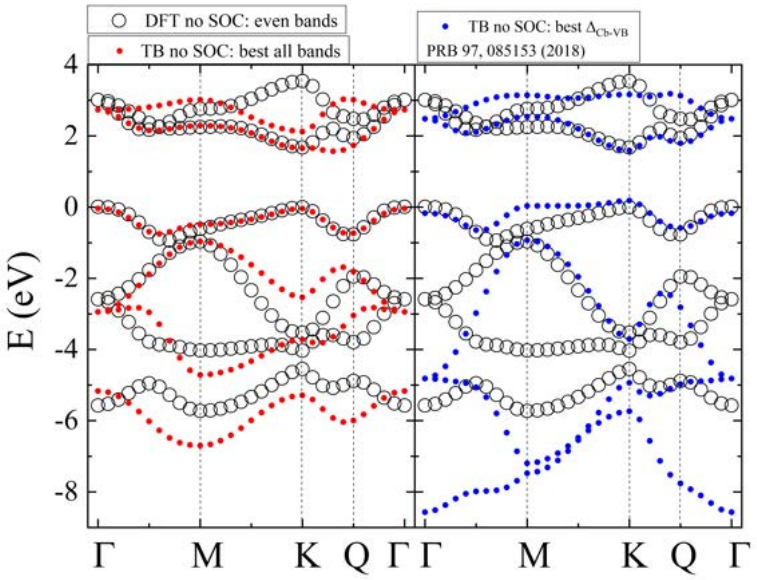

Figure 2.9: Left: TB dispersion obtained after optimizing SK parameters to reproduce all even DFT bands as well as possible. Right: TB dispersion optimized to reproduce transition energy between VB and CB. We note that the former reproduces very well VB, while the latter one - CB, especially on K-Γ line.

used, first increasing weights for VB and CB (by 20 times) on whole Γ-M-K-Γ line and then in subsequent sweeps weights around K point in VB and CB and Q point in CB were further increased (100 times with respect to their initial values). Due to those weighting procedure, it is not surprising that both VB and CB along K-Γ line are reproduced very well, while e.g. on Γ-M-K line TB energies deviate from target DFT values. We note that in general choices of SK parameters are not unique, which is main defect of the tight-binding method. Those parametrization are also not constructed and tested to tackle substitution effects, e.g. simulating alloys like $M_{1-x}W_xS_{1-y}Se_y$. On the other hand, when SK parameters are found, they allow for realistic simulations of many physical phenomena, otherwise impossible to tackle using DFT based methods, e.g study of multi-million nanostructure systems or converged simulations of excitonic spectrum.

2.2.4 Spin-orbit coupling

As discussed previously, an important aspect of MX_2 TMD's materials is relativistic spin-orbit interaction. DFT calculations suggest, that spin-orbit splitting in conduction band is always smaller than in valence band in all MX_2 family. Exact values of this splitting are, however, highly sensitive to material choice, ranging from 3 to 52 meV at minimum of conduction bands and between 148 and 484 meV in valence bands. Specifically, for MoS_2 we obtained 3 meV in CB

parameter	best all bands	best Δ_{CB-VB}
$E_{m_d=0,\pm2}$	0.07	-0.03
$E_{m_p=\pm1}$	-1.85	-3.36
$E_{m_p=0}$	-3.58	-4.78
$V_{dp\sigma}$	2.38	-3.39
$V_{dp\pi}$	-0.93	1.10
$V_{dd\sigma}$	-0.95	-1.10
$V_{dd\pi}$	0.75	0.76
$V_{dd\delta}$	0.14	0.27
$V_{pp\sigma}$	0.60	1.19
$V_{pp\pi}$	-0.15	-0.83

Table 2.2: Slater-Koster parameters fitted to DFT MoS_2 bandstructure tailored for various problems. Structural parameters are taken as $d_{\parallel} = 1.8393$ Å and $d_{\perp} = 1.5622$ Å. All values in table are given in eV.

and 148 meV in VB splitting, as shown in Fig. 2.6 and Fig. 2.7.

To include spin - orbit coupling in our tight-binding model, we analyze matrix elements of the following operator

$$\vec{L} \cdot \vec{S} = \frac{1}{2}\left(L_+ S_- + L_- S_+\right) + L_z S_z. \tag{2.19}$$

Using relations $L_z|L,m\rangle = m|L,m\rangle$ and

$$L_\pm|L,m\rangle = \sqrt{L(L+1) - m(m\pm1)}|L,m\pm1\rangle \tag{2.20}$$

we obtain, e.g. for first diagonal element of spinfull Hamiltonian,

$$\langle d_{m_d=-2}|\lambda_M \vec{L}\cdot\vec{S}|d_{m_d=-2}\rangle = -2\cdot\frac{1}{2}\cdot\lambda_M. \tag{2.21}$$

It turns out that only non-zero spin-orbit operator matrix elements are diagonal in our basis and read for spin up ($\sigma = +1$)

$$\hat{H}_{SOC} = \mathrm{diag}\left(-\lambda_M, 0, \lambda_M, -\frac{1}{2}\lambda_{X_2}, 0, \frac{1}{2}\lambda_{X_2}\right). \tag{2.22}$$

Full Hamiltonian with SOC can be written therefore as:

$$H\left(\vec{k}\right) = \begin{bmatrix} H_{Mo-Mo} & H_{Mo-S_2} \\ H^\dagger_{Mo-S_2} & H_{S_2-S_2} \end{bmatrix} \otimes \begin{bmatrix} 1 & 0 \\ 0 & 1 \end{bmatrix} + \begin{bmatrix} H_{SO}(\sigma=1) & 0 \\ 0 & H_{SO}(\sigma=-1) \end{bmatrix} \tag{2.23}$$

where spin-dependent matrix is given by

$$H_{SO}(\sigma) = \begin{bmatrix} -\sigma\cdot\lambda_{Mo} & 0 & 0 & 0 & 0 & 0 \\ & 0 & 0 & 0 & 0 & 0 \\ & & \sigma\cdot\lambda_{Mo} & 0 & 0 & 0 \\ & & & -\sigma\cdot\frac{\lambda_{S_2}}{2} & 0 & 0 \\ & & & & 0 & 0 \\ & & & & & \sigma\cdot\frac{\lambda_{S_2}}{2} \end{bmatrix}. \tag{2.24}$$

Parameters λ_{Mo} and λ_{S_2} (λ_M and λ_{X_2} in general) have to be chosen such as to reproduce splitting of bands. This choice, however, generally changes dispersion of bands due to modification of diagonal parts of Hamiltonian and in principle requires additional fitting. We checked that, e.g. for MoS_2, setting $\lambda_{Mo} = 0.148/2$ eV and $\lambda_{S_2} = 0.03/2$ reproduces correct splittings in VB (0.148 eV) and CB (0.003 eV). We note that order of magnitude larger value of λ_{S_2} stems from different contribution of $m_p \neq 0$ orbitals to CB (order of 20%). To avoid difficult re-fitting of our SOC results optimizing VB-CB transition, one can for example fit VB+SOC and CB+SOC separately, keeping λ_M and λ_{X_2} parameters as above. Result of such procedure compared to DFT + SOC band-structure are shown in Fig. 2.10. One can see that this reproduces dispersion and spin splitting correctly, however it affects negatively either band gap for CB fit and second minimum dispersion at Q point for VB fit. Parameters for best VB and CB with SOC for MoS_2 are presented in Appendix 6.5.

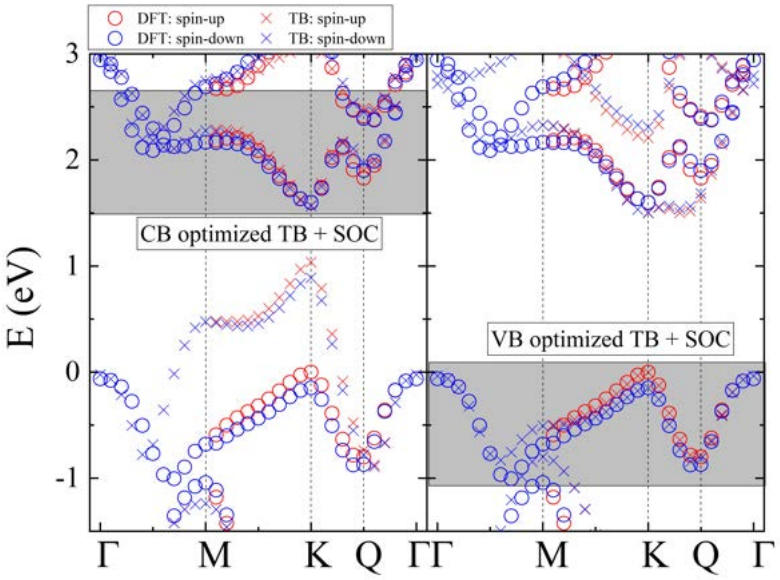

Figure 2.10: Best fit for SOC Hamiltonian for MoS_2 performed separately for CB and VB.

To understand better how SOC affects band structure across BZ, let us first plot spin-split bands along (+K)-Γ-(-K) direction, as shown in Fig. 2.11 (a). One can notice, that our choice of parameters reproduces well spin splitting in VB and CB at K points and our model catches spin inversion between +K and -K points. Interestingly, general feature of whole MX_2 family is spin inversion of bands in CB close to the K point, taking place between K and Q points. This feature is better visible when lowest spin-split band is shown across whole BZ, as shown in Fig. 2.11 (b). For example of MoS_2 at the +K point, bottom of CB has spin orientation same as top of VB. However, region of BZ where this property holds is very small (red region around +K in Fig. 2.11 (b)) and quickly other spin becomes lower. This situation changes again approximately

half-way between K and Q point, around which spin is again oriented in the same way as at +K point in VB. Interestingly, in both Mo and W based TMD's spin at Q point is always oriented the same way as in VB at K point, irrespective of spin ordering change in W based materials in CB at K point with respect to Mo based TMD's. This property might have interesting implications on spin-selective charging of quantum dots confining electron states from CB, as discussed later in thesis. Same spin orientation between VB at K and Q at CB means also, that all momentum-indirect excitons with momentum $|Q-K|$ will have spin "bright" configuration and when activated e.g. by phonons, should be optically detectable, in contrast to spin-forbidden lowest excitons with small momentum around K-points in tungsten-based TMD's.

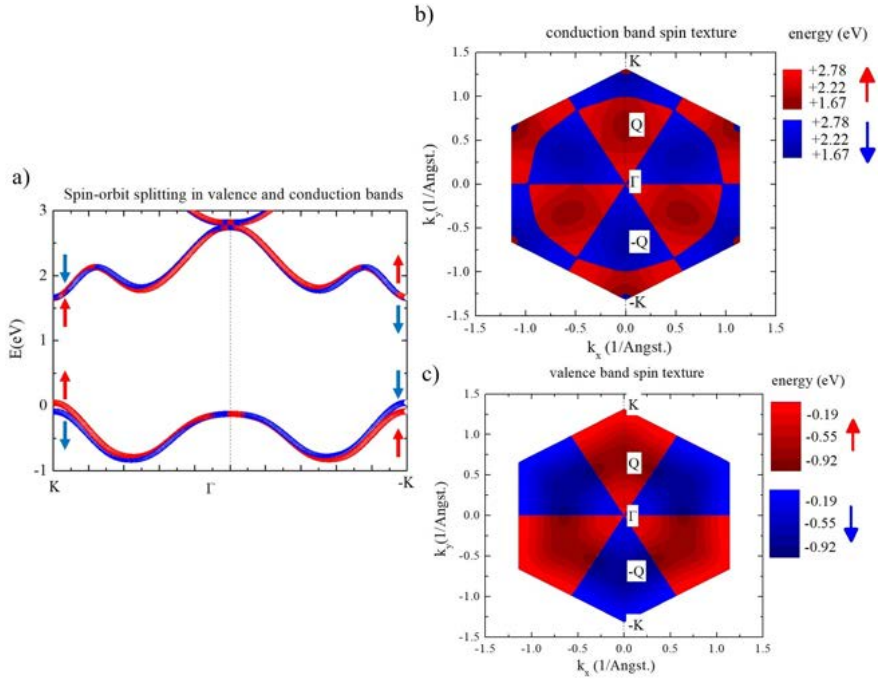

Figure 2.11: (a) Band structure along (+K)-Γ-(-K) line with SOC, obtained using parametrization dubbed "best Δ_{CB-VB}" and parameters $\lambda_{Mo} = 0.148/2$ eV and $\lambda_{S_2} = 0.03/2$. (b) Spin texture of CB, showing spin orientation of lowest CB spin-split band. (c) Corresponding VB spin texture.

2.2.5 Massive Dirac fermion and parabolic effective models

In the next step we discuss the low energy Hamiltonian around K-point. We begin with noticing, that at K point top of the VB is build almost solely from $m_d = +2$ orbital (with small admixture of $m_p = +1$ orbital), while bottom of the CB is build from combination of $m_d = 0$ and $m_p = -1$ orbitals. However, assuming low-energy basis as $m_d = 0$ and $m_d = +2$ and expanding g_0 and g_2

functions around K point ($\vec{k} = \vec{K} + \delta\vec{k}$) as

$$g_0 = -3 + \frac{9}{4}q^2, \qquad g_2 = -i\frac{9}{2}q_- + \frac{9}{8}q_+^2, \tag{2.25}$$

where $q_{x(y)} = \delta k_{x(y)} \cdot d_{\parallel}$, $q^2 = q_x^2 + q_y^2$ and $q_\pm = q_x \pm iq_y$, one can immediately end up with massive Dirac fermion (mDF) Hamiltonian with correction called "trigonal warping[474]":

$$\begin{aligned} H_{eff} &= H_{Dirac} + H_{mass} + H_{warp.} \\ H_{Dirac} &= \begin{pmatrix} 0 & at(-iq_x - q_y) \\ at(iq_x - q_y) & 0 \end{pmatrix}, \\ H_{mass} &= \begin{pmatrix} \frac{\Delta}{2} + \alpha q^2 & 0 \\ 0 & -\frac{\Delta}{2} + \beta q^2 \end{pmatrix}, \\ H_{warp.} &= \gamma \begin{pmatrix} 0 & q_+^2 \\ q_-^2 & 0 \end{pmatrix}. \end{aligned} \tag{2.26}$$

We note that there is a relation between parameters $\Delta, a, t, \alpha, \beta, \gamma$ to E_d, W_1, W_2, W_3, however to predict these values reliably one has to include coupling to other orbitals. This can be done by using Löwdin perturbation theory,[462,463] however we take alternative route. We note only that this procedure leads to further correction

$$H_\eta = \frac{\eta}{2}q^2 \begin{pmatrix} 0 & q_+ \\ q_- & 0 \end{pmatrix}, \tag{2.27}$$

which is already in third power of expansion of wavevector around K point parameter $q_{x(y)}$. To fit model parameters we choose to take another route and simply treat them as variational and fit their values to our DFT-based tight-binding model to reproduce VB and CB close to the K point. Best parametrization for dispersion including up to 1/4 distance between K and Q point we found is $\Delta = 1.6850$ eV, $a = 3.193$ Å,$t = 1.411$ eV, $\alpha = 0.8341$ eV·Å^2, $\beta = 0.8066$ eV·Å^2, $\gamma = -0.0354$ eV·Å^2, $\eta = -0.0833$ eV·Å^3. As a further simplification, we can tune parameters to keep only massive Dirac fermion model Hamiltonian:

$$H_{mDF} = \begin{pmatrix} \frac{\Delta}{2} & at(-iq_x - q_y) \\ at(iq_x - q_y) & -\frac{\Delta}{2} \end{pmatrix}, \tag{2.28}$$

for which best fit is obtained for $\Delta = 1.6848$ eV, $a = 3.193$ Å, $t = 1.4677$ eV. We note that complicated model described by Eq. 2.26 and Eq. 2.27 and simple mDF model defined by Eq. 2.28 give very similar results of dispersion and when applied e.g. to excitonic calculations there is no qualitative and very little quantitative difference, therefore in the rest of the thesis we will use only simplified mDF model without introducing further corrections. We note that mDF can be even further reduced to parabolic (effective mass) model. This can be done noting, that eigenergies of mDF are:

$$E = \pm\sqrt{\frac{\Delta^2}{4} + a^2t^2q^2} = \pm\frac{\Delta}{2}\sqrt{1 + \underbrace{\frac{4a^2t^2}{\Delta^2}q^2}_{\varepsilon}} \underbrace{\approx}_{\varepsilon<<1} = \pm\frac{\Delta}{2}\left(1 + \frac{1}{2}\varepsilon - \frac{1}{8}\varepsilon^2 + ...\right) \tag{2.29}$$

Keeping only first order of ε we end up with

$$E = \pm\left(\frac{\Delta}{2} + \frac{\hbar^2 q^2}{2m^*}\right). \tag{2.30}$$

Effective electron mass is given $m^* = \frac{\Delta\hbar^2}{2a^2t^2}$. We note that choice of parameters Δ, t, m^* depends heavily on how large portion of BZ we want to fit as closely as possible. One can note also, that top of VB and bottom of CB is described better if different effective masses of electrons (m_e) and holes (m_h) are taken. For MoS_2, when using parabolic model we take $m_e = 0.54m_0$ and $m_h = 0.44m_0$. For other MX_2 materials best effective mass parameters can be found easily in literature.[421]

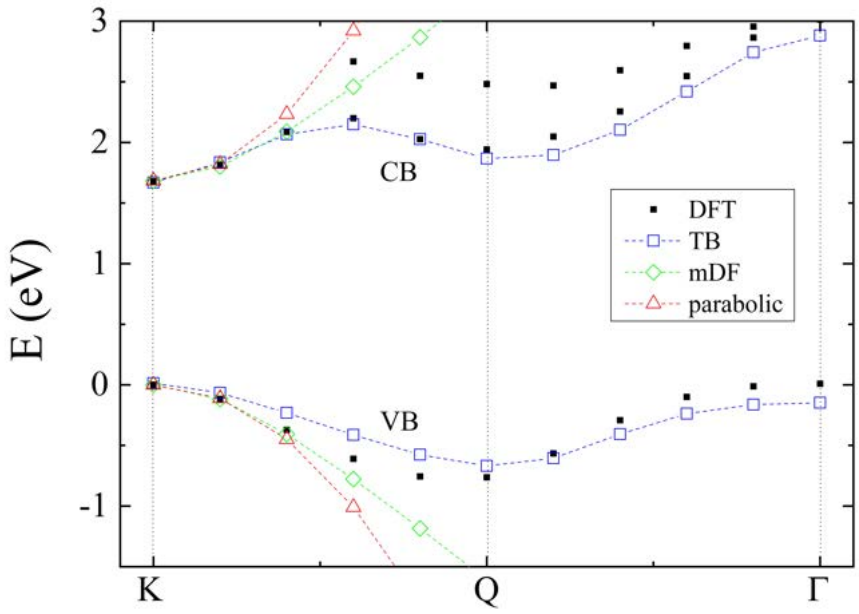

Figure 2.12: Comparison between dispersion models along K-Γ line. DFT dispersion is denoted by black circles, TB - by blue rectangles, massive Dirac fermion by green diamonds and parabolic (effective mass) model by red triangles. Corresponding connecting lines are shown as a guide to the eye.

As a summary, in Fig. 2.12 we present *ab initio* result and different discussed low energy models of VB and CB: tight-binding optimized for VB and CB separately, massive Dirac fermion model (without quadratic, trigonal wrapping and "η"corrections) and parabolic model. One can observe, that all of them describes well neighborhood of K point, however only using TB model it is possible to obtain second minimum at Q point in CB and correct second maximum of VB at Γ point. Approximately 10% of K-Γ line from K point is described properly by both mDF and parabolic models, mDF model being better for CB description. We note also, that both mDF and parabolic models can be extended to include spin, however in both cases it is necessary to find different parametrization for two spin species (e.g two effective electron and hole masses and two

gap parameters Δ for parabolic model). All those parametrization are available in literature[421] for all MX_2 crystals, however in the rest of the thesis, when discussing spin physics, only TB model will be utilized.

2.3 Analysis of single-particle bandstructure of MX_2

2.3.1 Mechanism of band-gap opening

At first, let us discuss band gap opening process at K - point, focusing on MoS_2 as a representative of MX_2 family. As identified previously, we know that only non-zero matrix elements at K point are those proportional to function $f_0\left(\vec{k}\right)$. Assuming Mo d- orbital energies at K point as $E_{m_d=\pm 2} = E_{m_d=0} = 0$ (reference energy) and $E_{m_p=\pm 1} = E_{m_p=0} \approx -3.5$ eV (rough estimate based on energy of first band below valence one with majority contribution from p - orbitals), we fit parameters $V_{dp\sigma}$, $V_{dp\pi}$ to obtain as good band gap at K-point as possible, comparing against DFT calculations. Then we multiply all non-zero matrix elements by some parameter 't' and we check what happens when we slowly turn on the interaction between p and d orbitals, as shown in Fig. 2.13 (a). As one can notice, interaction between d- and p-orbitals lifts the degeneracy

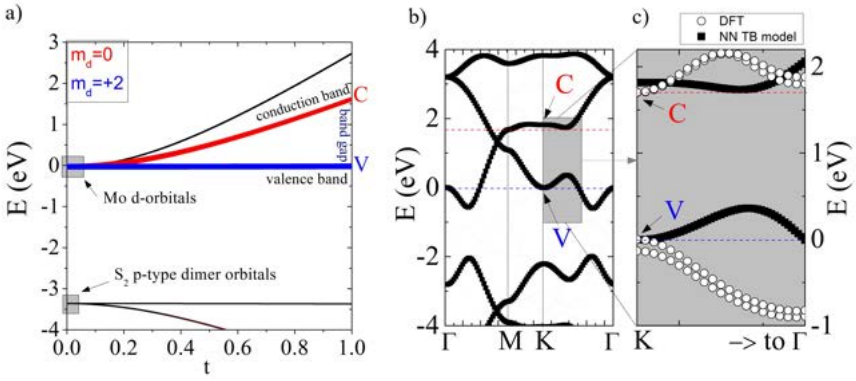

Figure 2.13: (a) Orbital - resolved positions of bands at K-point with respect to d-p orbitals coupling strength t. For all t values bottom of the valence band is set to 0. (b) Best fit for band structure obtained using nearest-neighbor tight-binding model along Γ - M - K - Γ line. (c) Comparison between DFT (white dots) and TB (black dots) dispersions near K- point along K - Γ line. Figure reproduced from Ref. 1.

of three d- orbitals. At K - point, when interaction is turned on, the band gap between $m_d = +2$ and $m_d = 0$ opens. We conclude, therefore, that major process of band gap creation in MX_2 materials stems from d- orbitals interactions with p-orbitals.

Despite correct description of band gap opening process, we find that NN TB

model is not sufficient to describe correctly band structure around Fermi level. As one can see in Fig. 2.13 (b), even though band gap is opened at K - point, due to change of the orbital symmetry character between K and Γ points (major contribution of $m_d = 0$ at K in CB changes to major contribution to VB at Γ), no matter what parameters we choose, there is always a crossing of the bands. This crossing creates analog of "Dirac" cone somewhere in the BZ, see Fig. 2.13 (b). Due to this effect we were also not able to find reasonable approximation for effective mass around K - point in NN TB model, as shown in Fig. 2.13 (c).

As shown e.g. in Fig. 2.9 we need next-NN Hamiltonian to correctly capture band gap opening in whole BZ and dispersion around K, Q and Γ points in both conduction and valence bands. Comparing results of first and second NN TB models, we see that gap opening at K can be understood as d- and p- orbitals interaction, however it is crucial to add to TB model second nearest neighbors metal - metal orbitals interactions (d-d interaction) described by Eq. 2.15, to open band gap across whole d-orbital group. We note that not only dispersion of TB model reproduces very well result obtained using *ab initio*, but also orbital compositions trends are well resolved. For example, our tight-binding model captures correctly that majority of orbital composition of bands at +K / -K points in valence band comes from $m_d = +2/-2$ orbitals, as represented by red circles in Fig. 2.14. Also, major contribution to conduction band at ±K points is coming from $m_d = 0$ orbital (black circles).

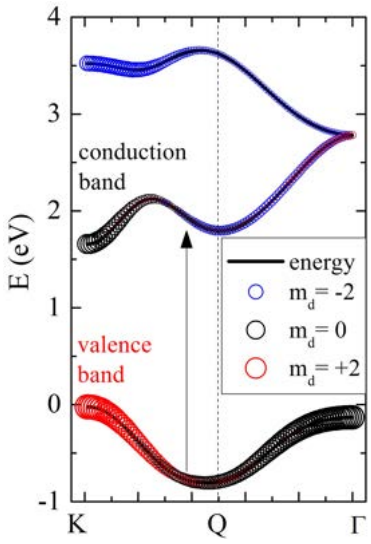

Figure 2.14: Evolution of orbital compositions from K to Γ point in MoS_2. Size of circle encodes value of orbital contribution, while color - m_d quantum number of M d-orbital. Figure reproduced from Ref. 1.

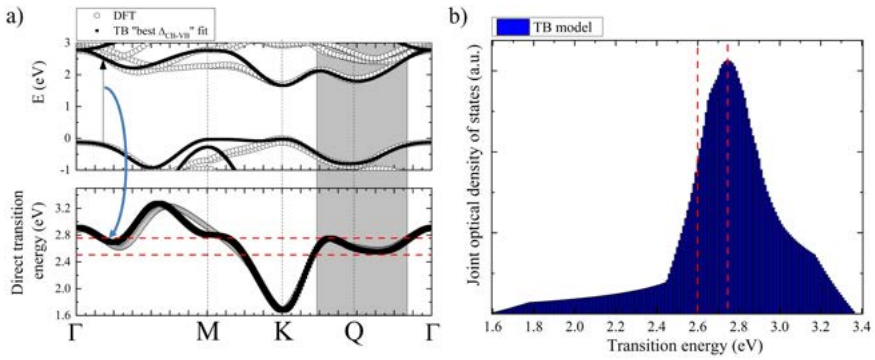

Figure 2.15: (a) Direct transition energy between VB and CB for both DFT and TB optimized to reproduce transition energy. (b) Joint optical density of states, showing pronounced peak for band nesting transition energy, resulting from existence of Q points.

2.3.2 Q-points and band nesting

Due to the exchange of orbital symmetries between valence and conduction bands, one can expect that second minimum in CB may occur. This minimum, at so-called Q - point (however usual naming convention for points inside BZ should be Greek, therefore names Σ or Λ are also in use), due to lack of the second maximum in valence band, creates peculiar situation, when both conduction and valence bands are parallel in large portion of the Brillouin zone, see Fig. 2.15 (a). This phenomenon, which is reminiscent of parallel electron and hole pockets is superconductors (however not on the same Fermi level), is called band nesting.[747] It is responsible for record high absorption by TMD's monolayers. For uncorrelated electron-hole transition we identify peak energy of joint optical density of states at energetic window between 2.58 eV and 2.75 eV for MoS_2, see Fig. 2.15 (a,b), red dashed lines. We note that other contribution to this peak comes from portion of BZ between Γ and M line. We checked, that when Q points are "turned off" and not included in joint optical density of states, before mentioned peak drops significantly, establishing that it is mainly related to transitions from neighborhood of Q points. We note again, that second minimum at Q point becomes true minimum for $n > 1$ layers of MX_2 family, which are indirect gap semiconductors with gaps between Γ and Q points.

2.3.3 Theory of Landé and valley Zeeman effect

Understanding response of material to applied magnetic field can greatly enhance our knowledge of electronic structure. In the following section we study how electrons in center of the $\pm K$ valleys react to external magnetic field $\vec{B}$. We assume that field is always perpendicular to the sample, $\vec{B} = (0, 0, B_z)$. In MX_2 materials there are 3 contributions to overall Zeeman splitting of a given valley, summarized in Fig. 2.16. They are:

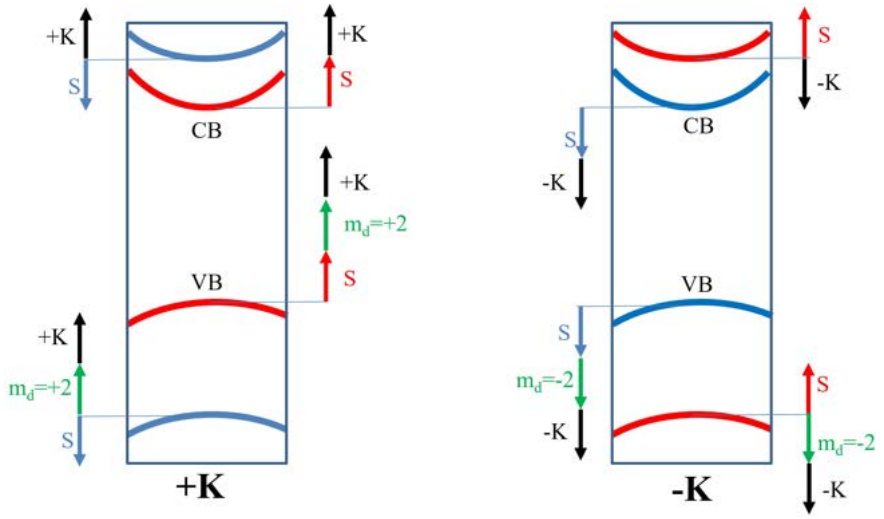

Figure 2.16: Different contributions to +K and -K valleys response to magnetic fields. Blue and red arrows show bare electron Zeeman contribution in magnetic field $\vec{B} = (0, 0, B_z)$, green - atomic orbital Landé contribution and black ones - valley Zeeman contribution.

- Bare electron Zeeman effect, related to intrinsic electrons spin and described by Hamiltonian $H_1 = g_0 \mu_B \vec{B} \cdot \vec{s}$
- Orbital Landé splitting, caused by electron orbital rotation, proportional to azimuthal quantum number m from which electron at given k-space region is build, described by Hamiltonian $H_2 = \mu_B \vec{B} \cdot \vec{L}$
- Valley Zeeman splitting, caused by wavepacket rotation and corresponding wavepacket orbital magnetic moment related to Berry's curvature. This effect is described by Hamiltonian $H_3 = \tilde{\mu}_V \vec{B} \cdot \vec{L}_{wp}$ and corresponding energy shift is given by $\Delta_{VZ} = \vec{m}_{wp} \cdot \vec{B}$.

Now we aim to calculate energy shifts caused by three effects described above. First, the bare spin Zeeman splitting gives standard $\Delta E_1 = 2 s_z \mu B \approx \pm B \cdot 5.79 \cdot 10^{-5}$ eV/T, so even in 100 Tesla it gives shifts of the order of meV.

Calculation of the second contribution is more difficult due to usually complicated orbital structure of electron Bloch wavefunctions in crystal. Our goal is to calculate expectation value of H_2 in form

$$\Delta E_n(k) = \langle \Psi_n(k) | \hat{L}_z/\hbar | \Psi_n(k) \rangle \mu_B B_z, \tag{2.31}$$

where n is band (CB or VB). Details of such matrix element evaluation in our TB model are presented in Appendix 6.6. Final matrix element of $\hat{L}_z$ operator, for example in CB at K point, is given by

$$\langle \Psi_{CB}\left(\vec{K}\right) | L_z/\hbar | \Psi_{CB}\left(\vec{K}\right) \rangle = (-1) \left| \nu_4^{CB}(K) \right|^2, \tag{2.32}$$

where $\nu_i^n(\vec{k})$ is i-th eigenvector component of TB spinor of n-th band at given $\vec{k}$ - point. Analogous calculation for valence band at K point yields

$$\langle \Psi_{VB}\left(\vec{K}\right)|L_z/\hbar|\Psi_{VB}\left(\vec{K}\right)\rangle = 2\cdot\left|\nu_3^{VB}(K)\right|^2 + 1\cdot\left|\nu_6^{VB}(K).\right|^2 \tag{2.33}$$

Matrix elements at $-K$ are obtained simply by changing signs of all m, resulting in opposite matrix elements than in $+K$ valley. Interestingly, we see that splitting due to chalcogen dimers affects orbital Zeeman splitting (ν_4 and ν_6 in Eq. (2.32) and Eq. (2.33)), entering with opposite signs to VB and CB, "conspiring" to give only metal ($m_d = \pm 2$) contribution, as usually described in experimental papers.[178] Small deviation from total g-factor 4 for valley Zeeman splitting can be understood then as sensitive probe of imbalance between chalcogen dimer contributions to CB and VB. Interestingly, in MoS_2 experimental exciton g-factors may deviate strongly from value 4, which was proposed to be related to many-body effects, possibly interactions of 1s bright excitonic state with several dark states.[180]

Third contribution to total Zeeman shift in magnetic field stems from Bloch electron wave-packet (wp) rotation. This orbital magnetic moment $\vec{m}_{wp}$ can be analytically derived for massive Dirac fermion model for $\vec{B} = (0, 0, B_z)$ and yields[748]

$$\Delta_{VZ} = \vec{m}_{wp}(q)\cdot\vec{B} = \tau_z\frac{2ea^2\Delta t^2 B_z}{2\hbar\left(\Delta^2 + 4q^2a^2t^2\right)}\underbrace{=}_{q=0}\frac{a^2t^2}{\Delta}\frac{eB_z}{\hbar}. \tag{2.34}$$

Interestingly, exactly the same result for q = 0 can be obtained differently, analyzing Landau levels constructed out of massive Dirac fermions. Standard procedure[1,567,749] introducing ladder operators and transforming massive Dirac fermion Hamiltonian defined in Eq. 2.28 to harmonic oscillator problem yields difference between bottom Landau levels in respective valleys in CB (zeroth Landau level in -K valley and first Landau level in +K valley) given by:

$$\Delta_{VZ} = \frac{\Delta}{2}\left(\frac{\sqrt{2}at}{l_0\Delta}\right)^2 = \frac{a^2t^2}{\Delta}\frac{eB_z}{\hbar} \tag{2.35}$$

where magnetic length l_0 is given by $l_0 = \sqrt{\hbar/(eB_z)}$.

We note that the orbital magnetic moment can be in principle calculated for every k-point in BZ within TB model for n-th band using formula[748]

$$\vec{m}_{wp}(\vec{k}) = i\frac{e\hbar}{2m^2}\sum_{i\neq n}\frac{\langle u_{n,k}|\hat{p}|u_{i,k}\rangle\times\langle u_{i,k}|\hat{p}|u_{n,k}\rangle}{E_n(\vec{k}) - E_i(\vec{k})}, \tag{2.36}$$

where $\hat{p}$ are momentum operators, $|u_{n,k}\rangle$ - Bloch wavefunctions constructed out of TB coefficients and $E_n(\vec{k})$ - TB eigenenergies. Interestingly, interplay of orbital and valley Zeeman splittings may be an additional way of tuning respective K and Q valleys positions minima in CB, especially in QD systems. This effects is left, however, for a future study.

Chapter 3

Optical properties of MX_2: exciton theory

In the following Chapter properties of excitons, complexes dominating optical response of 2D semiconductors are studied. First we derive an equation describing correlated bound electron-hole state, analogous to Bethe-Salpeter theory. Then, a lot of attention is devoted to realistic description of matrix elements describing interactions between excited carriers. Next we present ladder of approximations starting from simplest, analytically solvable excitonic model, finishing with full tight-binding theory of exciton with model, but realistic theory of screening. Particularly, role of band nesting and topology of wavefunctions on excitonic spectrum is uncovered. Then, we use knowledge of excitonic fine structure to rationalize novel type of fine structure of trions in MoS_2 when compared with other TMD's.

3.1 Non-interacting optical excitations in hexagonal semiconductors

The simplest picture of light absorption by semiconducting material can be understood in terms of transitions of carriers from valence to conduction band due to photon excitation with energy $E_{exc.}$, changing angular momentum by ± 1 when circularly polarized light is used. In MX_2 semiconductors situation get's more complicated, because dipole transitions between d orbitals ($m_d = \pm 2$ in VB and $m_d = 0$ in CB) and negligible p-d transitions cannot explain that circularly polarized light excites carriers within one valley. Solution to this problem comes from realization that velocity matrix elements inside transition matrix elements in general have two contributions:[750] dipole transitions between localized orbitals and terms related to electron hopping between lattice sites. This hopping contribution set's phase of velocity matrix element between VB and CB Bloch wavefunctions and defines optical selection rules, generally not

only in MX_2, but in all gapped" chiral" fermion systems, e.g. graphene multilayers.[630,631]

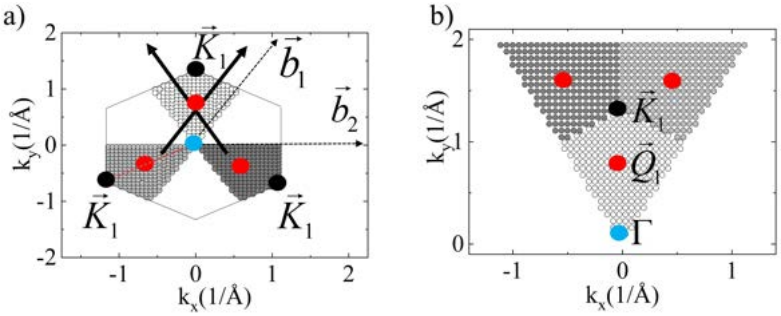

Figure 3.1: (a) Choice of +K valley on whole BZ. (b) Construction of valley around single K-point. Figure reproduced from Ref. 5.

Because it is possible to selectively excite carriers from band edge of one valley (e.g. +K), in theoretical investigations it is useful to think about two-non equivalent parts of the hexagonal Brillouin zone (BZ). Unique association of k-points to belong to one or the other valley have to be done as shown in Fig. 3.1. Starting from cutting "wedges" around 3 equivalent (related to each other by reciprocal lattice vector G translations) K - points, as shown in Fig. 3.1 (a), one can move respective wedges to one neighborhood of K-point, creating triangle around it as in Fig. 3.1 (b). We note that similarly constructed triangle for -K valley has to be rotated by C_3 symmetry, and both triangles for +K and -K valley put next to each other create rhomboidal BZ equivalent to full hexagonal BZ.

In next step let us discuss energy of transitions inside one valley. As shown in Fig. 3.2 (a) along K-Q-Γ line, TB model (optimized to reproduce Kohn-Sham transition energies) shows steep rise of transition energy to approximately half - way between K and Q points. In this region, ΔE is described quite well by both parabolic and massive Dirac fermion models. However, around Q - point, density of states becomes flat, which results in large peak in joint optical density of states, as discussed and depicted in Fig. 2.15. This means, that in terms of mean energy of transition across +K valley TB model has the lowest, and parabolic model - the highest value. Similar effect might be "on average" obtained by increasing effective mass of bands when switching from parabolic to mDF to TB approximations. This picture will help later to rationalize increased binding energy of excitons for TB model compared with parabolic one under approximation of the same form of electron-hole interaction.

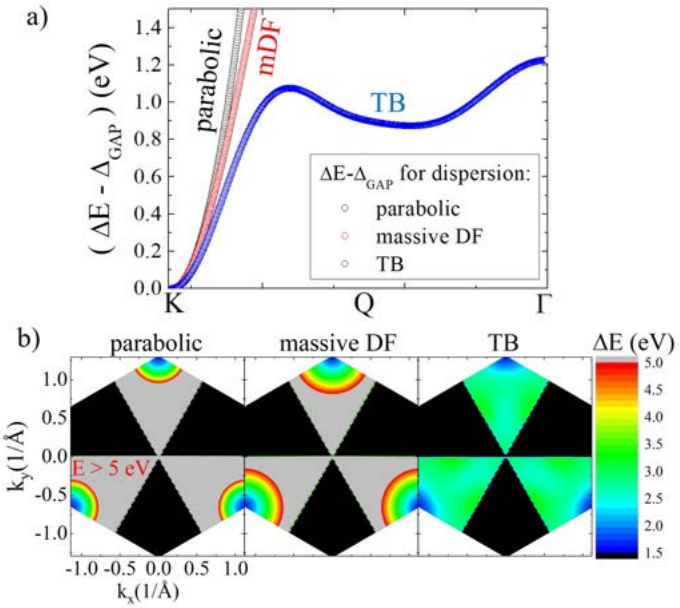

Figure 3.2: (a) Comparison of three models of energy transitions ($\Delta E = E_{CB} - E_{VB}$) set with respect to band gap Δ_{GAP} at K point. (b) The same transition energy (without subtraction of Δ_{GAP}) for all points in +K valley in BZ. Figure reproduced from Ref. 5.

3.2 Effect of electron-electron interactions on optical properties

"Free particle" transitions, described in previous Section, are well known to give incorrect optical band gaps in materials in which interactions are strong. As discussed in introduction, those energies have to be first corrected by electron and hole self-energies, and then electron - hole interaction has be included. In simple hydrogen-like picture, positive hole charge interacts by Coulomb potential with negative electron charge, creating series of ground and excited bound states, as shown schematically in Fig. 3.3 (a).

We begin description of our theory from defining the ground state. From now on we assume that we have only one valence and one conduction band. Next, to construct the ground state we fill all states in the valence band, as shown in Fig. 3.3 (b), as

$$|GS\rangle = \sum c_k^\dagger |0\rangle, \tag{3.1}$$

where $|0\rangle$ is vacuum state. Let's note that ground state contains some interactions on the Kohn-Sham level, because tight-binding theory used is constructed to reproduce DFT band structures. These interactions are equivalent conceptually to Hartree-Fock theory corrections, both affecting single-particle energies. Next step is construction of single excitation shown in Fig. 3.3(b) as $c^\dagger_{c,k+Q_{CM},\sigma} c_{v,k,\sigma} |GS\rangle$, where $c_{v,k,\sigma}$ annihilates electron from valence band state

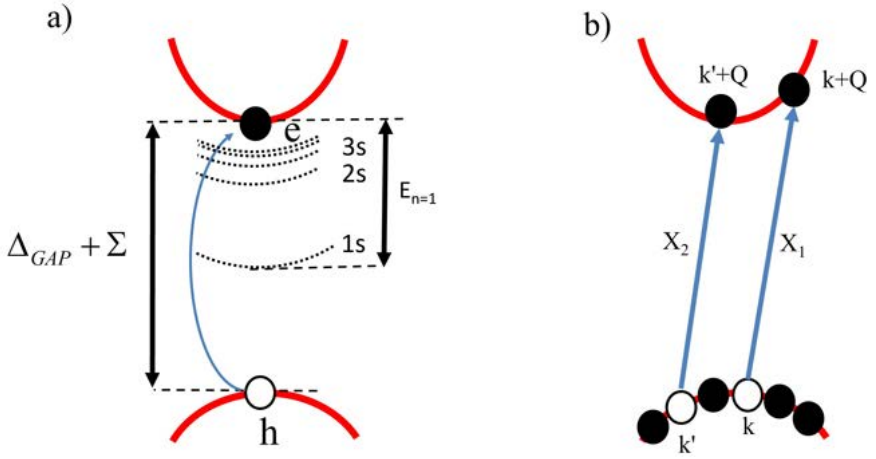

Figure 3.3: (a) Single electron - single hole picture (exciton in effective mass approximation) in which interaction creates spectrum of bound states. (b) Exact picture where "hole" is created by exciting electron from filled ground state in VB. Exciton is then constructed as coherent superposition of all possible excitations for a given center-of-mass momentum $\vec{Q}_{CM}$ interacting via Coulomb interaction.

with wavevector $\vec{k}$ and spin σ and $c^{\dagger}_{c,k+Q_{CM},\sigma}$ creates electron in conduction band with momentum $k + Q_{CM}$ and the same spin σ as electron annihilated from valence band. Q_{CM} is center-of-mass momentum of electron-hole pair.

In the next step exciton state is formed as linear combination of excitations with coefficients $A_n^{Q_{CM}}$ being complex electron-hole amplitudes

$$|X, Q_{\mathrm{CM}}\rangle = \sum_{k}^{1^{st}BZ} A_n^{Q_{\mathrm{CM}}}\left(\vec{k}\right) c^{\dagger}_{c,k+Q_{\mathrm{CM}},\sigma} c_{v,k,\sigma}|GS\rangle \tag{3.2}$$

Because we are interested in optically excited exciton states and we do not consider phonon-assisted processes, we can assume that Q_{CM} is zero and drop this index from now on. Exciton states can be calculated using standard eigenvalue problem

$$\hat{H}_X|X\rangle_n = E_n|X\rangle_n \tag{3.3}$$

where interacting excitonic Hamiltonian $\hat{H}_X$ is given in notation hiding both band index $b = v = VB$ or $b = c = CB$, wavevector $\vec{k}$ and spin σ in single index, for example $|i\rangle = |b, \vec{k}, \sigma\rangle$ as

$$\hat{H}_X = \underbrace{\sum_i \varepsilon_i c_i^{\dagger} c_i}_{\hat{H}_X^{(1)}} + \underbrace{\frac{1}{2}\sum_{ijkl} \langle i\,|j\,|V|\,k|\,l\rangle\, c_i^{\dagger} c_j^{\dagger} c_k c_l}_{\hat{H}_X^{(2)}} \tag{3.4}$$

In the next step we face a problem of calculating matrix elements of this Hamiltonian. As a first step let's consider single particle part $\hat{H}_X^{(1)}$. For two arbitrary excitonic states $|X_1\rangle = c^{\dagger}_{f_1} c_{i_1}|GS\rangle$, $|X_2\rangle = c^{\dagger}_{f_2} c_{i_2}|GS\rangle$, where $i_1 = (k, v)$,

$f_1 = (k, c)$, $i_2 = (k', v)$, $f_2 = k', c$, we have for single particle part of the Hamiltonian

$$\langle X_2|\hat{H}_X^1|X_1\rangle = \sum_{m=1}^{N_{all}} \varepsilon_m \langle X_2|c_m^\dagger c_m|X_1\rangle = \sum_{i=m}^{N_{all}} \varepsilon_m \langle GS|c_{i_2}^\dagger c_{f_2} c_m^\dagger c_m c_{f_1}^\dagger c_{i_1}|GS\rangle \tag{3.5}$$

Detailed steps showing how Wick theorem is used to reduce six component operators are presented in Appendix 6.8 and the result is given by

$$\langle X_2|\hat{H}_X^{(1)}|X_1\rangle = \delta(i_1, i_2)\delta(f_1, f_2)\left[\varepsilon_{f_1} - \varepsilon_{i_1} + \sum_{m=1}^{N_{occ.}} \varepsilon_m\right], \tag{3.6}$$

where last sum inside bracket over all occupied states is a non-interacting contribution to ground state energy, that can be subtracted from diagonal energy in B.-S. matrix.

Analysis of interaction part $\hat{H}_X^2$ is more demanding, because now 8-operator product have to be reduced. Details of this process are again moved to Appendix 6.8. The final result gives several terms that can be arranged as

$$\langle X_2|\hat{H}_X^{(2)}|X_1\rangle = H_{V-GS} + H_{h-GS} + H_{e-GS} + H_{e-h}, \tag{3.7}$$

Part of full Hamiltonian denoted as H_{V-GS} describes interactions renormalizing energy of the ground state

$$H_{V-GS} = \frac{1}{2}\delta(i_1, i_2)\delta(f_1, f_2) \sum_{m_1, m_2=1}^{N_{occ.}} \left[\langle m_1 | m_2 | V | m_2 | m_1\rangle - \delta_{\sigma,\sigma'} \langle m_1 | m_2 | V | m_1 | m_2\rangle\right]. \tag{3.8}$$

Term H_{h-GS} is missing electron ("hole") interaction with all filled states (hole self-energy)

$$H_{h-GS} = -\delta(f_1, f_2) \sum_{m_1=1}^{N_{occ.}} \left[\langle i_1 | m_1 | V | m_1 | i_2\rangle - \delta_{\sigma,\sigma'} \langle m_1 | i_1 | V | m_1 | i_2\rangle\right], \tag{3.9}$$

and term H_{e-GS} is analogous electron interaction with all filled states (electron self-energy)

$$H_{h-GS} = \delta(i_1, i_2) \sum_{m1=1}^{N_{occ.}} \left[\langle m_1 | f_2 | V | f_1 | m_1\rangle - \delta_{\sigma,\sigma'} \langle m_1 | f_2 | V | m_1 | f_1\rangle\right]. \tag{3.10}$$

The most interesting part for us is electron - hole interaction H_{e-h} given by

$$H_{e-h} = -\langle i_1 | f_2 | V | f_1 | i_2\rangle + \langle f_2 | i_1 | V | f_1 | i_2\rangle. \tag{3.11}$$

Coming back to notation using wave vectors $\vec{k}$ and $\vec{k}'$, neglecting ground state energy correction due to interactions and incorporating electron and hole self-energies into dispersion energies $\varepsilon_{c,k}$ and $\varepsilon_{v,k}$ we obtain Bethe-Salpeter equation for exciton (center-of-mass momentum $Q_{CM} = 0$)

$$\left(\varepsilon_{c,k} - \varepsilon_{v,k}\right) A_n\left(\vec{k}\right) + \sum_{k'}^{\mathrm{BZ}} \left[-\left\langle v, \vec{k}' \middle| c, \vec{k} \middle| V \middle| c, \vec{k}' \middle| v, \vec{k} \right\rangle + \left\langle v, \vec{k}' \middle| c, \vec{k} \middle| V \middle| v, \vec{k} \middle| c, \vec{k}' \right\rangle\right] A_n\left(\vec{k}'\right) = E_n A_n\left(\vec{k}\right) \tag{3.12}$$

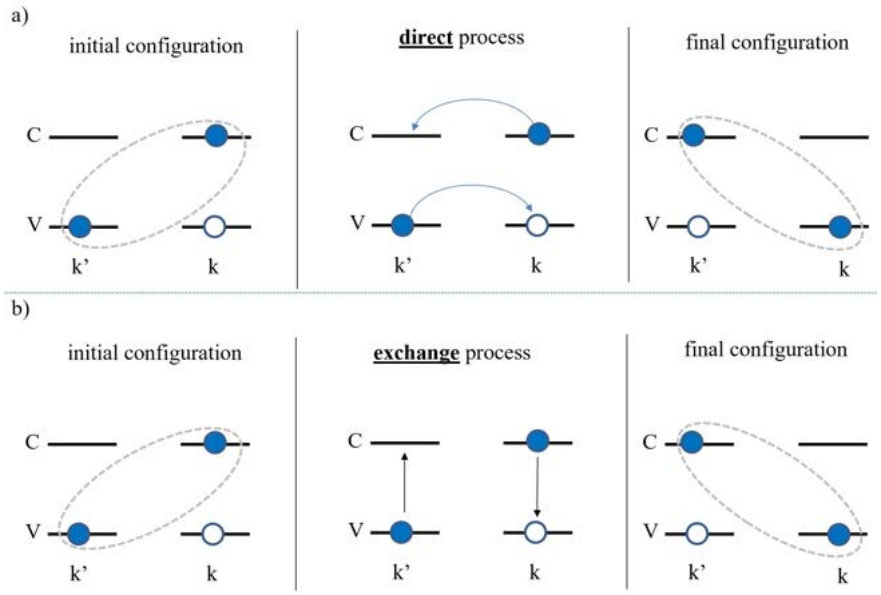

Figure 3.4: Graphical representation of two types of interaction between electron and hole: (a) direct process (b) exchange process.

In this equation summation over $\vec{k}'$ states is understood as over all vectors in first BZ, the same as number of atoms in the crystal. First let us identify type of matrix elements inside summation over $\vec{k}'$. Note that they are written in electron-only language. As shown in Fig. 3.4, first element (with minus sign) describes process in which electron in conduction band in state $\vec{k}$ and electron in valence band in state $\vec{k}'$ scatters via Coulomb interaction to electron in state $\vec{k}'$ in conduction band and electron in state $\vec{k}$ in valence band. This description is equivalent to electron-hole pair scattering from state $\vec{k}$ to $\vec{k}'$. Second process in Eq. (3.12) describes electrons starting as previously in $\vec{k}$ state in conduction band and $\vec{k}'$ state in valence band and scattering to same $\vec{k}$ and $\vec{k}'$, but changing band indices to valence and conduction, respectively. We identify first process as attractive direct electron-hole interaction, and second process as repulsive exchange electron-hole interaction.

Interestingly, when form of Eq. (3.12) is compared with the same equation for electron-hole binding energy[511] derived using two-particle Green's function method, there is a difference in exchange interaction screening. Question if exchange interaction should be screened was analyzed already in physics of quantum dots, for which better comparison with experiments was achieved when exchange was screened. In our theory we obtain same screening for both direct and exchange, however we will study further what happens if they are treated differently.

3.3 Coulomb matrix elements

We begin this Chapter with general definition of an arbitrary Coulomb matrix element

$$\left\langle n_1,\vec{k}_1\left|n_2,\vec{k}_2\right|V\left|n_3,\vec{k}_3\right|n_4,\vec{k}_4\right\rangle = \iint_{R^3} d^3rd^3r'V^{3\mathrm{D}}\left(\vec{r}-\vec{r}\right)\Psi^*_{n_1}\left(\vec{k}_1,\vec{r}\right)\Psi^*_{n_2}\left(\vec{k}_2,\vec{r}',\right)\Psi_{n_3}\left(\vec{k}_3,\vec{r}'\right)\Psi_{n_4}\left(\vec{k}_4,\vec{r}\right). \tag{3.13}$$

The wavefunctions can be written as

$$\Psi_n\left(\vec{k},\vec{r}\right) = e^{i\vec{k}\cdot\vec{r}}u_n\left(\vec{k},\vec{r}\right), \tag{3.14}$$

where Bloch part of the wavfunction is given by

$$u_n\left(\vec{k},\vec{r}\right) = \frac{1}{\sqrt{N_{UC}}}\sum_{i=1}^{N_{UC}}\sum_{\alpha=1}^{2}\sum_{\mu=1}^{3}e^{-i\vec{k}\cdot\left(\vec{r}-\vec{U}_i-\vec{\tau}_\alpha\right)}\nu^{(n)}_{\alpha\mu}\left(\vec{k}\right)\varphi_{\alpha\mu}\left(\vec{r}-\vec{U}_i-\vec{\tau}_\alpha\right) \tag{3.15}$$

Index i goes over N_{UC} unit cells with positions U_i, α enumerates sublattice and μ corresponding orbital. Tight-binding model coefficients $\nu^{(n)}_{\alpha\mu}$ are calculated from Hamiltonian in Eq. 2.14. $\vec{\tau}_\alpha$ specifies atom (or dimer) position inside unit cell. Finally we take $\varphi_{\alpha\mu}$ as localized orbitals written in a form of Slater ζ-type orbitals:

$$\varphi_{\alpha\mu}\left(\vec{r}\right) = R_n(r)Y_{L,\mu}(\theta,\phi) \tag{3.16}$$

where radial function is approximated as

$$R_n = \frac{(2\zeta_{nLm})^{n+\frac{1}{2}}}{\sqrt{(2n)!}}r^{n-1}e^{-\zeta_{nLm}\cdot r} \tag{3.17}$$

where ζ_{nLm} Slater parameters are taken for isolated atom model.[744,745] Spherical harmonics are given by standard expression

$$Y_{L\mu} = \sqrt{\frac{2L+1}{4\pi}\frac{(L-m)!}{(L+m)!}}P^m_L(\cos\theta)e^{im\phi} \tag{3.18}$$

where P^m_L are associated Legendre polynomials with Condon-Shortley phase $(-1)^m$ inside them. For $\alpha = 1$ we have Mo atom with $L = 2$, $\mu \in \{-2, 0, +2\}$ and for $\alpha = 2$ we have S_2 top and bottom atoms with $L = 1$, $\mu \in \{-1, 0, +1\}$.

3.3.1 Electron-hole direct matrix elements

For concreteness, let us first analyze direct electron - hole Coulomb matrix elements. Paying attention to index arrangement we have

$$\left\langle v,\vec{k}'\left|c,\vec{k}\right|V\left|c,\vec{k}'\right|v,\vec{k}\right\rangle = \iint_{R^3} d^3rd^3r'\Big[V^{3\mathrm{D}}\left(\vec{r}^{\,3\mathrm{D}}-\vec{r}^{\,3\mathrm{D}'}\right)\Psi^*_v\left(\vec{k}',\vec{r},z\right)\Psi^*_c\left(\vec{k},\vec{r}',z'\right)\times ... \\ ...\times\Psi_c\left(\vec{k}',\vec{r}',z'\right)\Psi_v\left(\vec{k},\vec{r},z\right)\Big]. \tag{3.19}$$

where $V^{3\mathrm{D}}$ is the bare electron-electron interaction, which screening will be discussed later. Note that in Eq. (3.19) $\vec{r}^{\,3D}$ vector is explicitly separated into two dimensional vector $\vec{r}$ (in which crystal is periodic) and out-of-plane coordinate z ($d^3r = d^2rdz$). Substituting the Bloch form of the wavefunctions we get after re-grouping

$$\iint_{R^3} d^3r d^3r' \Big[e^{i\left(\vec{k}-\vec{k'}\right)\cdot\left(\vec{r}-\vec{r'}\right)} V^{3\mathrm{D}}\left(\vec{r}^{\,3\mathrm{D}} - \vec{r}^{\,3\mathrm{D}'}\right) u_v^*\left(\vec{k'},\vec{r},z\right) u_v\left(\vec{k},\vec{r},z\right) \times ... \\ ... \times u_c^*\left(\vec{k},\vec{r'},z'\right) u_c\left(\vec{k'},\vec{r'},z'\right) \Big]. \tag{3.20}$$

In next step we utilize the property, that because electrons move in 2D crystal, their coordinates in that plane (we set it to xy) can be analyzed in reciprocal space. Two dimensional Fourier transform $V^{2\mathrm{D}}(q) = \frac{e^2}{4\pi\epsilon_0}\frac{2\pi}{q}$ (in SI) of three dimensional interaction gives

$$V^{3\mathrm{D}}\left(\vec{r}^{\,3\mathrm{D}} - \vec{r}^{\,3\mathrm{D}'}\right) = \frac{1}{(2\pi)^2}\iint_{-\infty}^{\infty} d^2q V^{2\mathrm{D}}(q) e^{-|z-z'|\cdot|\vec{q}|} e^{i\vec{q}\cdot\left(\vec{r}-\vec{r'}\right)}. \tag{3.21}$$

where z, z' coordinates are not transformed because there is no periodicity in z-th direction. Similarly to interaction, one can note that products of Bloch wavefunctions depending on the same coordinates ($\vec{r}^{\,3D}$ or $\vec{r}'^{3D}$) can also be written in terms of their 2D Fourier series

$$u_v^*\left(\vec{k'},\vec{r},z\right) u_v\left(\vec{k},\vec{r},z\right) \equiv \rho_{vv}^{\vec{k'}\vec{k}}\left(\vec{r},z\right) = \sum_{\vec{G}} e^{i\vec{G}\cdot\vec{r}} \tilde{\rho}_{vv}^{\vec{k'}\vec{k}}\left(\vec{G},z\right). \tag{3.22}$$

Fourier coefficients of such pairs of Bloch functions, called in literature either "pair densities" or "co-densities", are given by

$$\tilde{\rho}_{vv}^{\vec{k'}\vec{k}}\left(\vec{G},z\right) = \frac{1}{S}\iint_{R^2} d^2r e^{-i\vec{G}\cdot\vec{r}} u_v^*\left(\vec{k'},\vec{r},z\right) u_v\left(\vec{k},\vec{r},z\right), \tag{3.23}$$

where S is the crystal area. Those pair densities have to be calculated numerically due to a complicated structure of our tight-binding Bloch wavefunctions. In principle, integration should be performed over R^2 plane, however we do it only inside radius including all atoms inside central unit cell and all first neighboring unit cells. We have checked that for larger radii results are not affected. In next step we put all Fourier transforms into one expression (Eq. (3.20)). This allows us to integrate out many delta functions, however during this step one has to be careful and pay attention to changing continuous delta's to discrete one's $\delta\left(\vec{G'}+\vec{G}\right) \to \frac{S}{(2\pi)^2}\delta_{\vec{G'}+\vec{G}}$. Otherwise, there is no cancellation of crystal area S and results of final matrix elements have wrong scaling in limit of an infinite crystal. Final expression for direct matrix element (with coefficient $S/(2\pi)^2$ resulting from sum to integral transition) is

$$V^D\left(\vec{k},\vec{k'}\right) = \frac{S}{(2\pi)^2}\left\langle v,\vec{k'}\left|c,\vec{k}\right|V\left|c,\vec{k'}\right|v,\vec{k}\right\rangle = \gamma\sum_{\vec{G}}\frac{F^D\left(\vec{k},\vec{k'},\vec{G}\right)}{\left|\vec{k'}-\vec{k}-\vec{G}\right|}, \tag{3.24}$$

where $\gamma = e^2/\left(8\pi^2\varepsilon_0\right)$ and interaction form factor F^D is given by:

$$F^D\left(\vec{k},\vec{k'},\vec{G}\right) = \int dz \int dz' \rho_{vv}^{\vec{k'}\vec{k}}\left(\vec{G},z\right)\rho_{cc}^{\vec{k}\vec{k'}}\left(-\vec{G},z'\right)e^{-|z-z'|\cdot|\vec{k'}-\vec{k}-\vec{G}|}. \quad (3.25)$$

Pair densities can be evaluated numerically for every coordinate z by using explicit form of the Bloch wavefunctions, constructed using localized Slater orbitals φ as described before, as

$$\begin{aligned}\rho_{vv}^{\vec{k'}\vec{k}}\left(\vec{G},z\right) &= \frac{1}{N_{\mathrm{UC}}}\sum_{\alpha,\beta=1}^{2}\sum_{\mu,\nu=1}^{3}\left[v_{\alpha\mu}^{\mathrm{VB}}\left(\vec{k'}\right)\right]^{*}v_{\beta\nu}^{\mathrm{VB}}\left(\vec{k}\right)\times \\ &\sum_{i,j=1}^{N_{\mathrm{UC}}}\exp\left[-i\vec{k'}\cdot\left(\vec{U}_i+\vec{\tau}_\alpha\right)+i\vec{k}\cdot\left(\vec{U}_j+\vec{\tau}_\beta\right)\right]\times \\ &\iint_{R^2} d^2r\left\{e^{-i\left(\vec{G}-\vec{k'}+\vec{k}\right)\cdot\vec{r}}\varphi_{\alpha\mu}\left(\vec{r}-\vec{U}_i-\vec{\tau}_\alpha,z\right)^{*}\varphi_{\beta\nu}\left(\vec{r}-\vec{U}_j-\vec{\tau}_\beta,z\right)\right\}.\end{aligned} \quad (3.26)$$

We note that further discussion of details of properties of direct Coulomb interaction, e.g. behavior of pair densities, convergence issues, matrix elements symmetries, complex phase properties and description of their inter-valley behavior is moved to Appendix 6.9.

3.3.2 Electron-hole exchange matrix elements

In next step exchange Coulomb matrix elements are discussed. Expression for them, derived analogously to Eq. (3.24) is given by

$$V^X\left(\vec{k},\vec{k'}\right) = \frac{S}{(2\pi)^2}\left\langle v,\vec{k'}\left|c,\vec{k}\right|V\left|v,\vec{k}\right|c,\vec{k'}\right\rangle = \gamma\sum_{\vec{G}\neq 0}\frac{F^X\left(\vec{k},\vec{k'},\vec{G}\right)}{\left|\vec{G}\right|}, \quad (3.27)$$

with form factors

$$F^X\left(\vec{k},\vec{k'},\vec{G}\right) = \int dz \int dz' \rho_{vc}^{\vec{k'}\vec{k'}}\left(\vec{G},z\right)\rho_{cv}^{\vec{k}\vec{k}}\left(-\vec{G},z'\right)e^{-|z-z'|\cdot|\vec{G}|}. \quad (3.28)$$

There are several differences between direct and exchange electron-hole interaction. As can be seen from Eq. (3.12) direct interaction comes with negative sing (electron-hole attraction) and exchange one comes with positive sign (electron-hole repulsion). Contrary to direct matrix elements, there is no $1/|k-k'|$ overall dependence of magnitude of those elements, therefore potentially exchange interaction can be large whenever direct matrix elements are small due to large $|k-k'|$ distance. We note also, that interaction form factors F^D consist of pair densities diagonal in band indices ($\rho_{vv/cc}$) and off-diagonal with wave vector indices ($\rho^{kk'}$), while for exchange interaction form factors situation is opposite, i.e. there is off-diagonal dependence on band indices ($\rho_{vc/cv}$) and diagonal wavevector dependence ($\rho^{kk/kk''}$). Due to those properties, we found that direct matrix elements are in general complex numbers, while exchange matrix elements are real within numerical precision. Also, due to dependence only on

diagonal wavevector, exchange matrix element can be computed much faster that direct matrix elements. Further comparison of direct and exchange interaction is again moved to Appendix 6.9.

At this point we note also that at first look there is $G = 0$ singularity in V^X in Eq. (3.27). This singularity is generally problematic for 3D crystals and different methods of dealing with it has been discussed in literature.[751] However, we note that for 2D crystal, taking a limit result in zero

$$\lim_{\vec{G}\to 0} \frac{\int dz \int dz' \rho_{vc}^{\vec{k}'\vec{k}'}\left(\vec{G}, z\right) \rho_{cv}^{\vec{k}\vec{k}}\left(-\vec{G}, z'\right)}{\left|\vec{G}\right|} = 0. \tag{3.29}$$

Singular term, therefore, does not contribute to sum adding up to total value of V^X and can be excluded from summation over G vectors in Eq. (3.27).

3.3.3 Gauge choice in Coulomb matrix elements

As can be seen from Eq. (3.19) direct matrix elements are in general complex quantities, which phase is determined by numerical routines diagonalizing tight-binding Hamiltonian defined in Eq. (2.14) and therefore is rather random. One may wonder if Bethe-Salpeter-like equation defined in Eq. (3.12) is gauge-invariant, i.e., it does not depend on gauge choice of wavefunctions, which can be done arbitrarily for every band and k-point. To prove that eigenvalues of BSE and modules of exciton wavefunctions do not depend on gauge choice, it is instructive to analyze BSE eigenvalue problem for 3 k-points and direct interaction only. Because all matrix elements have the following arrangement of bands $\langle v|c|V|c|v\rangle$, we drop it for a moment for clarity and measure energy with respect to the band gap $\tilde{E} = E - \Delta_{gap}$:

$$\begin{vmatrix} \tilde{E} - \Delta E(k_1) & \langle k_2|k_1|V|k_2|k_1\rangle e^{i\varphi} & \langle k_3|k_1|V|k_3|k_1\rangle e^{i\varphi} \\ e^{-i\varphi}\langle k_1|k_2|V|k_1|k_2\rangle & \tilde{E} - \Delta E(k_2) & \langle k_3|k_2|V|k_3|k_2\rangle \\ e^{-i\varphi}\langle k_1|k_3|V|k_1|k_3\rangle & \langle k_2|k_3|V|k_2|k_3\rangle & \tilde{E} - \Delta E(k_3) \end{vmatrix} = 0 \tag{3.30}$$

To show how gauge choice affects this problem, $|v, k_1\rangle$ wavefunction has been multiplied by arbitrary phase $\exp(i\varphi)$. As known from theory of matrix diagonalization, when both row and column (without diagonal element) are multiplied by phase and conjugated phase, respectively, eigenvalues are not affected. We have checked that for such matrix also absolute values of eigenvectors are not affected. On the other hand, unsurprisingly, phase φ affects phase of exciton coefficients A defined in Eq. (3.2). This arbitrariness of phase choice may influence apparent symmetry of ground excitonic state, as already noted in literature.[545] One of the solutions to this problem is studying only observable quantities, like imaginary part of dielectric function ε_2, in which complex exciton amplitudes are multiplied by velocity operator matrix elements, which are constructed also from wavefunctions. Keeping track of phase in both should be enough to get gauge independent answer. On the other hand, one is sometimes interested in studying excitonic wavefunctions themselves. To obtain ground excitonic state

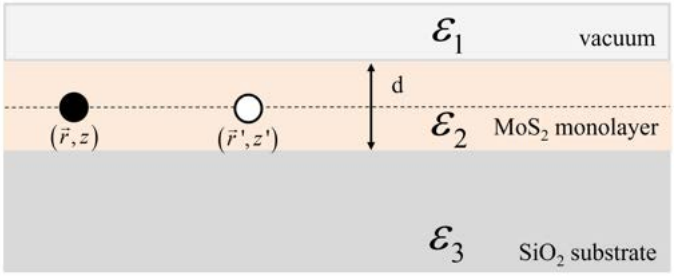

Figure 3.5: Schematic picture of dielectric environment of MX_2 monolayer.

with 1s symmetry various numerical approaches are used, however their details are rarely discussed in literature.[511,545] In our procedure, we follow idea introduced by Rohlfing and Louie,[511] in which global phase of tight-binding wavefunctions is chosen in such way, that the sum of imaginary parts is 0, i.e. $\sum_{\alpha=1}^{2}\sum_{\mu=1}^{3} \mathrm{Im} v_{\alpha\mu}^{(n)} = 0$. In next step, we rotate global phase in such a way to get phase 0 on $m_d = 0$ orbital, which means that phase of second TB coefficient is set to zero ($\mathrm{Im}\ v_{12} = 0$). Second gauge procedure actually breaks first property, however we found that this procedure is necessary to obtain numerically excitons in +K and -K valleys, which wavefunctions have the following property expected from time-reversal symmetry arguments

$$A_n(-k) = A_n^*(k). \tag{3.31}$$

3.3.4 Screening of Coulomb interactions

Additional complication in realistic description of Coulomb electron-hole interaction stems from screening of interaction by other carriers. As noted early in studies of graphene,[752] electron-electron interaction screening in 2D crystals behaves differently that in 3D crystals. It is, therefore, not enough to choose some "average" static screening, but more involved model has be used. Simplest known model that catches major linear dependence of screening in k space was derived in physics of thin dielectric slabs and is called Rytova - Keldysh (R.-K.) model.[563,564,752] In this theory bare Coulomb matrix elements $V^{D/X}$ are divided by function

$$V_{R-K}^{D/X}(q) = \frac{V_{bare}^{D/X}(q)}{[\varepsilon_r^{\text{R-K}}\,(1 + 2\pi\alpha\,|\vec{q}|)]}. \tag{3.32}$$

Counter-intuitively, static-like screening part ε_r depends not on material itself, but on surrounding material's dielectric properties $\varepsilon_r^{\text{R-K}} = (\varepsilon_1 + \varepsilon_3)/2$. This expression comes from theory of dielectric slab with finite width d surrounded by two semi-infinite dielectric with electric permeability $\varepsilon_1, \varepsilon_3$. In such theory

momentum transfer dependent screening can be derived in form

$$\varepsilon(q) = \underbrace{(\varepsilon_1 + \varepsilon_3)/2}_{\varepsilon_r^{\text{R-K}}} \left[1 + \underbrace{\frac{2\varepsilon_2^2 - (\varepsilon_1^2 + \varepsilon_3^2)}{2\varepsilon_2(\varepsilon_1 + \varepsilon_3)} d \cdot q}_{2\pi\alpha} \right]. \tag{3.33}$$

In the numerical results for MoS_2 discussed in next sections we take for concrete case of MoS_2 (with "effective " thickness $d = 6.14$ Å) on top of bulk SiO_2 ($\varepsilon_3 = 4$) crystal,[143,753] as shown schematically in Fig. 3.5. Next we assume that from the top crystal is surrounded by vacuum, therefore we take $\varepsilon_3 = 1$. As known from literature,[754] more advanced models of screening do not affect significantly exciton spectra. This is related to the property, that R.-K. model describes well screening from *ab initio* and only for large k-space distance (when matrix elements are small due to $1/|k - k'|$ dependence) there is substantial difference between "correct" and approximated screening model.

We note that for testing purposes and to gain insight we use also static dielectric constant model $\varepsilon_r^{\text{stat.}}$ as simply $V_{stat.}^{D/X}(q) = V_{bare}^{D/X}(q)/\varepsilon_r^{\text{stat.}}$. Value of $\varepsilon_r^{\text{stat.}}$ is taken as 5.74 to yield 1s A exciton binding energy close to experimental value (400 meV) when parabolic model of bands is assumed with effective electron and hole masses 0.44 and 0.54 m_0, respectively. We point also to the issue of (already mentioned) screening of exchange interaction, which is absent in field-theoretically derived Bethe-Salpeter equation. Role of screened exchange interaction and possible higher-order corrections of this approach are left for future study, because in CI language they naturally have to include coupling to more-than-single excitation basis (e.g. bi-excitons), which is beyond our current computational possibilities for excitonic problem in reciprocal space language.

3.3.5 Singularity in Coulomb matrix elements

Just as for exchange Coulomb interaction discussed above, it is easy to understand that diagonal term of direct electron-hole interaction in BSE given by Eq. (3.12) is singular at $k = k'$ and $G = 0$. Renormalization due to this singularity has to be included in simulations on finite lattice, otherwise numerical results (which we have done for parabolic model) give vastly different results when compared with theoretical predictions. We note that dealing with singularity is connected with discretization of BZ associated with single valley. Below we discuss rectangular discretization of the lattice, which will be described better in next Section. Confining our discussion to the case of G=0 for a moment, one of the methods allowing to integrate out singularity is to note that form factor $F^D(k = k', G = 0) = 1$ and make an approximation that inside box centered around point (k_x,k_y) exciton wavefunction takes constant value. This approximation is naturally more and more exact with increasing number of points (and decreasing area associated with each k point) into which BZ is discretized. This

allows us to approximate diagonal of BSE interaction kernel as

$$\int_{k_x-\delta k/2}^{k_x+\delta k/2}\int_{k_y-\delta k/2}^{k_y+\delta k/2} dk'_x dk'_y \frac{A_n\left(\vec{k'}\right)}{\left|\vec{k}-\vec{k'}\right|} \approx$$
$$A_n\left(\vec{k}\right)\int_{-\delta k/2}^{\delta k/2}\int_{-\delta k/2}^{\delta k/2} dk'_x dk'_y \frac{1}{\sqrt{k_x'^2+k_y'^2}} = \tag{3.34}$$
$$A_n\left(\vec{k}\right)\left[2\ln\frac{\sqrt{2}+1}{\sqrt{2}-1}\right]\delta k = A_n\left(\vec{k}\right)\mathrm{V_{sin.}}\delta k.$$

We note that this result assumes constant, static screening of electron - hole interaction and in principle should be re-calculated when R.-K. screening model is used. Also, the $G = 0$ term is the leading one, however summation over G vectors introduces further corrections into singular term. We checked numerically that both effects introduce contributions that are at least 2 orders of magnitude smaller than expression given in Eq. (3.34) and are neglected in further studies. We note that constant $V_{sin.} \approx 3.5255$ is calculated for rectangular lattice with area of BZ around single point given by $(\delta k)^2$ and it should be changed to $V_{sin.} \approx 3.2325$ for rhomboidal lattice with analogous rhombus area given by $\sqrt{3}(\delta k)^2/2$ under the same approximations as for rectangular discretization scheme.

3.3.6 Interaction form factor approximation theory

In the last part of this section we build systematic theory of approximation of direct electron-hole matrix elements. As a first step we note that in equation for matrix elements entering BSE are

$$V^D\left(\vec{k},\vec{k'}\right) = \gamma\sum_{\vec{G}}\frac{1}{\left|\vec{k'}-\vec{k}-\vec{G}\right|}\times F^D\left(\vec{k},\vec{k'},\vec{G}\right). \tag{3.35}$$

Calculation of interaction form factors F^D is a major bottleneck of both *ab initio* and TB calculations due to necessity of calculating them for all combinations of k and k' and additional summation over reciprocal lattice vectors G. Simplest solution is to assume all form factors to be one (their highest possible value, exact for k=k' and G=0) and note, that highest value entering sum over G vectors comes from G's minimizing $|k - k' - G|$ distance. We checked that this approximation is relatively useful around K point, for which neighborhood form factor absolute value deviates from one rather slowly. Example of such "additional" $1/|K - k'|$ dependence can be observed in Fig. 3.6 (a). In Fig. 3.6 (b) we present why distance between k and k' points should be calculated with respect to reciprocal lattice vector. Because we are in first Brillouin zone, there are three equivalent K point per valley. However, if we take k point from neighborhood of one K point and k' from other, naively this distance is large (of the order of reciprocal lattice vectors G). One the other hand, when points in hexagonal BZ are transformed to create triangle around one K-point (which

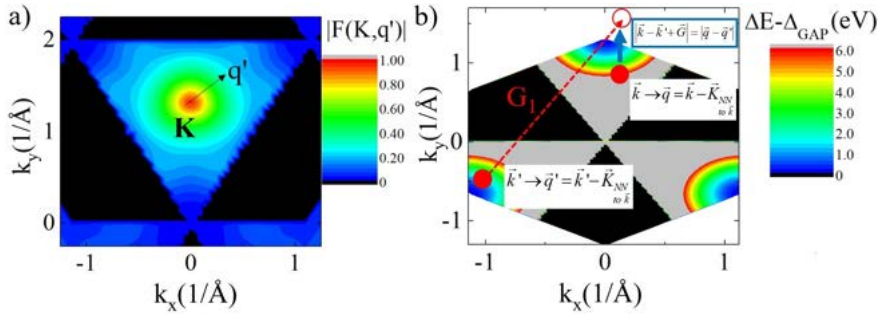

Figure 3.6: (a) Absolute value of form factor $F^D(K, k', G = 0)$. (b) Construction of simplified "$1\|q - q'|$" interaction model. Figure reproduced from Ref. 5.

gives 3 equivalent Γ points in vertices), it is clear that correct way of measuring distance in reciprocal space is given by $|q-q'|$, where q vectors are now measured from nearest K - point. This reasoning resembles well known problem of "Umklapp scattering", known from theory of electron-phonon and phonon-phonon scattering. Due to $1/|q - q'|$ dependence we call this approximation "simplified $1/|q - q'|$ interaction".

Approximation described above allows to reproduce numerically analytical solutions for simple model of exciton with electron/hole dispersion in parabolic approximation. It's main deficiency is that it does not include any effects related to orbital composition of bands (no Bloch function effect) and is purely real, which always gives degenerate states in exciton spectrum with the same exciton angular momentum quantum numbers, e.g. $2p_x$ excitonic state is degenerate with $2p_y$ state. To motivate a way around this problem, let us first discuss which parts of full, complex form factor influence mostly it's value. For concreteness, let us check for example difference between form factor describing scattering between one chosen k point to some $k' + \Delta k'$ point ($\Delta k'$ is assumed to be small):

$$V^D\left(\vec{k}, \vec{k'} + \Delta\vec{k'}\right) = \gamma \sum_{\vec{G}} \frac{1}{\left|\vec{k'} + \Delta\vec{k'} - \vec{k} - \vec{G}\right|} \times F^D\left(\vec{k}, \vec{k'} + \Delta\vec{k'}, \vec{G}\right). \quad (3.36)$$

Form factor for such matrix element is given by

$$F^D\left(\vec{k}, \vec{k'} + \Delta\vec{k'}, \vec{G}\right) = \int dz \int dz' \rho_{vv}^{\vec{k'}+\Delta\vec{k'}\vec{k}}\left(\vec{G}, z\right) \rho_{cc}^{\vec{k}\vec{k'}+\Delta\vec{k'}}\left(-\vec{G}, z'\right) \times \times e^{-\left|z-z'\right|\cdot\left|\vec{k'}+\Delta\vec{k'}-\vec{k}-\vec{G}\right|}. \quad (3.37)$$

One can observe that effect of $\Delta\vec{k'}$ on matrix element V^D is complicated, because it affects

- denominator in Eq. (3.36)
- tight-binding coefficients inside $\rho_{vv/cc}$
- exponent value depending on z,z'

- details of in-plane integration of Slater orbitals and summation over unit cells (inside $\rho_{vv/cc}$ as apparent from Eq. (3.26)).

We checked numerically, implementing in code selective turning on/off of all above contributions, that actually first two corrections (denominator and TB coefficient) yield very good approximation to matrix elements and the last two (exponent and details of integration) do not contribute too much. This motivated us to extract TB coefficients from form factors, giving expression formally equivalent to Eq. (3.25) with implicit summation over sublattices (α, β) and orbitals (μ, ν) that can be written as

$$F^D\left(\vec{k},\vec{k'},\vec{G}\right) = \sum_{\alpha\beta\alpha'\beta'=1}^{2}\sum_{\mu\nu\mu'\nu'=1}^{3} C^{TB}_{\alpha\beta\alpha'\beta'\mu\nu\mu'\nu'}\left(\vec{k},\vec{k'}\right)\cdot F_{\alpha\beta\alpha'\beta'\mu\nu\mu'\nu'}\left(\vec{k},\vec{k'},\vec{G}\right), \tag{3.38}$$

where C^{TB} coefficient is given by product of 4 wavefunction coefficients

$$C^{TB}_{\alpha\beta\alpha'\beta'\mu\nu\mu'\nu'}\left(\vec{k},\vec{k'}\right) = \left[v^{VB}_{\alpha\mu}\left(\vec{k'}\right)\right]^* v^{VB}_{\beta\nu}\left(\vec{k}\right)\left[v^{CB}_{\alpha'\mu'}\left(\vec{k}\right)\right]^* v^{CB}_{\beta'\nu'}\left(\vec{k'}\right) \tag{3.39}$$

and quantity we call "orbital form factor" $F^D_{\alpha\beta\ldots}$ given by

$$\begin{aligned} &F_{\alpha\beta\alpha'\beta'\mu\nu\mu'\nu'}\left(\vec{k},\vec{k'},\vec{G}\right) = \\ &\int dz \int dz' \tilde{\rho}^{\vec{k'}\vec{k}}_{\alpha\beta\mu\nu}\left(\vec{G},z\right)\tilde{\rho}^{\vec{k}\vec{k'}}_{\alpha'\beta'\mu'\nu'}\left(-\vec{G},z'\right)e^{-|z-z'|\cdot|\vec{k'}-\vec{k}-\vec{G}|}. \end{aligned} \tag{3.40}$$

Those orbital form factors depend on analogues of product densities, now in the form that does not depend on TB coefficient's v:

$$\begin{aligned} &\tilde{\rho}^{\vec{k'}\vec{k}}_{\alpha\beta\mu\nu}\left(\vec{G},z\right) = \frac{1}{N_{UC}}\sum_{i=1}^{N_{UC}}\sum_{j=1}^{N_{UC}}\exp\left[i\left(\vec{k'}\left(\vec{U}_i+\vec{\tau}_\alpha\right)+\vec{k}\left(\vec{U}_j+\vec{\tau}_\beta\right)\right)\right]\times \\ &\times\int d^2r \exp\left[-i\left(\vec{G}-\vec{k'}+\vec{k}\cdot\vec{r}\right)\right]\left[\phi_{\alpha\mu}\left(\vec{r}-\vec{U}_i-\vec{\tau}_\alpha,z\right)\right]^*\phi_{\beta\nu}\left(\vec{r}-\vec{U}_j-\vec{\tau}_\beta,z\right) \end{aligned} \tag{3.41}$$

This method, being equivalent to Eq. (3.25) is not faster, however it helps to realize, that C^{TB} coefficient can be calculated very fast from TB model and we can take only orbital form factor at $k'-k-G=0$ limit. This approximation is conceptually equivalent to treating long-range Coulomb interaction as not dependent on details of orbital structure. Taking this limit gives

$$F_{\alpha\beta\alpha'\beta'\mu\nu\mu'\nu'}\left(\vec{k}-\vec{k'}-\vec{G}=0\right) = \delta_{\alpha\beta}\delta_{\alpha'\beta'}\delta_{\mu\nu}\delta_{\mu'\nu'}e^{i\vec{G}\left(-\vec{\tau}_\alpha+\vec{\tau}+\alpha'\right)}. \tag{3.42}$$

Final equation for direct form factor is therefore simplified to

$$\begin{aligned} F^D\left(\vec{k},\vec{k'},\vec{G}\right) = \sum_{\alpha\alpha'=1}^{2}\sum_{\mu\mu'=1}^{3}&\left[v^{VB}_{\alpha\mu}\left(\vec{k'}\right)\right]^* v^{VB}_{\alpha\nu}\left(\vec{k}\right)\left[v^{CB}_{\alpha'\mu'}\left(\vec{k}\right)\right]^* v^{CB}_{\alpha'\mu'}\left(\vec{k'}\right)\times \\ &\times e^{i\vec{G}\left(-\vec{\tau}_\alpha+\vec{\tau}+\alpha'\right)}. \end{aligned} \tag{3.43}$$

Up to our knowledge this expression is different to similar ones available in literature,[539,541,543,755] which are always taken for G=0. We note that phase rotation given by this term is either 1 or C_3 rotation (by phase factor $\exp(\pm 2\pi/3)$) and allows to choose arbitrarily centered Brillouin zones. Discussion comparing excitonic spectrum obtained by using full form factors and approximate ones in moved to Appendix 6.9. We note that all our main results have been obtained with full form factors without reducing orbital form factors.

3.4 Exciton fine structure

As known from literature and from our own experience, computation of excitonic spectrum is a numerically challenging task. To lower computational complexity let us discuss now precisely how excitonic fine structure calculations are performed. First, we discretize Eq. (3.12) neglecting electron - hole exchange interaction, since it is much weaker than direct electron - hole interaction. Also, we choose in summation over k' wavevectors only those associated with one valley, as shown in Fig. 3.1. Remembering about singular terms as discussed previously, Bethe-Salpeter like equation for one valley takes form

$$\begin{aligned} &\left[\Delta E\left(\vec{k}\right) - \Delta_{\mathrm{GAP}} - V_{\mathrm{sin.}}\right] A_n\left(\vec{k}\right) \\ &- \sum_{\vec{k}' \neq \vec{k}}^{1/2\mathrm{BZ}} (\delta k)^2 V^D\left(\vec{k}, \vec{k}'\right) A_n\left(\vec{k}'\right) = E_n A_n\left(\vec{k}\right). \end{aligned} \tag{3.44}$$

This equation represents dense, Hermitean matrix problem that is solved numerically. Primary convergence parameter is number of k vectors into which single valley was discretized. Details of computations and convergence studies will be presented in next Section.

Now let's discuss further steps of fine structure calculations. First we add spin splitting to both valence and conduction bands. Spin-splitting modifies electron-hole energy difference $\Delta E\left(\vec{k}\right) = \varepsilon^{\sigma}_{\mathrm{CB}}\left(\vec{k}\right) - \varepsilon^{\sigma'}_{\mathrm{VB}}\left(\vec{k}\right)$. To calculate matrix elements, we choose to use spinless wavefunctions due to their negligible dependence on spin. By this method we are able to obtain fine structure in one valley (e.g. +K), i.e. bright (spin-like) and dark (spin-unlike) A and B excitonic series. Calculation of fine structure in one valley (+K) automatically gives fine structure in the other one (-K) due to symmetry of energies $E_n(+K) = E_n(-K)$ for spin-flipped configurations of excitons. We found also that with proper gauge of matrix elements (first Rohlfing, Louie method, then setting phase of $m_{d=0}$ spinor component to 0), the following property of matrix elements between valleys is satisfied $V\left(-\vec{k}, -\vec{k}'\right) = V\left(\vec{k}', \vec{k}\right)$. Implementing this symmetry in BSE one can prove formally, that exciton wavefunctions have to be related to each other as $A^*_n\left(-\vec{k}\right) = A_n\left(\vec{k}\right)$. We checked numerically, performing separate, full calculations in +K and -K valleys that our implementation satisfies this properties, giving within numerical precision same excitonic spectrum and phases of excitonic states related by mirror symmetry of k vector and complex conjugation

$\left(A_n^*\left(-\vec{k}\right) = A_n\left(\vec{k}\right)\right)$.

Having obtained fine structure spectrum for spin, next step is to include interactions "missing" from Eq. (3.44). We follow and expand the idea of "Ising excitons" basis,[527] taking 4 lowest states (1st and 2nd shell of 2D exciton) ordered in matrix notation as ${}^{\uparrow}_{\uparrow}\hat{A}^{+K}_{\text{bright}} = \text{diag}\left(E_{1s}, E_{2p_1}, E_{2p_2}, E_{2s}\right)$. Then, full Bethe-Salpeter-like problem, including intra- and inter-valley exchange interactions and inter-valley direct interaction, can be written as

$$\hat{H}^{FS} = \begin{bmatrix} H_{+K,+K} & H_{+K,-K} \\ H^{\dagger}_{+K,-K} & H_{-K,-K} \end{bmatrix} \tag{3.45}$$

$$H_{+K,+K} = \begin{bmatrix} {}^{\uparrow}_{\uparrow}\hat{A}^{+K}_{\text{bright}} + V^X & 0 & V^X & 0 \\ 0 & {}^{\downarrow}_{\uparrow}\hat{A}^{+K}_{\text{dark}} & 0 & 0 \\ V^{X\dagger} & 0 & {}^{\downarrow}_{\downarrow}\hat{B}^{+K}_{\text{bright}} + V^X & 0 \\ 0 & 0 & 0 & {}^{\uparrow}_{\downarrow}\hat{B}^{+K}_{\text{dark}} \end{bmatrix}$$

$$H_{-K,-K} = \begin{bmatrix} {}^{\downarrow}_{\downarrow}\hat{A}^{-K}_{\text{bright}} + V^X & 0 & V^X & 0 \\ 0 & {}^{\uparrow}_{\downarrow}\hat{A}^{-K}_{\text{dark}} & 0 & 0 \\ V^{X\dagger} & 0 & {}^{\uparrow}_{\uparrow}\hat{B}^{-K}_{\text{bright}} + V^X & 0 \\ 0 & 0 & 0 & {}^{\downarrow}_{\uparrow}\hat{B}^{-K}_{\text{dark}} \end{bmatrix}$$

$$H_{+K,-K} = \begin{bmatrix} V^X & 0 & -V^D + V^X & 0 \\ 0 & 0 & 0 & -V^D \\ -V^D + V^X & 0 & V^X & 0 \\ 0 & -V^D & 0 & 0 \end{bmatrix}$$

We note that to solve such matrix problem, it is necessary to know matrix elements constructed using excitonic wavefunctions $A(\vec{k})$. For example, matrix elements for intra-valley exchange interaction V^X are given by

$$\left[UV^XU^{\dagger}\right]_{ij} = \sum_{\vec{k},\vec{k'}}^{1/2\text{ BZ}} A_i^*\left(\vec{k}\right) A_j\left(\vec{k'}\right) V^X\left(\vec{k},\vec{k'}\right). \tag{3.46}$$

where U are matrices diagonalizing single-valley, direct-interaction only Bethe-Salpeter-like equation. We note that using this method allows to undersand role of exchange interaction from the point of view of coupling between different excitonic states. Also, due to high localization of excitons in k-space, summation in Eq. (3.46) doesn't have to run through all k points in single valley, but might be easily restricted to part of BZ in which exciton wavefunctions are nonzero. This reduces greatly number of electron-hole exchange inetractions matrix elements V^X that need to be calculated.

3.5 Computational details

In the following section let us discuss several numerical aspects of exciton calculations. First, as mentioned previously, equation for exciton has to be discretized

on part of the Brillouin zone associated with one valley. This discretization can be performed in several ways. As shown in Fig. 3.7 (a), one can either discretize whole Brillouin zone using rectangular grid and then choose points associated with one valley or chose only one "wedge" in one valley ("kite" inside rectangle in Fig. 3.7 (a)) and then rotate it by $\pm C_3$ operation. Those two choices, in

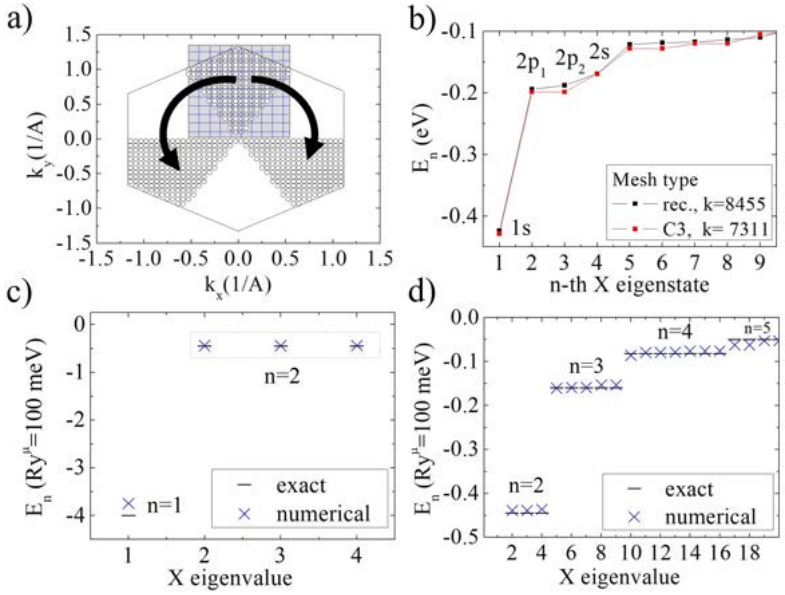

Figure 3.7: (a) Possible two choices of k-points grid, either by rectangular discretization of whole BZ and choice of one valley, or choice of one wedge and then wedge rotation by $\pm C_3$ symmetry operation. (b) Comparison of exciton spectra for two choices of lattice discretization. (c), (d) Comparison of theoretical result for parabolic exciton model and highly converged numerical calculation performed on 120 000 k-points lattice for (c) first two excitonic shells and (d) 2-5 excitonic shells. Figure reproduced from Ref. 5.

principle, should give exactly the same results in the limit of large number of k points (very dense grid). However, because of calculation can be done only for limited number of k - points (which sets our dense matrix size, limited mainly by RAM memory available on a given node in HPC clusters and diagonalization of such large matrix time), finite size effect distinguish between those two choices. As shown in Fig. 3.7 (b), in second shell expected degeneracy of p states is much better for C_3 grid. We note that 2s state is not degenerate with 2p states due to too small number of k - points. We studied systematically how many k-points we need to include to reliably talk about excited excitonic shells, comparing analytical and numerical results for a parabolic model. Our findings are summarized in Table 3.1.

As presented in Fig. 3.7 (c-d) excitonic spectrum is well converged to theoretical values for shells 2-4, however for higher shells relative precision is getting worse. Surprisingly at first sight, 1s excitonic state seems to deviate significantly from theoretical value -4 Ry. We traced this effect back to shape of our computa-

excitonic shell	precision (meV)	# of k-points
n=1	20	≈3200
n=2	20	≈7300
n=3	14	≈40 000
n=4	4	≈120 000

Table 3.1: Estimation of number of k-points necessary to converge n-th excitonic shell.

tional box in k-space, which in parabolic exciton model in principle should be circular and infinitely large. In our calculation it has triangular shape, therefore for strongly bound excitons (small in real space, large in k-space) exciton wavefunction "feels" boundaries of computational box. One can get rid of this effect by increasing screening and making excitons larger in real (small in reciprocal) space and simultaneously increasing number of k points.

Results presented above are calculated for parabolic model dispersion of electron and hole energies and simplified "1/|q-q'|" type of interaction which does not include effects related to carrier wavefunctions. Inclusion of those is computationally hard procedure that we discuss now. For example of lattice giving reasonably converged second shell of exciton, one needs ≈ 7000 k-point k grid. This requires calculating $\approx 7000^2/2 \approx 10^6$ matrix elements. We perform this calculation in HPC cluster, calculating first form factors F^D as defined in Eq. (3.25) and saving them in permanent memory. When all form factors are available, we use them in BSE calculations, during which form factor database is used for $V^D = \sum_G^{|G_{cutoff}|} \frac{F^D(k,k',G)}{|k'-k-G|}$ matrix elements evaluation. Summation over reciprocal lattice vectors sets how many form factors are necessary and greatly affects computational time. In Fig. 3.8 we show convergence of one exemplary matrix element $V^D(k = K, k' = Q)$. In our calculation we were able to reach only $G_{cutoff} = G_1$, therefore we estimate precision of magnitude of our matrix elements to be underestimated by $\approx 20\%$. Even though relative error of value of matrix element is similar to only one G=0, we perform summation of 7 - G's to assure proper symmetry for scattering between k' and k when distance in "shortened" by G - vector, as discussed previously. Further details of numerical integrations, performed using trapezoid numerical integration methods (we always do only 2D integrals, first for ρ's, then for z, z' integration) are $N_{UC} = 7$, integration grid density set to $0.5a_B$ (Bohr radius), $z_{min/max} = \mp 5.0a_B$. Whenever possible, we first calculate values of integrals on some sparse real-space grids and if value is above properly defined threshold, we improve numerical convergence of a given integral by increasing grid density 50x fold. We estimate that our choice of details of integrations affects single form factor $F^D(k, k', G)$ by less than 10%.

Having discussed convergence of energies E_n and form factors F^D, let us turn to study of exciton wavefunctions $A_n(k)$, focusing on how we identify their symmetry (how we assign labels s, p, d). Wavefunctions A_n are obtained from diagonalization of BSE given by Eq. (3.44). In Fig. 3.9 (a) and (b) we show for reference how excitons look in k-space in simplest parabolic exciton model.

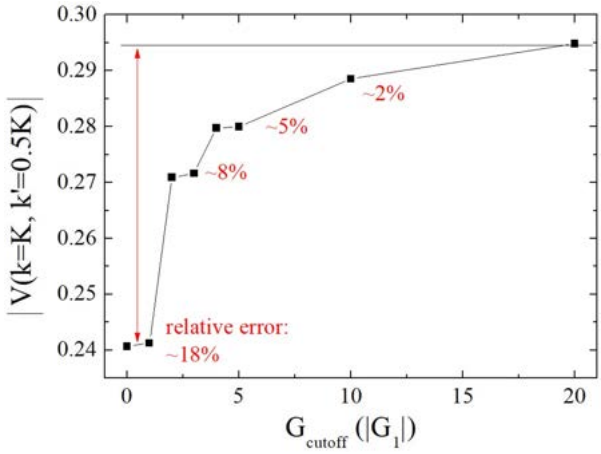

Figure 3.8: Convergence of exemplary direct Coulomb matrix element in function of G_{cutoff} which defines number of G vectors included in summation inside those elements. Figure reproduced from Ref. 5.

One can clearly distinguish 1s and $2p_x$ states, first having maximum at K point (center of triangle representing +K valley) and rotational symmetry and second having node structure and minimum at +K. This behavior is in contrast with results obtained for full tight-binding calculations with complex electron-hole interaction, shown in Fig. 3.9 (c-d). Although 1s state amplitude is similar (even though there is a complex phase present even for 1s state), novel $2p_-$ state no longer posses nodal structure, but interestingly has circular symmetry, just as s-like state. On the other hand, contrary to s-like state, it has minimum at it's center. We trace this state to be linear combination of p_x and p_y states ($2p_\pm = 1/\sqrt{2}(2p_x \pm i2p_y)$) which has exactly these properties. As will be discussed later, this mixing results from the fact that electron - hole direct interaction is complex. Due to topology of electron and hole wavefunctions, states with non-zero L feel "geometric" analog of magnetic field, usually called Berry's field strength and couple to each other.

3.6 Excitonic spectrum of MoS_2

In the following Section results of numerical studies of Bethe-Salpeter-like equation for excitonic states will be discussed. In presentation that follows we detach theory describing electron-hole transition energies from model of electron-hole interaction used (e.g. we study tight-binding model with simple $1/|q-q'|$ interaction model). Two types of screening are used, i.e., static and R.-K. screening. Rationale for subsequent parts is to present different renormalization processes affecting excitonic spectrum, leading to more and more realistic description of excitonic series. In our results we decide to discuss excitonic binding energies in units of excitonic Rydberg $\text{Ry}^\mu = \frac{\mu e^2}{2\hbar^2\varepsilon^2}$ to detach them from specific value of static screening. Value of Ry depends in parabolic approximation on effec-

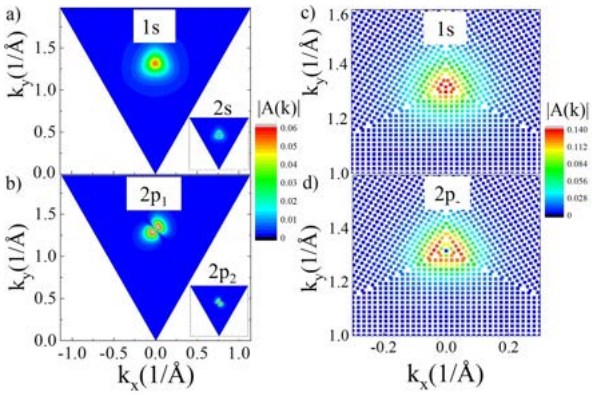

Figure 3.9: Exciton wavefunction amplitudes on numerical k-grid with K point at the center. (a) 1s type state (2s in the inset), (b) 2p1 (2p2 in the inset) excitonic states for simplified $1/|q-q'|$ interaction model. Results in (c) and (d) show how full tight-binding energies and wavefunctions do not modify in principle amplitude of 1s state, however influence strongly 2p - like state, that due to chirality of interaction becomes mixture of $2p_x$ and $2p_y$ state. Figure reproduced from Ref. 5.

tive masses of electron and hole through reduced mass $\mu = (1/m_e^* + 1/m_h^*)^{-1}$ and static screening parametrized by $\varepsilon = 4\pi\varepsilon_0\varepsilon_r^{stat.}$. Discussion of analytically solvable problem of exciton in effective mass approximation is presented in Appendix 6.7.

3.6.1 Role of Q-points and band nesting

In the following Section effect of band structure (electron and hole dispersion) on excitonic levels is discussed. How different dispersion models affect electron-hole dispersion energies is summarized in Fig. 3.10. Those direct transition energies enter as diagonal of Bethe-Salpeter-like equation that is corrected by singular term. Eq. 3.44 is solved first for parabolic dispersion model, simplified $1/|q-q'|$ interaction and static screening. Excitonic spectrum gives numerically (as expected from theory) binding energy of first $1s$ state close to -4 Ry$^\mu$ (deviation already identified as finite BZ effect) and degenerate second shell of three states: $2s$, $2p_x$, $2p_y$, which energy is close to theoretically known value $E_{n=2-4} = -4/9$ Ry$^\mu$.

In next calculation, we change the dispersion model to massive Dirac fermion, keeping interaction as $1/|q-q'|$. We notice that binding energy of 1s state lowers to ≈ -5.5 Ry$^\mu$. This behavior can be understood as increased "average" effective mass, i.e. carriers in massive Dirac fermion model on average taken over BZ are described better by higher effective mass than in parabolic model. This naturally leads to stronger binding corresponding to lower energy of 1s state. We observe also larger separation between first and second shell and small breaking of degeneracy between $2s$ and $2p_x, 2p_y$ states within second shell.

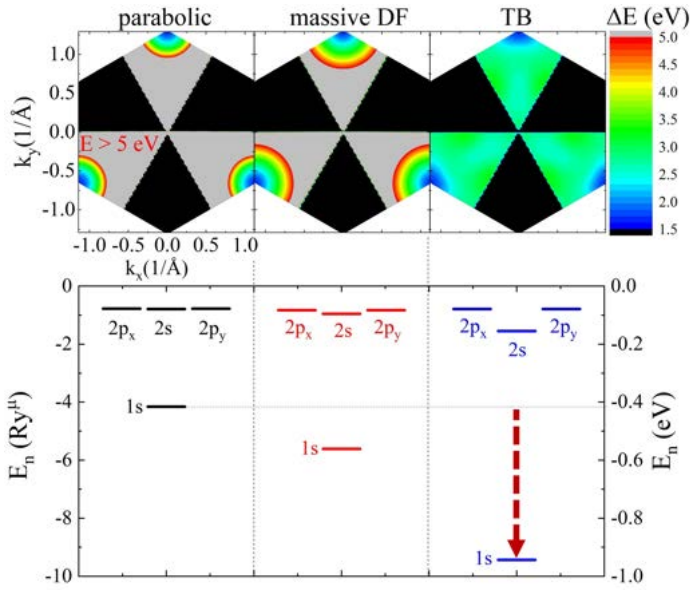

Figure 3.10: (Top panel) Electron-hole transition energies obtained using three different dispersion models, displayed in one valley. (Bottom panel) Excitonic spectrum calculated using simplified interaction $1/|q-q'|$. Parameters of screening are chosen in such way to reproduce Ry = 100 meV, corresponding to experimental estimates for 1s exciton binding energy $E_1 \approx 400$ meV for MoS_2 on SiO_2. Red arrow shows general trend and should be compared with opposite effect presented in Fig. 3.12. Figure reproduced from Ref. 5.

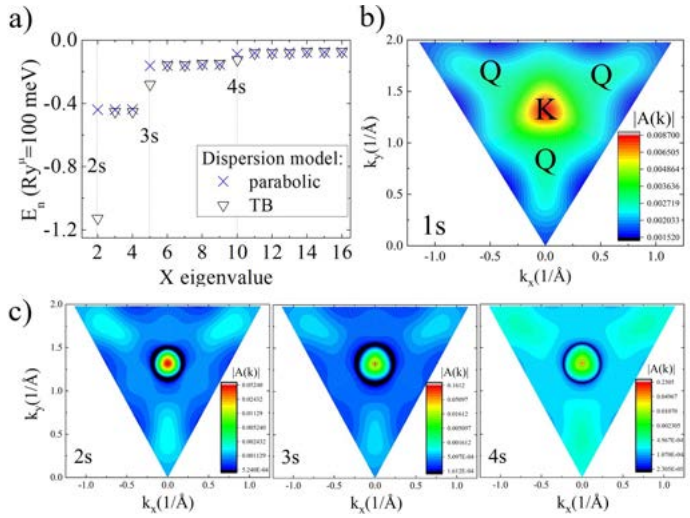

Figure 3.11: (a) n>1 excitonic shells calculated for parabolic and TB dispersion models, simplified $1/|q-q'|$ interaction and static screening. Exciton wavefunction for (b) 1s and (c) 2s to 4s states. Logarithmic color scale representing magnitude of $|A_n(k)|$ is used. Single valley BZ is discretized to 120 000 k-points, necessary for converged calculation up to 4-th excitonic shell. Figure reproduced from Ref. 5.

Finally, when tight-binding dispersion model is used, effects described for massive DF model become even more pronounced. Energy of $1s$ lowers as much as to -10 Ry^{μ}, there is large renormalization of 1s - 2s states energy difference and states with exciton angular momentum L=0 (2s) and |L|=1 are clearly no longer degenerate, as shown in Fig. 3.10. Similar effect is observed for higher shells, as shown in Fig. 3.11 (a). In addition to "average lowering" of effective mass process, there is pronounced contribution coming from existence of Q points, that can be observed in excitonic wavefunctions, as shown for $1s-4s$ states in Fig. 3.11 (b-d). Breaking of degeneracy of 3s and 4s state for $L \neq 0$ is also clearly observed, together with breaking of degeneracy of states with different L. We conclude that due to existence of 3 Q points around K point in single valley, full rotational symmetry of s-like states in broken and therefore those states react more strongly than others to dispersion model change from parabolic to TB.

3.6.2 Role of interactions screening

As discussed in subsection "Screening of Coulomb interactions", static screening does not describe faithfully actual screening of interactions in 2D semiconductors. Simplest correction, capturing non-locality of screening via it's $|q-q'|$ dependence can be modeled by Rytova-Keldysh theory and parametrized by polarizability parameter α. In our calculation we use simplified direct matrix

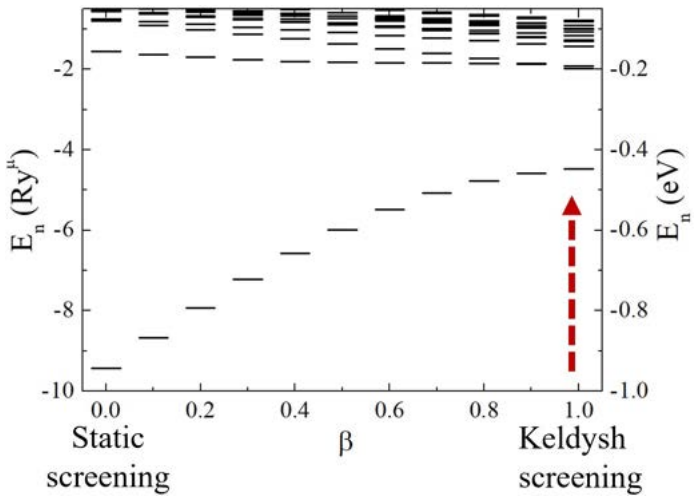

Figure 3.12: Difference between static ($\beta = 0$) and Rytova-Keldysh ($\beta = 1$) screening for TB dispersion and $1/|q-q'|$ interaction V^D. Polarizability is taken as $\alpha = 2.2$ Å. Renormalization trend is shown with red arrow, which should be compared with Fig. 3.10. Figure reproduced from Ref. 5.

element entering Eq. (3.44) in the following form:

$$V^D\left(\vec{k},\vec{k'}\right) = \frac{1}{|q-q'|} \times \left(\frac{1-\beta}{\varepsilon_r^{\text{st at.}}} + \frac{\beta}{\varepsilon_r^{\text{R-K}}\left(1+2\pi\alpha\left|\vec{k'}-\vec{k}-\vec{G}\right|\right)} \right), \tag{3.47}$$

where β controls switching between static and R.-K. screening.

In Figure 3.12 we present how excitonic spectrum gets renormalized for TB model dispersion and $1/|q-q'|$ interaction when static screening is switched from homogenous one ($\beta = 0$) to R.-K. model ($\beta = 1$). One can observe, that non-local screening has opposite effect than changing dispersion from parabolic to TB, and $1s$ state energy rises from -10 Ry$^\mu$ back to approximately - 4 Ry$^\mu$. Also, split $L = 0$ and $L \neq 0$ excited exciton states change their energies drastically, reversing order of states as well, i.e., for $\beta = 0$ order of states is $1s - 2s - 2p_{x,y}$, while for $\beta = 1$ we obtain $1s - 2p_{x,y} - 2s$, consistent with literature.[195,203]

3.6.3 Renormalization of spectrum from "2D-like"to "3D-like"

In addition to effects of dispersion and screening renormalizing 2D exciton spectrum, direct - electron hole interaction form factors F^D have to be taken into account. Generally speaking, because their value is ≤ 1, their averaged effect translates into lowering absolute value of binding energy and pushing excitonic shells towards each other. Focusing for a moment on absolute values of form factors, result of calculation on 7000 k-point grid (largest we were able to study with full effect of wave functions calculated with form factors given by Eq. (3.28)

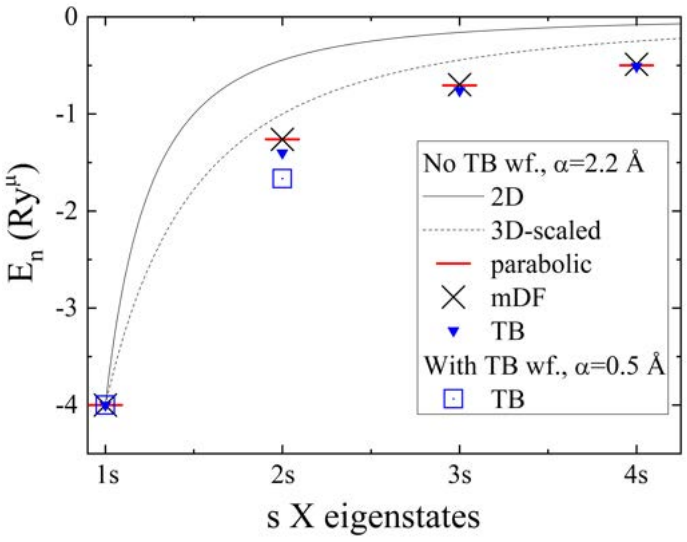

Figure 3.13: Excitonic series of s states for different models of dispersion (calculated with R.-K. screening and simplified $1/|q-q'|$ interaction) and with effect of full TB wavefunctions vs 2D and 3D exciton spectrum, all scaled to give the same energy of 1s state. Figure reproduced from Ref. 5.

) that allows for reliable discussion of only first and second shell is shown in Fig. 3.13. We conclude that collective effect of renormalization of 2D Rydberg series by dispersion, interaction screening and carrier wavefunctions is to make s-like series look like "more than 3D" exciton. It means that even though exciton is physically confined to 2D plane of MX_2, it's excited state series resembles more 3D excitonic Rydberg ladder of states. We note that non-hydrogenic Rydberg series is usually explained as effect of non-local screening.[173] With respect to literature known to us, we add to this understanding that it is not only related to screening, but depends also heavily on proper dispersion modeling (especially secondary minima in CB at Q points) and inclusion of proper wavefunction effects affecting interaction form factors F^D.

3.6.4 Effects of form-factor and topology of interactions

As mentioned before, taking into account electron and hole wavefunctions affects exciton fine structure by contributing to renormalization of s-like states. In addition to that, another interesting effect occurs. Because direct electron-hole interaction depends on wavefunctions, it's value is in general complex and phase of matrix elements $V^D(\vec{k},\vec{k}')$ cannot be transformed to zero by any gauge transformation. Taking as an example matrix elements describing scattering of excitons from $\vec{K}$ point to some $\vec{k}'$ points close to $\vec{K}$ and described as $\vec{k}' = \vec{K} + qe^{i\phi}$ we have

$$V^D\left(\vec{k}=K,\vec{k}'=\vec{K}+qe^{i\varphi}\right) = \left|V^D\left(\vec{k}=K,\vec{k}'=\vec{K}+qe^{i\varphi}\right)\right| e^{i\theta}. \qquad (3.48)$$

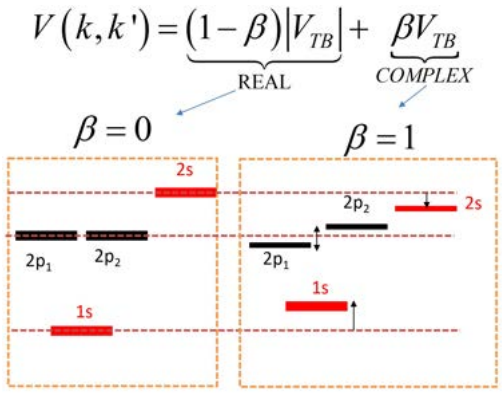

Figure 3.14: Schematic diagram how turning on phase of matrix elements affects first two shells of excitonic spectrum.

Our numerical result is such that absolute values of such matrix elements calculated between $\vec{K}$ point and points on the circle around with radius $|q|$ are constant, but their phase rotates continuously up to 2π on the complex plane, see Fig. 6.6 (b) in Appendix 6.9 . This means that electron - hole direct interaction can be called chiral. This chirality is interesting itself, however let us turn to discussion how it affects excitonic fine structure. Role of complex interaction phase manifest itself in two effects: first, it slightly renormalizes positions of s - like states, however this effect is subtle, and is magnified on schematic Fig. 3.14. On the other hand, clearly visible effect is that e.g. on second shell, normally degenerate p-like states become split in energy and mix, forming $2p_{\pm 1} = 2p_x \pm i2p_y$ states. More generally, due to complex interaction, all states with non zero exciton momentum L also mix and split (e.g. $3p_{\pm}$, $3d_{\pm}$ etc.).

Focusing on exact value of splitting of $L \neq 0$ state in second excitonic shell, we discovered that it's value depends heavily on screening. If screening parameters for full TB model (TB dispersion and form factors with wavefunction effects making them complex) and R.-K. screening are chosen such to give binding energy of 1s state 378 meV ($\alpha = 1.0$), value of 2p-2p splitting is $\Delta_{2p-2p} = 3.5$ meV, see Fig. 3.15 (a). However, if screening parameters are chosen such to give 1s state energy 458 meV ($\alpha = 0.5$), we obtain Δ_{2p-2p} as large as 13.0 meV. More systematic study of how polarizability parameter α affects 2p - 2p splitting is presented in Fig. 3.15 (b). For the case of $\alpha = 0.0$, splitting of p states can be as large as 120 meV. For more realistic parameters of α giving binding energies of 1s state below 500 meV (inset of Fig. 3.15 (b)), this splitting is predicted to be below 20 meV. In addition to that we check how much summation over G vectors in complex form factors affects this value ("error bars" in Fig. 3.15 (b)). We calculate this "error" comparing p state splittings obtained from single G vector that minimizes $\left|\vec{k'} - \vec{k} - \vec{G}\right|$ distance in k space with summation performed up to $G_{cutoff} = |G_1|$. We conclude that error introduced is large only for un-physical $\alpha = 0$ case, but for more realistic values is rather small.

Splitting of states with non-zero L reminds of situation when magnetic field is

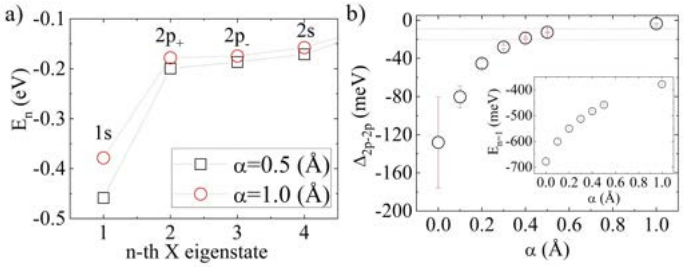

Figure 3.15: (a) Fine structure of exciton spectrum in full TB model with inclusion of effect of complex electron hole interaction. Two parameters of R.-K. screening model are studied. (b) 2p-2p energy splitting dependence on polarizability α. Error bars estimate how large error associated with lack of summation over G vectors is (only one term vs more correct summation up to $G_{cutoff} = |G_1|$). Inset in (b) shows corresponding energy of 1s state vs screening. Figure reproduced from Ref. 5.

applied, which distinguishes between states with non-zero angular momenta. In our case there is no magnetic field but instead there is "geometric " field resulting from topology of wavefunctions. This field, described by gauge invariant Berry's connection has to come from properties of wavefunctions. Now we trace this Berry's connection effect on electron - hole interaction. Starting with direct interaction matrix element for $\vec{k} = \vec{K} + \vec{q}$ and $\vec{k}' = \vec{K} + \vec{q}'$ points close to the $\vec{K}$ point, we can expand Bloch wavefunctions u_n formally in first order of $\vec{q}$ as

$$u_n\left(\vec{K}+\vec{q},\vec{r}\right) \approx u_n\left(\vec{K},\vec{r}\right) + \left[\vec{\nabla}_{\vec{q}} u_n\left(\vec{K}+\vec{q},\vec{r}\right)\right]_{\vec{q}=0} \cdot \vec{q}. \tag{3.49}$$

Using this approximation one can re-arrange terms under 6 dimensional $\vec{r}$, $\vec{r}'$ integral as

$$\begin{aligned} \iint_{R^3} \Big[& e^{i(\vec{q}-\vec{q}')\cdot(\vec{r}-\vec{r}')} V^{3D}\left(\vec{r}-\vec{r}'\right) \times \\ & \times \left[|u_v(\vec{K},\vec{r})|^2 |u_c(\vec{K},\vec{r})|^2 + \Delta_q \cdot \vec{q} + \Delta_q^* \cdot \vec{q}' \right] \Big], \end{aligned} \tag{3.50}$$

where Δ_q is given by

$$\Delta_q = |u_v(\vec{K},\vec{r})|^2 \cdot \underbrace{u_c(\vec{K},\vec{r}')\left[\vec{\nabla}_{\vec{q}} u_c(\vec{K}+\vec{q},\vec{r}')\right]}_{\text{Berry's connection}} + (v \leftrightarrow c)\Big]. \tag{3.51}$$

Equation above shown how (in general non-Abelian[756,757]) Berry's connection enters kernel of matrix elements and therefore, constitutes an example how topology affects not only single - particle, but also many body properties of correlated states.

To conclude this subsection, we note that similar values of 2p-2p states splitting are reported to come out from calculations using massive Dirac fermion model to both dispersion and form factor of direct electron-hole interaction.[430,541] This approach is, however, valid only close to the K point and whole calculation has

to be restricted to small fraction of BZ. If one uses mDF Hamiltonian applicable to all points in given valley in form

$$\hat{H}^{mDF}\left(\vec{k}\right) = \begin{bmatrix} \Delta/2 & g_k e^{i\theta_k} \\ g_k^* e^{-i\theta_k} & -\Delta/2 \end{bmatrix}, \tag{3.52}$$

with $g_k e^{i\theta_k} = t\exp(-i\vec{k}\vec{b})(1+\exp(i\vec{k}\vec{a_2})+\exp(i\vec{k}(\vec{a}_1+\vec{a}_2)))$, $\vec{b} = \left(d_{\|},0\right)$ and $3/2d_{\|}t = \hbar v_{\mathrm{F}}$. In principle, it is possible to derive form factor of interaction for such model

$$F(k,k') = \left[\sin\frac{\varphi_{k'}}{2}\sin\frac{\varphi_k}{2}\exp\left[-i\left(\theta_k-\theta_{k'}\right)\right]+\cos\frac{\varphi_{k'}}{2}\cos\frac{\varphi_{k'}}{2}\right]^2, \tag{3.53}$$

with $\cos\varphi_k = \frac{\Delta/2}{\sqrt{\Delta^2/4+g_k^2}}$. When such model is used consistently for whole valley, we find approximately 20 μeV splitting of $2p_{\pm}$ states, which is much smaller value than our TB result. Only unphysical extension $g_k e^{i\theta_k} \approx \hbar v_{\mathrm{F}}(iq_x - q_y)$ to whole valley gives approximately 30 meV splitting comparable to TB model. We conclude therefore, that massive Dirac fermion model (and wavefunctions obtained from it) does not capture correctly not only renormalization of spectrum due to dispersion, but also underestimates topological splittings and should be treated rather qualitatively.

3.6.5 Effect of spin orbit coupling in conduction band

In the following section let us focus on the effect of spin splitting on exciton fine structure. Largest effect, related to splitting of bands in VB, is A - B exciton splitting. For $\Delta_{VB}^{SOC} = 148$ meV we obtain A-B 1s excitonic states split by ≈ 125 meV for $\alpha = 0.5$ and full TB model. Much more subtle effect, introducing splitting of A exciton state to spin bright (same spin arrangement in VB and CB) and spin dark (opposite spins) is related to interplay between spin splitting in CB and different dispersion of bands, that can be understood approximately as different effective masses for carriers with different spins. Starting with clear situation of 10 meV splitting in CB one can see in Fig. 3.16 that, intuitively, lowest state is bright A_{bright}^{+K} and dark state A_{dark}^{+K} lies above it. We note that value of this splitting (5 meV in specific case here) is not the same as spin-splitting at K point. We trace this effect to before-mentioned effective masses difference. Therefore, if value of this splitting in CB is further reduced, one can end up in situation when even though single-particle arrangement of bands points to "bright < dark" arrangement, different effective masses cause inversion of excitonic states and spin dark state becomes ground excitonic state. We conclude that this situation happens in MoS_2, which has very small $\Delta_{CB}^{SOC} \approx 3$ meV. This conclusion is consistent with recent GW-BSE calculations[387,533] and some experiments.[192]

3.6.6 The role of electron-hole exchange interaction

On top of spin splitting effects, up to this point we consistently neglected generally small electron-hole exchange interaction. This interaction, however, controls

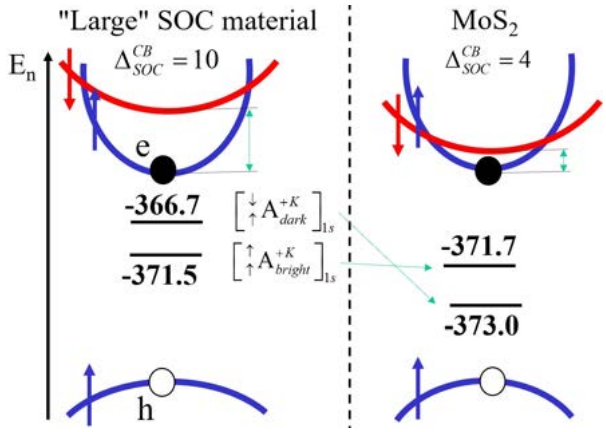

Figure 3.16: Comparison between spin-polarized bands and resulting bright - dark arrangement of states in materials with spin-like arrangement of bands around Fermi level. For materials with large splitting in CB, it is clear that lowest exciton is bright (same spin in VB and CB) and above it lies dark excitonic state (opposite spin in VB and CB). On the other hand, higher spin-polarized band in CB has larger effective mass, therefore even without exchange interaction effect it's binding energy may be larger that single-particle spin splitting at K point. Black bars denote two lowest s-like states. All presented energies are given in meV. Lower spin-split and in VB is not shown. Presented values are calculated using full TB model and polarizability $\alpha = 0.5$. Figure reproduced from Ref. 5.

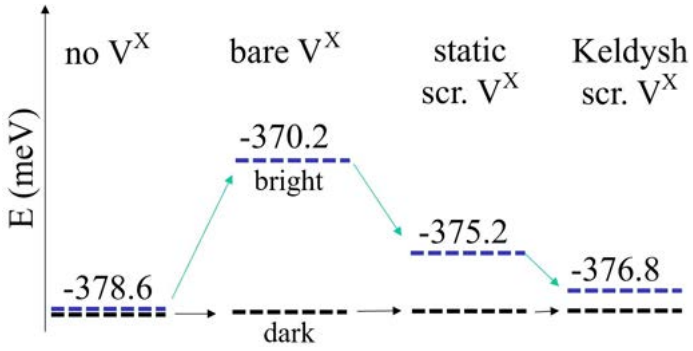

Figure 3.17: Role of electron-hole exchange interaction V^X and it's screening on fine structure. For clarity we start with spin-degenerate bands to disentangle effect of spin splitting and e.-h. exchange. When no V^X is present, 1s excitonic states are degenerate. When exchange is turned on, dark - bright splitting value depends on model of screening, as discussed in text. All values presented are given in meV. Figure reproduced from Ref. 5. Figure reproduced from Ref. 6.

subtle splitting of dark and bright states, because it affects only bound states of excitons with the same spin, increasing their energy (due to quantum mechanical electron - hole repulsion) in opposite to direct interaction. Starting with spin-degenerate states to make our analysis more transparent, when no exchange interaction V^X is present, dark and bright states are degenerate, as shown in Fig. 3.17. When unscreened electron-hole interaction ("bare V^X") is turned on, energy of bright state is increased (binding energy is lowered) up to ≈ 20 meV (in Fig. 3.17 8 meV), depending on details of screening used and 1s ground state energy. When either homogenous screening or R.-K. models are applied also to exchange interaction, this value is significantly lowered. We conclude that in all cases, trend is such that dark excitonic state in MoS_2 is lowest one, adding up to similar conclusion from spin splitting discussion above. We note that in field theory based DFT+GW+Bethe-Salpeter approach[387] electron-hole exchange interaction is always taken as bare, unscreened one. In our approach derived from CI approach, both direct and exchange interactions are treated on equal footing and should be screened in the same way. This issue has been discussed in literature,[533,758] but in our view further studies are necessary to understand source of this discrepancy. On the other hand, irrespective to details of screening, we conclude that in MoS_2 lowest excitonic state should be dark due to spin and exchange effects.

3.6.7 Inter-valley exciton scattering

Before we dwell into discussion of charged excitons fine structure, let us mentioned briefly issue of inter-valley exchange interaction. From our calculations presented above, we conclude that in $+K$ and $-K$ valleys $1s$ excitonic states are degenerate. This conclusion does not, however, include inter-valley exchange, which in principle may be of the order of intra-valley exchange due to lack of $1/|k-k'|$ asymptotic behavior, known for direct interaction. Focusing on excitonic states with center-of-mass momentum $Q_{CM} = 0$, it is known from theoretical arguments[387,522] that inter-valley exchange exciton coupling J can be divided into short-range and long range part as $J = J_{Q_{CM}}^{short-range-G\neq 0} + J_{Q_{CM}}^{long-range-G=0}$. It can be proven formally, that short-range part $J_{Q_{CM}}^{short-range-G\neq 0}$ vanishes for $Q_{CM} = 0$ by C_3 symmetry of excitonic states. On the other hand, long-range interaction can be expanded in second power of exciton momentum $J_{Q_{CM}}^{long-range-G=0} \sim |Q_{CM}|^2$, which still gives no coupling between excitons in +K and -K for $Q_{CM} = 0$. We checked numerically that this effect is actually difficult to reproduce because of finite precision with which exchange matrix elements could be calculated. Only when screening of exchange interaction was turned on, we were able to converge our results to give $+K$ and $-K$ exciton splitting below 1 meV.

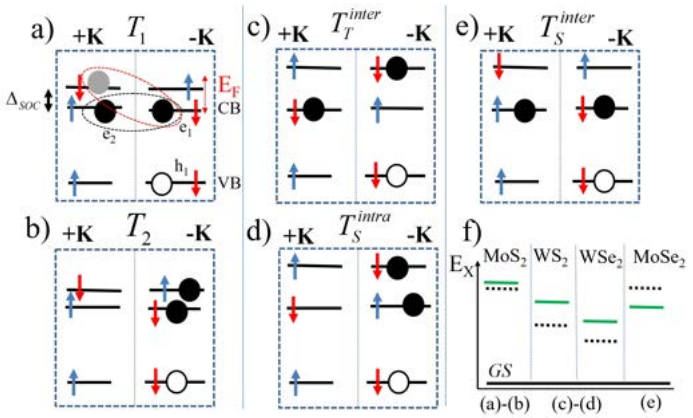

Figure 3.18: Trions in different MX_2 materials with electron-hole pair in bright configuration enabling optical activity. Single - particle levels in +K and -K valleys are shown in left and right panels, respectively. In VB only one spin band is shown due to large spin-splitting. In CB both bands are presented. (a) Inter-valley singlet and triplet trion states in material with small SOC in CB (MoS_2), along with intra-valley singlet shown in (b). (c-d) Bright trion species in materials with dark excitonic state and large SOC in CB, (c) showing inter-valley triplet and (d) intra-valley singlet. In bright material with large SOC in CB (e.g. $MoSe_2$) only one bright trion state is possible, i.e., inter-valley singlet shown in (e). (f) Scheme of dark-bright excitonic (not trionic) state arrangement corresponding to (a-b), (c-d) and (f) trion schemes.

3.7 Exciton interaction with additional carriers

It is well known, that in realistic samples electron gas concentration might be significant, leading to interaction of excitons with excess carriers, usually n-type. Under assumption of small concentration of this gas, one can imagine additional bound state of exciton + electron, called charged exciton or trion. Those optical complexes have very large photo-luminescence response and can even dominate PL signal.[6] As discussed in Introduction, quantitative calculations for those states are extremely challenging due to problem of renormalization of bands with excess carriers, much larger Hilbert space of possible 3-body excitations and slower convergence with respect to k-space discretization. In the following subsection we discuss only qualitatively how our understanding of exciton fine structure of exciton in MoS_2 may help with understanding of trion fine structure.

Our analysis is summarized in Fig. 3.18. We show there valley configuration possibilities of bright, negative trion states such that electron and hole reside in the same valley and have the same spin, allowing for optical recombination. Then, second electron in CB may have different possibilities of valley and spin arrangement. In addition to this different configurations, problem of dark-bright splitting of exciton comes into play. In Fig. 3.18 (a-b) we show most interesting effect that allows to propose explanation of experimentally observed trion fine structure in MoS_2. Because of bright-dark inversion, as described in previous section, bright excitonic state has higher energy than dark one. It is possible for exciton, therefore, to bind carrier from both (a) +K and (b) -K (b), effect known from materials with large negative SOC splitting (c-d), i.e., WX_2. Interestingly, in contrast to WX_2, inter-valley configuration of trion has both spins oriented in the same direction, forming singlet trion state instead of triplet. Inter-valley triplet state in MoS_2 is predicted to have higher energy and be unbound.[759] Trion fine structure cannot be observed in material with large SOC in CB and bright ground excitonic state (Fig. 3.18 (e)) like $MoSe_2$ due to large repulsion if electrons have the same spin and reside in the same valley (intra-valley triplet trion is unbound). In conclusion, MoS_2 is a special material with respect to both $MoSe/Te_2$ and tungsten based WX_2 TMD's due to it's small SOC and dark excitonic ground state combination with bright arrangement of single - particle bands (which are unlikely, but possible to invert due to presence of addition electron gas, as we discuss in Ref. 6).

Under assumption that trion fine structure is described by T_1 inter- and T_2 intra-valley singlet states, let us comment on what controls their energy splitting. Total energy difference between their configurations in MoS_2 is given by

$$\begin{aligned} E_{T_1} - E_{T_2} = \Delta_{CB}^{SOC} + \Big(& - \left[V_{tot.}^{D} \left(h_1^{+K}, e_2^{+K} \right) - V_{tot.}^{D} \left(h_1^{+K}, e_2^{-K} \right) \right] \\ & + \left[V_{tot.}^{D} \left(e_1^{+K}, e_2^{+K} \right) - V_{tot.}^{D} \left(e_1^{+K}, e_2^{-K} \right) \right] \Big). \end{aligned} \tag{3.54}$$

In contrast to equation above, energy splitting between intra-valley singlet T_S

and inter-valley triplet T_T in tungsten based materials is given by

$$E_{T_S} - E_{T_T} = V^X_{tot.}\left(e_1^{+K}, e_2^{-K}\right) + \Big(- \left[V^D_{tot.}\left(h_1^{+K}, e_2^{+K}\right) - V^D_{tot.}\left(h_1^{+K}, e_2^{-K}\right)\right] + \left[V^D_{tot.}\left(e_1^{+K}, e_2^{+K}\right) - V^D_{tot.}\left(e_1^{+K}, e_2^{-K}\right)\right] \Big). \tag{3.55}$$

In both expressions $V_{tot.}$ symbolize total energy associated with direct / exchange interactions. We conclude that because $V^D_{tot.}$ terms have similar magnitude and mostly cancel each other contribution to total splitting, value of trion fine structure splitting in MoS_2 depends mostly on spin-orbit coupling in CB, while in WX_2 measures mostly total exchange energy between electrons in CB. We note that precise comparison with experiment is unfortunately challenging due to increased splitting of trion fine structure in function of electron gas concentration, while our result are valid for vanishing density regime. More advanced study of effects of density of excess carriers on exciton and trion fine structure is left for future study.

Chapter 4

Physics of gate - defined quantum dots in MX_2 materials

In the following Chapter tight-binding model derived in Section 2 is used to study quantum dots, defined electrostatically by metallic gates. These gates are modeled using parabolic confining potential, trapping additional electron added into conduction band. First, a model of computational box is presented along with rudimentary tests. In next step harmonic oscillator spectrum resulting from K- points derived and Q-points derived states is analyzed, paying attention to topological effects and special symmetry of Q-point derived states. Then, interplay of dot radius and spin splitting is analyzed from the point of view of electronic shells arrangement, which influences charging spectrum of quantum dots.

4.1 Model of a quantum dot

We begin our discussion with a model of electrostatic quantum dot. First, we define some computational box describing our MX_2 semiconductor, using real space tight-binding hopping matrix elements described by Eq. (3.29-3.29) and Eq. (6.25-6.27), as shown in Fig. 4.1. We implement and test below possibility of turning on and off periodic boundary conditions (PBC) and selective modification of on-site energies on the edges of box, simulating in approximate way passivation of a box. Our confining potential induced by metallic gates[686] has minimum at the center of rectangular region and is set to 0 when touching dot radius R_{QD}. Depth of confining potential is parametrized by constant V_0. The total Hamiltonian of our system can be written, therefore, as

$$H = H_0 + \sum_{i\alpha} V_i c^+_{i\alpha} c_{i\alpha}. \tag{4.1}$$

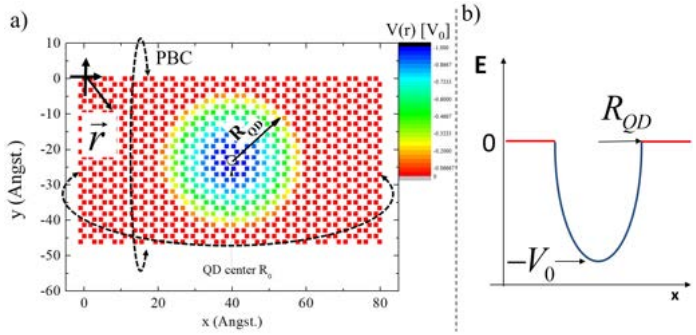

Figure 4.1: (a) Model of computational box and confining potential viewed from the top. (b) Side view of confining potential.

Potential V_i on i-th atoms is modeled as

$$V_i = V(r_i) = \begin{cases} \frac{1}{2}\omega^2 r_i^2 - V_0, \text{ for } r_i < R_{QD} \\ 0 \qquad\qquad\quad , \text{ for } r_i > R_{QD}, \end{cases} \tag{4.2}$$

where both quantum dot radius R_{QD} and potential depth V_0 are hidden inside harmonic oscillator frequency $\omega^2 = 2|V_0|/R_{QD}^2$. Except stated otherwise, we take $V_0 = 300$ meV. At the edge of the quantum dot we set our confining potential to 0, because we were forced to use periodic boundary condition to deal with edge states of our computational box, as described below.

As discussed in Introduction, there are many studies available for MoS_2 (which are expected to be similar in other MX_2 materials) showing that on physical edges of samples metallic states occur with energy in the gap. We have checked that our tight-binding model reproduces DFT predictions and, e.g. in nanoribbon geometry (equivalent to our computational box extended to infinity in one dimension), it gives in-gap edge states. We move those nanoribbon results to Appendix 6.10. Those in-gap states, when further quantization by cutting finite box is induced, naturally lead to many in-gap edge states if we use open boundary conditions, as shown in Fig. 4.2. However, when PBC is applied, they naturally disappear and in such torus geometry, as expected, we recover bandgap between VB- and CB- derived states. Interestingly, we tested another method of dealing with such states by changing energy of on-site matrix elements, which effectively simulates passivating edges of physical samples by e.g. hydrogen atoms. We found that those edge states shift their energy, however it is not possible to move them out of band gap energetic region, situation similar to topological insulator quantum dots.[760]

Edge states that are visible in Fig. 4.2 when no PBC is applied are interesting themselves. However in our setup, in which confinement is induced by metallic gates, in realistic physical situation we are very far from dot center and edge states cannot influence behavior of states localized inside QD. Because of this, we choose to use PBC. One may wonder how confining potential works in this setup and if results for opened / closed boundary condition are comparable to

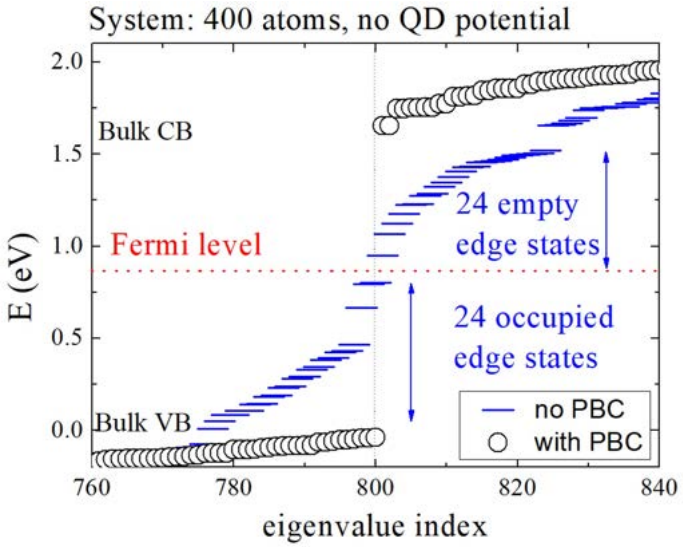

Figure 4.2: Comparison between eigenvalues when computational box (without QD potential) Hamiltonian is diagonalized with and without PBC. Only states around Fermi level are shown.

each other. In Fig. 4.3 (a) we show how increasing depth of potential V_0 lowers states from bottom of CB of torus inside gap region. Then we compare spectrum with and without PBC in Fig. 4.3 (b), proving that states localized inside QD (as shown in inset) are not affected by presence of edge states, depicted as small blue symbols in Fig. 4.3 (b). We conclude that PBC are not affecting QD states, therefore whenever dot potential does not "touch" edges of computational domain, we can use model with PBC in which numerical results are easier to interpret.

Another issue that one may rise, is that we model our QD with TB model which uses only symmetric orbitals with respect to Mo plane. One may expect, that application of perpendicular electric field E induces mixing between even and odd orbitals due to breaking of mirror symmetry in z direction. We estimate, however, that with experimentally realistic[761] gate voltages (e.g. ± 100 V for sample thickness 103 nm) difference between potential in top and bottom sulfur atoms is $\delta V = 0.19$ V. Simplifying discussion to states in CB at K point only, anti-symmetric band not included in our TB model is 1.37 eV apart, contributing below 0.5% to wavefunction of state derived from bottom of CB. Therefore, we neglect this contribution and leave precise estimation of this effect with full TB including symmetric and antisymmetric orbitals to future study.

We finish description of our model with technical comment on numerical procedure used in our calculation. Because we are interested in rather large quantum dots comparable to those available experimentally,[734,735] e.g. for dot with $R_{QD} = 100$ nm we need approximately 220×220 nm computational box that includes approximately $1.1 \cdot 10^6$ atoms. To perform diagonalization of such large matrix efficiently it is usually enough to use iterative Krylov - like methods,

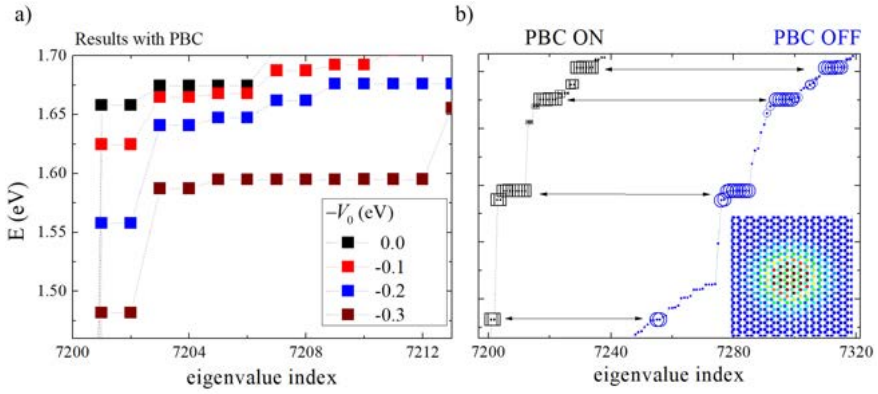

Figure 4.3: (a) Effect of lowering of depth of potential $-V_0$ on states from bottom of torus CB. (b) Comparison of spectra with and without PBC. Size of the symbol codes how much given eigenstate is localized inside QD (large symbol - state fully inside QD, small symbol - state localized away from QD region). Inset: example of electron wavefunction localized inside QD region.

e.g. Lanczos algorithm. In the following work we have taken another route, utilizing new algorithm based on contour integration technique, called FEAST[762] as implemented in Intel MKL numerical libraries. This method is interesting, because it's performance depends on number of eigenvalues in a given energy range, therefore we are able to speed up calculations by getting rid of edge states and focus only on those in-gap states localized inside QD. Because our TB model is short - ranged in real space (uses only NN and NNN), we are able to avoid producing large matrices by coding so-called CSR3 matrix storage format. Internal convergence parameters for diagonalization inside FEAST routine are set to 6 contour integral points and sum of all eigenvalues found (usually 100) error is set to be below 1 meV, so average error per 1 eigenvalue is approximately 1 μeV.

4.2 Study of size dependence of the quantum dot electronic spectrum

Before we go into details of physical understanding of spectrum, let us describe simple, but useful results of size studies of different QD's. Results obtained for different radii of QD's are summarized in Fig. 4.4. To simplify discussion, we begin with states calculated without inclusion of spin-orbit coupling. Fig. 4.4 (a) presents results of diagonalization for few QD radii in energetic window in which all states are localized strictly inside QD, fact we checked studying localization of wavefunctions associated with each state. First, one can observe, that with increasing dot radius more and more states "fall into" quantum dot due to decreasing distance between consecutive shells. Also, position of lowest two states goes down in energy, as presented in Fig. 4.4 (b). In Fig. 4.4 (c)

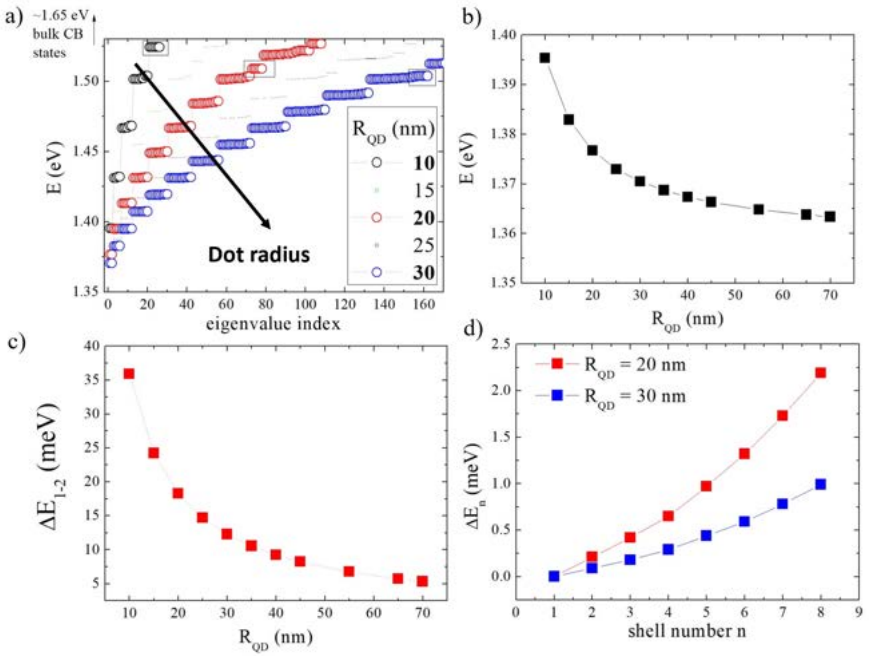

Figure 4.4: (a) States localized inside parabolic quantum dots for few different radii R_{QD}. (b) Energetic position of lowest energy state doublet. (c) Energy difference between first and second shell in function of R_{QD}. (d) Internal splitting of n-th energy shell for two different QD sizes.

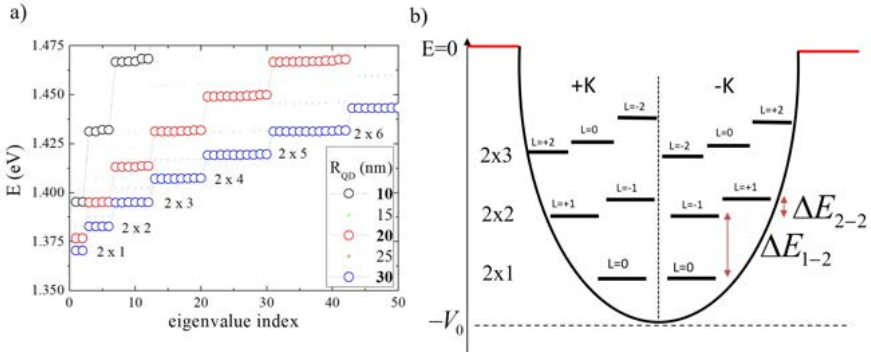

Figure 4.5: (a) Degeneracy of each shell of $\pm K$ - point derived spectrum. (b) Schematic of 2D parabolic Fock-Darwin ladder associated with each valley (+K, -K) with energy difference between shells ΔE_{1-2} as in Fig. 4.4 (c) and internal splitting of n=2 shell ΔE_{1-2}, as in Fig. 4.4 (d).

energetic distance between first and second shell (approximating distance of almost equidistant higher shells) is shown in function of R_{QD}. One can observe monotonic decrease of this value following $1/R_{QD}$ dependence and helping to asses what would happen if dot radius is so large that exact calculation becomes unfeasible. In Fig. 4.4 (d) we show interesting effect explained later in details, that within each shell states are not degenerate. We checked that this splitting of usually degenerate shells in 2D parabolic QD model is not the result of numerical error, but comes from topological properties of MX_2 wavefunctions. We note here only that this effect is more pronounced in smaller QD's and is consistent with similar splittings in strain-induced QD calculations.[708]

4.3 K-point-derived spectrum of electronic states

We begin analysis of spectrum from comment about k-space origin of states inside QD. By studying lowest states wavefunctions shown in Fig. 4.5 (a) , one can quickly realize that vast majority of electron density localizes on Mo metal atoms. On each Mo (S_2) atom (dimer) there are 3 complex numbers obtained from Hamiltonian diagonalization that describe spinor composition of states. We checked that for our lowest states, always $m_d = 0$ component of the spinor is largest (and p_{-1} for part of wavefunction localized in S_2 dimers), meaning that states have the same composition as bottom of CB at K point. This allows us to distinguish quantized states formed from k - vectors close to the K - points. We have checked also, that working with plane - wave basis of functions (done by this thesis author's collaborators)[4,7] defined on torus one can get to the same conclusion. We distinguish between +K and -K valley states either by checking $m_{p_{\pm 1}}$ component of spinors or by plotting which plane-waves with given k - vector from torus projected on BZ give largest contribution. We note that both methods allow to distinguish states formed from neighborhood of Q points in BZ. Specifically, first method works because spinor components at Q

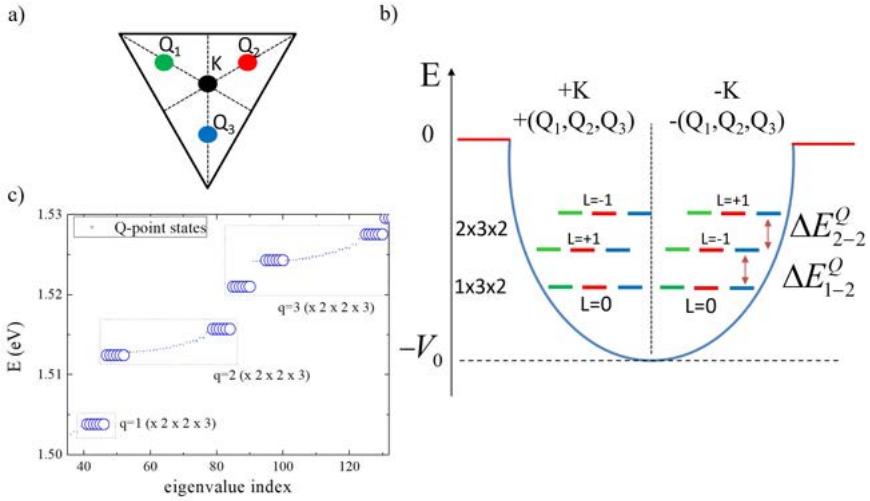

Figure 4.6: (a) Three Q-points surrounding one K point in valley. (b) Schematic arrangement of states derived from Q-points in QD, analogous to spectrum in Fig. 4.5 (b). (c) Large dots show ground and excited Q-point states in QD using spinor composition detection mechanism. Small dots represent K-point derived states.

point are different than at K and allow for easy and quick identification from which minimum given state is derived from in multivalley system.

Having identified valley from which given state is, one can notice immediately that for state within each valley we can associate states with degeneracy increasing by one with every shell, see Fig. 4.5 (a), just as in 2D harmonic oscillator spectrum known e.g. from self-assembled GaAs quantum dots.[763] Doubling of number of states in given shell due to existence of two minima in CB (+K, -K) instead of usual one (Γ in GaAs) is therefore proven and schematic of states arrangement is shown in Fig. 4.5 (b). We note also, that unlike in GaAs QD's, degeneracy breaking for $n \geq 2$ occurs, as explained further in text.

4.4 Q-point-derived spectrum of electronic states

As shown in Fig. 4.5 (a) in small rectangular boxes, when we follow Fock-Darwin ladder of states derived from K point, somewhere at higher energy we always find 6 fold perfectly degenerate states breaking this ladder. Their existence and degeneracy can be easily understood from multivalley structure of MX_2 conduction band. From *ab initio* studies and our TB model reproducing them one can observe that every minimum in CB at K point in one valley is surrounded by 3 secondary minima at Q points, as shown in Fig. 4.6 (a). With each of these minima there is associated Fock-Darwin series of states inside QD, as shown schematically in Fig. 4.6 (b). Because there are 2 valleys, we obtain $1 \times 2 \times 3 = 6$ degeneracy of first Q-point derived shell, $2 \times 2 \times 3 = 12$ degeneracy for second

etc. In Fig. 4.6 (c) we show that analogously to K - point derived states second shell splits and we associate this effect again with topological effect as discussed below.

Before we elucidate on new physics behind those states, let us discuss their energetic position in different TMD's. In MoS_2, as shown in Fig. 4.4, Q-point derived states are 21-st counting from ground state in QD with radius $R_{QD} = 10$ nm derived from K-point valley. One may argue, that because they are so high in energy and so many electrons are necessary to probe them, they are uninteresting. However, we know from our own and other studies, that for tungsten based TMD's WX_2 energetic difference between K and Q points in CB is significantly smaller than in Mo- based compounds (32 vs 230 meV, see Fig. 2.7). Also, in tungsten based compounds band ordering between K and Q point reverses. Therefore, due to significant spin splitting at K point (38 meV for WSe_2) for specific spin in chosen valley Q - point states may become the ground ones. This effect can be further magnified by processes lowering Q point position in CB with respect to K point position, e.g. strain as discussed in Introduction.

4.5 SU(3) "quarks" in TMD quantum dots

Let us focus for a moment on three Q-point derived states in one valley. One one hand, triple degeneracy is not surprising in QD, e.g. third shell of 2D harmonic oscillator is triply degenerate. However, those states can be distinguished by angular momentum quantum number. In our case in MX_2 crystals, even though it is clear that triple degeneracy comes from existence of 3 Q-points surrounding K - point, situation is different, because 3 degenerate states are mixture of all three valleys and have exactly the same angular momentum quantum number L=0. It has been proposed in literature[764] (for case of odd numbers of many-layer TMD's) that such states are manifestation of so-called flavor SU(3) symmetry and we call them "QD quarks". Such symmetry has been proposed in early theories of up, down and strange quarks in high energy physics[765,766] by Gell-Mann. Interestingly, in high energy physics this symmetry is only approximate due to different masses of quarks, while in our case it should be an exact one. We note that SU(3) symmetry is also associated with more widely used "color charge" and it is tempting to associate some "valley color" and understand each QD quark as mixture of all colors (property of all free particles in high energy physics). Also, each Q-point derived QD quark state should be described by some quantum number generalizing spin, analog of e.g. isospin. What is also important, no electrons on such QD quark states and complete filling of all of them are both "QD quark vacuum state",[764] suggesting analogy between "true quantum" and "Dirac" vacua, which possibly are not equivalent in QD setup due to electron - electron interactions. Qualitative and quantitative analysis how far those analogies are correct and can be pushed forward will be subject of our future studies. We note that study of those states may be interesting not only from fundamental reasons, but also because of practical utilization of 3-state analogs of qubits, i.e., "qutrit".[764]

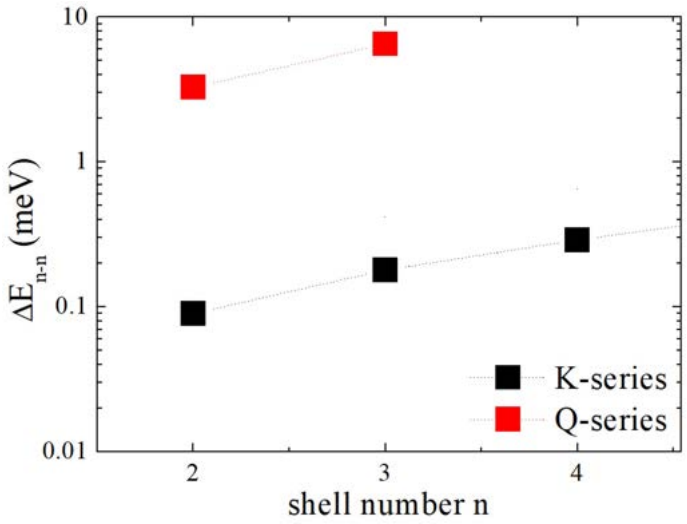

Figure 4.7: Internal splitting of shells of K- and Q- point derived QD states shown in logarithmic scale. QD radius here is 30 nm.

4.6 Topological splitting of electronic shells

As already mentioned in Fig. 4.4 (d) consecutive $n > 1$ shells of both K - point series and shells identified as Q-point derived states (Fig. 4.6 (c)) exhibit internal structure. We observe that splitting within shells becomes larger with increased shell number n, as shown in Fig. 4.7. As mentioned before, this effect is not merely numerical one, but it is associated with topological properties of MX_2 crystals. Splitting within $n > 1$ shells can be understood, in analogy to similar splittings when magnetic field is applied to 2D harmonic oscillator, as result of "geometric field" (Berry's curvature) acting on states with non-zero angular momentum L.[708] We note that L states in +K valley split in opposite direction than in -K due to sign reverse of Berry's curvature between +K and -K valleys.[430,545] Also, as shown in Fig. 4.7, shells associated with Q-point series exhibit topological splitting that is an order of magnitude larger than those associated with K-point series. Source of this effect and means of controlling value of this splittings in TMD's will be subject of future studies. We note that such topological splitting seems to influence also $L = 0$ states (e.g. splitting in third shell of states with $L = \pm 2$ is not symmetric around $L = 0$ state), in analogy to s-series topological splitting in excitonic series.[5,551]

To support our identification of splitting within QD shells as effect of Berry's curvature resulting from topological properties of wavefunctions, we studied simplest toy model, i.e. Kane-Mele model of graphene, in which strength of Berry's curvature is controlled by the band gap that can be opened in two topologically non-equivalent ways: trivial gap opened by opposite on-site potential on A-B atoms and topological gap opened by "toy-model" Kane-Mele spin-orbit coupling. We present details of those calculations in Appendix 6.11. Here we quote

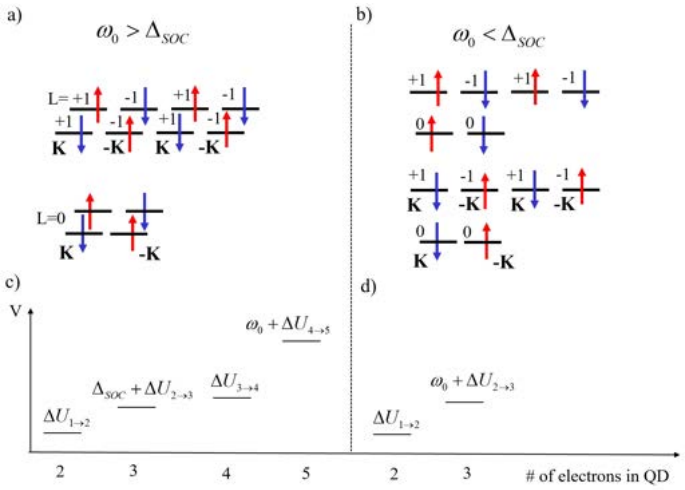

Figure 4.8: (a) Schematic arrangement of spin-split K-point derived states in QD when shell spacing ω_0^K is larger than spin splitting Δ_{SOC}. (b) Similar scheme when Δ_{SOC} dominates over shell splitting. (c-d) Corresponding schemes of charging energies for two shell splitting regimes. In (c) addition of third electron to QD is dominated by Δ_{SOC} and Coulomb energy U, while in (d) - by shell splitting and U. Figure reproduced from Ref. 4.

only central result that when Berry's curvature is larger (gap is smaller), for two different QD's with the same inter-shell splitting (ΔE_{1-2}) we observe systematically larger intra-shell splittings (ΔE_{2-2}), proving inter-shell splitting directly depends on Berry's curvature strength. We note that the same value of splitting is obtained for both topologically trivial and non-trivial phases, however we note that scheme of splittings of states described by valley and $L \neq 0$ angular momentum is different. We note that effect of splitting of $L \neq 0$ states might be, unfortunately, difficult to measure experimentally due similar splitting induced by deformation of QD potential, e.g. elliptical deformation.

4.7 Interplay of spin-orbit coupling and shell splitting

Finally, let us discuss how spin-orbit coupling modifies shell splitting inside MX_2 quantum dots, focusing on K-point derived spectrum which is lowest in molybdenum based TMD's. First, we note that spin arrangement of states in +K and -K is opposite, as shown for lowest states in Fig. 4.8 (a-b). Value of splitting between first two degenerate states and second pair of degenerate states (Fig. 4.8 (a)) is controlled by value of splitting at K - point in CB. Due to size quantization this value of splitting is smaller for smaller dots and reaches bulk value only for very large QD's.[4]

In next step, we note that shell ordering of spin-split states depends heavily on

interplay of Δ_{SOC} and shell splitting ω_0 controlled by QD size. For small dots it is clear that $\omega_0 > \Delta_{SOC}$. In such situation, first states above lowest Kramers dublet shown in Fig. 4.8 (a) are states from the same shell (n=1) split by SOC. However, when inter-shell splitting becomes smaller, one can note different shell ordering. When dot is large, $\Delta_{SOC} > \omega_0$ and next states above lowest pair are states from second shell (n=2, Fig. 4.8 (b)) with $L \neq 0$. Neglecting for a moment order of magnitude smaller topological splitting of $L = \pm 1$ states, one can see that states above lowest pair are 4-fold degenerate, oppositely 2-fold degeneracy when $\omega_0 > \Delta_{SOC}$. We note that those two regimes can be realized by fabricating QD's with different sizes. Possible experimental manifestation of this effects is discussed in Fig. 4.8 (c-d), which shows schematically charging spectrum[767] of multi-electron QD's, which depending on ω_0 and Δ_{SOC} should be controlled either by Δ_{SOC} or ω, depending on size of QD.

We note also, that multi - electron QD's discussed in regime $\omega_0 > \Delta_{SOC}$ have interesting broken symmetry ground state.[7] Due to the interplay of Ising-like spin SOC and weak inter-valley exchange effects, as discussed for excitonic properties of TMD's in previos Chapter, one can tune ground state of dot between inter-valley anti-ferromagnetic state with even number of electrons in +K and -K valley derived states (and no spin polarization due to spin - reversal between valleys) and spin- and valley- polarized state in which all electrons prefer to be in one valley and have the same spin.[167] Precise estimation of values of shell splitting ω_0 controlling transition between these two phases depends on SOC value and number of electrons.[7]

Chapter 5

Conclusions and plan for future work

To sum up, in the following thesis I presented results of study of TMD semiconductors electronic and optical properties, focusing on simple, yet physically well-motivated tight-binding approximation. In the first part I presented introduction to vast literature on 2D systems, focusing on novel atomically thin MX_2 (M=Mo, W, X=S, Se, Te) transition metal dichalcogenides in 2H phase. Those fascinating materials, combining advances related to graphene with semiconductor physics, are predicted to become more and more technology relevant. It is crucial, therefore, to build theories that are on one hand physically simple, intuitive and numerically trackable, and quantitatively correct on the other hand.

In the first Chapter presenting original results of this thesis, I presented minimal, graphene-like tight-binding model built using understanding derived from *ab initio* studies. This model simplicity comes from identification of band symmetries in terms of orbitals and realization, that it is enough to take only metal and dimer chalcogenide orbitals even with respect to metal plane to reliably describe bands around Fermi energy (valence and conduction bands). This model allowed me to understand band gap opening physics within metal d-orbital group, emergence of fundamental gap at K point and orbital quantum numbers associated with VB and CB. It also pointed to the origin of secondary minima of conduction band at Q points. Then I explained how existence of those Q points is related to the band nesting phenomenon. Also, successive further simplifications of TB model to massive Dirac fermion and effective mass models has been rigorously derived. Chapter was concluded with study of magnetic field effect on electronic structure close to the K - point.

In next part of the thesis, I built a theory of correlated electron - hole pairs, using interacting excitonic state language, that has many parallels with field-theoretical *ab initio* + GW + Bethe-Salpeter method. I uncovered that main difference between those methods lies in screening of electron-hole exchange in-

teraction. This method, in which significant time and effort has to be devoted to studying effect of wavefunctions on interaction form factors modeled using tight-binding theory, allowed me to study fine structure of excitonic spectrum in numerically convergent way. This fine structure, involving not only spin bright and dark, but also excited excitonic states, helped me with understanding of experimental results of my collaborators not only with respect to excitonic response that I calculated quantitatively, but also with qualitative understanding of spin arrangement in trion complexes in MoS_2.

In last part of this thesis, I applied tight-binding model from Chapter 2 to the problem of gate defined quantum dots. I was able to understand numerical results of parabolic quantum dots in terms of simple picture of 2D harmonic oscillator states resulting from 2 valleys at K point and additional higher energy spectrum resulting from existence of Q points. Then, I uncovered topological reasons behind splitting of K and Q -point derived shells and discussed how Q-point derived states can be understood in analogy with high energy physics quarks, proposing "SU(3) flavor quantum dots" in TMD's monolayers in realistic setting. I concluded last Chapter with discussion of interplay of spin-orbit interaction and shell spacing controlled by QD radius, affecting ladder of ground states in those quantum dots.

Future plans to extend results presented in this thesis can be broken in 3 groups. First, I plan to extend tight-binding model to include both even and odd orbitals, which should open possibility to study not only monolayers, but also bilayers. Those odd orbitals induce also interesting effect of mixing between bright and dark exciton, activating optical response of grey excitons that are currently under intense experimental study. Important step would be also to build and implement theory of "GW-like" re-normalization of excited electrons and holes, where converged calculations due to high localization of orbitals are a bottleneck of *ab initio* plane wave methods.

Second group of problems I'm planning to develop is connected with understanding properties of excitons with non-zero center-of-mass momentum Q. which activated by phonons lead to rich "excitonic landscape". Also, larger optical complexes like trions, biexcitons and charged biexcitons are of great interest nowadays. Configuration-interaction method presented in Chapter 3 can be, as known from physics of many-body complexes in quantum dots, extended to deal with such bound states. I plan also to understand more deeply how additional carriers affect exciton states and study exciton - trion coupling dynamics by phonons in a quantitative way.

Last group of problems I'm interested in is connected with flavor symmetry of Q - point state, which studies are only at it's infancy. It is possible, in principle, to imagine that out of those Q-point derived "QD quarks" one can construct composite particles in analogy to particles in Standard Model. To do this, it is crucial to understand Coulomb interactions between those states and how those interactions affect analogy between quarks and QD states and how far those analogies can be pushed forward. From the point of view of topological effects in the electronic spectrum, I plan to perform further studies on topological splitting, especial how it can be observed in realistic settings.

Chapter 6

Appendix

6.1 Details of DFT calculations

Density functional theory is nowadays standard framework for investigating electronic properties of materials. We do not repeat density-functional theory due confined space and many excellent expositions. All DFT calculations are performed using Abinit 8.10.2 software[768–772] installed on Compute Canada clusters (Beluga, Cedar, Graham, Niagara). This code allows for first principles calculations of electronic properties of many body systems, using several standard approximations within density functional theory framework. In our calculations we consistently use PBE version of GGA[773] exchange correlation potential. Because Abinit is 3D periodic code, we have to introduce vacuum between monolayers in study. We know from literature that 10 Å is enough co converge GGA level calculation due to short range nature of interactions included (which is no longer true if e.g. polarizability have to be calculated[404]). We take therefore 10 Å vacuum in all our calculations. Kinetic energy cut-off is taken as 30 Ha $\approx$ 816 eV (1 Ha = 27.2113845 eV). As standard PAW pseudo-potential method is used to reduce computational complexity associated with core electrons, energy cut-off for FFT grids taken as 60 Ha. Calculations are performed on 12 x 12 x 1 k-point grids. In first step of the calculations atomic positions are relaxed using Broyden–Fletcher–Goldfarb–Shanno algorithm with stopping criterion of maximal force set to 10^{-5} Ha/Bohr. In next step both unit cell and atom positions are relaxed, keeping z-th component of unit cell fixed (we do not relax vacuum between periodic images of monolayers). When band structure calculations are performed, criterion when total energy difference between self-consistent steps is converged was set to 10^{-10} Ha.

6.2 Localized Slater - like atomic orbitals

Through this work Slater-like localized orbitals $\varphi_{\alpha\mu}$ are used in the form

$$\varphi_{\alpha\mu}(\vec{r}) = R_n(r)Y_{L,\mu}(\theta,\phi) \tag{6.1}$$

where radial function is approximated as

$$R_n = \frac{(2\zeta_{nLm})^{n+\frac{1}{2}}}{\sqrt{(2n)!}} r^{n-1} e^{-\zeta_{nLm}\cdot r} \tag{6.2}$$

where ζ_{nLm} Slater parameters are taken for isolated atom model.[744,745] Spherical harmonics are given by standard expression

$$Y_{L\mu} = \sqrt{\frac{2L+1}{4\pi}\frac{(L-m)!}{(L+m)!}} P_L^m(\cos\theta)e^{im\phi} \tag{6.3}$$

where P_L^m are associated Legendre polynomials with Condon-Shortley phase $(-1)^m$ inside them. For $\alpha = 1$ we have Mo atom with $L = 2$, $\mu \in \{-2, 0, +2\}$ and for $\alpha = 2$ we have S_2 top and bottom atoms with $L = 1$, $\mu \in \{-1, 0, +1\}$. We note that ζ parameters are detached from values of Slater - Koster integrals, as usually assumed.

Now let us discuss how we use these orbitals in the tight-binding model. For d orbitals of metals situation is clear, namely orbital with given L and m is centered around atom center. On the other hand, orbital construction for two chalcogen atoms can be done differently. We define so-called dimer orbitals, that are centered around the same plane as metal atoms. Therefore, this construction has to be performed with care. We begin with upper (U) and lower (L) p-orbitals with quantum numbers $L = 1$, $m = \pm 1$ ϕ and define dimer orbital φ as proper combination of those two:

$$\varphi_{L=1,m_p=\pm1}(\vec{r}) = \frac{1}{\sqrt{2}}\left[\varphi^U_{L=1,m_p=\pm1}(\vec{r}-\vec{R}_S^{up}) + \varphi^L_{L=1,m_p=\pm1}(\vec{r}-R_S^{down})\right] \tag{6.4}$$

For $L = 1$, $m = 0$, due to the nodal structure of p_z orbitals, dimer has to be symmetric with respect to z inversion. This can be achieved by changing sign of one of the orbitals (we choose to change sign of the bottom one):

$$\varphi_{L=1,m_p=\pm0}(\vec{r}) = \frac{1}{\sqrt{2}}\left[\varphi^U_{L=1,m_p=0}(\vec{r}) - \varphi^L_{L=1,m_p=0}(\vec{r})\right]. \tag{6.5}$$

Projections of DFT wavefunctions in form

$$\psi_n^\sigma(\vec{k},\vec{r}) = \sum_\sigma \sum_{\vec{G}<|G_{cutoff}|} c_n^\sigma(\vec{k},\vec{G})e^{i(\vec{k}+\vec{G})\cdot\vec{r}} \tag{6.6}$$

are performed inside spheres around M and X atoms, as described in Subsection 2.1.3 "Analysis of orbital composition". We note that to obtain overlap integral $\iiint_{S^3} d^3r\psi^{*DFT}\psi^{TB}$ both wavefunctions are normalized to give 1 inside spheres due to localized nature of Slater orbitals and general lack of numerical normalization of DFT wavefunctions inside Abinit.

6.3 Summary of DFT results on different MX_2 crystals

In the following Appendix we collect additional results of DFT calculations of MX_2 crystals. First, we present in Fig. 6.1, that similarly to MoS_2, for WSe_2 conduction and valence bands are built from even orbitals with respect to tungsten plane. Additionally, projection of Kohn-Sham wavefunctions onto localized orbitals confirms trend that 3 upper symmetric bands are mainly composed of W - orbitals and 3 lower bands - from Se_2 dimers. Bottom of CB at K point is composed mainly from metal orbitals, just as for MoS_2, while second minimum in CB and both maxima in VB are constructed from combinations of orbitals on both sublattices.

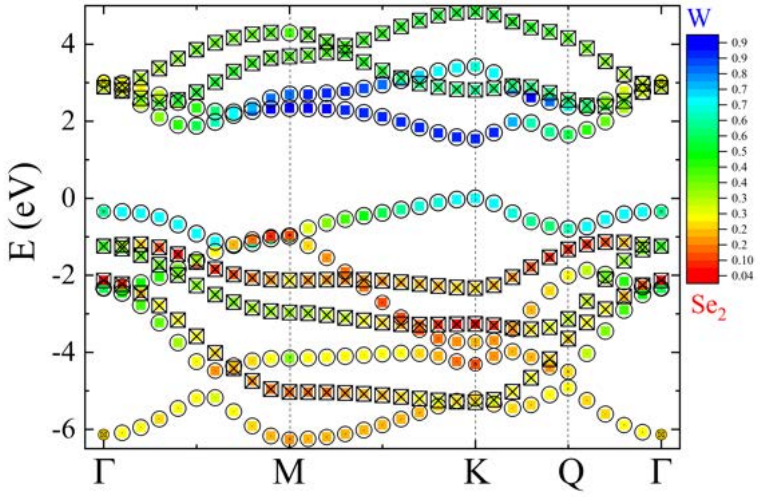

Figure 6.1: Color-mapped localization of a given k-resolved eigenenergy on W and Se_2 spheres and symmetry of eigenvalues across Brillouin zone. Circles (crossed rectangles) denote symmetric (anti-symmetric) orbitals with respect to metal plane. Compare with Fig. 2.4.

Next, in Fig. 6.2 we show orbital-resolved decomposition, similarly to result presented in Fig. 2.5. Let us note first that our method of projection clearly captures the fact that largest overlaps are coming from 4d and 3p orbitals for MoS_2, while 5d and 4p for WSe_2. We confirm that all coupling rules (e.g. d_0 and p_{-1} in CB at +K point) for even orbitals are the same as for MoS_2. These results support conclusion that our TB Hamiltonian is well suited to describe MX_2 family of semiconductors in 2H phase.

In the third step we present collected results of gaps between spin-split extrema of valence and conduction bands, as shown in Fig. 2.6. Those results are summarized in Table 6.1.

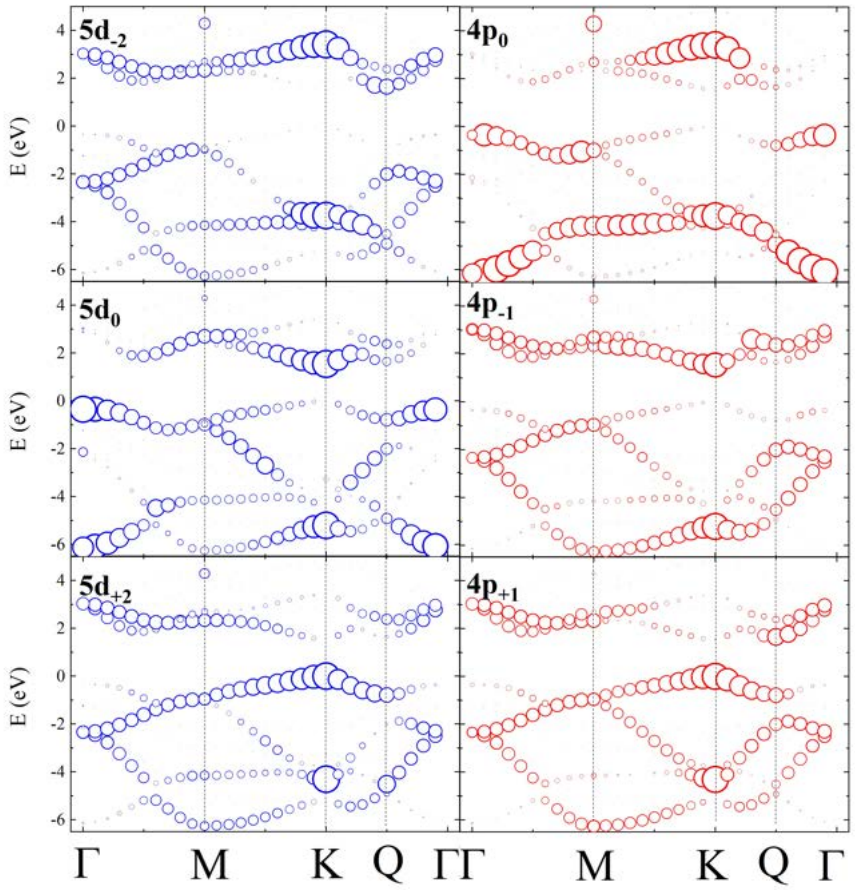

Figure 6.2: Collected symmetric contributions to bands in WSe_2.

6.4 Details of NN and NNN TB Hamiltonian derivation

Now we discuss details of tight-binding model derivation. First we introduce notion of directional cosines defined as $(l,m,n) = \left(\frac{d_x}{d}, \frac{d_y}{d}, \frac{d_z}{d}\right)$, where $\vec{d} = (d_x, d_y, d_z)$ denotes bond from metal to chalcogen atom and $d = |\vec{d}|$ is distance between two atoms, which can be written as $d = \sqrt{d_\perp^2 + d_\parallel^2}$. For three chalcogen dimers ($j = 1, 2, 3$) surrounding central metal atom we have therefore:

$$\begin{aligned} l_1 &= \frac{d_\parallel}{d}, m_1 = 0, n_1 = \pm\frac{d_\perp}{d} \\ l_2 &= -\frac{d_\parallel}{2d}, m_2 = \frac{\sqrt{3}d_\parallel}{2d}, n_2 = \pm\frac{d_\perp}{d} \\ l_3 &= \frac{d_\parallel}{2d}, m_3 = -\frac{\sqrt{3}d_\parallel}{2d}, n_3 = \pm\frac{d_\perp}{d} \end{aligned} \tag{6.7}$$

energy difference	MoS_2	$MoSe_2$	$MoTe_2$	WS_2	WSe_2	WTe_2
Δ_{VB}^{SOC}	148	186	218	435	473	498
Δ_{CB}^{SOC}	3	21	32	30	38	58
$\Delta_{K-\Gamma}^{SOC}$	65	351	544	255	520	655
Δ_{K-Q}^{SOC}	227	143	159	94	30	155

Table 6.1: Absolute values of gaps between spin-split extrema of valence and conduction bands calculated using DFT + SOC. All values are given in meV.

where for all z-th directional cosines n plus sign is for upper chalcogen in dimer, and minus sign for lower one.

Next we discuss linear transformation between complex and real spherical harmonics. Because basis we work in is defined via orbitals with well defined L and m quantum numbers, to use Slater - Koster rules we have to express those orbitals in terms of real harmonics. Let us introduce for convenience notation

$$\varphi_{L=2,m_d} \equiv |d_{m_d}\rangle, \qquad \varphi_{L=1,m_p} \equiv |p_{m_p}\rangle. \tag{6.8}$$

This mapping we need is defined for d - orbitals in the following way:

$$\begin{aligned} |d_{m_d=-2}\rangle &= \frac{1}{\sqrt{2}}\left(|d_{x^2-y^2}\rangle - i|d_{xy}\rangle\right), \\ |d_{m_d=0}\rangle &= |d_{3z^2-r^2}\rangle, \\ |d_{m_d=2}\rangle &= \frac{1}{\sqrt{2}}\left(|d_{x^2-y^2}\rangle + i|d_{xy}\rangle\right). \end{aligned} \tag{6.9}$$

For p orbitals analogous relation yields

$$\begin{aligned} |p_{m_p=-1}\rangle &= \frac{1}{\sqrt{2}}\left(|p_x\rangle - i|p_y\rangle\right), \\ |p_{m_p=0}\rangle &= |p_z\rangle, \\ |p_{m_p=1}\rangle &= -\frac{1}{\sqrt{2}}\left(|p_x\rangle + i|p_y\rangle\right). \end{aligned} \tag{6.10}$$

Necessary Slater-Koster rules for two - center energy integrals, depending on

directional cosines are[18]

$$
\begin{aligned}
\langle d_{3z^2-r^2}|V|p_x\rangle &= -\frac{1}{2}l\left[\left(3n^2-1\right)V_{dp\sigma}-2\sqrt{3}n^2V_{dp\pi}\right],\\
\langle d_{3z^2-r^2}|V|p_y\rangle &= -\frac{1}{2}m\left[\left(3n^2-1\right)V_{dp\sigma}-2\sqrt{3}n^2V_{dp\pi}\right],\\
\langle d_{3z^2-r^2}|V|p_x\rangle &= -\frac{1}{2}n\left[\left(3n^2-1\right)V_{dp\sigma}-2\sqrt{3}\left(n^2-1\right)V_{dp\pi}\right],\\
\langle d_{x^2-y^2}|V|p_x\rangle &= -\frac{1}{2}l\left[\sqrt{3}\left(l^2-m^2\right)V_{dp\sigma}+2\left(2m^2+n^2\right)V_{dp\pi}\right],\\
\langle d_{x^2-y^2}|V|p_y\rangle &= -\frac{1}{2}m\left[\sqrt{3}\left(l^2-m^2\right)V_{dp\sigma}-2\left(2l^2+n^2\right)V_{dp\pi}\right],\\
\langle d_{x^2-y^2}|V|p_z\rangle &= -\frac{1}{2}n\left(l^2-m^2\right)\left[\sqrt{3}V_{dp\sigma}-2V_{dp\pi}\right],\\
\langle d_{xy}|V|p_x\rangle &= -m\left[l^2\left(\sqrt{3}V_{dp\sigma}-2V_{dp\pi}\right)+V_{dp\pi}\right],\\
\langle d_{xy}|V|p_y\rangle &= -l\left[m^2\left(\sqrt{3}V_{dp\sigma}-2V_{dp\pi}\right)+V_{dp\pi}\right],\\
\langle d_{xy}|V|p_z\rangle &= -lmn\left[\sqrt{3}V_{dp\sigma}-2V_{dp\pi}\right]
\end{aligned}
\tag{6.11}
$$

In next step those rules can be used to calculate rules for complex orbitals, e.g. for $L=2, m_d=-2$ to $L=1, m_p=-1$ element we have, remembering about dimer construction $|p_{m_p=-1}\rangle = 1/\sqrt{2}\left(|p^U_{m_p=-1}\rangle + |p^L_{m_p=-1}\rangle\right)$:

$$
\begin{aligned}
&\langle d_{m_d=-2}|V|p_{m_p=-1}\rangle = \frac{1}{\sqrt{2}}\left[\langle d_{x^2-y^2}|V|p_{m_p=-1}\rangle + i\langle d_{xy}|V|p_{m_p=-1}\rangle\right] =\\
&\frac{1}{2}\left[\langle d_{x^2-y^2}|V|p^U_{m_p=-1}\rangle + \langle d_{x^2-y^2}|V|p^L_{m_p=-1}\rangle + i\langle d_{xy}|V|p^U_{m_p=-1}\rangle + i\langle d_{xy}|V|p^L_{m_p=-1}\rangle\right] =\\
&\frac{1}{2\sqrt{2}}\Big[\langle d_{x^2-y^2}|V|p^U_x\rangle - i\langle d_{x^2-y^2}|V|p^U_y\rangle + \langle d_{x^2-y^2}|V|p^L_x\rangle - i\langle d_{x^2-y^2}|V|p^L_y\rangle +\\
&\qquad i\langle d_{xy}|V|p^U_x\rangle + \langle d_{xy}|V|p^U_y\rangle + i\langle d_{xy}|V|p^L_x\rangle + \langle d_{xy}|V|p^L_y\rangle\Big] =\\
&\frac{l+im}{\sqrt{2}}\left[\frac{\sqrt{3}}{2}V_{dp\sigma}\left(\frac{d_\perp^2}{d^2}-1\right)-V_{dp\pi}\left(\frac{d_\perp^2}{d^2}+1\right)\right]
\end{aligned}
\tag{6.12}
$$

Using the same rules rest of the remaining hopping matrix elements can be

evaluated:

$$
\begin{aligned}
\langle d_{m_d=-2}|V|p_{m_p=0}\rangle &= -\frac{(l+im)^2}{2}\frac{d_\perp}{d}\left[\sqrt{3}V_{dp\sigma}-2V_{dp\pi}\right],\\
\langle d_{m_d=-2}|V|p_{m_p=1}\rangle &= -\frac{(l+im)^3}{\sqrt{2}}\left[\frac{\sqrt{3}}{2}V_{dp\sigma}-V_{dp\pi}\right],\\
\langle d_{m_d=0}|V|p_{m_p=-1}\rangle &= -\frac{l-im}{2}\left[\left(3\frac{d_\perp^2}{d^2}-1\right)V_{dp\sigma}-2\sqrt{3}\frac{d_\perp^2}{d^2}V_{dp\pi}\right],\\
\langle d_{m_d=0}|V|p_{m_p=0}\rangle &= -\frac{1}{\sqrt{2}}\frac{d_\perp}{d}\left[\left(3\frac{d_\perp^2}{d^2}-1\right)V_{dp\sigma}-2\sqrt{3}\left(\frac{d_\perp^2}{d^2}-1\right)V_{dp\pi}\right],\\
\langle d_{m_d=0}|V|p_{m_p=1}\rangle &= -\frac{l+im}{2}\left[\left(3\frac{d_\perp^2}{d^2}-1\right)V_{dp\sigma}-2\sqrt{3}\frac{d_\perp^2}{d^2}V_{dp\pi}\right],\\
\langle d_{m_d=2}|V|p_{m_p=-1}\rangle &= -\frac{(l-im)^3}{\sqrt{2}}\left[\frac{\sqrt{3}}{2}V_{dp\sigma}-V_{dp\pi}\right],\\
\langle d_{m_d=2}|V|p_{m_p=0}\rangle &= -\frac{(l-im)^2}{2}\frac{d_\perp}{d}\left[\sqrt{3}V_{dp\sigma}-2V_{dp\pi}\right],\\
\langle d_{m_d=2}|V|p_{m_p=1}\rangle &= \frac{l-im}{\sqrt{2}}\left[\frac{\sqrt{3}}{2}V_{dp\sigma}\left(\frac{d_\perp^2}{d^2}-1\right)-V_{dp\pi}\left(\frac{d_\perp^2}{d^2}+1\right)\right].
\end{aligned}
\tag{6.13}
$$

Final step to obtain Hamiltonian matrix element is evaluation of matrix elements between Bloch sums:

$$
\langle\Psi^{\vec{k}}_{A,m_d}|\hat{H}|\Psi^{\vec{k}}_{B,m_p}\rangle = \frac{1}{N_{UC}}\sum_{i=1}^{N_{UC}}\sum_{j=1}^{N_{UC}} e^{i\vec{k}\cdot\left(\vec{R}_{B,i}-\vec{R}_{A,j}\right)}\langle d_{m_d}\left(\vec{R}_{A,j}\right)|\hat{H}|p_{m_p}\left(\vec{R}_{B,i}\right)\rangle,
\tag{6.14}
$$

where notation

$$
\begin{aligned}
|d_{m_d}\left(\vec{R}_{A,j}\right)\rangle &= \varphi_{L=2,m_d}\left(\vec{r}-\vec{R}_{A,j}\right)\\
|p_{m_p}\left(\vec{R}_{B,i}\right)\rangle &= \varphi_{L=1,m_p}\left(\vec{r}-\vec{R}_{B,i}\right)
\end{aligned}
\tag{6.15}
$$

has been introduced. Applying usual two-center approximation and keeping only three nearest-neighbor chalcogen dimers we end up with expression

$$
\langle\Psi^{\vec{k}}_{A,m_d}|\hat{H}|\Psi^{\vec{k}}_{B,m_p}\rangle \approx \sum_{j=1}^{3} e^{i\vec{k}\cdot\vec{R}_{B,i}}\langle d_{m_d}|V|p_{m_p}\left(\vec{R}_{B,i}\right)\rangle,
\tag{6.16}
$$

Let us evaluate one full, k - dependent tunneling matrix element

$$
\begin{aligned}
&\langle\Psi^{\vec{k}}_{A,m_d=-2}|\hat{H}|\Psi^{\vec{k}}_{B,m_p=-1}\rangle =\\
&\sum_{j=1}^{3} e^{i\vec{k}\cdot\vec{R}_j}\frac{(l_j+im_j)}{\sqrt{2}}\left[\frac{\sqrt{3}}{2}V_{dp\sigma}\left(\frac{d_\perp^2}{d^2}-1\right)-V_{dp\pi}\left(\frac{d_\perp^2}{d^2}+1\right)\right].
\end{aligned}
\tag{6.17}
$$

For nearest chalcogen dimer positions we have (see Fig. 1.1) $\vec{R}_{B_1}=\left(d_\parallel,0\right)$, $\vec{R}_{B_2}=\left(-d_\parallel/2,\sqrt{3}d_\parallel/2\right)$, $\vec{R}_{B_3}=\left(-d_\parallel/2,-\sqrt{3}d_\parallel/2\right)$, which give $l_1+im_1=$

$e^{i0}\frac{d_\parallel}{d}$, $l_2+im_2=e^{i\frac{2\pi}{3}}\frac{d_\parallel}{d}$, $l_3+im_3=e^{i\frac{4\pi}{3}}\frac{d_\parallel}{d}$, respectively. Noting that prefactors depending on Slater - Koster parameters are j - independent, we can finally write matrix element as

$$\langle\Psi^{\vec{k}}_{A,m_d=-2}|\hat{H}|\Psi^{\vec{k}}_{B,m_p=-1}\rangle=\underbrace{\frac{1}{\sqrt{2}}\frac{d_\parallel}{d}\left[\frac{\sqrt{3}}{2}V_{dp\sigma}\left(\frac{d_\perp^2}{d^2}-1\right)-V_{dp\pi}\left(\frac{d_\perp^2}{d^2}+1\right)\right]}_{V_1}\cdot$$
$$\underbrace{\left[e^{ik_xd_\parallel}+e^{-ik_xd_\parallel/2}e^{i\sqrt{3}k_yd_\parallel/2}e^{i2\pi/3}+e^{-ik_xd_\parallel/2}e^{i\sqrt{3}k_yd_\parallel/2}e^{i4\pi/3}\right]}_{f_{-1}(\vec{k})}. \tag{6.18}$$

We note that this complicated expression can be written in terms of k-dependent function $f(\vec{k})$ and functions V which depend on Slater-Koster integrals and structural parameters. Using this approach, rest of the matrix elements can be expressed as

$$\begin{aligned}
\langle\Psi^{\vec{k}}_{A,m_d=-2}|\hat{H}|\Psi^{\vec{k}}_{B,m_p=0}\rangle&=-V_2f_0\left(\vec{k}\right),\\
\langle\Psi^{\vec{k}}_{A,m_d=-2}|\hat{H}|\Psi^{\vec{k}}_{B,m_p=1}\rangle&=V_3f_1\left(\vec{k}\right),\\
\langle\Psi^{\vec{k}}_{A,m_d=0}|\hat{H}|\Psi^{\vec{k}}_{B,m_p=-1}\rangle&=-V_4f_0\left(\vec{k}\right),\\
\langle\Psi^{\vec{k}}_{A,m_d=0}|\hat{H}|\Psi^{\vec{k}}_{B,m_p=0}\rangle&=-V_5f_1\left(\vec{k}\right),\\
\langle\Psi^{\vec{k}}_{A,m_d=0}|\hat{H}|\Psi^{\vec{k}}_{B,m_p=1}\rangle&=-V_4f_{-1}\left(\vec{k}\right),\\
\langle\Psi^{\vec{k}}_{A,m_d=2}|\hat{H}|\Psi^{\vec{k}}_{B,m_p=-1}\rangle&=-V_3f_1\left(\vec{k}\right),\\
\langle\Psi^{\vec{k}}_{A,m_d=2}|\hat{H}|\Psi^{\vec{k}}_{B,m_p=0}\rangle&=-V_2f_{-1}\left(\vec{k}\right),\\
\langle\Psi^{\vec{k}}_{A,m_d=2}|\hat{H}|\Psi^{\vec{k}}_{B,m_p=1}\rangle&=V_1f_0\left(\vec{k}\right),
\end{aligned} \tag{6.19}$$

where

$$\begin{aligned}
f_{-1}\left(\vec{k}\right)&=\left[e^{ik_xd_\parallel}+e^{-ik_xd_\parallel/2}e^{i\sqrt{3}k_yd_\parallel/2}e^{i2\pi/3}+e^{-ik_xd_\parallel/2}e^{i\sqrt{3}k_yd_\parallel/2}e^{i4\pi/3}\right],\\
f_0\left(\vec{k}\right)&=\left[e^{ik_xd_\parallel}+e^{-ik_xd_\parallel/2}e^{i\sqrt{3}k_yd_\parallel/2}e^{-i2\pi/3}+e^{-ik_xd_\parallel/2}e^{-i\sqrt{3}k_yd_\parallel/2}e^{i2\pi/3}\right],\\
f_1\left(\vec{k}\right)&=\left[e^{ik_xd_\parallel}+e^{-ik_xd_\parallel/2}e^{i\sqrt{3}k_yd_\parallel/2}+e^{-ik_xd_\parallel/2}e^{-i\sqrt{3}k_yd_\parallel/2}\right],
\end{aligned} \tag{6.20}$$

and k-independent elements are given by:

$$
\begin{aligned}
V_1 &= \frac{1}{\sqrt{2}}\frac{d_\parallel}{d}\left[\frac{\sqrt{3}}{2}\left(\frac{d_\perp^2}{d^2}-1\right)V_{dp\sigma}-\left(\frac{d_\perp^2}{d^2}+1\right)V_{dp\pi}\right],\\
V_2 &= \frac{1}{2}\frac{d_\perp}{d}\left(\frac{d_\parallel}{d}\right)^2\left[\sqrt{3}V_{dp\sigma}-2V_{dp\pi}\right],\\
V_3 &= \frac{1}{\sqrt{2}}\left(\frac{d_\parallel}{d}\right)^3\left[\frac{\sqrt{3}}{2}V_{dp\sigma}-V_{dp\pi}\right],\\
V_4 &= \frac{1}{2}\frac{d_\parallel}{d}\left[\left(3\frac{d_\perp^2}{d^2}-1\right)V_{dp\sigma}-2\sqrt{3}\frac{d_\perp^2}{d^2}V_{dp\pi}\right],\\
V_5 &= \frac{1}{2}\frac{d_\perp}{d}\left[\left(3\frac{d_\perp^2}{d^2}-1\right)V_{dp\sigma}-2\sqrt{3}\left(\frac{d_\perp^2}{d^2}-1\right)V_{dp\pi}\right]
\end{aligned}
\tag{6.21}
$$

Final form of nearest - neighbor tight-binding Hamiltonian reads:

$$
H\left(\vec{k}\right)=\begin{pmatrix}
E_{m_d=-2} & 0 & 0 & V_1 f_{-1}(\vec{k}) & -V_2 f_0(\vec{k}) & V_3 f_1(\vec{k})\\
 & E_{m_d=0} & 0 & -V_4 f_0(\vec{k}) & -V_5 f_1(\vec{k}) & V_4 f_{-1}(\vec{k})\\
 & & E_{m_d=2} & -V_3 f_1(\vec{k}) & -V_2 f_{-1}(\vec{k}) & -V_1 f_0(\vec{k})\\
 & & & E_{m_p=-1} & 0 & 0\\
 & & & & E_{m_p=0} & 0\\
 & & & & & E_{m_p=1}
\end{pmatrix}
\tag{6.22}
$$

Motivated by failure of the nearest neighbor tight-binding Hamiltonian do describe properly bands around Fermi level, we turn to derivation of next-nearest neighbor hopping elements. As one can see in Fig. 2.1, central metal atom has six next - nearest neighbor metal atoms in positions $R_{A_1}-R_{A_6}$. For next nearest neighbors we introduce new notation for directional cosines (l_2, m_2, n_2), not to be confused with index 2 for (l, m, n) for atom at position R_{B_2}. Analogously to first NN model derivation, we begin with listing Slater - Koster rules for two-center integrals between d orbitals:[18]

$$
\begin{aligned}
&\langle d_{3z^2-r^2}|V|d_{3z^2-r^2}\rangle = \left(\frac{1}{2}l_2^2+\frac{1}{2}m_2^2-n_2^2\right)^2 V_{dd\sigma}+3n_2^2\left(1-n_2^2\right)V_{dd\pi}+\frac{3}{4}\left(n_2^2-1\right)^2 V_{dd\delta},\\
&\langle d_{3z^2-r^2}|V|d_{x^2-y^2}\rangle = \frac{\sqrt{3}}{4}\left(l_2^2-m_2^2\right)\left[\left(3n_2^2-1\right)V_{dd\sigma}-4n_2^2V_{dd\pi}+\left(n_2^2+1\right)V_{dd\delta}\right],\\
&\langle d_{3z^2-r^2}|V|d_{xy}\rangle = \frac{\sqrt{3}}{2}l_2m_2\left[\left(3n_2^2-1\right)V_{dd\sigma}-4n_2^2V_{dd\pi}+\left(n_2^2+1\right)V_{dd\delta}\right],\\
&\langle d_{x^2-y^2}|V|d_{x^2-y^2}\rangle = \frac{3}{4}\left(l_2^2-m_2^2\right)V_{dd\sigma}+\left[l_2^2+m_2^2-\left(l_2^2-m_2^2\right)^2\right]V_{dd\pi}+\left[\frac{1}{4}\left(l_2^2-m_2^2\right)n_2^2\right]V_{dd\delta},\\
&\langle d_{x^2-y^2}|V|d_{xy}\rangle = \frac{1}{2}l_2m_2\left(l_2^2-m_2^2\right)\left[3V_{dd\sigma}-4V_{dd\pi}+V_{dd\delta}\right],\\
&\langle d_{xy}|V|d_{xy}\rangle = 3l_2^2m_2^2V_{dd\sigma}+\left(l_2^2m_2^2-4l_2^2m_2^2\right)V_{dd\pi}+\left(l_2^2m_2^2+n_2^2\right)V_{dd\delta}
\end{aligned}
\tag{6.23}
$$

Rules for p-orbitals are:

$$\begin{aligned}
\langle p_x|V|p_x\rangle &= l_2^2 V_{pp\sigma} + \left(1-l_2^2\right) V_{pp\pi},\\
\langle p_x|V|p_y\rangle &= l_2 m_2 \left(V_{pp\sigma} - V_{pp\pi}\right),\\
\langle p_x|V|p_z\rangle &= l_2 n_2 \left(V_{pp\sigma} - V_{pp\pi}\right),\\
\langle p_y|V|p_y\rangle &= m_2^2 V_{pp\sigma} + \left(1-m_2^2\right) V_{pp\pi},\\
\langle p_y|V|p_z\rangle &= m_2 n_2 \left(V_{pp\sigma} - V_{pp\pi}\right),\\
\langle p_z|V|p_z\rangle &= n_2^2 V_{pp\sigma} + \left(1-n_2^2\right) V_{pp\pi}.
\end{aligned} \tag{6.24}$$

Using above formulas we get for complex orbitals:

$$\begin{aligned}
\langle d_{m_d=-2}|V|d_{m_d=-2}\rangle =& \frac{1}{2}\left(\langle d_{x^2-y^2}| + i\langle d_{xy}|\right) V \left(|d_{x^2+y^2}\rangle - i|d_{xy}\rangle\right) =\\
&= \frac{1}{8}\left(3V_{dd\sigma} + 4V_{dd\pi} + V_{dd\delta}\right)
\end{aligned} \tag{6.25}$$

Remaining hopping elements read:

$$\begin{aligned}
\langle d_{m_d=-2}|V|d_{m_d=0}\rangle &= -\frac{\sqrt{3}}{4\sqrt{2}}\left(l_2+im_2\right)^2\left[V_{dd\sigma} - V_{dd\delta}\right],\\
\langle d_{m_d=-2}|V|d_{m_d=2}\rangle &= \frac{1}{8}\left(l_2+im_2\right)^4\left[3V_{dd\sigma} - 4V_{dd\pi} + V_{dd\delta}\right],\\
\langle d_{m_d=0}|V|d_{m_d=0}\rangle &= \frac{1}{4}V_{dd\sigma} + \frac{3}{4}V_{dd\delta},\\
\langle d_{m_d=0}|V|d_{m_d=2}\rangle &= -\frac{\sqrt{3}}{4\sqrt{2}}\left(l_2+im_2\right)^2\left[V_{dd\sigma} - V_{dd\delta}\right],\\
\langle d_{m_d=-2}|V|d_{m_d=2}\rangle &= \frac{1}{8}\left(l_2+im_2\right)^4\left(3V_{dd\sigma} - 4V_{dd\pi} + V_{dd\delta}\right)
\end{aligned} \tag{6.26}$$

Before we list similar hopping elements for chalcogen dimers, we note that we neglect in next - nearest interaction cross terms of interaction between top and bottom chalcogens, keeping only terms that are within the same plane (top-top, bottom-bottom). In this approximation hopping elements yield:

$$\begin{aligned}
\langle p_{m_1=-1}|V|p_{m_p=-1}\rangle &= \frac{1}{2}\left(V_{pp\sigma} + V_{pp\pi}\right),\\
\langle p_{m_1=-1}|V|p_{m_p=0}\rangle &= 0,\\
\langle p_{m_1=-1}|V|p_{m_p=1}\rangle &= \frac{1}{2}\left(l_2+im_2\right)^2\left(V_{pp\sigma} - V_{pp\pi}\right),\\
\langle p_{m_1=0}|V|p_{m_p=0}\rangle &= V_{pp\pi},\\
\langle p_{m_1=0}|V|p_{m_p=1}\rangle &= 0,\\
\langle p_{m_1=1}|V|p_{m_p=1}\rangle &= \frac{1}{2}\left(V_{pp\sigma} + V_{pp\pi}\right).
\end{aligned} \tag{6.27}$$

Remembering that because metal atoms are in the same plane and we neglected top-bottom chalcogen interactions, we always have $n_2 = 0$, which results also in $l_2^2 + m_2^2 = 1$. Using this we can obtain for second nearest neighbor TB Hamilto-

nian matrix elements:

$$
\begin{aligned}
&\langle \Psi^{\vec{k}}_{A,m_d=-2} | \hat{H} | \Psi^{\vec{k}}_{A,m_d=-2} \rangle = E_{d=-2} + W_1 g_0 \left(\vec{k} \right), \\
&\langle \Psi^{\vec{k}}_{A,m_d=-2} | \hat{H} | \Psi^{\vec{k}}_{A,m_d=0} \rangle = W_3 g_2 \left(\vec{k} \right), \\
&\langle \Psi^{\vec{k}}_{A,m_d=-2} | \hat{H} | \Psi^{\vec{k}}_{A,m_d=2} \rangle = W_4 g_4 \left(\vec{k} \right), \\
&\langle \Psi^{\vec{k}}_{A,m_d=0} | \hat{H} | \Psi^{\vec{k}}_{A,m_d=0} \rangle = E_{d=0} + W_2 g_0 \left(\vec{k} \right), \\
&\langle \Psi^{\vec{k}}_{A,m_d=0} | \hat{H} | \Psi^{\vec{k}}_{A,m_d=2} \rangle = W_3 g_2 \left(\vec{k} \right), \\
&\langle \Psi^{\vec{k}}_{A,m_d=2} | \hat{H} | \Psi^{\vec{k}}_{A,m_d=2} \rangle = E_{d=2} + W_1 g_0 \left(\vec{k} \right), \\
&\langle \Psi^{\vec{k}}_{B,m_p=-1} | \hat{H} | \Psi^{\vec{k}}_{B,m_p=-1} \rangle = E_{p=-1} + W_5 g_0 \left(\vec{k} \right), \\
&\langle \Psi^{\vec{k}}_{B,m_p=-1} | \hat{H} | \Psi^{\vec{k}}_{B,m_p=0} \rangle = 0, \\
&\langle \Psi^{\vec{k}}_{B,m_p=-1} | \hat{H} | \Psi^{\vec{k}}_{B,m_p=1} \rangle = W_7 g_2 \left(\vec{k} \right), \\
&\langle \Psi^{\vec{k}}_{B,m_p=0} | \hat{H} | \Psi^{\vec{k}}_{B,m_p=0} \rangle = E_{p=0} + W_6 g_0 \left(\vec{k} \right), \\
&\langle \Psi^{\vec{k}}_{B,m_p=0} | \hat{H} | \Psi^{\vec{k}}_{B,m_p=1} \rangle = 0, \\
&\langle \Psi^{\vec{k}}_{B,m_p=1} | \hat{H} | \Psi^{\vec{k}}_{B,m_p=1} \rangle = E_{p=1} + W_5 g_0 \left(\vec{k} \right).
\end{aligned}
\tag{6.28}
$$

Functions W_i, which are independent of $\vec{k}$, are given by:

$$
\begin{aligned}
W_1 &= \frac{1}{8} \left(3V_{dd\sigma} + 4V_{dd\pi} + V_{dd\delta} \right), \\
W_2 &= \frac{1}{4} \left(V_{dd\sigma} + 3V_{dd\delta} \right), \\
W_3 &= -\frac{\sqrt{3}}{4\sqrt{2}} \left(V_{dd\sigma} - V_{dd\delta} \right), \\
W_4 &= \frac{1}{8} \left(3V_{dd\sigma} - 4V_{dd\pi} + V_{dd\delta} \right), \\
W_5 &= \frac{1}{2} \left(V_{pp\sigma} + V_{pp\pi} \right), \\
W_6 &= V_{pp\pi}, \\
W_7 &= \frac{1}{2} \left(V_{pp\sigma} - V_{pp\pi} \right).
\end{aligned}
\tag{6.29}
$$

k-dependent $g\left(\vec{k}\right)$ functions can be expressed as:

$$
\begin{aligned}
g_0 \left(\vec{k} \right) &= 4 \cos \left(\frac{3}{2} k_x d_{\parallel} \right) \cos \left(\frac{\sqrt{3}}{2} k_y d_{\parallel} \right) + 2 \cos \left(\sqrt{3} k_y d_{\parallel} \right), \\
g_2 \left(\vec{k} \right) &= 2 \cos \left(\frac{3}{2} k_x d_{\parallel} + \frac{\sqrt{3}}{2} k_y d_{\parallel} \right) e^{i\frac{\pi}{3}} + 2 \cos \left(\frac{3}{2} k_x d_{\parallel} - \frac{\sqrt{3}}{2} k_y d_{\parallel} \right) e^{-i\frac{\pi}{3}} - 2 \cos \left(\sqrt{3} k_y d_{\parallel} \right), \\
g_4 \left(\vec{k} \right) &= 2 \cos \left(\frac{3}{2} k_x d_{\parallel} + \frac{\sqrt{3}}{2} k_y d_{\parallel} \right) e^{i\frac{2\pi}{3}} + 2 \cos \left(\frac{3}{2} k_x d_{\parallel} - \frac{\sqrt{3}}{2} k_y d_{\parallel} \right) e^{-i\frac{2\pi}{3}} + 2 \cos \left(\sqrt{3} k_y d_{\parallel} \right)
\end{aligned}
\tag{6.30}
$$

The final Hamiltonian matrix is given by:

$$H\left(\vec{k}\right) = \begin{pmatrix} \begin{matrix} E_{m_d=-2} \\ +W_1 g_0(\vec{k}) \end{matrix} & W_3 g_2(\vec{k}) & W_4 g_4(\vec{k}) & V_1 f_{-1}(\vec{k}) & -V_2 f_0(\vec{k}) & V_3 f_1(\vec{k}) \\ & \begin{matrix} E_{m_d=0} \\ +W_2 g_0(\vec{k}) \end{matrix} & W_3 g_2(\vec{k}) & -V_4 f_0(\vec{k}) & -V_5 f_1(\vec{k}) & V_4 f_{-1}(\vec{k}) \\ & & \begin{matrix} E_{m_d=2} \\ +W_1 g_0(\vec{k}) \end{matrix} & -V_3 f_1(\vec{k}) & -V_2 f_{-1}(\vec{k}) & -V_1 f_0(\vec{k}) \\ & & & \begin{matrix} E_{m_p=-1} \\ +W_5 g_0(\vec{k}) \end{matrix} & 0 & -W_7 g_2(\vec{k}) \\ & & & & \begin{matrix} E_{m_p=0} \\ +W_6 g_0(\vec{k}) \end{matrix} & 0 \\ & & & & & \begin{matrix} E_{m_p=1} \\ +W_5 g_0(\vec{k}) \end{matrix} \end{pmatrix} \tag{6.31}$$

6.5 Slater-Koster parameters for best VB and CB with SOC

In the following Appendix we list SK parameters for fit presented in Fig. 2.10. In Fig. 6.3, presenting same information as Fig. 2.10, we zoom into two conduction bands and valence band on the left and right panels, respectively.

parameter	best CB	best VB
$E_{m_d=0,\pm2}$	0.0086	-0.0124
$E_{m_p=\pm1}$	-2.6743	-1.8464
$E_{m_p=0}$	-2.8824	-3.4268
$V_{dp\sigma}$	-2.4255	2.4894
$V_{dp\pi}$	1.0283	-0.9028
$V_{dd\sigma}$	-0.9230	-1.0190
$V_{dd\pi}$	0.0595	0.7564
$V_{dd\delta}$	0.0367	0.2077
$V_{pp\sigma}$	1.3672	0.6881
$V_{pp\pi}$	-0.0777	-0.1977

Table 6.2: Slater-Koster parameters fitted to DFT MoS_2 bandstructure tailored for best reproduction of CB and VB with SOC. For both fits we use $\lambda_{Mo} = 0.148/2$ eV and $\lambda_{S_2} = 0.03/2$ eV. All values in table are given in eV.

6.6 Orbital Zeeman splitting in TB model

In the following Appendix we are interested in evaluating orbital Zeeman matrix element H_2 in the form

$$\Delta E_n(K) = \langle \Psi_n(K) | \frac{\hat{L}_z}{\hbar} | \Psi_n(K) \rangle \mu_B B_z, \tag{6.32}$$

where n is band (CB or VB). To do that, we first consider arbitrary matrix element between sublattice Bloch wavefunctions, constructed from localized or-

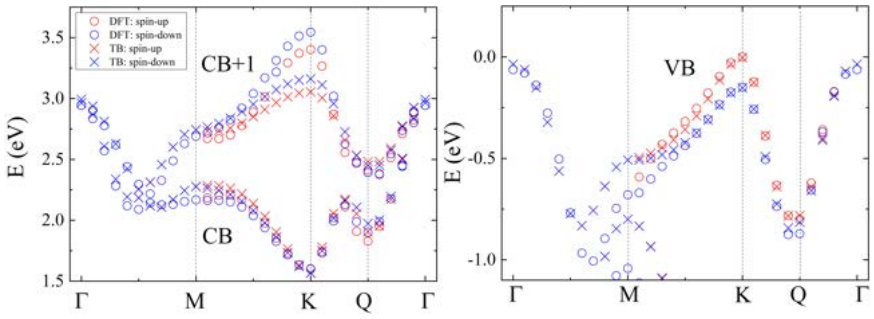

Figure 6.3: Zoom into CB and VB + SOC bandstructure fitted separately using TB+SOC model.

bitals with specific quantum numbers L, m

$$\begin{aligned}\Psi_A^m\left(\vec{k},\vec{r}\right) &= \frac{1}{\sqrt{N_{UC}}}\sum_{i=1}^{N_{UC}} e^{i\vec{k}\cdot\vec{R}_{A,i}}\varphi_m\left(\vec{r}-\vec{R}_{A,i}\right),\\ \Psi_B^l\left(\vec{k},\vec{r}\right) &= \frac{1}{\sqrt{N_{UC}}}\sum_{j=1}^{N_{UC}} e^{i\vec{k}\cdot\vec{R}_{B,j}}\varphi_l\left(\vec{r}-\vec{R}_{B,j}\right).\end{aligned} \tag{6.33}$$

For orbital angular momentum operator defined as $L_z = -i\hbar\left(\vec{r}\times\vec{\nabla}_{\vec{r}}\right)_z$ and introducing $\vec{R}_{AB} = \vec{R}_{A,i} - \vec{R}_{B,j}$ our matrix element yields

$$\begin{aligned}&-i\hbar\langle\Psi_B^l\left(\vec{k},\vec{r}\right)|\left(\vec{r}\times\vec{\nabla}_{\vec{r}}\right)_z|\Psi_A^m\left(\vec{k},\vec{r}\right)\rangle =\\ &=\frac{-i\hbar}{N_{UC}}\sum_{i,j=1}^{N_{UC}}\int_{R^3} d\vec{r}e^{i\vec{k}\cdot\vec{R}_{AB}}\varphi_l^*\left(\vec{r}-\vec{R}_{B,j}\right)\left(\vec{r}\times\vec{\nabla}_{\vec{r}}\right)_z\varphi_m\left(\vec{r}-\vec{R}_{A,i}\right).\end{aligned} \tag{6.34}$$

In next step we introduce new vector $\vec{u}_i$ describing coordinates around given $\vec{R}_{A/B,i}$ atomic center as

$$\vec{u}_i = \vec{r}-\vec{R}_{A,i} \rightarrow \vec{r} = \vec{u}_i + \vec{R}_{A,i} \rightarrow d\vec{r} = d\vec{u}_i. \tag{6.35}$$

This allows us to write how L_z acts on orbital φ

$$\begin{aligned}&-i\hbar\left(\vec{r}\times\frac{\partial}{\partial\vec{r}}\right)_z\varphi_m\left(\vec{r}-\vec{R}_{A,i}\right) = -i\hbar\left(\left(\vec{u}_i+\vec{R}_{A,i}\right)\times\frac{\partial}{\partial\vec{u}_i}\underbrace{\frac{\partial\vec{u}_i}{\partial r}}_{=1}\right)_z\varphi_m\left(\vec{u}_i\right),\\ &=\underbrace{-i\hbar\left(\vec{u}_i\times\frac{\partial}{\partial\vec{u}_i}\right)_z}_{L_z}\varphi_m\left(\vec{u}_i\right)+\left(\vec{R}_{A,i}\times\underbrace{(-i\hbar)\frac{\partial}{\partial\vec{u}_i}}_{\vec{p}_{u_i}}\right)_z\varphi_m\left(\vec{u}_i\right),\\ &=m\varphi_m\left(\vec{u}_i\right)+\left(\vec{R}_{A,i}\times\vec{p}_{u_i}\right)_z\varphi_m\left(\vec{u}_i\right).\end{aligned} \tag{6.36}$$

Knowing how L_z operator acts on orbital, using previously defined u_i, $\vec{r}-\vec{R}_{B,j} = \vec{u}_i + \vec{R}_{A,i} - \vec{R}_{B,j} = \vec{u}_i + \vec{R}_{AB}$ and changing summation over i,j to $\vec{R}_{AB}, \vec{R}_A$ we obtain

$$
\begin{aligned}
&-i\hbar\langle\Psi_B^l\left(\vec{k},\vec{r}\right)|\left(\vec{r}\times\vec{\nabla}_{\vec{r}}\right)_z|\Psi_A^m\left(\vec{k},\vec{r}\right)\rangle \\
&= \frac{m}{N_{UC}}\sum_{\vec{R}_{AB},\vec{R}_A}^{N_{UC}}\int d\vec{u}e^{i\vec{k}\cdot\vec{R}_{AB}}\underbrace{\varphi_l^*\left(\vec{u}+\vec{R}_{AB}\right)\varphi_m\left(\vec{u}\right)}_{\neq 0 \text{ only for } \vec{R}_{AB}=0}+ \\
&\frac{-i\hbar}{N_{UC}}\sum_{\vec{R}_{AB},\vec{R}_A}^{N_{uc}}\int d\vec{u}e^{i\vec{k}\cdot\vec{R}_{AB}}\varphi_l^*\left(\vec{u}+\vec{R}_{AB}\right)\left(\vec{R}_A\times\vec{p}_u\right)_z\varphi_m\left(\vec{u}\right) \\
&= \frac{m}{N_{UC}}\sum_{\vec{R}_A}^{N_{UC}}\underbrace{\int d\vec{u}\varphi_l^*\left(\vec{u}\right)\varphi_m\left(\vec{u}\right)}_{=\delta_{lm}}+ \\
&\frac{-i\hbar}{N_{UC}}\sum_{\vec{R}_A}^{N_{UC}}\left[\vec{R}_A\times\underbrace{\sum_{\vec{R}_{AB}}^{N_{UC}}e^{i\vec{k}\cdot\vec{R}_{AB}}\int d\vec{u}\varphi_l^*\left(\vec{u}+\vec{R}_{AB}\right)\cdot\vec{p}_{u_i}\varphi_m\left(\vec{u}\right)}_{\vec{R}_A \text{ independent}}\right]_z \\
&= m\delta_{lm}+0,
\end{aligned}
\tag{6.37}
$$

where second term vanished due to summation $\vec{R}_A$ over isotropic system.

Remembering that at K point in conduction band Bloch wavefunction is constructed mostly from orbitals with symmetry $m_d = 0$ and $m_p = -1$. This is reproduced by solution of TB Hamiltonian $\hat{H}^{TB}\bar{\nu}_i = E_i\bar{\nu}_i$, where $\bar{\nu}_i$ describes vector of TB coefficients corresponding to choice of basis in Eq. (2.3) ($m_d = 0 \leftrightarrow \nu_2$, $m_p = -1 \leftrightarrow \nu_4$). We can write therefore simplified Bloch wavefunction as

$$
\begin{aligned}
\Psi_{CB}\left(K,\vec{r}\right) \approx \nu_2^{CB}\underbrace{\frac{1}{\sqrt{N_{UC}}}\sum_{i=1}^{N_{UC}}e^{i\vec{K}\cdot\vec{R}_{a,i}}\varphi_{l=2,m=0}\left(\vec{r}-\vec{R}_{A,i}\right)}_{\Psi^{m=0}_{CB,A,K}(\vec{r})}+ \\
+\nu_4^{CB}\underbrace{\frac{1}{\sqrt{N_{UC}}}\sum_{i=1}^{N_{UC}}e^{i\vec{K}\cdot\vec{R}_{B,i}}\varphi_{l=1,m=-1}\left(\vec{r}-\vec{R}_{B,i}\right)}_{\Psi^{m=-1}_{CB,B,K}(\vec{r})}.
\end{aligned}
\tag{6.38}
$$

Final matrix element of $\hat{L}_z$ operator in CB at K point is therefore

$$
\begin{aligned}
&\langle\Psi_{CB}\left(\vec{K}\right)|L_z|\Psi_{CB}\left(\vec{K}\right)\rangle = \\
&\left[\nu_2^{CB*}\langle\Psi^{m=0}_{CB,A,K}| + \nu_4^{CB*}\langle\psi^{m=-1}_{CB,B,K}|\right]\hat{L}_z\left[\nu_2^{CB}|\Psi^{m=0}_{CB,A,K}\rangle + \nu_4^{CB}|\Psi^{m=-1}_{CB,B,K}\rangle\right] = \\
&\left|\nu_2^{CB}\right|^2\cdot 0 + \nu_2^{CB*}\nu_4^{CB}\cdot 0 + \nu_4^{CB*}\nu_2^{CB}\cdot 0 + \left|\nu_4^{CB}\right|^2\cdot(-1) = \\
&(-1)\left|\nu_4^{CB}\right|^2.
\end{aligned}
\tag{6.39}
$$

Analogous calculation for valence band yields

$$\langle \Psi_{VB}\left(\vec{K}\right)|L_z|\Psi_{VB}\left(\vec{K}\right)\rangle = 2\cdot\left|\nu_3^{VB}\right|^2 + 1\cdot\left|\nu_6^{VB}\right|^2. \tag{6.40}$$

6.7 Analytically solvable excitonic problem

In this Appendix we study analytically solvable, hydrogen-like model of exciton in 2D. We consider optically excited electron, which leaves empty state behind, which we call "hole". Assuming positive electron and hole effective masses $m_e^*, m_h^* > 0$ of carriers with parabolic dispersion approximation, we can write energies of carriers as

$$\begin{aligned} E_e &= E_c + \frac{\hbar^2 k_e^2}{2m_e^*}, \\ E_h &= E_v - \frac{\hbar^2 k_h^2}{2m_h^*}, \end{aligned} \tag{6.41}$$

where electron (hole) wavevector is defined by

$$\vec{k}_{e(h)} = -i\vec{\nabla}_{e(h)} = -i\left(\frac{\partial}{\partial x_{e(h)}}, \frac{\partial}{\partial y_{e(h)}}\right). \tag{6.42}$$

E_v and E_c are valence and conduction band edges, respectively. We define band gap as $\Delta_{GAP} = E_c - E_v$. Exciton Hamiltonian in real space yields

$$\hat{H}_X = E_c + \frac{\hbar^2 k_e^2}{2m_e^*} - \left(E_v - \frac{\hbar^2 k_h^2}{2m_h^*}\right) + \frac{(+e)(-e)}{4\pi\varepsilon_0\varepsilon_r^{stat.}\left|\vec{r}_e - \vec{r}_h\right|}, \tag{6.43}$$

where ϵ_0 is vacuum permittivity, $\varepsilon_r^{stat.}$ describes static screening of a given materials (we consider generic semiconductor here) and $\vec{r}_e, \vec{r}_h$ describe positions of electron and hole with charges (+e) and (-e). Introducing $\varepsilon = 4\pi\varepsilon_0\varepsilon_r^{stat.}$ and using definition of $\vec{k}_{e(h)}$ we obtain

$$\hat{H}_X = \Delta_{GAP} - \frac{\hbar^2\vec{\nabla}_e^2}{2m_e^*} - \frac{\hbar^2\vec{\nabla}_h^2}{2m_h^*} - \frac{e^2}{\varepsilon\left|\vec{r}_e - \vec{r}_h\right|}. \tag{6.44}$$

In next step, we want to transform problem in Eq. (6.44) to relative coordinates. We do this by introducing new variables describing relative motion of electron hole pair $\vec{r} = \vec{r}_e - \vec{r}_h$ and center-of-mass motion $\vec{R} = \frac{\vec{r}_e m_e^* + \vec{r}_h m_h^*}{m_e^* + m_h^*}$. Using chain rule we can write for derivatives

$$\begin{aligned} \frac{\partial}{\partial r} &= \frac{\partial}{\partial r_e}\frac{\partial r_e}{\partial r} + \frac{\partial}{\partial r_h}\frac{\partial r_h}{\partial r} = \frac{m_h^*}{m_e^* + m_h^*}\frac{\partial}{\partial r_e} - \frac{m_e^*}{m_e^* + m_h^*}\frac{\partial}{\partial r_h}, \\ \frac{\partial}{\partial R} &= \frac{\partial}{\partial r_e}\frac{\partial r_e}{\partial R} + \frac{\partial}{\partial r_h}\frac{\partial r_h}{\partial R} = \frac{\partial}{\partial r_e} + \frac{\partial}{\partial r_h}. \end{aligned} \tag{6.45}$$

Inverse relations, expressing old coordinates and derivatives in terms of new

ones are given by

$$\begin{aligned}
\vec{r}_e &= \frac{m_h^*}{m_e^* + m_h^*} r + R, \\
\vec{r}_h &= -\frac{m_e^*}{m_e^* + m_h^*} r + R, \\
\frac{\partial}{\partial r_e} &= \frac{\partial}{\partial r} + \frac{m_e^*}{m_e^* = m_h^*} \frac{\partial}{\partial R}, \\
\frac{\partial}{\partial r_h} &= -\frac{\partial}{\partial r} + \frac{m_h^*}{m_e^* + m_h^*} \frac{\partial}{\partial R}.
\end{aligned} \tag{6.46}$$

Introducing total $M = m_e^* + m_h^*$ and reduced $\mu = (1/m_e^* + 1/m_h^*)^{-1}$ masses, we can write excitonic Hamiltonian as

$$\hat{H}_X = \Delta_{GAP} - \frac{\hbar^2 \nabla_R^2}{2M} - \frac{\hbar^2 \nabla_r^2}{2\mu} - \frac{e^2}{\varepsilon r}. \tag{6.47}$$

We can note that because now interaction doesn't mix relative and center-of-mass motions, we can factorize our excitonic wavefunction to free particle movement with wavevector $\vec{Q}$ and relative motion

$$\Psi_n \left(\vec{r}, \vec{R} \right) = e^{i\vec{Q}\cdot\vec{R}} \varphi_n \left(r \right), \tag{6.48}$$

which is a solution of eigenproblem

$$\hat{H}_X \Psi_n \left(\vec{r}, \vec{R} \right) = E_n \Psi_n \left(\vec{r}, \vec{R} \right). \tag{6.49}$$

Substituting Eq. (6.47) and Eq. (6.48) into Eq. (6.49) and acting with $\vec{\nabla}_R$ operator we obtain

$$e^{i\vec{Q}\cdot\vec{R}} \left[\frac{\hbar^2 Q^2}{2M} - \frac{\hbar^2 \nabla_r^2}{2\mu} - \frac{e^2}{\varepsilon r} \right] \varphi_n(r) = e^{i\vec{Q}\cdot\vec{R}} \left(E_n - \Delta_{GAP} \right) \varphi_n(r) \tag{6.50}$$

Introducing new "reference" energy $E_n^Q = E_n - \Delta_{GAP} - \frac{\hbar^2 Q^2}{2M}$ we get

$$\left[-\frac{\hbar^2 \nabla_r^2}{2\mu} - \frac{e^2}{\varepsilon r} \right] \varphi_n(r) = E_n^Q \varphi_n(r) \tag{6.51}$$

Problem defined in Eq. (6.51) can be solved using different methods. First lets us show method to get eigenvalues by transforming to parabolic coordinate system u, v,[774] e.g., $x = \frac{1}{2}\left(u^2 - v^2\right)$ and $y = u \cdot v$. Then, for operators occurring in Eq. (6.61) we get

$$\begin{aligned}
\frac{1}{r} &= \frac{1}{\sqrt{x^2 + y^2}} = \frac{2}{u^2 + v^2}, \\
\frac{\partial^2}{\partial x^2} + \frac{\partial^2}{\partial y^2} &= \frac{1}{u^2 + v^2} \left(\frac{\partial^2}{\partial u^2} + \frac{\partial^2}{\partial v^2} \right),
\end{aligned} \tag{6.52}$$

and Eq. (6.51) takes the form

$$\left[\frac{1}{u^2 + v^2} \frac{p_u^2 + p_v^2}{2\mu} - \frac{2}{u^2 + v^2} \frac{e^2}{\varepsilon} \right] \varphi_n(u, v) = E_n^Q \varphi_n(u, v). \tag{6.53}$$

Rearranging terms and aiming for the form of equation similar to 2D quantum harmonic oscillator we get

$$\left[\frac{p_u^2+p_v^2}{2\mu}+\frac{1}{2}\mu\underbrace{\left[-\frac{2}{\mu}E_n^Q\right]}_{"\omega^2"}\left(u^2+v^2\right)\right]\varphi_n(u,v)=\underbrace{\frac{2e^2}{\varepsilon}}_{"E"}\varphi_n(u,v). \tag{6.54}$$

Using the solution of 2D harmonic oscillator we get

$$\left[\frac{2e^2}{\varepsilon}\right]^2=\left[\hbar\omega\left(n+m+1\right)\right]^2=-\frac{2}{\mu}E_n^Q\hbar^2\left(n+m+1\right)^2, \tag{6.55}$$

leading finally to

$$E_n^Q=-\frac{\mu e^4}{2\varepsilon^2\hbar^2}\frac{1}{\left[\frac{1}{2}(n+m)+\frac{1}{2}\right]^2}=-\frac{4}{\left(n+m+1\right)^2}\left[\mathrm{Ry}^\mu\right], \tag{6.56}$$

where so-called excitonic Rydberg $\mathrm{Ry}^\mu=\frac{\mu e^2}{2\hbar^2\varepsilon^2}$ was introduced and the following condition for n,m has to be fulfilled $n-m=\pm 2p, p=0,1,2,....$ This series is equivalent to

$$E_n^Q=-\frac{1}{\left(n-\frac{1}{2}\right)^2}\left[\mathrm{Ry}^\mu\right], \qquad n=1,2,... \tag{6.57}$$

with degeneracy as every second shell of 2D harmonic oscillator (n=1: 1 degenerate state, n=2: 3, n=3: 5 etc.).

Alternative approach[775] to solve Eq. (6.51) (written in excitonic Rydberg units)to assume factorization of $\varphi=\frac{1}{\sqrt{2}}R(r)e^{im\phi}$ and transform from Cartesian to polar coordinates r,ϕ

$$\left(-\left[\frac{1}{r}\frac{\partial}{\partial r}\left(r\frac{\partial\varphi_n(r)}{\partial r}\right)+\frac{1}{r^2}\frac{\partial^2\varphi_n(r)}{\partial\phi^2}\right]-\frac{2}{r}\varphi_n(r)\right)=E_n^Q\varphi_n(r). \tag{6.58}$$

Assumption of form of radial function $R(r)=Cr^{|m|}e^{-r\sqrt{E_n}}L(r)$ transforms problem to equation defining associated Laguerre polynomials $L(r)$

$$\begin{aligned}&r\frac{d^2L(r)}{dr^2}+\left(2|m|+1-2r\sqrt{-E_n^Q}\right)\frac{dL(r)}{dr}+\\&+\left(2-2|m|\sqrt{-E_n^Q}-\sqrt{-E_n^Q}\right)L(r)=0,\end{aligned} \tag{6.59}$$

giving as previously $E_n^Q=-1/(n+1/2)^2$ (note that n start from 0 now) and excitonic relative motion wavefunction

$$\varphi_n(r,\phi)=\sqrt{\frac{\left(\sqrt{-E_n^Q}\right)^3(n-|m|)!}{\pi(n+|m|)!}}\left[2r\sqrt{-E_n^Q}\right]^{|m|}e^{-r\sqrt{-E_n^Q}}L_{n-|m|}^{2|m|}\left(2r\sqrt{-E_n^Q}\right)e^{im\phi}. \tag{6.60}$$

First 3 shell eigenenergies and relative motion wavefunctions are listed in Table 6.7.

n	E_n [Ry$^\mu$]	deg. m	wf. $\varphi_{n,m}(r,\phi)$
0	-4	$\{0\}$	$\varphi_{0,0} = \sqrt{\frac{8}{\pi}} e^{-2r}$
1	$-4/9$	$\{-1,0,1\}$	$\varphi_{1,m} = \sqrt{\frac{8}{27\pi(1+\lvert m\rvert)!}} \left(\frac{4}{3}r\right)^{\lvert m\rvert} e^{-\frac{2}{3}r} L^{2\lvert m\rvert}_{1-\lvert m\rvert}\left(\frac{4}{3}r\right) e^{im\phi}$
2	$-4/25$	$\{-2,-1,0,1,2\}$	$\varphi_{2,m} = \sqrt{\frac{8(2-\lvert m\rvert)!}{125\pi(2+\lvert m\rvert)!}} \left(\frac{4}{5}r\right)^{\lvert m\rvert} e^{-\frac{4}{5}r} L^{2\lvert m\rvert}_{2-\lvert m\rvert}\left(\frac{4}{5}r\right) e^{im\phi}$

Table 6.3: List of first three 2D excitonic shells n, degeneracies (deg.) and wavefunctions (wf.).

First few associated Laguerre polynomials are:

$$\begin{aligned} L_0^0(x) &= 1, \\ L_1^0(x) &= -x+1, \\ L_0^2(x) &= 1, \\ L_0^4(x) &= 1, \\ L_1^2(x) &= -x+3, \\ L_2^0(x) &= 1/2\left(x^2-4x+2\right). \end{aligned} \tag{6.61}$$

Analytical solutions to excitonic problem are, however, available only for very simple dispersion relation (parabolic model) and no effect of electron and hole Bloch wavefunctions on their interaction. Interestingly, first problem with calculating excitonic states for more sophisticated dispersion models can be overcome by Fourier transform of Eq. (6.47). First step in this direction is writing electron-hole wavefunction as linear combination of plane waves with coefficients $A_n\left(\vec{k}_e,\vec{k}_h\right)$:

$$\Psi_n\left(\vec{r}_e,\vec{r}_h\right) = \frac{1}{S}\sum_{\vec{k}_e,\vec{k}_h} A_n\left(\vec{k}_e,\vec{k}_h\right) e^{i\vec{k}_e\cdot\vec{r}_e} e^{i\vec{k}_h\cdot\vec{r}_h}, \tag{6.62}$$

where S is crystal surface, which should vanish from calculation at some point and $\vec{k}_{e(h)}$ are electron (hole) wavevectors. Using previously defined relative motion coordinates r, R and collecting them inside exponents as

$$\vec{k} = \frac{m_h^*}{m_e^*+m_h^*}\vec{k}_e - \frac{m_e^*}{m_e^*+m_h^*}\vec{k}_h, \qquad \vec{Q} = \vec{k}_e + \vec{k}_h, \tag{6.63}$$

we can write

$$\Psi_n\left(\vec{r}_e,\vec{r}_h\right) = \frac{1}{S}\sum_{k,Q} A_n\left(\vec{k},\vec{Q}\right) e^{i\vec{k}\cdot\vec{r}} e^{i\vec{Q}\cdot\vec{R}} = \Psi_n\left(\vec{r},\vec{R}\right). \tag{6.64}$$

Acting with Hamiltonian $\hat{H}_X$ from Eq. (6.47) on such wavefunction we get

$$\begin{aligned} &\frac{1}{S}\sum_{\vec{k},\vec{Q}} A_n\left(\vec{k},\vec{Q}\right) e^{i\left(\vec{k}\cdot\vec{r}+\vec{Q}\cdot\vec{R}\right)}\left[\Delta_{GAP} + \frac{\hbar^2Q^2}{2M} + \frac{\hbar^2k^2}{2\mu} - \frac{e^2}{\varepsilon r}\right] = \\ &E_n\frac{1}{S}\sum_{\vec{k},\vec{Q}} A_n\left(\vec{k},\vec{Q}\right) e^{i\left(\vec{k}\cdot\vec{r}+\vec{Q}\cdot\vec{R}\right)}. \end{aligned} \tag{6.65}$$

Integrating both sides by $\int_S dr \int_S dR...$ and changing some integrals to delta functions (note distinct notation for continuous delta $\delta(\vec{k}-\vec{k}')$ vs discrete one $\delta_{\vec{k}\vec{k}'}$)

$$\begin{aligned}\int_S dr \exp\left[-i\left(\vec{k}-\vec{k}'\right)\cdot\vec{r}\right] &= (2\pi)^2\,\delta\left(\vec{k}-\vec{k}'\right) = S\cdot\delta_{\vec{k}\vec{k}'},\\ \int_S dR \exp\left[-i\left(\vec{Q}-\vec{Q}'\right)\cdot\vec{R}\right] &= (2\pi)^2\,\delta\left(\vec{Q}-\vec{Q}'\right) = S\cdot\delta_{\vec{Q}\vec{Q}'},\end{aligned} \tag{6.66}$$

we obtain

$$\begin{aligned}&\frac{S^2}{S}\sum_{\vec{k},\vec{Q}} A_n\left(\vec{k},\vec{Q}\right) E(\vec{k},\vec{Q})\delta_{\vec{k}\vec{k}'}\delta_{\vec{Q}\vec{Q}'} - \frac{S}{S}\sum_{\vec{k},\vec{Q}} A_n\left(\vec{k},\vec{Q}\right)\int_S e^{i\left(\vec{k}-\vec{k}'\right)\cdot\vec{r}}\frac{e^2}{\varepsilon r}\delta_{\vec{Q}\vec{Q}'} =\\ &\frac{S^2}{S}E_n\sum_{\vec{k},\vec{Q}} A_n\left(\vec{k},\vec{Q}\right)\delta_{\vec{k}\vec{k}'}\delta_{\vec{Q}\vec{Q}'}.\end{aligned} \tag{6.67}$$

Executing delta's, changing notation $(k,Q)\leftrightarrow(k',Q')$, dividing by S and noting, that Fourier transform of $1/r$ interaction is:

$$\int_S dr\frac{e^{i\left(\vec{k}-\vec{k}'\right)\cdot\vec{r}}}{r} = \frac{2\pi}{\left|\vec{k}-\vec{k}'\right|} \tag{6.68}$$

we obtain

$$E\left(\vec{k},\vec{Q}\right)A_n\left(\vec{k},\vec{Q}\right) - \frac{1}{S}\sum_{\vec{k}'}\frac{2\pi e^2}{\varepsilon\left|\vec{k}-\vec{k}'\right|}A_n\left(\vec{k}',\vec{Q}\right) = E_n A_n\left(\vec{k},\vec{Q}\right). \tag{6.69}$$

This equation, even tough equivalent to Eq. (6.47), gives more insight, because now one can easily generalize electron-hole dispersion E(k,Q) beyond parabolic model. This equation is equivalent to so-called Wannier equation and constitutes simplified version of Bethe-Salpeter equation. For parabolic model of electron and hole dispersions it can be solved analytically[775] and yields same as previously mentioned binding energies E_n and k-dependence of amplitudes A_n, for example for 1s exciton state, is given by:

$$A_n\left(\vec{k}\right) = \sqrt{2\pi}\left(\frac{4}{k^2+4}\right)^{\frac{3}{2}} \tag{6.70}$$

However, as mentioned earlier, this approach does not contain electron - hole Bloch form factors (which in principle could be introduced in Ψ_n in Eq. (6.62) and it misses crucial corrections coming from quantum mechanical exchange interaction.

6.8 Details of CI derivation of Bethe-Salpeter-like equation

We begin with excitonic Hamiltonian

$$\hat{H}_X|X\rangle_n = E_n|X\rangle_n \tag{6.71}$$

where interacting excitonic Hamiltonian $\hat{H}_X$ is given in notation hiding both band index $b = v = VB$ or $b = c = CB$, wavevector $\vec{k}$ and spin σ in single index, for example $|i\rangle = |b, \vec{k}, \sigma\rangle$ as

$$\hat{H}_X = \underbrace{\sum_i \varepsilon_i c_i^\dagger c_i}_{\hat{H}_X^{(1)}} + \underbrace{\frac{1}{2}\sum_{ijkl} \langle i\,|j\,|V|\,k|\,l\rangle\, c_i^\dagger c_j^\dagger c_k c_l}_{\hat{H}_X^{(2)}}\,. \tag{6.72}$$

In next step we face problem of calculating matrix elements of this Hamiltonian. As a first step let's consider single particle part $\hat{H}_X^{(1)}$. For two arbitrary excitonic states $|X_1\rangle = c_{f_1}^\dagger c_{i_1}|GS\rangle$, $|X_2\rangle = c_{f_2}^\dagger c_{i_2}|GS\rangle$, where $i_1 = (k, v)$, $f_1 = (k, c)$, $i_2 = (k', v)$, $f_2 = k', c$, we have for single particle part of the Hamiltonian

$$\langle X_2|\hat{H}_X^1|X_1\rangle = \sum_{m=1}^{N_{all}} \varepsilon_m \langle X_2|c_m^\dagger c_m|X_1\rangle = \sum_{i=m}^{N_{all}} \varepsilon_m \langle GS|c_{i_2}^\dagger c_{f_2} c_m^\dagger c_m c_{f_1}^\dagger c_{i_1}|GS\rangle \tag{6.73}$$

To attack $\hat{H}_X^1$ expectation value, we use Wick theorem to reduce 6-component operator

$$\begin{aligned}
&\langle GS|c_{i2}^\dagger c_{f2} c_m^\dagger c_m c_{f1}^\dagger c_{i1}|GS\rangle = \underbrace{\langle GS|c_{i2}^\dagger c_{f2}|GS\rangle}_{=0}\langle GS|...|GS\rangle - \underbrace{\langle GS|c_{i2}^\dagger c_m^\dagger|GS\rangle}_{=0}\langle GS|...|GS\rangle + \\
&\langle GS|c_{i2}^\dagger c_m|GS\rangle\langle GS|...|GS\rangle - \underbrace{\langle GS|c_{i2}^\dagger c_{f1}^\dagger|GS\rangle}_{=0}\langle GS|...|GS\rangle + \langle GS|c_{i2}^\dagger c_{i1}|GS\rangle\langle GS|...|GS\rangle = \\
&\underbrace{\langle GS|c_{i2}^\dagger c_m|GS\rangle}_{\delta(m,i2)}\langle GS|c_{f2} c_m^\dagger c_{f1}^\dagger c_{i1}|GS\rangle + \underbrace{\langle GS|c_{i2}^\dagger c_{i1}|GS\rangle}_{\delta(i1,i2)}\langle GS|c_{f2} c_m^\dagger c_m c_{f1}^\dagger|GS\rangle = \\
&\delta(m,i2)\langle GS|c_{f2} c_m^\dagger c_{f1}^\dagger c_{i1}|GS\rangle + \delta(i1,i2)\langle GS|c_{f2} c_m^\dagger c_m c_{f1}^\dagger|GS\rangle.
\end{aligned} \tag{6.74}$$

Further reduction of 4-component operators can be performed analogously for first one as

$$\begin{aligned}
&\langle GS|c_{f2} c_m^\dagger c_{f1}^\dagger c_{i1}|GS\rangle = \\
&\langle GS|c_{f2} c_m^\dagger|GS\rangle\langle GS|...|GS\rangle - \langle GS|c_{f2} c_{f1}^\dagger|GS\rangle\langle GS|...|GS\rangle + \underbrace{\langle GS|c_{f2} c_{i1}|GS\rangle}_{=0}\langle GS|...|GS\rangle = \\
&\langle GS|c_{f2} c_m^\dagger|GS\rangle\underbrace{\langle GS|c_{f1}^\dagger c_{i1}|GS\rangle}_{=0} - \langle GS|c_{f2} c_{f1}^\dagger|GS\rangle\langle GS|c_m^\dagger c_{i1}|GS\rangle = \\
&-\delta(f1,f2)\delta(m,i1),
\end{aligned} \tag{6.75}$$

and for the second as

$$\begin{aligned}
&\langle GS|c_{f2} c_m^\dagger c_m c_{f1}^\dagger|GS\rangle = \\
&\langle GS|c_{f2} c_m^\dagger|GS\rangle\langle GS|...|GS\rangle - \underbrace{\langle GS|c_{f2} c_m|GS\rangle}_{=0}\langle GS|...|GS\rangle + \langle GS|c_{f2} c_{f1}^\dagger|GS\rangle\langle GS|...|GS\rangle = \\
&\langle GS|c_{f2} c_m^\dagger|GS\rangle\langle GS|c_m c_{f1}^\dagger|GS\rangle + \langle GS|c_{f2} c_{f1}^\dagger|GS\rangle\langle GS|c_m^\dagger c_m|GS\rangle = \\
&\delta(m,f2)\delta(m,f1) + \delta(f1,f2)\delta(m \leq N_{occ.})
\end{aligned} \tag{6.76}$$

Combining all reduced operators we get

$$\langle X_2|\hat{H}_X^{(1)}|X_1\rangle = \sum_{m=1}^{N_{all}} \varepsilon_m \langle X_2|c_m^\dagger c_m|X_1\rangle =$$
$$\sum_{i=m}^{N_{all}} \varepsilon_m \left(\delta(m,i2)[-\delta(f1,f2)\delta(m,i1)] + \delta(i1,i2)[\delta(m,f2)\delta(m,f1) + \delta(f1,f2)\delta(m \leq N_{occ.})]\right) =$$
$$\delta(i1,i2)\delta(f1,f2)\left[\varepsilon_{f1} - \varepsilon_{i1} + \sum_{m=1}^{N_{occ.}} \varepsilon_m\right]. \tag{6.77}$$

For two-body interaction part of the Hamiltonian $H_X^{(2)}$ situation is more complicated due to 8-component operators that need to be reduced:

$$\begin{aligned}
&\langle GS|c_{i2}^\dagger c_{f2} c_{m1}^\dagger c_{m2}^\dagger c_{m3} c_{m4} c_{f1}^\dagger c_{i1}|GS\rangle = \underbrace{\langle GS|c_{i2}^\dagger c_{f2}|GS\rangle}_{=0}\langle GS|...|GS\rangle + \\
&- \underbrace{\langle GS|c_{i2}^\dagger c_{m1}^\dagger|GS\rangle}_{=0}\langle GS|...|GS\rangle + \underbrace{\langle GS|c_{i2}^\dagger c_{m2}^\dagger|GS\rangle}_{=0}\langle GS|...|GS\rangle + \\
&- \underbrace{\langle GS|c_{i2}^\dagger c_{m3}|GS\rangle}_{\delta(i2,m3)}\langle GS|...|GS\rangle + \underbrace{\langle GS|c_{i2}^\dagger c_{m4}|GS\rangle}_{\delta(i2,m4)}\langle GS|...|GS\rangle + \\
&- \underbrace{\langle GS|c_{i2}^\dagger c_{f1}^\dagger|GS\rangle}_{=0}\langle GS|...|GS\rangle + \underbrace{\langle GS|c_{i2}^\dagger c_{i1}}_{\delta(i1,i2)}|GS\rangle\langle GS|...|GS\rangle = \\
&- \delta(i2,m3)\langle GS|c_{f2} c_{m1}^\dagger c_{m2}^\dagger c_{m4} c_{f1}^\dagger c_{i1}|GS\rangle + \\
&+ \delta(i2,m4)\langle GS|c_{f2} c_{m1}^\dagger c_{m2}^\dagger c_{m3} c_{f1}^\dagger c_{i1}|GS\rangle + \\
&+ \delta(i1,i2)\langle GS|c_{f2} c_{m1}^\dagger c_{m2}^\dagger c_{m3} c_{m4} c_{f1}^\dagger|GS\rangle.
\end{aligned} \tag{6.78}$$

Remaining 6-operator product can be calculated analogously to 1-operator case. As a result one can obtain 14 non-zero terms, which can be further reduced using symmetry $\vec{r} \leftrightarrow \vec{r}'$ inside matrix elements V_{ijkl} to give Bethe - Salpeter equation with ground state energy correction and self-energy corrections that can be easily subtracted from the diagonal of BSE.

6.9 Study of direct and exchange Coulomb matrix elements

To understand better product densities entering direct electron-hole interaction form factors, let us analyze simplest co-densities calculated from $k = K$ point to some other points along $K - \Gamma$ line (because our K point can be chosen to have only k_y component, this path on BZ can be represented as $x \cdot K$). As one can observe in Fig. 6.4 (a,b) for absolute values of ρ, z dependence of pair density for $k = k' = K$ for $G = 0$ is simply describing in-plane integrated density of Slater orbitals with weights coming from their orbital composition obtained from tight-binding model. As shown for ρ_{cc} describing conduction band in Fig. 6.4 (a), in z dependence one can clearly see both Mo and S_2 orbitals, because they both contribute to the conduction band (70 an 30 %, respectively). Three peaks in central region stem from $m_d = 0$ shape of orbital. Situation is even simpler for

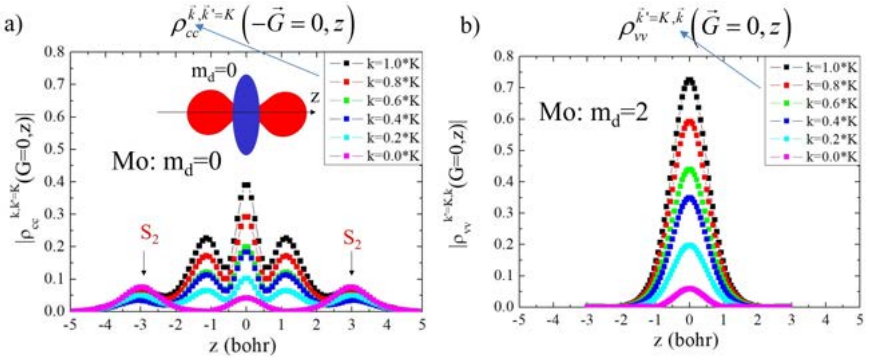

Figure 6.4: Simplest pair densities k' and z-th dependence for both (a) valence and (b) conduction band ρ's. For simplicity both cases wavevector k is set to K point (corner of hexagonal BZ) and reciprocal lattice vector G is set to 0. Figure partly reproduced from Ref. 5.

valence band co-density, see Fig. 6.4 (b), in which only $m_{d=+2}$ contributes in practice and in-plane summation of contributions of this orbital gives single peak without additional features. Decreasing peak heights when distance between k and k' points is increased stems from simple property that for increased $k-k'$ (or non - zero G) in integral there is oscillating factor $e^{i(k-k'-G)\cdot r}$ that when integrated out spatially, decreased absolute value of the integral.

We note that numerical integration of co-densities, because their dependence on two wavevectors k and k', necessary fine resolution of z-dependence and necessity of evaluation for different G's, is generally hard computationally. This makes summation of G vectors in Eq. (3.24) challenging. Example of convergence of absolute value of some representative matrix element $V(k=K, k'=0.5K=Q)$ is shown in Fig. 3.8. Convergence parameter G_{cutoff} sets radius of G summation in reciprocal space in units of length of primitive reciprocal lattice vector $|G_1|$. One can observe that relative error in matrix element, when no summation is performed and only one $G=0$, is of the order of 20%. One can argue, however, that this value is overestimated, because it describes bare matrix elements, which later will be screened. In practice, we were able to calculate matrix elements for 7000 k-points lattice only for $G_{cutoff} = 1 \cdot |G_1|$, therefore our numerical results using full form factors should be understood as possibly under-estimating strength of electron-hole attraction.

Let us discuss now symmetry of direct interaction form factors across BZ. In Fig. 6.5 we present absolute values of $F_D(+K, k', G)$ for k' vectors in +K valley and three different G's chosen in such way to produce triangle centered around +K point, as shown in Fig. 3.1. One can observe that even if k=K is taken, G vector translates overall $1/|K-k'|$ dependence to the respective corner of the hexagon, rationalizing taking as an approximate interaction $1/|q-q'|$ simplified model. This property ensures that interaction around K point in sense of it's magnitude is isotropic.

Having checked magnitude of interaction, let us study it's phase. Considering

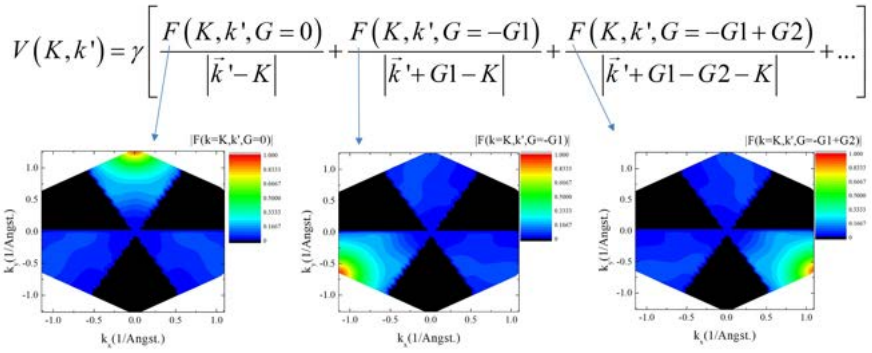

Figure 6.5: Absolute value of form factors of Coulomb interaction from +K point to all other points in +K valley calculated for three different G-vectors translating wedges centered around Γ point to triangle around +K point.

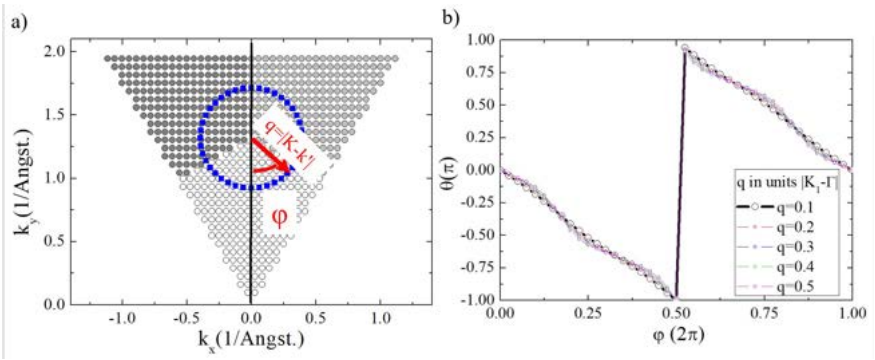

Figure 6.6: (a) Circle of k' vectors around +K point parametrized using complex number coordinate representation as $\vec{k}' = qe^{i\varphi}$. (b) Phase θ of matrix element $V^D(+K, k') = |V|e^{i\theta}$.

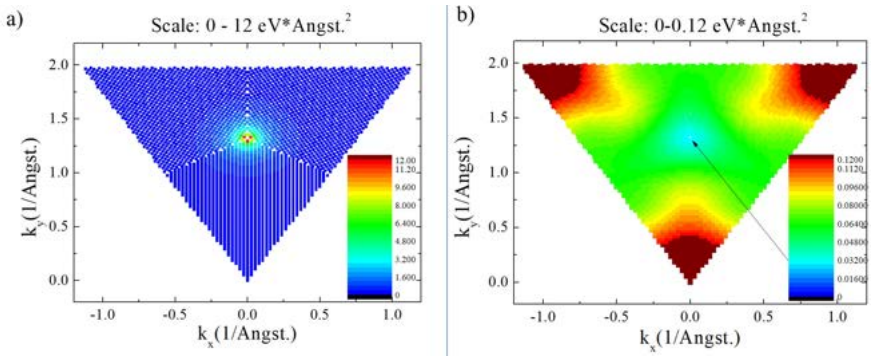

Figure 6.7: Highly converged calculation comparing numerical results of magnitude of (a) direct and (b) exchange interactions inside one valley. In both cases matrix elements are calculated for k=K and G=0. Color scale is given in eV·Å^2 units.

triangular picture of the +K valley, we circle around +K point (Fig. 6.6 (a)) and calculate complex element $V^D(K, k' = qe^{i\varphi}) = |V|e^{i\theta}$. Next, we plot phase θ of such element for different $q's$ denoting distance of k' from K point. As shown in Fig. 6.6 (b) for large q's, reaching from K to Q points, there is a consistent 2π rotation (with 2π jump discontinuity coming from numerics) of matrix element. We note that this behavior is not general for all points across BZ and circles around them, therefore cannot be utilized to build some systematic approximation theory of V^D across BZ.

Having established numerical properties of direct interaction, let us now compare it with exchange one. In Fig. 6.7 (a-b) we calculated with large numerical precision magnitudes of complex direct interaction and real exchange, using Eq. 3.24 and Eq. 3.27, respectively. In general one can observe that exchange interaction magnitude is at least two orders of magnitude smaller than direct one. Interestingly, it does not follow $1/|q-q'|$ dependence, visibly growing with larger $|q-q'|$ separation. As apparent from Eq. 3.27 this is purely orbital effect associated with F^X form factors.

Finally, let us discuss excitonic spectrum obtained with simplified form factors of direct interaction taking fully into account tight-binding coefficients, as discussed in Section 3.3.6 "Interaction form factor approximation theory". As shown in Fig. 6.8, for k-grid including almost 30000 k-points in one valley and Rytova - Keldysh screening parameter $\alpha = 2.0$ Å, one can observe topological splittings of $2p_-$ - $2p_+$ states, fully consistent with full form factor calculation. We note that exact value of this splitting is larger (22 meV) than this obtained from full form factor theory (3.5 meV) for screening parameters giving similar energy of the ground state ($\approx$ 350 meV). We note also that due to high precision of this calculation we were able to obtain well separated n=3 excitonic shell and we observed there internal splitting of states (with energetic hierarchy $(3d_-, 3d_+) < (3d_-, 3d_+) < 3s$) due to chirality of interaction consistent with picture built to explain topological nature of $2p_+$-$2p_-$ splitting.

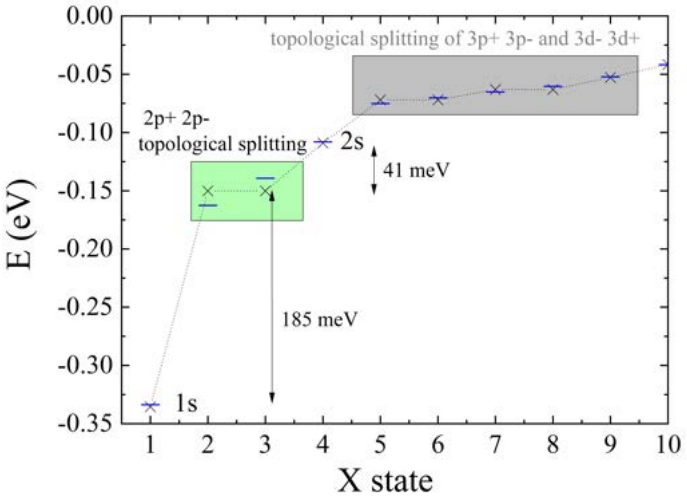

Figure 6.8: Valley excitonic spectrum obtained with approximated direct interaction form factors. Screening parameter α is taken as 2.0 Å. Exact number of k-points used in calculation is 29231.

6.10 Study of MoS_2 nanoribbon

Low energy band structure of zigzag and armchair nanoribbons is shown in Fig. 6.9 (a-b). We choose system size to be 40 and 42 atoms (in y-direction, infinite in x). One can observe in both cases bulk bands of nanoribbons, valence bands below $E = 0$ eV and conduction bands above $E = 1.6$ eV, as expected from bulk 2D crystal tight-binding model. Consistently with DFT results,[776] in both cases in-gap states are observed. First, we study where these states are localized. To do that, we check how much of a given state wavefunction is localized on the top and bottom of the nanoribbons. Clearly, in both cases in-gap states are almost solely localized on edge Mo (S_2) atom (dimer). Main difference between two types of edge terminations is lack of band gap in zigzag case. Also, lower and upper branches of in-gap states in zigzag nanoribbon are localized on different edges (Fig. 1), contrary to the armchair case.

For transport calculations we use standard two-lead geometry[500] and Landauer formula for conductance $G = \frac{e^2}{h}T$, in which transmission coefficient T is calculated using Caroli formula $T = \mathrm{Tr}\left[\Gamma_L G^r_{1,N} \Gamma_R \left(G^r_{1,N}\right)^\dagger\right]$, where $G^r_{1,N}$ is retarded Green's function matrix obtained using recursive scheme. Surface Green's functions of semi-infinite leads are calculated using Sancho-Rubio algorithm. Left (right) lead self-energies Σ_L (Σ_R) give $\Gamma_{L(R)}$ matrices via formula $\Gamma_{R(L)} = \Gamma_{L(R)} - \Gamma^\dagger_{L(R)}$. We note that all calculations are performed for 1-body non-interacting electrons at $T = 0$ K. Local density of states $A(i, E)$ (at atom i, for a given energy E) is calculated using imaginary part of Green's function as $A(i, E) = -\frac{1}{\pi}\mathrm{Im}\left[\sum_\alpha G^r(i, i, \alpha, E)\right]$, where α represents summation over proper orbitals and spins, depending on atom type (Mo or S_2). Another method allowing us to study real space distribution of electrons and their localization is

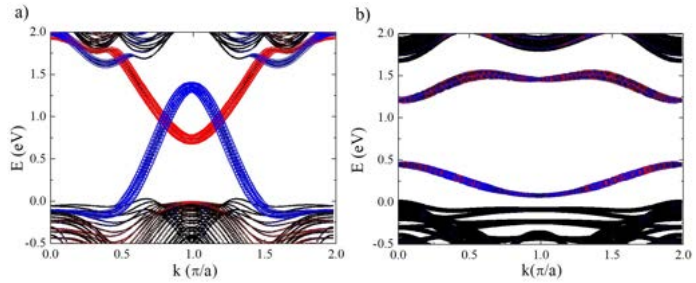

Figure 6.9: Band structure of (a) zigzag- and (b) armchair - type MoS_2 nanoribbon. The width of one slice is set to 40 and 42 atoms, respectively. One can clearly observe in-gap edge states between VB and CB bulk bands. Size of the blue (red) dots represents how much state for a given 1D wavevector k and energy E is localized on Mo (S_2) site on the edge of the nanoribbon.

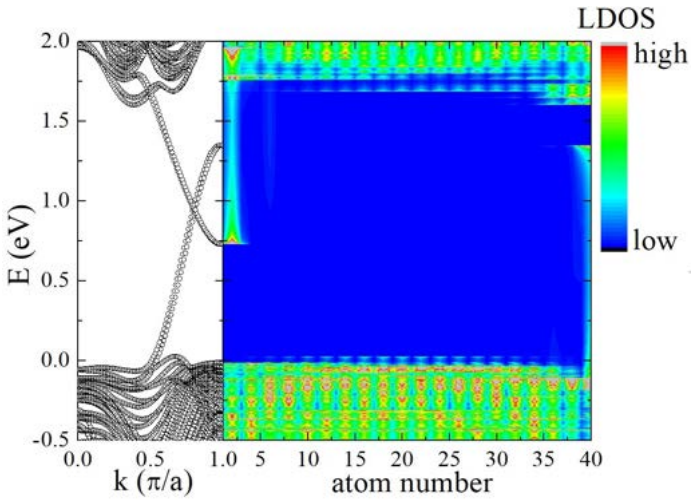

Figure 6.10: Atom-resolved local density of states (LDOS) for zigzag nanoribbon. For every energy value E of nanoribbon band structure (left panel, k show for values from 0 to π/a) atom resolved LDOS is shown on the right panel. Colors denote arbitrary scaled LDOS intensities.

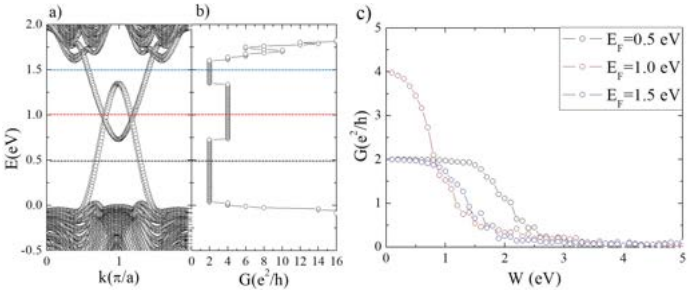

Figure 6.11: (a)Bandstructure and (b) conductance G of clean zigzag nanoribbons for a given energy E. It is clear that there are different regimes of conductance depending on number of edge states. (c) Transport properties of disordered zigzag nanoribbons (size 40 by 80 atoms). For 3 different Fermi energies E_F we calculate averaged conductance G for different Anderson-disorder strengths W.

local density of states (LDOS), presented for zigzag nanoribbon in Fig. 6.10. For every energy E we can plot atom resolved LDOS, and we observe that when moving across the bulk gap, states are either from bottom edge of the nanoribbon (atom number 1), or from topmost one (atom number 40). There exists also range of energies for which these two branches overlap ($E = 0.75 - 1.25$ eV). We observe also that close to the top and bottom of edge states parabolas seen on the left panel of Fig. 6.10, edge states are becoming more de-localized, comparing to regions far from bulk states and crossover region.

In the last part we check also how much conducting in-gap states are robust to non-magnetic disorder, described by Anderson-like impurity model. We choose to study systems with 40 by 80 (zigzag) and 42 by 84 atoms (armchair). For armchair nanoribbons (not presented) we observe quick disappearance of conductance with respect to disorder strength W. Contrary to that, in zigzag nanoribbon (Fig. 6.11) we observe that if top and bottom branches of in-gap states do not cross, conductance is protected against backscattering (plateaus for E=0.5 and E=1.5 eV). One can notice that transport by states localized on Mo atoms is slightly more robust than transport via states localized on S_2 dimers. When in-gap states cross, we observe that for e.g. $E_F = 1.0$ eV, conductance at the beginning is larger ($G = 4e^2/h$), but drops showing no plateau feature. However, due to relatively small system size we cannot conclude if conductance for this regime is unprotected, which will be left for further studies.

6.11 Topological splitting in QD in Kane-Mele model

In the following Appendix we study the effect of Berry's curvature and topology on states confined in gate defined parabolic QD's. We choose to study Kane-Mele model,[52,53] in which two topologically non-equivalent routes to gap opening can be realized. This model was shown to realistically describe low en-

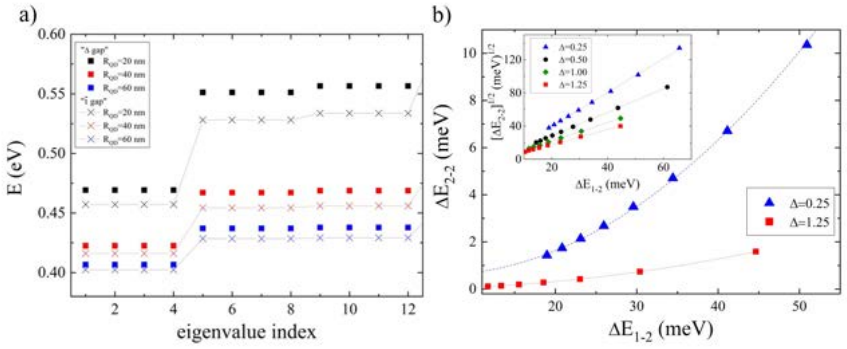

Figure 6.12: Quantum dot spectrum in Kane-Mele model. (a) The first three energy shells of the conduction band. Squares represent results obtained for Δ and crosses corresponding t_2. Quantum dot radius varied from 20 to 60 Å (see legend). (b) The first intra-shell energy split ΔE_{12} versus δE_{22} for $\Delta = 0.25$ (blue triangles) and $\Delta = 1.00$ (black dots). Dashed lines represent parabolic fits. Inset: $(\Delta E_{12})^{1/2}$ against ΔE_{22} for Δ up to 1.25 (details in legend).

ergy sector of mono-[54,777,778] and bi-[779] layers of graphene on top of different monolayer transition metal dichalcogenides, monolayers of jacutingaite[780] and it's recently proposed[495] counterpart Pd_2HgSe_3. We show the relation between shell splitting, QD size quantization, magnitude of Berry's curvature controlled by size of the band-gap and topological phase of the system.

First we describe briefly Kane-Mele TB model. We consider generic honeycomb lattice with constant $a_0 = 1.42$ Å, value usually taken for graphene. The simulations are performed in computational box with periodic boundary conditions (PBC). Model Hamiltonian yields

$$H_0 = \sum_{\langle i\alpha, j\beta\rangle} t_{i\alpha,j\beta} c^+_{i\alpha} c_{j\beta} + \sum_{i\alpha} \left(\pm \frac{\Delta}{2}\right) c^+_{i\alpha} c_{i\alpha} + \sum_{\langle\langle i\alpha, j\beta\rangle\rangle} \tilde{t}_{i\alpha,j\beta} e^{-i\nu_{ij}\phi} c^+_{i\alpha} c_{j\beta}, \tag{6.79}$$

where the summation extends over atoms i, j and spins α, β. $c^+_{i\alpha}$ and $c_{i\alpha}$ are fermion creation and annihilation operators, respectively. In first sum over nearest neighbor (<>) atoms, $t_{i\alpha,j\beta}$ is the hopping integral. Next two sums describe two ways of opening the gap in the systems. In second sum, staggered sublattice potential opens trivial gap Δ in the system, while in third sum Kane-Mele spin-orbit term with strength $\tilde{t}$ opens non-trivial gap.

In Fig. 6.12 (a) we show shells of QD calculated in Kane-Mele model analogous K-point derived spectrum of MoS_2 quantum dot shown in Fig. 4.5. Four-fold degeneracy results from spin and valley degeneracy. We note that results of the same R_{QD} are slightly different between trivial ("Δ gap") and topological system ("$\tilde{t}$ gap") due to different effective masses at band edges in both models. One can clearly see, however, that both exhibit splitting in n=2 shell. Now we

quantify this splitting in Fig. 6.12 (b) by plotting value of intra-shell splitting ΔE_{2-2} vs corresponding inter-shell splitting ΔE_{1-2}. Because we do this for two different gap parameters $\Delta = 0.25$ eV and $\Delta = 1.25$ eV, dots with same radii give different inter-shell energies. Therefore, we study different sizes of the dots giving different Δ_{1-2} and then show corresponding topological splitting in second shell. One can observe in Fig. 6.12 (b) that for system with larger magnitude of Berry's curvature at K point ($\Delta = 0.25$ eV) one has significantly larger topological splitting than system with smaller value of Berry's curvature ($\Delta = 1.25$ eV), supporting our interpretation that inter-shell splitting is topological effect. Inset of Fig. 6.12 (b) shows that basically square root value of topological splitting is linearly dependent of intra-shell splitting for different gaps, therefore for different magnitudes if Berry's curvature. Theoretical explanation of this numerically discovered dependence requires further studies.

Bibliography

[1] M. Bieniek, M. Korkusiński, L. Szulakowska, P. Potasz, I. Ozfidan, and P. Hawrylak, "Band nesting, massive Dirac fermions, and valley Landé and Zeeman effects in transition metal dichalcogenides: A tight-binding model," *Phys. Rev. B*, vol. 97, p. 085153, Feb 2018. [Online]. Available: https://link.aps.org/doi/10.1103/PhysRevB.97.085153

[2] J. Jadczak, L. Bryja, J. Kutrowska-Girzycka, P. Kapuscinski, M. Bieniek, Y.-S. Huang, and P. Hawrylak, "Room temperature multi-phonon upconversion photoluminescence in monolayer semiconductor WS_2," *Nature Communications*, vol. 10, no. 1, p. 107, 2019. [Online]. Available: https://doi.org/10.1038/s41467-018-07994-1

[3] L. Szulakowska, M. Bieniek, and P. Hawrylak, "Electronic structure, magnetoexcitons and valley polarized electron gas in 2D crystals," *Solid-State Electronics*, vol. 155, pp. 105 – 110, 2019, selected Papers from the Future Trends in Microelectronics (FTM-2018) Workshop. [Online]. Available: http://www.sciencedirect.com/science/article/pii/S0038110118306348

[4] M. Bieniek, L. Szulakowska, and P. Hawrylak, "Effect of valley, spin, and band nesting on the electronic properties of gated quantum dots in a single layer of transition metal dichalcogenides," *Phys. Rev. B*, vol. 101, p. 035401, Jan 2020. [Online]. Available: https://link.aps.org/doi/10.1103/PhysRevB.101.035401

[5] M. Bieniek, L. a. Szulakowska, and P. Hawrylak, "Band nesting and exciton spectrum in monolayer MoS2," *Phys. Rev. B*, vol. 101, p. 125423, Mar 2020. [Online]. Available: https://link.aps.org/doi/10.1103/PhysRevB.101.125423

[6] J. Jadczak, J. Kutrowska-Girzycka, M. Bieniek, T. Kazimierczuk, P. Kossacki, J. Schindler, J. Debus, K. Watanabe, T. Taniguchi, C.-H. Ho, A. Wójs, P. Hawrylak, and L. Bryja, "Fine structure of negatively charged and neutral excitons in monolayer MoS_2," *arXiv e-prints*, p. arXiv:2001.07929, Jan. 2020. [Online]. Available: https://arxiv.org/abs/2001.07929

[7] L. Szulakowska, M. Cygorek, M. Bieniek, and P. Hawrylak, "Valley and spin polarized broken symmetry states of interacting electrons in gated MoS_2 quantum dots," 2020. [Online]. Available: https://arxiv.org/abs/2005.04467

[8] A. Y. Cho, "Growth of periodic structures by the molecular-beam method," *Applied Physics Letters*, vol. 19, no. 11, pp. 467–468, 1971. [Online]. Available: https://doi.org/10.1063/1.1653775

[9] T. Ando, A. B. Fowler, and F. Stern, "Electronic properties of two-dimensional systems," *Rev. Mod. Phys.*, vol. 54, pp. 437–672, Apr 1982. [Online]. Available: https://link.aps.org/doi/10.1103/RevModPhys.54.437

[10] L. L. Chang, L. Esaki, and R. Tsu, "Resonant tunneling in semiconductor double barriers," *Applied Physics Letters*, vol. 24, no. 12, pp. 593–595, 1974. [Online]. Available: https://doi.org/10.1063/1.1655067

[11] R. Dingle, W. Wiegmann, and C. H. Henry, "Quantum States of Confined Carriers in Very Thin $Al_xGa_{1-x}As$-GaAs-$Al_xGa_{1-x}As$ Heterostructures," *Phys. Rev. Lett.*, vol. 33, pp. 827–830, Sep 1974. [Online]. Available: https://link.aps.org/doi/10.1103/PhysRevLett.33.827

[12] P. M. Petroff, A. C. Gossard, R. A. Logan, and W. Wiegmann, "Toward quantum well wires: Fabrication and optical properties," *Applied Physics Letters*, vol. 41, no. 7, pp. 635–638, 1982. [Online]. Available: https://doi.org/10.1063/1.93610

[13] M. A. Reed, R. T. Bate, K. Bradshaw, W. M. Duncan, W. R. Frensley, J. W. Lee, and H. D. Shih, "Spatial quantization in GaAs–AlGaAs multiple quantum dots," *Journal of Vacuum Science & Technology B: Microelectronics Processing and Phenomena*, vol. 4, no. 1, pp. 358–360, 1986. [Online]. Available: https://avs.scitation.org/doi/abs/10.1116/1.583331

[14] L. Jacak, P. Hawrylak, and A. Wójs, *Quantum dots.* Springer, Berlin, Heidelberg, 1998. [Online]. Available: https://doi.org/10.1007/978-3-642-72002-4

[15] Y. Masumoto and T. Takagahara, *Quantum dots.* Springer, Berlin, Heidelberg, 2002. [Online]. Available: https://doi.org/10.1007/978-3-662-05001-9

[16] J. M. Luttinger and W. Kohn, "Motion of Electrons and Holes in Perturbed Periodic Fields," *Phys. Rev.*, vol. 97, pp. 869–883, Feb 1955. [Online]. Available: https://link.aps.org/doi/10.1103/PhysRev.97.869

[17] R. Winkler, *Spin-Orbit Coupling Effects in Two-Dimensional Electron and Hole Systems*, ser. Springer Tracts in Modern Physics. Springer, 2003. [Online]. Available: https://doi.org/10.1007/b13586

[18] J. C. Slater and G. F. Koster, "Simplified LCAO Method for the Periodic Potential Problem," *Phys. Rev.*, vol. 94, p. 1498, Jun 1954. [Online]. Available: https://link.aps.org/doi/10.1103/PhysRev.94.1498

[19] M. L. Cohen and V. Heine, "The Fitting of Pseudopotentials to Experimental Data and Their Subsequent Application," in *Solid State Physics*, ser. Solid State Physics, H. Ehrenreich, F. Seitz, and D. Turnbull, Eds. Academic Press, 1970, vol. 24, pp. 37 – 248. [Online]. Available: http://www.sciencedirect.com/science/article/pii/S0081194708600703

[20] J. Ihm, A. Zunger, and M. L. Cohen, "Momentum-space formalism for the total energy of solids," *Journal of Physics C: Solid State Physics*, vol. 12, no. 21, pp. 4409–4422, nov 1979. [Online]. Available: https://doi.org/10.1088%2F0022-3719%2F12%2F21%2F009

[21] L.-W. Wang and A. Zunger, "Pseudopotential calculations of nanoscale CdSe quantum dots," *Phys. Rev. B*, vol. 53, pp. 9579–9582, Apr 1996. [Online]. Available: https://link.aps.org/doi/10.1103/PhysRevB.53.9579

[22] W. Kohn and L. J. Sham, "Self-Consistent Equations Including Exchange and Correlation Effects," *Phys. Rev.*, vol. 140, pp. A1133–A1138, Nov 1965. [Online]. Available: https://link.aps.org/doi/10.1103/PhysRev.140.A1133

[23] D. Porezag, T. Frauenheim, T. Köhler, G. Seifert, and R. Kaschner, "Construction of tight-binding-like potentials on the basis of density-functional theory: Application to carbon," *Phys. Rev. B*, vol. 51, pp. 12947–12957, May 1995. [Online]. Available: https://link.aps.org/doi/10.1103/PhysRevB.51.12947

[24] M. Elstner, D. Porezag, G. Jungnickel, J. Elsner, M. Haugk, T. Frauenheim, S. Suhai, and G. Seifert, "Self-consistent-charge density-functional tight-binding method for simulations of complex materials properties," *Phys. Rev. B*, vol. 58, pp. 7260–7268, Sep 1998. [Online]. Available: https://link.aps.org/doi/10.1103/PhysRevB.58.7260

[25] P. Koskinen and V. Mäkinen, "Density-functional tight-binding for beginners," *Computational Materials Science*, vol. 47, no. 1, pp. 237 – 253, 2009. [Online]. Available: http://www.sciencedirect.com/science/article/pii/S0927025609003036

[26] N. Marzari, A. A. Mostofi, J. R. Yates, I. Souza, and D. Vanderbilt, "Maximally localized Wannier functions: Theory and applications," *Rev. Mod. Phys.*, vol. 84, pp. 1419–1475, Oct 2012. [Online]. Available: https://link.aps.org/doi/10.1103/RevModPhys.84.1419

[27] P. Dirac, *The Principles of Quantum Mechanics.* Oxford University Press, 1930.

[28] G. W. Semenoff, "Condensed-Matter Simulation of a Three-Dimensional Anomaly," *Phys. Rev. Lett.*, vol. 53, pp. 2449–2452, Dec 1984. [Online]. Available: https://link.aps.org/doi/10.1103/PhysRevLett.53.2449

[29] K. S. Novoselov, A. K. Geim, S. V. Morozov, D. Jiang, Y. Zhang, S. V. Dubonos, I. V. Grigorieva, and A. A. Firsov, "Electric Field Effect in Atomically Thin Carbon Films," *Science*, vol. 306, no. 5696, pp. 666–669, 2004. [Online]. Available: https://science.sciencemag.org/content/306/5696/666

[30] K. S. Novoselov, A. K. Geim, S. V. Morozov, D. Jiang, M. I. Katsnelson, I. V. Grigorieva, S. V. Dubonos, and A. A. Firsov, "Two-dimensional gas of massless Dirac fermions in graphene," *Nature*, vol. 438, no. 7065, pp. 197–200, 2005. [Online]. Available: https://doi.org/10.1038/nature04233

[31] Y. Zhang, Y.-W. Tan, H. L. Stormer, and P. Kim, "Experimental observation of the quantum Hall effect and Berry's phase in graphene," *Nature*, vol. 438, no. 7065, pp. 201–204, 2005. [Online]. Available: https://doi.org/10.1038/nature04235

[32] G. Giovannetti, P. A. Khomyakov, G. Brocks, P. J. Kelly, and J. van den Brink, "Substrate-induced band gap in graphene on hexagonal boron nitride: Ab initio density functional calculations," *Phys. Rev. B*, vol. 76, p. 073103, Aug 2007. [Online]. Available: https://link.aps.org/doi/10.1103/PhysRevB.76.073103

[33] B. Hunt, J. D. Sanchez-Yamagishi, A. F. Young, M. Yankowitz, B. J. LeRoy, K. Watanabe, T. Taniguchi, P. Moon, M. Koshino, P. Jarillo-Herrero, and R. C. Ashoori, "Massive Dirac Fermions and Hofstadter Butterfly in a van der Waals Heterostructure," *Science*, vol. 340, no. 6139, pp. 1427–1430, 2013. [Online]. Available: https://science.sciencemag.org/content/340/6139/1427

[34] D. Xiao, G.-B. Liu, W. Feng, X. Xu, and W. Yao, "Coupled Spin and Valley Physics in Monolayers of MoS_2 and Other Group-VI Dichalcogenides," *Phys. Rev. Lett.*, vol. 108, p. 196802, May 2012. [Online]. Available: https://link.aps.org/doi/10.1103/PhysRevLett.108.196802

[35] B. Yan and C. Felser, "Topological Materials: Weyl Semimetals," *Annual Review of Condensed Matter Physics*, vol. 8, no. 1, pp. 337–354, 2017. [Online]. Available: https://doi.org/10.1146/annurev-conmatphys-031016-025458

[36] V. Mourik, K. Zuo, S. M. Frolov, S. R. Plissard, E. P. A. M. Bakkers, and L. P. Kouwenhoven, "Signatures of Majorana Fermions in Hybrid Superconductor-Semiconductor Nanowire Devices," *Science*, vol. 336, no. 6084, pp. 1003–1007, 2012. [Online]. Available: https://science.sciencemag.org/content/336/6084/1003

[37] J. Alicea, "New directions in the pursuit of Majorana fermions in solid state systems," *Reports on Progress in Physics*, vol. 75, no. 7, p. 076501, jun 2012. [Online]. Available: https://doi.org/10.1088%2F0034-4885%2F75%2F7%2F076501

[38] B. Bradlyn, J. Cano, Z. Wang, M. G. Vergniory, C. Felser, R. J. Cava, and B. A. Bernevig, "Beyond Dirac and Weyl fermions: Unconventional quasiparticles in conventional crystals," *Science*, vol. 353, no. 6299, 2016. [Online]. Available: https://science.sciencemag.org/content/353/6299/aaf5037

[39] C. Beenakker, "Bringing order to the expanding fermion zoo," *Science*, vol. 353, no. 6299, pp. 539–540, 2016. [Online]. Available: https://science.sciencemag.org/content/353/6299/539

[40] S. M. Young and C. L. Kane, "Dirac Semimetals in Two Dimensions," *Phys. Rev. Lett.*, vol. 115, p. 126803, Sep 2015. [Online]. Available: https://link.aps.org/doi/10.1103/PhysRevLett.115.126803

[41] Z. F. Wang, B. Liu, and W. Zhu, "Hourglass Fermion in Two-Dimensional Material," *Phys. Rev. Lett.*, vol. 123, p. 126403, Sep 2019. [Online]. Available: https://link.aps.org/doi/10.1103/PhysRevLett.123.126403

[42] K. v. Klitzing, G. Dorda, and M. Pepper, "New Method for High-Accuracy Determination of the Fine-Structure Constant Based on Quantized Hall Resistance," *Phys. Rev. Lett.*, vol. 45, pp. 494–497, Aug 1980. [Online]. Available: https://link.aps.org/doi/10.1103/PhysRevLett.45.494

[43] D. J. Thouless, M. Kohmoto, M. P. Nightingale, and M. den Nijs, "Quantized Hall Conductance in a Two-Dimensional Periodic Potential," *Phys. Rev. Lett.*, vol. 49, pp. 405–408, Aug 1982. [Online]. Available: https://link.aps.org/doi/10.1103/PhysRevLett.49.405

[44] D. C. Tsui, H. L. Stormer, and A. C. Gossard, "Two-Dimensional Magnetotransport in the Extreme Quantum Limit," *Phys. Rev. Lett.*, vol. 48, pp. 1559–1562, May 1982. [Online]. Available: https://link.aps.org/doi/10.1103/PhysRevLett.48.1559

[45] R. B. Laughlin, "Anomalous Quantum Hall Effect: An Incompressible Quantum Fluid with Fractionally Charged Excitations," *Phys. Rev. Lett.*, vol. 50, pp. 1395–1398, May 1983. [Online]. Available: https://link.aps.org/doi/10.1103/PhysRevLett.50.1395

[46] J. K. Jain, "Composite-fermion approach for the fractional quantum Hall effect," *Phys. Rev. Lett.*, vol. 63, pp. 199–202, Jul 1989. [Online]. Available: https://link.aps.org/doi/10.1103/PhysRevLett.63.199

[47] ——, *Composite Fermions*. Cambridge University Press, 2007. [Online]. Available: https://doi.org/10.1017/CBO9780511607561

[48] X.-G. Wen, "Topological orders and edge excitations in fractional quantum Hall states," *Advances in Physics*, vol. 44, no. 5, pp. 405–473, 1995. [Online]. Available: https://doi.org/10.1080/00018739500101566

[49] ——, "Colloquium: Zoo of quantum-topological phases of matter," *Rev. Mod. Phys.*, vol. 89, p. 041004, Dec 2017. [Online]. Available: https://link.aps.org/doi/10.1103/RevModPhys.89.041004

[50] F. D. M. Haldane, "Model for a Quantum Hall Effect without Landau Levels: Condensed-Matter Realization of the "Parity Anomaly"," *Phys. Rev. Lett.*, vol. 61, pp. 2015–2018, Oct 1988. [Online]. Available: https://link.aps.org/doi/10.1103/PhysRevLett.61.2015

[51] G. Jotzu, M. Messer, R. Desbuquois, M. Lebrat, T. Uehlinger, D. Greif, and T. Esslinger, "Experimental realization of the topological Haldane model with ultracold fermions," *Nature*, vol. 515, no. 7526, p. 237, 2014. [Online]. Available: https://doi.org/10.1038/nature13915

[52] C. L. Kane and E. J. Mele, "Z_2 Topological Order and the Quantum Spin Hall Effect," *Phys. Rev. Lett.*, vol. 95, p. 146802, Sep 2005. [Online]. Available: https://link.aps.org/doi/10.1103/PhysRevLett.95.146802

[53] ——, "Quantum Spin Hall Effect in Graphene," *Phys. Rev. Lett.*, vol. 95, p. 226801, Nov 2005. [Online]. Available: https://link.aps.org/doi/10.1103/PhysRevLett.95.226801

[54] M. Gmitra, D. Kochan, P. Högl, and J. Fabian, "Trivial and inverted Dirac bands and the emergence of quantum spin Hall states in graphene on transition-metal dichalcogenides," *Phys. Rev. B*, vol. 93, p. 155104, Apr 2016. [Online]. Available: https://link.aps.org/doi/10.1103/PhysRevB.93.155104

[55] A. Avsar, H. Ochoa, F. Guinea, B. Ozyilmaz, B. J. van Wees, and I. J. Vera-Marun, "Colloquium: Spintronics in graphene and other two-dimensional materials," *arXiv e-prints*, p. arXiv:1909.09188, Sep 2019.

[56] B. A. Bernevig, T. L. Hughes, and S.-C. Zhang, "Quantum Spin Hall Effect and Topological Phase Transition in HgTe Quantum Wells," *Science*, vol. 314, no. 5806, pp. 1757–1761, 2006. [Online]. Available: https://science.sciencemag.org/content/314/5806/1757

[57] M. König, S. Wiedmann, C. Brüne, A. Roth, H. Buhmann, L. W. Molenkamp, X.-L. Qi, and S.-C. Zhang, "Quantum Spin Hall Insulator State in HgTe Quantum Wells," *Science*, vol. 318, no. 5851, pp. 766–770, 2007. [Online]. Available: https://science.sciencemag.org/content/318/5851/766

[58] I. Knez, R.-R. Du, and G. Sullivan, "Evidence for Helical Edge Modes in Inverted InAs/GaSb Quantum Wells," *Phys. Rev. Lett.*, vol. 107, p. 136603, Sep 2011. [Online]. Available: https://link.aps.org/doi/10.1103/PhysRevLett.107.136603

[59] I. K. Drozdov, A. Alexandradinata, S. Jeon, S. Nadj-Perge, H. Ji, R. J. Cava, B. A. Bernevig, and A. Yazdani, "One-dimensional topological edge states of bismuth bilayers," *Nature Physics*, vol. 10, no. 9, p. 664, 2014. [Online]. Available: https://doi.org/10.1038/nphys3048

[60] F. Reis, G. Li, L. Dudy, M. Bauernfeind, S. Glass, W. Hanke, R. Thomale, J. Schäfer, and R. Claessen, "Bismuthene on a SiC substrate: A candidate for a high-temperature quantum spin Hall material," *Science*, vol. 357, no. 6348, pp. 287–290, 2017. [Online]. Available: https://science.sciencemag.org/content/357/6348/287

[61] Y. Ren, Z. Qiao, and Q. Niu, "Topological phases in two-dimensional materials: a review," *Reports on Progress in Physics*, vol. 79, no. 6, p. 066501, may 2016. [Online]. Available: https://doi.org/10.1088%2F0034-4885%2F79%2F6%2F066501

[62] M. Z. Hasan and C. L. Kane, "Colloquium: Topological insulators," *Rev. Mod. Phys.*, vol. 82, pp. 3045–3067, Nov 2010. [Online]. Available: https://link.aps.org/doi/10.1103/RevModPhys.82.3045

[63] X.-L. Qi and S.-C. Zhang, "Topological insulators and superconductors," *Rev. Mod. Phys.*, vol. 83, pp. 1057–1110, Oct 2011. [Online]. Available: https://link.aps.org/doi/10.1103/RevModPhys.83.1057

[64] S. Ryu, A. P. Schnyder, A. Furusaki, and A. W. W. Ludwig, "Topological insulators and superconductors: tenfold way and dimensional hierarchy," *New Journal of Physics*, vol. 12, no. 6, p. 065010, jun 2010. [Online]. Available: https://doi.org/10.1088%2F1367-2630%2F12%2F6%2F065010

[65] C.-K. Chiu, J. C. Y. Teo, A. P. Schnyder, and S. Ryu, "Classification of topological quantum matter with symmetries," *Rev. Mod. Phys.*, vol. 88, p. 035005, Aug 2016. [Online]. Available: https://link.aps.org/doi/10.1103/RevModPhys.88.035005

[66] A. Bansil, H. Lin, and T. Das, "Colloquium: Topological band theory," *Rev. Mod. Phys.*, vol. 88, p. 021004, Jun 2016. [Online]. Available: https://link.aps.org/doi/10.1103/RevModPhys.88.021004

[67] S. Rachel, "Interacting topological insulators: a review," *Reports on Progress in Physics*, vol. 81, no. 11, p. 116501, oct 2018. [Online]. Available: https://doi.org/10.1088%2F1361-6633%2Faad6a6

[68] R. Yu, W. Zhang, H.-J. Zhang, S.-C. Zhang, X. Dai, and Z. Fang, "Quantized Anomalous Hall Effect in Magnetic Topological Insulators," *Science*, vol. 329, no. 5987, pp. 61–64, 2010. [Online]. Available: https://science.sciencemag.org/content/329/5987/61

[69] C.-Z. Chang, J. Zhang, X. Feng, J. Shen, Z. Zhang, M. Guo, K. Li, Y. Ou, P. Wei, L.-L. Wang, Z.-Q. Ji, Y. Feng, S. Ji, X. Chen, J. Jia, X. Dai, Z. Fang, S.-C. Zhang, K. He, Y. Wang, L. Lu, X.-C. Ma, and Q.-K. Xue, "Experimental Observation of the Quantum Anomalous Hall Effect in a Magnetic Topological Insulator," *Science*, vol. 340, no. 6129, pp. 167–170, 2013. [Online]. Available: https://science.sciencemag.org/content/340/6129/167

[70] L. Fu, "Topological Crystalline Insulators," *Phys. Rev. Lett.*, vol. 106, p. 106802, Mar 2011. [Online]. Available: https://link.aps.org/doi/10.1103/PhysRevLett.106.106802

[71] P. Dziawa, B. J. Kowalski, K. Dybko, R. Buczko, A. Szczerbakow, M. Szot, E. Lusakowska, T. Balasubramanian, B. M. Wojek, M. H. Berntsen, O. Tjernberg, and T. Story, "Topological crystalline insulator states in Pb1-xSnxSe," *Nature Materials*, vol. 11, no. 12, pp. 1023–1027, 2012. [Online]. Available: https://doi.org/10.1038/nmat3449

[72] F. Schindler, A. M. Cook, M. G. Vergniory, Z. Wang, S. S. P. Parkin, B. A. Bernevig, and T. Neupert, "Higher-order topological insulators," *Science Advances*, vol. 4, no. 6, 2018. [Online]. Available: https://advances.sciencemag.org/content/4/6/eaat0346

[73] D. Xiao, M.-C. Chang, and Q. Niu, "Berry phase effects on electronic properties," *Rev. Mod. Phys.*, vol. 82, pp. 1959–2007, Jul 2010. [Online]. Available: https://link.aps.org/doi/10.1103/RevModPhys.82.1959

[74] R. Resta, "Manifestations of Berrys phase in molecules and condensed matter," *Journal of Physics: Condensed Matter*, vol. 12, no. 9, pp. R107–R143, feb 2000. [Online]. Available: https://doi.org/10.1088%2F0953-8984%2F12%2F9%2F201

[75] T. Fukui, Y. Hatsugai, and H. Suzuki, "Chern Numbers in Discretized Brillouin Zone: Efficient Method of Computing (Spin) Hall Conductances," *Journal of the Physical Society of Japan*, vol. 74, no. 6, pp. 1674–1677, 2005. [Online]. Available: https://doi.org/10.1143/JPSJ.74.1674

[76] M. Nakahara, *Geomtery, Topology and Physics*. Taylor and Francis Group, 2003.

[77] A. Rycerz, J. Tworzydlo, and C. W. J. Beenakker, "Valley filter and valley valve in graphene," *Nature Physics*, vol. 3, no. 3, pp. 172–175, 2007. [Online]. Available: https://doi.org/10.1038/nphys547

[78] K. F. Mak, D. Xiao, and J. Shan, "Light–valley interactions in 2D semiconductors," *Nature Photonics*, vol. 12, p. 451, AUG 2018. [Online]. Available: https://doi.org/10.1038/s41566-018-0204-6

[79] J. R. Schaibley, H. Yu, G. Clark, P. Rivera, J. S. Ross, K. L. Seyler, W. Yao, and X. Xu, "Valleytronics in 2D materials," *Nature Reviews Materials*, vol. 1, no. 11, p. 16055, 2016. [Online]. Available: https://doi.org/10.1038/natrevmats.2016.55

[80] J. Pawłowski, D. Żebrowski, and S. Bednarek, "Valley qubit in a gated MoS 2 monolayer quantum dot," *Physical Review B*, vol. 97, no. 15, p. 155412, Apr. 2018. [Online]. Available: https://link.aps.org/doi/10.1103/PhysRevB.97.155412

[81] A. D. Güçlü, P. Potasz, M. Korkusinski, and P. Hawrylak, *Graphene quantum dots*. Springer, 2014.

[82] T. Wehling, A. Black-Schaffer, and A. Balatsky, "Dirac materials," *Advances in Physics*, vol. 63, no. 1, pp. 1–76, 2014. [Online]. Available: https://doi.org/10.1080/00018732.2014.927109

[83] X. Wan, A. M. Turner, A. Vishwanath, and S. Y. Savrasov, "Topological semimetal and Fermi-arc surface states in the electronic structure of pyrochlore iridates," *Phys. Rev. B*, vol. 83, p. 205101, May 2011. [Online]. Available: https://link.aps.org/doi/10.1103/PhysRevB.83.205101

[84] Z. K. Liu, B. Zhou, Y. Zhang, Z. J. Wang, H. M. Weng, D. Prabhakaran, S.-K. Mo, Z. X. Shen, Z. Fang, X. Dai, Z. Hussain, and Y. L. Chen, "Discovery of a Three-Dimensional Topological Dirac Semimetal, Na3Bi," *Science*, vol. 343, no. 6173, pp. 864–867, 2014. [Online]. Available: https://science.sciencemag.org/content/343/6173/864

[85] C.-H. Park, L. Yang, Y.-W. Son, M. L. Cohen, and S. G. Louie, "New Generation of Massless Dirac Fermions in Graphene under External Periodic Potentials," *Phys. Rev. Lett.*, vol. 101, p. 126804, Sep 2008. [Online]. Available: https://link.aps.org/doi/10.1103/PhysRevLett.101.126804

[86] L. A. Ponomarenko, R. V. Gorbachev, G. L. Yu, D. C. Elias, R. Jalil, A. A. Patel, A. Mishchenko, A. S. Mayorov, C. R. Woods, J. R. Wallbank, M. Mucha-Kruczynski, B. A. Piot, M. Potemski, I. V. Grigorieva, K. S. Novoselov, F. Guinea, V. I. Fal'ko, and A. K. Geim, "Cloning of Dirac fermions in graphene superlattices," *Nature*, vol. 497, no. 7451, pp. 594–597, 2013. [Online]. Available: https://doi.org/10.1038/nature12187

[87] P. R. Wallace, "The Band Theory of Graphite," *Phys. Rev.*, vol. 71, pp. 622–634, May 1947. [Online]. Available: https://link.aps.org/doi/10.1103/PhysRev.71.622

[88] G. Connell, J. Wilson, and A. Yoffe, "Effects of pressure and temperature on exciton absorption and band structure of layer crystals: Molybdenum disulphide," *Journal of Physics and Chemistry of Solids*, vol. 30, no. 2, pp. 287 – 296, 1969. [Online]. Available: http://www.sciencedirect.com/science/article/pii/0022369769903102

[89] J. Wilson and A. Yoffe, "The transition metal dichalcogenides discussion and interpretation of the observed optical, electrical and structural properties," *Advances in Physics*, vol. 18, no. 73, pp. 193–335, 1969. [Online]. Available: https://doi.org/10.1080/00018736900101307

[90] M. S. Dresselhaus and G. Dresselhaus, "Intercalation compounds of graphite," *Advances in Physics*, vol. 51, no. 1, pp. 1–186, 2002. [Online]. Available: https://doi.org/10.1080/00018730110113644

[91] J. E. Fischer and T. E. Thompson, "Graphite intercalation compounds," *Physics Today*, vol. 31, no. 7, p. 36, 1978. [Online]. Available: https://doi.org/10.1063/1.2995104

[92] K. S. Novoselov, D. Jiang, F. Schedin, T. J. Booth, V. V. Khotkevich, S. V. Morozov, and A. K. Geim, "Two-dimensional atomic crystals," *Proceedings of the National Academy of Sciences*, vol. 102, no. 30, pp. 10 451–10 453, 2005. [Online]. Available: https://www.pnas.org/content/102/30/10451

[93] N. Mounet, M. Gibertini, P. Schwaller, D. Campi, A. Merkys, A. Marrazzo, T. Sohier, I. E. Castelli, A. Cepellotti, G. Pizzi, and N. Marzari, "Two-dimensional materials from high-throughput computational exfoliation of experimentally known compounds," *Nature Nanotechnology*, vol. 13, no. 3, pp. 246–252, 2018. [Online]. Available: https://doi.org/10.1038/s41565-017-0035-5

[94] A. J. Mannix, Z. Zhang, N. P. Guisinger, B. I. Yakobson, and M. C. Hersam, "Borophene as a prototype for synthetic 2D materials development," *Nature Nanotechnology*, vol. 13, no. 6, pp. 444–450, 2018. [Online]. Available: https://doi.org/10.1038/s41565-018-0157-4

[95] M. Ashton, J. Paul, S. B. Sinnott, and R. G. Hennig, "Topology-Scaling Identification of Layered Solids and Stable Exfoliated 2D Materials," *Phys. Rev. Lett.*, vol. 118, p. 106101, Mar 2017. [Online]. Available: https://link.aps.org/doi/10.1103/PhysRevLett.118.106101

[96] M. Chhowalla, H. S. Shin, G. Eda, L.-J. Li, K. P. Loh, and H. Zhang, "The chemistry of two-dimensional layered transition metal dichalcogenide nanosheets," *Nature Chemistry*, vol. 5, no. 4, pp. 263–275, 2013. [Online]. Available: https://doi.org/10.1038/nchem.1589

[97] X. Duan, C. Wang, A. Pan, R. Yu, and X. Duan, "Two-dimensional transition metal dichalcogenides as atomically thin semiconductors: opportunities and challenges," *Chem. Soc. Rev.*, vol. 44, pp. 8859–8876, 2015. [Online]. Available: http://dx.doi.org/10.1039/C5CS00507H

[98] Q. H. Wang, K. Kalantar-Zadeh, A. Kis, J. N. Coleman, and M. S. Strano, "Electronics and optoelectronics of two-dimensional transition metal dichalcogenides," *Nature Nanotechnology*, vol. 7, no. 11, pp. 699–712, 2012. [Online]. Available: https://doi.org/10.1038/nnano.2012.193

[99] Z. Fei, T. Palomaki, S. Wu, W. Zhao, X. Cai, B. Sun, P. Nguyen, J. Finney, X. Xu, and D. H. Cobden, "Edge conduction in monolayer WTe2," *Nature Physics*, vol. 13, no. 7, pp. 677–682, 2017. [Online]. Available: https://doi.org/10.1038/nphys4091

[100] S. Wu, V. Fatemi, Q. D. Gibson, K. Watanabe, T. Taniguchi, R. J. Cava, and P. Jarillo-Herrero, "Observation of the quantum spin Hall effect up to 100 kelvin in a monolayer crystal," *Science*, vol. 359, no. 6371, pp. 76–79, 2018. [Online]. Available: https://science.sciencemag.org/content/359/6371/76

[101] B. Radisavljevic, A. Radenovic, J. Brivio, V. Giacometti, and A. Kis, "Single-layer mos2 transistors," *Nat. Nano.*, p. 50141, 2011. [Online]. Available: http://www.nature.com/nnano/journal/v6/n3/full/nnano.2010.279.html#correction1

[102] A. Splendiani, L. Sun, Y. Zhang, T. Li, J. Kim, C.-Y. Chim, G. Galli, and F. Wang, "Emerging photoluminescence in monolayer mos2," *Nano Letters*, vol. 10, no. 4, pp. 1271–1275, 2010, pMID: 20229981. [Online]. Available: http://dx.doi.org/10.1021/nl903868w

[103] K. F. Mak, C. Lee, J. Hone, J. Shan, and T. F. Heinz, "Atomically Thin MoS_2: A New Direct-Gap Semiconductor," *Phys. Rev. Lett.*, vol. 105, p. 136805, Sep 2010. [Online]. Available: https://link.aps.org/doi/10.1103/PhysRevLett.105.136805

[104] M. M. Ugeda, A. J. Bradley, S.-F. Shi, F. H. da Jornada, Y. Zhang, D. Y. Qiu, W. Ruan, S.-K. Mo, Z. Hussain, Z.-X. Shen, F. Wang, S. G. Louie, and M. F. Crommie, "Giant bandgap renormalization and excitonic effects in a monolayer transition metal dichalcogenide semiconductor," *Nature Materials*, p. 1091, 2014. [Online]. Available: https://doi.org/10.1038/nmat4061

[105] K. Kang, S. Xie, L. Huang, Y. Han, P. Y. Huang, K. F. Mak, C.-J. Kim, D. Muller, and J. Park, "High-mobility three-atom-thick semiconducting films with wafer-scale homogeneity," *Nature*, vol. 520, no. 7549, pp. 656–660, 2015. [Online]. Available: https://doi.org/10.1038/nature14417

[106] K. Novoselov, A. Mishchenko, A. Carvalho, and A. C. Neto, "2D materials and van der Waals heterostructures," *Science*, vol. 353, no. 6298, p. 9439, 2016. [Online]. Available: https://doi.org/10.1126/science.aac9439

[107] G. Wang, A. Chernikov, M. M. Glazov, T. F. Heinz, X. Marie, T. Amand, and B. Urbaszek, "Colloquium: Excitons in atomically thin transition metal dichalcogenides," *Rev. Mod. Phys.*, vol. 90, p. 021001, Apr 2018. [Online]. Available: https://link.aps.org/doi/10.1103/RevModPhys.90.021001

[108] S. El Kazzi, W. Mortelmans, T. Nuytten, J. Meersschaut, P. Carolan, L. Landeloos, T. Conard, I. Radu, M. Heyns, and C. Merckling, "MoS2 synthesis by gas source MBE for transition metal dichalcogenides integration on large scale substrates," *Journal of Applied Physics*, vol. 123, no. 13, p. 135702, 2018. [Online]. Available: https://doi.org/10.1063/1.5008933

[109] D. Fu, X. Zhao, Y.-Y. Zhang, L. Li, H. Xu, A.-R. Jang, S. I. Yoon, P. Song, S. M. Poh, T. Ren, Z. Ding, W. Fu, T. J. Shin, H. S. Shin, S. T. Pantelides, W. Zhou, and K. P. Loh, "Molecular Beam Epitaxy of Highly Crystalline Monolayer Molybdenum Disulfide on Hexagonal Boron Nitride," *Journal of the American Chemical Society*, vol. 139, no. 27, pp. 9392–9400, 2017, pMID: 28633527. [Online]. Available: https://doi.org/10.1021/jacs.7b05131

[110] X. Wang, M. Hossain, Z. Wei, and L. Xie, "Growth of two-dimensional materials on hexagonal boron nitride (h-BN)," *Nanotechnology*, vol. 30, no. 3, p. 034003, nov 2018. [Online]. Available: https://doi.org/10.1088%2F1361-6528%2Faaeb70

[111] X. Liu, I. Balla, H. Bergeron, G. P. Campbell, M. J. Bedzyk, and M. C. Hersam, "Rotationally Commensurate Growth of MoS2 on Epitaxial Graphene," *ACS Nano*, vol. 10, no. 1, pp. 1067–1075, 2016, pMID: 26565112. [Online]. Available: https://doi.org/10.1021/acsnano.5b06398

[112] M. R. Molas, A. O. Slobodeniuk, K. Nogajewski, M. Bartos, L. Bala, A. Babiński, K. Watanabe, T. Taniguchi, C. Faugeras, and M. Potemski, "Energy Spectrum of Two-Dimensional Excitons in a Nonuniform Dielectric Medium," *Phys. Rev. Lett.*, vol. 123, p. 136801, Sep 2019. [Online]. Available: https://link.aps.org/doi/10.1103/PhysRevLett.123.136801

[113] V. Nicolosi, M. Chhowalla, M. G. Kanatzidis, M. S. Strano, and J. N. Coleman, "Liquid Exfoliation of Layered Materials," *Science*, vol. 340, no. 6139, 2013. [Online]. Available: https://science.sciencemag.org/content/340/6139/1226419

[114] A. Jawaid, D. Nepal, K. Park, M. Jespersen, A. Qualley, P. Mirau, L. F. Drummy, and R. A. Vaia, "Mechanism for Liquid Phase Exfoliation of MoS2," *Chemistry of Materials*, vol. 28, no. 1, pp. 337–348, 2016. [Online]. Available: https://doi.org/10.1021/acs.chemmater.5b04224

[115] D.-H. Lien, J. S. Kang, M. Amani, K. Chen, M. Tosun, H.-P. Wang, T. Roy, M. S. Eggleston, M. C. Wu, M. Dubey, S.-C. Lee, J.-H. He, and A. Javey, "Engineering Light Outcoupling in 2D Materials," *Nano Letters*, vol. 15, no. 2, pp. 1356–1361, 2015, pMID: 25602462. [Online]. Available: https://doi.org/10.1021/nl504632u

[116] Y. Lin, X. Ling, L. Yu, S. Huang, A. L. Hsu, Y.-H. Lee, J. Kong, M. S. Dresselhaus, and T. Palacios, "Dielectric Screening of Excitons and Trions in Single-Layer MoS2," *Nano Letters*, vol. 14, no. 10, p. 5569, 2014. [Online]. Available: https://doi.org/10.1021/nl501988y

[117] A. Raja, A. Chaves, J. Yu, G. Arefe, H. M. Hill, A. F. Rigosi, T. C. Berkelbach, P. Nagler, C. Schüller, T. Korn, C. Nuckolls, J. Hone, L. E. Brus, T. F. Heinz, D. R. Reichman, and A. Chernikov, "Coulomb engineering of the bandgap and excitons in two-dimensional materials," *Nature Communications*, vol. 8, no. 1, p. 15251, 2017. [Online]. Available: https://doi.org/10.1038/ncomms15251

[118] O. A. Ajayi, J. V. Ardelean, G. D. Shepard, J. Wang, A. Antony, T. Taniguchi, K. Watanabe, T. F. Heinz, S. Strauf, X.-Y. Zhu, and J. C. Hone, "Approaching the intrinsic photoluminescence linewidth in transition metal dichalcogenide monolayers," *2D Materials*, vol. 4, no. 3, p. 031011, 2017. [Online]. Available: http://dx.doi.org/10.1088/2053-1583/aa6aa1

[119] F. Cadiz, E. Courtade, C. Robert, G. Wang, Y. Shen, H. Cai, T. Taniguchi, K. Watanabe, H. Carrere, D. Lagarde, M. Manca, T. Amand, P. Renucci, S. Tongay, X. Marie, and B. Urbaszek, "Excitonic Linewidth Approaching the Homogeneous Limit in MoS_2-Based van der Waals Heterostructures," *Phys. Rev. X*, vol. 7, p. 021026, May 2017. [Online]. Available: https://link.aps.org/doi/10.1103/PhysRevX.7.021026

[120] H. Haug and S. W. Koch, *Quantum Theory of the Optical and Electronic Properties of Semiconductors*, 5th ed. WORLD SCIENTIFIC, 2009. [Online]. Available: https://doi.org/10.1142/7184

[121] P. Y. Yu and M. Cardona, *Fundamentals of Semiconductors*, 4th ed. Springer, Berlin, Heidelberg, 2010. [Online]. Available: https://doi.org/10.1007/978-3-642-00710-1

[122] W. Schäfer and M. Wegener, *Semiconductor Optics and Transport Phenomena*, 1st ed. Springer, Berlin, Heidelberg, 2002. [Online]. Available: https://doi.org/10.1007/978-3-662-04663-0

[123] P. K. Gogoi, Z. Hu, Q. Wang, A. Carvalho, D. Schmidt, X. Yin, Y.-H. Chang, L.-J. Li, C. H. Sow, A. H. C. Neto, M. B. H. Breese, A. Rusydi, and A. T. S. Wee, "Oxygen Passivation Mediated Tunability of Trion and Excitons in MoS_2," *Phys. Rev. Lett.*, vol. 119, p. 077402, Aug 2017. [Online]. Available: https://link.aps.org/doi/10.1103/PhysRevLett.119.077402

[124] A. Allain, J. Kang, K. Banerjee, and A. Kis, "Electrical contacts to two-dimensional semiconductors," *Nature Materials*, vol. 14, no. 12, pp. 1195–1205, 2015. [Online]. Available: https://doi.org/10.1038/nmat4452

[125] X. Zhang, W. P. Han, J. B. Wu, S. Milana, Y. Lu, Q. Q. Li, A. C. Ferrari, and P. H. Tan, "Raman spectroscopy of shear and layer breathing modes in multilayer MoS_2," *Phys. Rev. B*, vol. 87, p. 115413, Mar 2013. [Online]. Available: https://link.aps.org/doi/10.1103/PhysRevB.87.115413

[126] G. Plechinger, S. Heydrich, J. Eroms, D. Weiss, C. Schüller, and T. Korn, "Raman spectroscopy of the interlayer shear mode in few-layer MoS2 flakes," *Applied Physics Letters*, vol. 101, no. 10, p. 101906, 2012. [Online]. Available: https://doi.org/10.1063/1.4751266

[127] C. Zhang, A. Johnson, C.-L. Hsu, L.-J. Li, and C.-K. Shih, "Direct Imaging of Band Profile in Single Layer MoS2 on Graphite: Quasiparticle Energy Gap, Metallic Edge States, and Edge Band Bending," *Nano Letters*, vol. 14, no. 5, pp. 2443–2447, 2014, pMID: 24783945. [Online]. Available: https://doi.org/10.1021/nl501133c

[128] D. J. Trainer, Y. Zhang, F. Bobba, X. Xi, S.-W. Hla, and M. Iavarone, "The Effects of Atomic-Scale Strain Relaxation on the Electronic Properties of Monolayer MoS2," *ACS Nano*, vol. 13, no. 7, pp. 8284–8291, 2019, pMID: 31268680. [Online]. Available: https://doi.org/10.1021/acsnano.9b03652

[129] W. Jin, P.-C. Yeh, N. Zaki, D. Zhang, J. T. Sadowski, A. Al-Mahboob, A. M. van der Zande, D. A. Chenet, J. I. Dadap, I. P. Herman, P. Sutter, J. Hone, and R. M. Osgood, "Direct Measurement of the Thickness-Dependent Electronic Band Structure of MoS_2 Using Angle-Resolved Photoemission Spectroscopy," *Phys. Rev. Lett.*, vol. 111, p. 106801, Sep 2013. [Online]. Available: https://link.aps.org/doi/10.1103/PhysRevLett.111.106801

[130] Y. Zhang, T.-R. Chang, B. Zhou, Y.-T. Cui, H. Yan, Z. Liu, F. Schmitt, J. Lee, R. Moore, Y. Chen, H. Lin, H.-T. Jeng, S.-K. Mo, Z. Hussain, A. Bansil, and Z.-X. Shen, "Direct observation of the transition from indirect to direct bandgap in atomically thin epitaxial MoSe2," *Nature Nanotechnology*, vol. 9, no. 2, pp. 111–115, 2014. [Online]. Available: https://doi.org/10.1038/nnano.2013.277

[131] N. Alidoust, G. Bian, S.-Y. Xu, R. Sankar, M. Neupane, C. Liu, I. Belopolski, D.-X. Qu, J. D. Denlinger, F.-C. Chou, and M. Z. Hasan, "Observation of monolayer valence band spin-orbit effect and induced quantum well states in MoX2," *Nature Communications*, vol. 5, no. 1, p. 4673, 2014. [Online]. Available: https://doi.org/10.1038/ncomms5673

[132] J. A. Miwa, S. Ulstrup, S. G. Sørensen, M. Dendzik, A. G. c. v. a. c. Čabo, M. Bianchi, J. V. Lauritsen, and P. Hofmann, "Electronic Structure of Epitaxial Single-Layer MoS_2," *Phys. Rev. Lett.*, vol. 114, p. 046802, Jan 2015. [Online]. Available: https://link.aps.org/doi/10.1103/PhysRevLett.114.046802

[133] Y. L. Huang, Y. Chen, W. Zhang, S. Y. Quek, C.-H. Chen, L.-J. Li, W.-T. Hsu, W.-H. Chang, Y. J. Zheng, W. Chen, and A. T. S. Wee, "Bandgap tunability at single-layer molybdenum disulphide grain boundaries," *Nature Communications*, vol. 6, no. 1, p. 6298, 2015. [Online]. Available: https://doi.org/10.1038/ncomms7298

[134] M.-H. Chiu, C. Zhang, H.-W. Shiu, C.-P. Chuu, C.-H. Chen, C.-Y. S. Chang, C.-H. Chen, M.-Y. Chou, C.-K. Shih, and L.-J. Li, "Determination of band alignment in the single-layer MoS2/WSe2 heterojunction," *Nature Communications*, vol. 6, no. 1, p. 7666, 2015. [Online]. Available: https://doi.org/10.1038/ncomms8666

[135] P. Eickholt, C. Sanders, M. Dendzik, L. Bignardi, D. Lizzit, S. Lizzit, A. Bruix, P. Hofmann, and M. Donath, "Spin Structure of K Valleys in Single-Layer WS_2 on Au(111)," *Phys. Rev. Lett.*, vol. 121, p. 136402, Sep 2018. [Online]. Available: https://link.aps.org/doi/10.1103/PhysRevLett.121.136402

[136] M. Bernardi, M. Palummo, and J. C. Grossman, "Extraordinary Sunlight Absorption and One Nanometer Thick Photovoltaics Using Two-Dimensional Monolayer Materials," *Nano Letters*, vol. 13, no. 8, pp. 3664–3670, 2013, pMID: 23750910. [Online]. Available: https://doi.org/10.1021/nl401544y

[137] G. Konstantatos, "Current status and technological prospect of photodetectors based on two-dimensional materials," *Nature Communications*, vol. 9, no. 1, p. 5266, 2018. [Online]. Available: https://doi.org/10.1038/s41467-018-07643-7

[138] F. Bonaccorso, L. Colombo, G. Yu, M. Stoller, V. Tozzini, A. C. Ferrari, R. S. Ruoff, and V. Pellegrini, "Graphene, related two-dimensional crystals, and hybrid systems for energy conversion and storage," *Science*, vol. 347, no. 6217, 2015. [Online]. Available: https://science.sciencemag.org/content/347/6217/1246501

[139] F. H. L. Koppens, T. Mueller, P. Avouris, A. C. Ferrari, M. S. Vitiello, and M. Polini, "Photodetectors based on graphene, other two-dimensional materials and hybrid systems," *Nature Nanotechnology*, vol. 9, no. 10, pp. 780–793, 2014. [Online]. Available: https://doi.org/10.1038/nnano.2014.215

[140] C.-H. Lee, G.-H. Lee, A. M. van der Zande, W. Chen, Y. Li, M. Han, X. Cui, G. Arefe, C. Nuckolls, T. F. Heinz, J. Guo, J. Hone, and P. Kim, "Atomically thin p-n junctions with van der Waals heterointerfaces," *Nature Nanotechnology*, vol. 9, no. 9, pp. 676–681, 2014. [Online]. Available: https://doi.org/10.1038/nnano.2014.150

[141] M.-L. Tsai, S.-H. Su, J.-K. Chang, D.-S. Tsai, C.-H. Chen, C.-I. Wu, L.-J. Li, L.-J. Chen, and J.-H. He, "Monolayer MoS2 Heterojunction Solar Cells," *ACS Nano*, vol. 8, no. 8, pp. 8317–8322, 2014, pMID: 25046764. [Online]. Available: https://doi.org/10.1021/nn502776h

[142] M. M. Furchi, A. Pospischil, F. Libisch, J. Burgdörfer, and T. Mueller, "Photovoltaic Effect in an Electrically Tunable van der Waals Heterojunction," *Nano Letters*, vol. 14, no. 8, pp. 4785–4791, 2014, pMID: 25057817. [Online]. Available: https://doi.org/10.1021/nl501962c

[143] J. Jadczak, J. Kutrowska-Girzycka, P. Kapuściński, Y. S. Huang, A. Wójs, and L. Bryja, "Probing of free and localized excitons and trions in atomically thin WSe2, WS2, MoSe2 and MoS2 in photoluminescence and reflectivity experiments," *Nanotechnology*, vol. 28, no. 39, p. 395702, sep 2017. [Online]. Available: https://doi.org/10.1088%2F1361-6528%2Faa87d0

[144] A. C. Ferrari, J. C. Meyer, V. Scardaci, C. Casiraghi, M. Lazzeri, F. Mauri, S. Piscanec, D. Jiang, K. S. Novoselov, S. Roth, and A. K. Geim, "Raman Spectrum of Graphene and Graphene Layers," *Phys. Rev. Lett.*, vol. 97, p. 187401, Oct 2006. [Online]. Available: https://link.aps.org/doi/10.1103/PhysRevLett.97.187401

[145] C. Lee, H. Yan, L. E. Brus, T. F. Heinz, J. Hone, and S. Ryu, "Anomalous Lattice Vibrations of Single- and Few-Layer MoS2," *ACS Nano*, vol. 4, no. 5, pp. 2695–2700, 2010, pMID: 20392077. [Online]. Available: https://doi.org/10.1021/nn1003937

[146] A. Splendiani, L. Sun, Y. Zhang, T. Li, J. Kim, C.-Y. Chim, G. Galli, and F. Wang, "Emerging Photoluminescence in Monolayer MoS2," *Nano Letters*, vol. 10, no. 4, p. 1271, 2010. [Online]. Available: https://doi.org/10.1021/nl903868w

[147] G. Eda, H. Yamaguchi, D. Voiry, T. Fujita, M. Chen, and M. Chhowalla, "Photoluminescence from Chemically Exfoliated MoS2," *Nano Letters*, vol. 11, no. 12, pp. 5111–5116, 2011, pMID: 22035145. [Online]. Available: https://doi.org/10.1021/nl201874w

[148] P. Tonndorf, R. Schmidt, P. Böttger, X. Zhang, J. Börner, A. Liebig, M. Albrecht, C. Kloc, O. Gordan, D. R. T. Zahn, S. M. de Vasconcellos, and R. Bratschitsch, "Photoluminescence emission and Raman response of monolayer MoS2, MoSe2, and WSe2," *Opt. Express*, vol. 21, no. 4, pp. 4908–4916, Feb 2013. [Online]. Available: http://www.opticsexpress.org/abstract.cfm?URI=oe-21-4-4908

[149] W. Zhao, Z. Ghorannevis, L. Chu, M. Toh, C. Kloc, P.-H. Tan, and G. Eda, "Evolution of Electronic Structure in Atomically Thin Sheets of WS2 and WSe2," *ACS Nano*, vol. 7, no. 1, pp. 791–797, 2013, pMID: 23256505. [Online]. Available: https://doi.org/10.1021/nn305275h

[150] C. Ruppert, O. B. Aslan, and T. F. Heinz, "Optical Properties and Band Gap of Single- and Few-Layer MoTe2 Crystals," *Nano Letters*, vol. 14, no. 11, pp. 6231–6236, 2014, pMID: 25302768. [Online]. Available: https://doi.org/10.1021/nl502557g

[151] I. G. Lezama, A. Arora, A. Ubaldini, C. Barreteau, E. Giannini, M. Potemski, and A. F. Morpurgo, "Indirect-to-Direct Band Gap Crossover in Few-Layer MoTe2," *Nano Letters*, vol. 15, no. 4, pp. 2336–2342, 2015, pMID: 25803208. [Online]. Available: https://doi.org/10.1021/nl5045007

[152] E. S. Kadantsev and P. Hawrylak, "Electronic structure of a single MoS2 monolayer," *Solid State Communications*, vol. 152, no. 10, p. 909, 2012. [Online]. Available: http://www.sciencedirect.com/science/article/pii/S0038109812000889

[153] A. Ramasubramaniam, "Large excitonic effects in monolayers of molybdenum and tungsten dichalcogenides," *Phys. Rev. B*, vol. 86, p. 115409, Sep 2012. [Online]. Available: https://link.aps.org/doi/10.1103/PhysRevB.86.115409

[154] R. Coehoorn, C. Haas, and R. A. de Groot, "Electronic structure of $MoSe_2$, MoS_2, and WSe_2. II. The nature of the optical band gaps," *Phys. Rev. B*, vol. 35, pp. 6203–6206, Apr 1987. [Online]. Available: https://link.aps.org/doi/10.1103/PhysRevB.35.6203

[155] T. Cao, G. Wang, W. Han, H. Ye, C. Zhu, J. Shi, Q. Niu, P. Tan, E. Wang, B. Liu, and J. Feng, "Valley-selective circular dichroism of monolayer molybdenum disulphide," *Nature Communications*, vol. 3, no. 1, p. 887, 2012. [Online]. Available: https://doi.org/10.1038/ncomms1882

[156] K. F. Mak, K. He, J. Shan, and T. F. Heinz, "Control of valley polarization in monolayer MoS2 by optical helicity," *Nature Nanotechnology*, vol. 7, no. 8, pp. 494–498, 2012. [Online]. Available: https://doi.org/10.1038/nnano.2012.96

[157] G. Sallen, L. Bouet, X. Marie, G. Wang, C. R. Zhu, W. P. Han, Y. Lu, P. H. Tan, T. Amand, B. L. Liu, and B. Urbaszek, "Robust optical emission polarization in MoS_2 monolayers through selective valley excitation," *Phys. Rev. B*, vol. 86, p. 081301, Aug 2012. [Online]. Available: https://link.aps.org/doi/10.1103/PhysRevB.86.081301

[158] H. Zeng, J. Dai, W. Yao, D. Xiao, and X. Cui, "Valley polarization in MoS2 monolayers by optical pumping," *Nature Nanotechnology*, vol. 7, no. 8, pp. 490–493, 2012. [Online]. Available: https://doi.org/10.1038/nnano.2012.95

[159] G. Wang, E. Palleau, T. Amand, S. Tongay, X. Marie, and B. Urbaszek, "Polarization and time-resolved photoluminescence spectroscopy of excitons in MoSe2 monolayers," *Applied Physics Letters*, vol. 106, no. 11, p. 112101, 2015. [Online]. Available: http://dx.doi.org/10.1063/1.4916089

[160] Y. Zhang, T. Oka, R. Suzuki, J. Ye, and Y. Iwasa, "Electrically switchable chiral light-emitting transistor," *Science*, vol. 344, no. 6185, pp. 725–728, 2014. [Online]. Available: http://dx.doi.org/10.1126/science.1251329

[161] G. Kioseoglou, A. T. Hanbicki, M. Currie, A. L. Friedman, D. Gunlycke, and B. T. Jonker, "Valley polarization and intervalley scattering in monolayer MoS2," *Applied Physics Letters*, vol. 101, no. 22, p. 221907, 2012. [Online]. Available: http://dx.doi.org/10.1063/1.4768299

[162] A. M. Jones, H. Yu, N. J. Ghimire, S. Wu, G. Aivazian, J. S. Ross, B. Zhao, J. Yan, D. G. Mandrus, D. Xiao, W. Yao, and X. Xu, "Optical generation of excitonic valley coherence in monolayer WSe2," *Nature Nanotechnology*, vol. 8, no. 9, pp. 634–638, 2013. [Online]. Available: https://doi.org/10.1038/nnano.2013.151

[163] G. Wang, X. Marie, B. L. Liu, T. Amand, C. Robert, F. Cadiz, P. Renucci, and B. Urbaszek, "Control of Exciton Valley Coherence in Transition Metal Dichalcogenide Monolayers," *Phys. Rev. Lett.*, vol. 117, p. 187401, Oct 2016. [Online]. Available: https://link.aps.org/doi/10.1103/PhysRevLett.117.187401

[164] K. Hao, G. Moody, F. Wu, C. K. Dass, L. Xu, C.-H. Chen, L. Sun, M.-Y. Li, L.-J. Li, A. H. MacDonald, and X. Li, "Direct measurement of exciton valley coherence in monolayer WSe2," *Nature Physics*, vol. 12, no. 7, pp. 677–682, 2016. [Online]. Available: https://doi.org/10.1038/nphys3674

[165] A. Srivastava, M. Sidler, A. V. Allain, D. S. Lembke, A. Kis, and A. Imamoglu, "Valley Zeeman effect in elementary optical excitations of monolayer WSe2," *Nature Physics*, vol. 11, no. 2, pp. 141–147, 2015. [Online]. Available: https://doi.org/10.1038/nphys3203

[166] G. Aivazian, Z. Gong, A. M. Jones, R.-L. Chu, J. Yan, D. G. Mandrus, C. Zhang, D. Cobden, W. Yao, and X. Xu, "Magnetic control of valley pseudospin in monolayer WSe2," *Nature Physics*, vol. 11, no. 2, pp. 148–152, 2015. [Online]. Available: https://doi.org/10.1038/nphys3201

[167] T. Scrace, Y. Tsai, B. Barman, L. Schweidenback, A. Petrou, G. Kioseoglou, I. Ozfidan, M. Korkusiński, and P. Hawrylak, "Magnetoluminescence and valley polarized state of a two-dimensional electron gas in WS2 monolayers," *Nat. Nano.*, vol. 10, no. 7, pp. 603–607, 2015. [Online]. Available: http://dx.doi.org/10.1038/nnano.2015.78

[168] J. E. H. Braz, B. Amorim, and E. V. Castro, "Valley-polarized magnetic state in hole-doped monolayers of transition-metal dichalcogenides," *Phys. Rev. B*, vol. 98, p. 161406, Oct 2018. [Online]. Available: https://link.aps.org/doi/10.1103/PhysRevB.98.161406

[169] J. G. Roch, G. Froehlicher, N. Leisgang, P. Makk, K. Watanabe, T. Taniguchi, and R. J. Warburton, "Spin-polarized electrons in monolayer MoS_2," *Nature Nanotechnology*, vol. 14, no. 5, pp. 432–436, 2019. [Online]. Available: https://doi.org/10.1038/s41565-019-0397-y

[170] D. Miserev, J. Klinovaja, and D. Loss, "Exchange intervalley scattering and magnetic phase diagram of transition metal dichalcogenide monolayers," *Phys. Rev. B*, vol. 100, p. 014428, Jul 2019. [Online]. Available: https://link.aps.org/doi/10.1103/PhysRevB.100.014428

[171] K. He, N. Kumar, L. Zhao, Z. Wang, K. F. Mak, H. Zhao, and J. Shan, "Tightly Bound Excitons in Monolayer WSe_2," *Phys. Rev. Lett.*, vol. 113, p. 026803, Jul 2014. [Online]. Available: https://link.aps.org/doi/10.1103/PhysRevLett.113.026803

[172] A. Arora, M. Koperski, K. Nogajewski, J. Marcus, C. Faugeras, and M. Potemski, "Excitonic resonances in thin films of WSe2: from monolayer to bulk material," *Nanoscale*, vol. 7, pp. 10 421–10 429, 2015. [Online]. Available: http://dx.doi.org/10.1039/C5NR01536G

[173] A. Chernikov, T. C. Berkelbach, H. M. Hill, A. Rigosi, Y. Li, O. B. Aslan, D. R. Reichman, M. S. Hybertsen, and T. F. Heinz, "Exciton Binding Energy and Nonhydrogenic Rydberg Series in Monolayer WS_2," *Phys. Rev. Lett.*, vol. 113, p. 076802, Aug 2014. [Online]. Available: https://link.aps.org/doi/10.1103/PhysRevLett.113.076802

[174] A. Hanbicki, M. Currie, G. Kioseoglou, A. Friedman, and B. Jonker, "Measurement of high exciton binding energy in the monolayer transition-metal dichalcogenides WS2 and WSe2," *Solid State Communications*, vol. 203, pp. 16 – 20, 2015. [Online]. Available: http://www.sciencedirect.com/science/article/pii/S0038109814004621

[175] H. M. Hill, A. F. Rigosi, C. Roquelet, A. Chernikov, T. C. Berkelbach, D. R. Reichman, M. S. Hybertsen, L. E. Brus, and T. F. Heinz, "Observation of Excitonic Rydberg States in Monolayer MoS2 and WS2 by Photoluminescence Excitation Spectroscopy," *Nano Letters*, vol. 15, no. 5, pp. 2992–2997, 2015, pMID: 25816155. [Online]. Available: https://doi.org/10.1021/nl504868p

[176] A. Arora, K. Nogajewski, M. Molas, M. Koperski, and M. Potemski, "Exciton band structure in layered MoSe2: from a monolayer to the bulk limit," *Nanoscale*, vol. 7, pp. 20 769–20 775, 2015. [Online]. Available: http://dx.doi.org/10.1039/C5NR06782K

[177] G. Wang, X. Marie, I. Gerber, T. Amand, D. Lagarde, L. Bouet, M. Vidal, A. Balocchi, and B. Urbaszek, "Giant Enhancement of the Optical Second-Harmonic Emission of WSe_2 Monolayers by Laser Excitation at Exciton Resonances," *Phys. Rev. Lett.*, vol. 114, p. 097403, Mar 2015. [Online]. Available: https://link.aps.org/doi/10.1103/PhysRevLett.114.097403

[178] A. V. Stier, K. M. McCreary, B. T. Jonker, J. Kono, and S. A. Crooker, "Exciton diamagnetic shifts and valley Zeeman effects in monolayer WS2 and MoS2 to 65 Tesla," *Nature Communications*, vol. 7, no. 1, p. 10643, Feb 2016. [Online]. Available: https://doi.org/10.1038/ncomms10643

[179] A. V. Stier, N. P. Wilson, K. A. Velizhanin, J. Kono, X. Xu, and S. A. Crooker, "Magnetooptics of Exciton Rydberg States in a Monolayer Semiconductor," *Phys. Rev. Lett.*, vol. 120, p. 057405, Feb 2018. [Online]. Available: https://link.aps.org/doi/10.1103/PhysRevLett.120.057405

[180] M. Goryca, J. Li, A. Stier, S. Crooker, T. Taniguchi, K. Watanabe, E. Courtade, S. Shree, C. Robert, B. Urbaszek, X. Marie, and S. A. Crooker, "Revealing exciton masses and dielectric properties of monolayer semiconductors with high magnetic fields," *Nature Communications*, vol. 10, p. 4172, 2019. [Online]. Available: https://doi.org/10.1038/s41467-019-12180-y

[181] A. Delhomme, G. Butseraen, B. Zheng, L. Marty, V. Bouchiat, M. R. Molas, A. Pan, K. Watanabe, T. Taniguchi, A. Ouerghi, J. Renard, and C. Faugeras, "Magneto-spectroscopy of exciton Rydberg states in a CVD grown WSe2 monolayer," *Applied Physics Letters*, vol. 114, no. 23, p. 232104, 2019. [Online]. Available: https://doi.org/10.1063/1.5095573

[182] X.-X. Zhang, Y. You, S. Y. F. Zhao, and T. F. Heinz, "Experimental Evidence for Dark Excitons in Monolayer WSe_2," *Phys. Rev. Lett.*, vol. 115, p. 257403, Dec 2015. [Online]. Available: https://link.aps.org/doi/10.1103/PhysRevLett.115.257403

[183] G. Wang, C. Robert, A. Suslu, B. Chen, S. Yang, S. Alamdari, I. C. Gerber, T. Amand, X. Marie, S. Tongay, and B. Urbaszek, "Spin-orbit engineering in transition metal dichalcogenide alloy monolayers," *Nature Communications*, vol. 6, no. 1, p. 10110, 2015. [Online]. Available: https://doi.org/10.1038/ncomms10110

[184] G. Wang, C. Robert, M. M. Glazov, F. Cadiz, E. Courtade, T. Amand, D. Lagarde, T. Taniguchi, K. Watanabe, B. Urbaszek, and X. Marie, "In-Plane Propagation of Light in Transition Metal Dichalcogenide Monolayers: Optical Selection Rules," *Phys. Rev. Lett.*, vol. 119, p. 047401, Jul 2017. [Online]. Available: https://link.aps.org/doi/10.1103/PhysRevLett.119.047401

[185] C. Robert, T. Amand, F. Cadiz, D. Lagarde, E. Courtade, M. Manca, T. Taniguchi, K. Watanabe, B. Urbaszek, and X. Marie, "Fine structure and lifetime of dark excitons in transition metal dichalcogenide monolayers," *Phys. Rev. B*, vol. 96, p. 155423, Oct 2017. [Online]. Available: https://link.aps.org/doi/10.1103/PhysRevB.96.155423

[186] Y. Tang, K. F. Mak, and J. Shan, "Long valley lifetime of dark excitons in single-layer WSe2," *Nature Communications*, vol. 10, no. 1, p. 4047, 2019. [Online]. Available: https://doi.org/10.1038/s41467-019-12129-1

[187] K.-D. Park, T. Jiang, G. Clark, X. Xu, and M. B. Raschke, "Radiative control of dark excitons at room temperature by nano-optical antenna-tip Purcell effect," *Nature Nanotechnology*, vol. 13, no. 1, pp. 59–64, 2018. [Online]. Available: https://doi.org/10.1038/s41565-017-0003-0

[188] Y. Zhou, G. Scuri, D. S. Wild, A. A. High, A. Dibos, L. A. Jauregui, C. Shu, K. De Greve, K. Pistunova, A. Y. Joe, T. Taniguchi, K. Watanabe, P. Kim, M. D. Lukin, and H. Park, "Probing dark excitons in atomically thin semiconductors via near-field coupling to surface plasmon polaritons," *Nature Nanotechnology*, vol. 12, no. 9, pp. 856–860, 2017. [Online]. Available: https://doi.org/10.1038/nnano.2017.106

[189] M. R. Molas, A. O. Slobodeniuk, T. Kazimierczuk, K. Nogajewski, M. Bartos, P. Kapuściński, K. Oreszczuk, K. Watanabe, T. Taniguchi, C. Faugeras, P. Kossacki, D. M. Basko, and M. Potemski, "Probing and Manipulating Valley Coherence of Dark Excitons in Monolayer WSe_2," *Phys. Rev. Lett.*, vol. 123, p. 096803, Aug 2019. [Online]. Available: https://link.aps.org/doi/10.1103/PhysRevLett.123.096803

[190] F. Withers, O. Del Pozo-Zamudio, S. Schwarz, S. Dufferwiel, P. M. Walker, T. Godde, A. P. Rooney, A. Gholinia, C. R. Woods, P. Blake, S. J. Haigh, K. Watanabe, T. Taniguchi, I. L. Aleiner, A. K. Geim, V. I. Fal'ko, A. I. Tartakovskii, and K. S. Novoselov, "WSe2 Light-Emitting Tunneling Transistors with Enhanced Brightness at Room Temperature," *Nano Letters*, vol. 15, no. 12, pp. 8223–8228, 2015, pMID: 26555037. [Online]. Available: http://dx.doi.org/10.1021/acs.nanolett.5b03740

[191] X.-X. Zhang, T. Cao, Z. Lu, Y.-C. Lin, F. Zhang, Y. Wang, Z. Li, J. C. Hone, J. A. Robinson, D. Smirnov, S. G. Louie, and T. F. Heinz, "Magnetic brightening and control of dark excitons in monolayer WSe2," *Nature Nanotechnology*, vol. 12, no. 9, pp. 883–888, 2017. [Online]. Available: https://doi.org/10.1038/nnano.2017.105

[192] M. R. Molas, C. Faugeras, A. O. Slobodeniuk, K. Nogajewski, M. Bartos, D. M. Basko, and M. Potemski, "Brightening of dark excitons in monolayers of semiconducting transition metal dichalcogenides," *2D Materials*, vol. 4, no. 2, p. 021003, jan 2017. [Online]. Available: https://doi.org/10.1088%2F2053-1583%2Faa5521

[193] Z. Lu, D. Rhodes, Z. Li, D. V. Tuan, Y. Jiang, J. Ludwig, Z. Jiang, Z. Lian, S.-F. Shi, J. Hone, H. Dery, and D. Smirnov, "Magnetic field mixing and splitting of bright and dark excitons in monolayer MoSe2," *2D Materials*, vol. 7, no. 1, p. 015017, nov 2019. [Online]. Available: https://doi.org/10.1088%2F2053-1583%2Fab5614

[194] Z. Li, T. Wang, C. Jin, Z. Lu, Z. Lian, Y. Meng, M. Blei, S. Gao, T. Taniguchi, K. Watanabe, T. Ren, S. Tongay, L. Yang, D. Smirnov, T. Cao, and S.-F. Shi, "Emerging photoluminescence from the dark-exciton phonon replica in monolayer WSe2," *Nature Communications*, vol. 10, no. 1, p. 2469, 2019. [Online]. Available: https://doi.org/10.1038/s41467-019-10477-6

[195] Z. Ye, T. Cao, K. O'Brien, H. Zhu, X. Yin, Y. Wang, S. G. Louie, and X. Zhang, "Probing excitonic dark states in single-layer tungsten disulphide," *Nature*, p. 214, 2014. [Online]. Available: https://doi.org/10.1038/nature13734

[196] G. Berghauser, A. Knorr, and E. Malic, "Optical fingerprint of dark 2p-states in transition metal dichalcogenides," *2D MATERIALS*, vol. 4, no. 1, MAR 2017. [Online]. Available: https://doi.org/10.1088/2053-1583/4/1/015029

[197] C. Pöllmann, P. Steinleitner, U. Leierseder, P. Nagler, G. Plechinger, M. Porer, R. Bratschitsch, C. Schüller, T. Korn, and R. Huber, "Resonant internal quantum transitions and femtosecond radiative decay of excitons in monolayer WSe2," *Nature Materials*, vol. 14, no. 9, p. 889, 2015. [Online]. Available: https://doi.org/10.1038/nmat4356

[198] S. Cha, J. H. Sung, S. Sim, J. Park, H. Heo, M.-H. Jo, and H. Choi, "1s-intraexcitonic dynamics in monolayer MoS2 probed by ultrafast mid-infrared spectroscopy," *Nature Communications*, vol. 7, p. 10768, 2016. [Online]. Available: https://doi.org/10.1038/ncomms10768

[199] P. Steinleitner, P. Merkl, A. Graf, P. Nagler, K. Watanabe, T. Taniguchi, J. Zipfel, C. Schüller, T. Korn, A. Chernikov, S. Brem, M. Selig, G. Berghäuser, E. Malic, and R. Huber, "Dielectric Engineering of Electronic Correlations in a van der Waals Heterostructure," *Nano Letters*, vol. 18, no. 2, p. 1402, 2018. [Online]. Available: https://doi.org/10.1021/acs.nanolett.7b05132

[200] G. Berghäuser, P. Steinleitner, P. Merkl, R. Huber, A. Knorr, and E. Malic, "Mapping of the dark exciton landscape in transition metal dichalcogenides," *Phys. Rev. B*, vol. 98, p. 020301, Jul 2018. [Online]. Available: https://link.aps.org/doi/10.1103/PhysRevB.98.020301

[201] S. Brem, J. Zipfel, M. Selig, A. Raja, L. Waldecker, J. D. Ziegler, T. Taniguchi, K. Watanabe, A. Chernikov, and E. Malic, "Intrinsic lifetime of higher excitonic states in tungsten diselenide monolayers," *Nanoscale*, vol. 11, pp. 12 381–12 387, 2019. [Online]. Available: http://dx.doi.org/10.1039/C9NR04211C

[202] P. Merkl, F. Mooshammer, P. Steinleitner, A. Girnghuber, K.-Q. Lin, P. Nagler, J. Holler, C. Schüller, J. M. Lupton, T. Korn, S. Ovesen, S. Brem, E. Malic, and R. Huber, "Ultrafast transition between exciton phases in van der Waals heterostructures," *Nature Materials*, vol. 18, no. 7, p. 691, 2019. [Online]. Available: https://doi.org/10.1038/s41563-019-0337-0

[203] C.-K. Yong, M. I. B. Utama, C. S. Ong, T. Cao, E. C. Regan, J. Horng, Y. Shen, H. Cai, K. Watanabe, T. Taniguchi, S. Tongay, H. Deng, A. Zettl, S. G. Louie, and F. Wang, "Valley-dependent exciton fine structure and Autler–Townes doublets from Berry phases in monolayer MoSe2," *Nature Materials*, vol. 18, no. 10, pp. 1065–1070, Oct 2019. [Online]. Available: https://doi.org/10.1038/s41563-019-0447-8

[204] T. C. Berkelbach, M. S. Hybertsen, and D. R. Reichman, "Bright and dark singlet excitons via linear and two-photon spectroscopy in monolayer transition-metal dichalcogenides," *Phys. Rev. B*, vol. 92, p. 085413, Aug 2015. [Online]. Available: https://link.aps.org/doi/10.1103/PhysRevB.92.085413

[205] M. Feierabend, G. Berghäuser, A. Knorr, and E. Malic, "Proposal for dark exciton based chemical sensors," *Nature Communications*, vol. 8, no. 1, p. 14776, 2017. [Online]. Available: https://doi.org/10.1038/ncomms14776

[206] D. Christiansen, M. Selig, G. Berghäuser, R. Schmidt, I. Niehues, R. Schneider, A. Arora, S. M. de Vasconcellos, R. Bratschitsch, E. Malic, and A. Knorr, "Phonon Sidebands in Monolayer Transition Metal Dichalcogenides," *Phys. Rev. Lett.*, vol. 119, p. 187402, Nov 2017. [Online]. Available: https://link.aps.org/doi/10.1103/PhysRevLett.119.187402

[207] M. Selig, G. Berghäuser, A. Raja, P. Nagler, C. Schüller, T. F. Heinz, T. Korn, A. Chernikov, E. Malic, and A. Knorr, "Excitonic linewidth and coherence lifetime in monolayer transition metal dichalcogenides," *Nature Communications*, vol. 7, no. 1, p. 13279, 2016. [Online]. Available: https://doi.org/10.1038/ncomms13279

[208] G.-H. Peng, P.-Y. Lo, W.-H. Li, Y.-C. Huang, Y.-H. Chen, C.-H. Lee, C.-K. Yang, and S.-J. Cheng, "Distinctive Signatures of the Spin- and Momentum-Forbidden Dark Exciton States in the Photoluminescence of Strained WSe2 Monolayers under Thermalization," *Nano Letters*, vol. 19, no. 4, pp. 2299–2312, 2019, pMID: 30860847. [Online]. Available: https://doi.org/10.1021/acs.nanolett.8b04786

[209] M. A. Lampert, "Mobile and Immobile Effective-Mass-Particle Complexes in Nonmetallic Solids," *Phys. Rev. Lett.*, vol. 1, pp. 450–453, Dec 1958. [Online]. Available: https://link.aps.org/doi/10.1103/PhysRevLett.1.450

[210] K. Kheng, R. T. Cox, M. Y. d' Aubigné, F. Bassani, K. Saminadayar, and S. Tatarenko, "Observation of negatively charged excitons X^- in semiconductor quantum wells," *Phys. Rev. Lett.*, vol. 71, pp. 1752–1755, Sep 1993. [Online]. Available: https://link.aps.org/doi/10.1103/PhysRevLett.71.1752

[211] P. Hawrylak, "Optical properties of a two-dimensional electron gas: Evolution of spectra from excitons to Fermi-edge singularities," *Phys. Rev. B*, vol. 44, pp. 3821–3828, Aug 1991. [Online]. Available: https://link.aps.org/doi/10.1103/PhysRevB.44.3821

[212] G. A. Narvaez, P. Hawrylak, and J. A. Brum, "The role of finite hole mass in the negatively charged exciton in two dimensions," *Physica E: Low-dimensional Systems and Nanostructures*, vol. 9, no. 4, pp. 716 – 722, 2001. [Online]. Available: http://www.sciencedirect.com/science/ARTICLE/pii/S1386947700002952

[213] K. F. Mak, K. He, C. Lee, G. H. Lee, J. Hone, T. F. Heinz, and J. Shan, "Tightly bound trions in monolayer MoS2," *Nature Materials*, vol. 12, no. 3, pp. 207–211, 2013. [Online]. Available: https://doi.org/10.1038/nmat3505

[214] A. A. Mitioglu, P. Plochocka, J. N. Jadczak, W. Escoffier, G. L. J. A. Rikken, L. Kulyuk, and D. K. Maude, "Optical manipulation of the exciton charge state in single-layer tungsten disulfide," *Phys. Rev. B*, vol. 88, p. 245403, Dec 2013. [Online]. Available: https://link.aps.org/doi/10.1103/PhysRevB.88.245403

[215] C. H. Lui, A. J. Frenzel, D. V. Pilon, Y.-H. Lee, X. Ling, G. M. Akselrod, J. Kong, and N. Gedik, "Trion-Induced Negative Photoconductivity in Monolayer MoS_2," *Phys. Rev. Lett.*, vol. 113, p. 166801, Oct 2014. [Online]. Available: https://link.aps.org/doi/10.1103/PhysRevLett.113.166801

[216] A. Singh, G. Moody, K. Tran, M. E. Scott, V. Overbeck, G. Berghäuser, J. Schaibley, E. J. Seifert, D. Pleskot, N. M. Gabor, J. Yan, D. G. Mandrus, M. Richter, E. Malic, X. Xu, and X. Li, "Trion formation dynamics in monolayer transition metal dichalcogenides," *Phys. Rev. B*, vol. 93, p. 041401, Jan 2016. [Online]. Available: https://link.aps.org/doi/10.1103/PhysRevB.93.041401

[217] C. Zhang, H. Wang, W. Chan, C. Manolatou, and F. Rana, "Absorption of light by excitons and trions in monolayers of metal dichalcogenide MoS_2: Experiments and theory," *Phys. Rev. B*, vol. 89, p. 205436, May 2014. [Online]. Available: https://link.aps.org/doi/10.1103/PhysRevB.89.205436

[218] A. R. Rezk, B. Carey, A. F. Chrimes, D. W. M. Lau, B. C. Gibson, C. Zheng, M. S. Fuhrer, L. Y. Yeo, and K. Kalantar-zadeh, "Acoustically-Driven Trion and Exciton Modulation in Piezoelectric Two-Dimensional MoS2," *Nano Letters*, vol. 16, no. 2, pp. 849–855, 2016, pMID: 26729449. [Online]. Available: https://doi.org/10.1021/acs.nanolett.5b02826

[219] G. Plechinger, P. Nagler, J. Kraus, N. Paradiso, C. Strunk, C. Schüller, and T. Korn, "Identification of excitons, trions and biexcitons in single-layer WS2," *physica status solidi (RRL) – Rapid Research Letters*, vol. 9, no. 8, pp. 457–461, 2015. [Online]. Available: https://onlinelibrary.wiley.com/doi/abs/10.1002/pssr.201510224

[220] J. Cuadra, D. G. Baranov, M. Wersall, R. Verre, T. J. Antosiewicz, and T. Shegai, "Observation of Tunable Charged Exciton Polaritons in Hybrid Monolayer WS2 Plasmonic Nanoantenna System," *Nano Letters*, vol. 18, no. 3, pp. 1777–1785, 2018, pMID: 29369640. [Online]. Available: https://doi.org/10.1021/acs.nanolett.7b04965

[221] J. Jadczak, A. Delgado, L. Bryja, Y. S. Huang, and P. Hawrylak, "Robust high-temperature trion emission in monolayers of $Mo(S_ySe_{1-y})_2$ alloys," *Phys. Rev. B*, vol. 95, p. 195427, May 2017. [Online]. Available: https://link.aps.org/doi/10.1103/PhysRevB.95.195427

[222] H. Nan, Z. Wang, W. Wang, Z. Liang, Y. Lu, Q. Chen, D. He, P. Tan, F. Miao, X. Wang, J. Wang, and Z. Ni, "Strong Photoluminescence Enhancement of MoS2 through Defect Engineering and Oxygen Bonding," *ACS Nano*, vol. 8, no. 6, pp. 5738–5745, 2014, pMID: 24836121. [Online]. Available: https://doi.org/10.1021/nn500532f

[223] S. Mouri, Y. Miyauchi, and K. Matsuda, "Tunable Photoluminescence of Monolayer MoS2 via Chemical Doping," *Nano Letters*, vol. 13, no. 12, pp. 5944–5948, 2013, pMID: 24215567. [Online]. Available: https://doi.org/10.1021/nl403036h

[224] N. Scheuschner, O. Ochedowski, A.-M. Kaulitz, R. Gillen, M. Schleberger, and J. Maultzsch, "Photoluminescence of freestanding single- and few-layer MoS_2," *Phys. Rev. B*, vol. 89, p. 125406, Mar 2014. [Online]. Available: https://link.aps.org/doi/10.1103/PhysRevB.89.125406

[225] T. Godde, D. Schmidt, J. Schmutzler, M. Aßmann, J. Debus, F. Withers, E. M. Alexeev, O. Del Pozo-Zamudio, O. V. Skrypka, K. S. Novoselov, M. Bayer, and A. I. Tartakovskii, "Exciton and trion dynamics in atomically thin $MoSe_2$ and WSe_2: Effect of localization," *Phys. Rev. B*, vol. 94, p. 165301, Oct 2016. [Online]. Available: https://link.aps.org/doi/10.1103/PhysRevB.94.165301

[226] J. S. Ross, S. Wu, H. Yu, N. J. Ghimire, A. M. Jones, G. Aivazian, J. Yan, D. G. Mandrus, D. Xiao, W. Yao, and X. Xu, "Electrical control of neutral and charged excitons in a monolayer semiconductor," *Nature Communications*, vol. 4, no. 1, p. 1474, 2013. [Online]. Available: https://doi.org/10.1038/ncomms2498

[227] J. S. Ross, P. Klement, A. M. Jones, N. J. Ghimire, J. Yan, D. G. Mandrus, T. Taniguchi, K. Watanabe, K. Kitamura, W. Yao, D. H. Cobden, and X. Xu, "Electrically tunable excitonic light-emitting diodes based on monolayer WSe2 p-n junctions," *Nature Nanotechnology*, vol. 9, no. 4, pp. 268–272, 2014. [Online]. Available: https://doi.org/10.1038/nnano.2014.26

[228] J. Shang, X. Shen, C. Cong, N. Peimyoo, B. Cao, M. Eginligil, and T. Yu, "Observation of Excitonic Fine Structure in a 2D Transition-Metal Dichalcogenide Semiconductor," *ACS Nano*, vol. 9, no. 1, pp. 647–655, 2015, pMID: 25560634. [Online]. Available: https://doi.org/10.1021/nn5059908

[229] K. Yao, A. Yan, S. Kahn, A. Suslu, Y. Liang, E. S. Barnard, S. Tongay, A. Zettl, N. J. Borys, and P. J. Schuck, "Optically Discriminating Carrier-Induced Quasiparticle Band Gap and Exciton Energy Renormalization in Monolayer MoS_2," *Phys. Rev. Lett.*, vol. 119, p. 087401, Aug 2017. [Online]. Available: https://link.aps.org/doi/10.1103/PhysRevLett.119.087401

[230] J. Yang, T. Lü, Y. W. Myint, J. Pei, D. Macdonald, J.-C. Zheng, and Y. Lu, "Robust Excitons and Trions in Monolayer MoTe2," *ACS Nano*, vol. 9, no. 6, pp. 6603–6609, 2015, pMID: 26039551. [Online]. Available: https://doi.org/10.1021/acsnano.5b02665

[231] E. Courtade, M. Semina, M. Manca, M. M. Glazov, C. Robert, F. Cadiz, G. Wang, T. Taniguchi, K. Watanabe, M. Pierre, W. Escoffier, E. L. Ivchenko, P. Renucci, X. Marie, T. Amand, and B. Urbaszek, "Charged excitons in monolayer WSe_2: Experiment and theory," *Phys. Rev. B*, vol. 96, p. 085302, Aug 2017. [Online]. Available: https://link.aps.org/doi/10.1103/PhysRevB.96.085302

[232] E. Liu, J. van Baren, Z. Lu, M. M. Altaiary, T. Taniguchi, K. Watanabe, D. Smirnov, and C. H. Lui, "Gate Tunable Dark Trions in Monolayer WSe_2," *Phys. Rev. Lett.*, vol. 123, p. 027401, Jul 2019. [Online]. Available: https://link.aps.org/doi/10.1103/PhysRevLett.123.027401

[233] P. Back, M. Sidler, O. Cotlet, A. Srivastava, N. Takemura, M. Kroner, and A. Imamoğlu, "Giant Paramagnetism-Induced Valley Polarization of Electrons in Charge-Tunable Monolayer $MoSe_2$," *Phys. Rev. Lett.*, vol. 118, p. 237404, Jun 2017. [Online]. Available: https://link.aps.org/doi/10.1103/PhysRevLett.118.237404

[234] G. Plechinger, P. Nagler, A. Arora, R. Schmidt, A. Chernikov, A. G. del Águila, P. C. M. Christianen, R. Bratschitsch, C. Schüller, and T. Korn, "Trion fine structure and coupled spin-valley dynamics in monolayer tungsten disulfide," *Nature Communications*, vol. 7, no. 1, p. 12715, 2016. [Online]. Available: https://doi.org/10.1038/ncomms12715

[235] D. Vaclavkova, J. Wyzula, K. Nogajewski, M. Bartos, A. O. Slobodeniuk, C. Faugeras, M. Potemski, and M. R. Molas, "Singlet and triplet trions in WS2 monolayer encapsulated in hexagonal boron nitride," *Nanotechnology*, vol. 29, no. 32, p. 325705, jun 2018. [Online]. Available: https://doi.org/10.1088%2F1361-6528%2Faac65c

[236] A. Boulesbaa, B. Huang, K. Wang, M.-W. Lin, M. Mahjouri-Samani, C. Rouleau, K. Xiao, M. Yoon, B. Sumpter, A. Puretzky, and D. Geohegan, "Observation of two distinct negative trions in tungsten disulfide monolayers," *Phys. Rev. B*, vol. 92, p. 115443, Sep 2015. [Online]. Available: https://link.aps.org/doi/10.1103/PhysRevB.92.115443

[237] V. Orsi Gordo, M. A. G. Balanta, Y. Galvão Gobato, F. S. Covre, H. V. A. Galeti, F. Iikawa, O. D. D. Couto, F. Qu, M. Henini, D. W. Hewak, and C. C. Huang, "Revealing the nature of low-temperature photoluminescence peaks by laser treatment in van der Waals epitaxially grown WS2 monolayers," *Nanoscale*, vol. 10, pp. 4807–4815, 2018. [Online]. Available: http://dx.doi.org/10.1039/C8NR00719E

[238] M. R. Molas, K. Nogajewski, A. O. Slobodeniuk, J. Binder, M. Bartos, and M. Potemski, "The optical response of monolayer, few-layer and bulk tungsten disulfide," *Nanoscale*, vol. 9, pp. 13 128–13 141, 2017. [Online]. Available: http://dx.doi.org/10.1039/C7NR04672C

[239] Z. Li, T. Wang, Z. Lu, M. Khatoniar, Z. Lian, Y. Meng, M. Blei, T. Taniguchi, K. Watanabe, S. A. McGill, S. Tongay, V. M. Menon, D. Smirnov, and S.-F. Shi, "Direct Observation of Gate-Tunable Dark Trions in Monolayer WSe2," *Nano Letters*, vol. 19, no. 10, pp. 6886–6893, 2019, pMID: 31487988. [Online]. Available: https://doi.org/10.1021/acs.nanolett.9b02132

[240] A. Arora, T. Deilmann, T. Reichenauer, J. Kern, S. Michaelis de Vasconcellos, M. Rohlfing, and R. Bratschitsch, "Excited-State Trions in Monolayer WS_2," *Phys. Rev. Lett.*, vol. 123, p. 167401, Oct 2019. [Online]. Available: https://link.aps.org/doi/10.1103/PhysRevLett.123.167401

[241] A. M. Jones, H. Yu, J. R. Schaibley, J. Yan, D. G. Mandrus, T. Taniguchi, K. Watanabe, H. Dery, W. Yao, and X. Xu, "Excitonic luminescence upconversion in a two-dimensional semiconductor," *Nature Physics*, vol. 12, no. 4, pp. 323–327, 2016. [Online]. Available: http://dx.doi.org/10.1038/nphys3604

[242] C. Mai, A. Barrette, Y. Yu, Y. G. Semenov, K. W. Kim, L. Cao, and K. Gundogdu, "Many-Body Effects in Valleytronics: Direct Measurement of Valley Lifetimes in Single-Layer MoS2," *Nano Letters*, vol. 14, no. 1, pp. 202–206, 2014, pMID: 24325650. [Online]. Available: https://doi.org/10.1021/nl403742j

[243] Y. You, X.-X. Zhang, T. C. Berkelbach, M. S. Hybertsen, D. R. Reichman, and T. F. Heinz, "Observation of biexcitons in monolayer WSe2," *Nature Physics*, vol. 11, no. 6, pp. 477–481, 2015. [Online]. Available: https://doi.org/10.1038/nphys3324

[244] E. J. Sie, A. J. Frenzel, Y.-H. Lee, J. Kong, and N. Gedik, "Intervalley biexcitons and many-body effects in monolayer MoS_2," *Phys. Rev. B*, vol. 92, p. 125417, Sep 2015. [Online]. Available: https://link.aps.org/doi/10.1103/PhysRevB.92.125417

[245] H. S. Lee, M. S. Kim, H. Kim, and Y. H. Lee, "Identifying multiexcitons in MoS_2 monolayers at room temperature," *Phys. Rev. B*, vol. 93, p. 140409, Apr 2016. [Online]. Available: https://link.aps.org/doi/10.1103/PhysRevB.93.140409

[246] M. Okada, Y. Miyauchi, K. Matsuda, T. Taniguchi, K. Watanabe, H. Shinohara, and R. Kitaura, "Observation of biexcitonic emission at extremely low power density in tungsten disulfide atomic layers grown on hexagonal boron nitride," *Scientific Reports*, vol. 7, no. 1, p. 322, 2017. [Online]. Available: https://doi.org/10.1038/s41598-017-00068-0

[247] P. Nagler, M. V. Ballottin, A. A. Mitioglu, M. V. Durnev, T. Taniguchi, K. Watanabe, A. Chernikov, C. Schüller, M. M. Glazov, P. C. M. Christianen, and T. Korn, "Zeeman Splitting and Inverted Polarization of Biexciton Emission in Monolayer WS_2," *Phys. Rev. Lett.*, vol. 121, p. 057402, Aug 2018. [Online]. Available: https://link.aps.org/doi/10.1103/PhysRevLett.121.057402

[248] M. S. Kim, S. J. Yun, Y. Lee, C. Seo, G. H. Han, K. K. Kim, Y. H. Lee, and J. Kim, "Biexciton Emission from Edges and Grain Boundaries of Triangular WS2 Monolayers," *ACS Nano*, vol. 10, no. 2, pp. 2399–2405, 2016, pMID: 26758415. [Online]. Available: https://doi.org/10.1021/acsnano.5b07214

[249] I. Paradisanos, S. Germanis, N. T. Pelekanos, C. Fotakis, E. Kymakis, G. Kioseoglou, and E. Stratakis, "Room temperature observation of biexcitons in exfoliated WS2 monolayers," *Applied Physics Letters*, vol. 110, no. 19, p. 193102, 2017. [Online]. Available: https://doi.org/10.1063/1.4983285

[250] J. Pei, J. Yang, X. Wang, F. Wang, S. Mokkapati, T. Lü, J.-C. Zheng, Q. Qin, D. Neshev, H. H. Tan, C. Jagadish, and Y. Lu, "Excited State Biexcitons in Atomically Thin MoSe2," *ACS Nano*, vol. 11, no. 7, pp. 7468–7475, 2017, pMID: 28672110. [Online]. Available: https://doi.org/10.1021/acsnano.7b03909

[251] Z. Li, T. Wang, Z. Lu, C. Jin, Y. Chen, Y. Meng, Z. Lian, T. Taniguchi, K. Watanabe, S. Zhang, D. Smirnov, and S.-F. Shi, "Revealing the biexciton and trion-exciton complexes in BN encapsulated WSe2," *Nature Communications*, vol. 9, no. 1, p. 3719, 2018. [Online]. Available: https://doi.org/10.1038/s41467-018-05863-5

[252] M. Barbone, A. R. P. Montblanch, D. M. Kara, C. Palacios-Berraquero, A. R. Cadore, D. De Fazio, B. Pingault, E. Mostaani, H. Li, B. Chen, K. Watanabe, T. Taniguchi, S. Tongay, G. Wang, A. C. Ferrari, and M. Atature, "Charge-tuneable biexciton complexes in monolayer WSe2," *Nature Communications*, vol. 9, no. 1, p. 3721, 2018. [Online]. Available: https://doi.org/10.1038/s41467-018-05632-4

[253] M. Paur, A. J. Molina-Mendoza, R. Bratschitsch, K. Watanabe, T. Taniguchi, and T. Mueller, "Electroluminescence from multi-particle exciton complexes in transition metal dichalcogenide semiconductors," *Nature Communications*, vol. 10, no. 1, p. 1709, 2019. [Online]. Available: https://doi.org/10.1038/s41467-019-09781-y

[254] S.-Y. Chen, T. Goldstein, T. Taniguchi, K. Watanabe, and J. Yan, "Coulomb-bound four- and five-particle intervalley states in an atomically-thin semiconductor," *Nature Communications*, vol. 9, no. 1, p. 3717, 2018. [Online]. Available: https://doi.org/10.1038/s41467-018-05558-x

[255] K. Hao, J. F. Specht, P. Nagler, L. Xu, K. Tran, A. Singh, C. K. Dass, C. Schüller, T. Korn, M. Richter, A. Knorr, X. Li, and G. Moody, "Neutral and charged inter-valley biexcitons in monolayer MoSe2," *Nature Communications*, vol. 8, no. 1, p. 15552, 2017. [Online]. Available: https://doi.org/10.1038/ncomms15552

[256] W. Liu, B. Lee, C. H. Naylor, H.-S. Ee, J. Park, A. T. C. Johnson, and R. Agarwal, "Strong Exciton–Plasmon Coupling in MoS2 Coupled with Plasmonic Lattice," *Nano Letters*, vol. 16, no. 2, pp. 1262–1269, 2016, pMID: 26784532. [Online]. Available: https://doi.org/10.1021/acs.nanolett.5b04588

[257] D. Van Tuan, B. Scharf, I. Žutić, and H. Dery, "Marrying Excitons and Plasmons in Monolayer Transition-Metal Dichalcogenides," *Phys. Rev. X*, vol. 7, p. 041040, Nov 2017. [Online]. Available: https://link.aps.org/doi/10.1103/PhysRevX.7.041040

[258] M. Sidler, P. Back, O. Cotlet, A. Srivastava, T. Fink, M. Kroner, E. Demler, and A. Imamoglu, "Fermi polaron-polaritons in charge-tunable atomically thin semiconductors," *Nature Physics*, vol. 13, no. 3, pp. 255–261, Mar 2017. [Online]. Available: https://doi.org/10.1038/nphys3949

[259] D. Van Tuan, A. M. Jones, M. Yang, X. Xu, and H. Dery, "Virtual Trions in the Photoluminescence of Monolayer Transition-Metal Dichalcogenides," *Phys. Rev. Lett.*, vol. 122, p. 217401, May 2019. [Online]. Available: https://link.aps.org/doi/10.1103/PhysRevLett.122.217401

[260] D. N. Basov, M. M. Fogler, and F. J. García de Abajo, "Polaritons in van der Waals materials," *Science*, vol. 354, no. 6309, 2016. [Online]. Available: https://science.sciencemag.org/content/354/6309/aag1992

[261] S. Dufferwiel, S. Schwarz, F. Withers, A. A. P. Trichet, F. Li, M. Sich, O. Del Pozo-Zamudio, C. Clark, A. Nalitov, D. D. Solnyshkov, G. Malpuech, K. S. Novoselov, J. M. Smith, M. S. Skolnick, D. N. Krizhanovskii, and A. I. Tartakovskii, "Exciton-polaritons in van der Waals heterostructures embedded in tunable microcavities," *Nature Communications*, vol. 6, no. 1, p. 8579, 2015. [Online]. Available: https://doi.org/10.1038/ncomms9579

[262] N. Lundt, S. Klembt, E. Cherotchenko, S. Betzold, O. Iff, A. V. Nalitov, M. Klaas, C. P. Dietrich, A. V. Kavokin, S. Höfling, and C. Schneider, "Room-temperature Tamm-plasmon exciton-polaritons with a WSe2 monolayer," *Nature Communications*, vol. 7, no. 1, p. 13328, 2016. [Online]. Available: https://doi.org/10.1038/ncomms13328

[263] A. K. Geim and I. V. Grigorieva, "Van der Waals heterostructures," *Nature*, vol. 499, no. 7459, p. 419, 2013. [Online]. Available: https://doi.org/10.1038/nature12385

[264] L. A. Ponomarenko, A. K. Geim, A. A. Zhukov, R. Jalil, S. V. Morozov, K. S. Novoselov, I. V. Grigorieva, E. H. Hill, V. V. Cheianov, V. I. Fal'ko, K. Watanabe, T. Taniguchi, and R. V. Gorbachev, "Tunable metal-insulator transition in double-layer graphene heterostructures," *Nature Physics*, vol. 7, no. 12, pp. 958–961, 2011. [Online]. Available: https://doi.org/10.1038/nphys2114

[265] T. Georgiou, R. Jalil, B. D. Belle, L. Britnell, R. V. Gorbachev, S. V. Morozov, Y.-J. Kim, A. Gholinia, S. J. Haigh, O. Makarovsky, L. Eaves, L. A. Ponomarenko, A. K. Geim, K. S. Novoselov, and A. Mishchenko, "Vertical field-effect transistor based on graphene-WS2 heterostructures for flexible and transparent electronics," *Nature Nanotechnology*, vol. 8, no. 2, pp. 100–103, 2013. [Online]. Available: https://doi.org/10.1038/nnano.2012.224

[266] C. Robert, M. A. Semina, F. Cadiz, M. Manca, E. Courtade, T. Taniguchi, K. Watanabe, H. Cai, S. Tongay, B. Lassagne, P. Renucci, T. Amand, X. Marie, M. M. Glazov, and B. Urbaszek, "Optical spectroscopy of excited exciton states in MoS_2 monolayers in van der Waals heterostructures," *Phys. Rev. Materials*, vol. 2, p. 011001, Jan 2018. [Online]. Available: https://link.aps.org/doi/10.1103/PhysRevMaterials.2.011001

[267] C. Jin, E. Y. Ma, O. Karni, E. C. Regan, F. Wang, and T. F. Heinz, "Ultrafast dynamics in van der Waals heterostructures," *Nature Nanotechnology*, vol. 13, no. 11, pp. 994–1003, 2018. [Online]. Available: https://doi.org/10.1038/s41565-018-0298-5

[268] H. Fang, C. Battaglia, C. Carraro, S. Nemsak, B. Ozdol, J. S. Kang, H. A. Bechtel, S. B. Desai, F. Kronast, A. A. Unal, G. Conti, C. Conlon, G. K. Palsson, M. C. Martin, A. M. Minor, C. S. Fadley, E. Yablonovitch, R. Maboudian, and A. Javey, "Strong interlayer coupling in van der Waals heterostructures built from single-layer chalcogenides," *Proceedings of the National Academy of Sciences*, vol. 111, no. 17, pp. 6198–6202, 2014. [Online]. Available: https://www.pnas.org/content/111/17/6198

[269] P. Rivera, J. R. Schaibley, A. M. Jones, J. S. Ross, S. Wu, G. Aivazian, P. Klement, K. Seyler, G. Clark, N. J. Ghimire, J. Yan, D. G. Mandrus, W. Yao, and X. Xu, "Observation of long-lived interlayer excitons in monolayer MoSe2-WSe2 heterostructures," *Nature Communications*, vol. 6, no. 1, p. 6242, 2015. [Online]. Available: https://doi.org/10.1038/ncomms7242

[270] H. Chen, X. Wen, J. Zhang, T. Wu, Y. Gong, X. Zhang, J. Yuan, C. Yi, J. Lou, P. M. Ajayan, W. Zhuang, G. Zhang, and J. Zheng, "Ultrafast formation of interlayer hot excitons in atomically thin MoS2/WS2 heterostructures," *Nature Communications*, vol. 7, no. 1, p. 12512, 2016. [Online]. Available: https://doi.org/10.1038/ncomms12512

[271] M. Baranowski, A. Surrente, L. Klopotowski, J. M. Urban, N. Zhang, D. K. Maude, K. Wiwatowski, S. Mackowski, Y. C. Kung, D. Dumcenco, A. Kis, and P. Plochocka, "Probing the Interlayer Exciton Physics in a MoS2/MoSe2/MoS2 van der Waals Heterostructure," *Nano Letters*, vol. 17, no. 10, pp. 6360–6365, 2017, pMID: 28895745. [Online]. Available: https://doi.org/10.1021/acs.nanolett.7b03184

[272] B. Miller, A. Steinhoff, B. Pano, J. Klein, F. Jahnke, A. Holleitner, and U. Wurstbauer, "Long-Lived Direct and Indirect Interlayer Excitons in van der Waals Heterostructures," *Nano Letters*, vol. 17, no. 9, pp. 5229–5237, 2017, pMID: 28742367. [Online]. Available: https://doi.org/10.1021/acs.nanolett.7b01304

[273] P. Nagler, G. Plechinger, M. V. Ballottin, A. Mitioglu, S. Meier, N. Paradiso, C. Strunk, A. Chernikov, P. C. M. Christianen, C. Schüller, and T. Korn, "Interlayer exciton dynamics in a dichalcogenide monolayer heterostructure," *2D Materials*, vol. 4, no. 2, p. 025112, jun 2017. [Online]. Available: https://doi.org/10.1088%2F2053-1583%2Faa7352

[274] T. Wang, S. Miao, Z. Li, Y. Meng, Z. Lu, Z. Lian, M. Blei, T. Taniguchi, K. Watanabe, S. Tongay, D. Smirnov, and S.-F. Shi, "Giant Valley-Zeeman Splitting from Spin-Singlet and Spin-Triplet Interlayer Excitons in WSe2/MoSe2 Heterostructure," *Nano Letters*, vol. 20, no. 1, pp. 694–700, 2020, pMID: 31865705. [Online]. Available: https://doi.org/10.1021/acs.nanolett.9b04528

[275] P. Rivera, K. L. Seyler, H. Yu, J. R. Schaibley, J. Yan, D. G. Mandrus, W. Yao, and X. Xu, "Valley-polarized exciton dynamics in a 2D semiconductor heterostructure," *Science*, vol. 351, no. 6274, pp. 688–691, 2016. [Online]. Available: https://science.sciencemag.org/content/351/6274/688

[276] P. Rivera, H. Yu, K. L. Seyler, N. P. Wilson, W. Yao, and X. Xu, "Interlayer valley excitons in heterobilayers of transition metal dichalcogenides," *Nature Nanotechnology*, vol. 13, no. 11, pp. 1004–1015, 2018. [Online]. Available: https://doi.org/10.1038/s41565-018-0193-0

[277] S. Mouri, W. Zhang, D. Kozawa, Y. Miyauchi, G. Eda, and K. Matsuda, "Thermal dissociation of inter-layer excitons in MoS2/MoSe2 hetero-bilayers," *Nanoscale*, vol. 9, pp. 6674–6679, 2017. [Online]. Available: http://dx.doi.org/10.1039/C7NR01598D

[278] T. Deilmann and K. S. Thygesen, "Interlayer Trions in the MoS2/WS2 van der Waals Heterostructure," *Nano Letters*, vol. 18, no. 2, pp. 1460–1465, 2018, pMID: 29377700. [Online]. Available: https://doi.org/10.1021/acs.nanolett.7b05224

[279] F. Vialla, M. Danovich, D. A. Ruiz-Tijerina, M. Massicotte, P. Schmidt, T. Taniguchi, K. Watanabe, R. J. Hunt, M. Szyniszewski, N. D. Drummond, T. G. Pedersen, V. I. Fal'ko, and F. H. L. Koppens, "Tuning of impurity-bound interlayer complexes in a van der Waals heterobilayer," *2D Materials*, vol. 6, no. 3, p. 035032, may 2019. [Online]. Available: https://doi.org/10.1088%2F2053-1583%2Fab168d

[280] E. V. Calman, L. H. Fowler-Gerace, D. J. Choksy, L. V. Butov, D. E. Nikonov, I. A. Young, S. Hu, A. Mishchenko, and A. K. Geim, "Indirect Excitons and Trions in MoSe2/WSe2 van der Waals Heterostructures," *Nano Letters*, vol. 0, no. 0, p. null, 0, pMID: 32069058. [Online]. Available: https://doi.org/10.1021/acs.nanolett.9b05086

[281] M. M. Fogler, L. V. Butov, and K. S. Novoselov, "High-temperature superfluidity with indirect excitons in van der Waals heterostructures," *Nature Communications*, vol. 5, no. 1, p. 4555, 2014. [Online]. Available: https://doi.org/10.1038/ncomms5555

[282] E. V. Calman, M. M. Fogler, L. V. Butov, S. Hu, A. Mishchenko, and A. K. Geim, "Indirect excitons in van der Waals heterostructures at room temperature," *Nature Communications*, vol. 9, no. 1, p. 1895, 2018. [Online]. Available: https://doi.org/10.1038/s41467-018-04293-7

[283] Z. Wang, D. A. Rhodes, K. Watanabe, T. Taniguchi, J. C. Hone, J. Shan, and K. F. Mak, "Evidence of high-temperature exciton condensation in two-dimensional atomic double layers," *Nature*, vol. 574, no. 7776, pp. 76–80, 2019. [Online]. Available: https://doi.org/10.1038/s41586-019-1591-7

[284] S. Bertolazzi, J. Brivio, and A. Kis, "Stretching and Breaking of Ultrathin MoS2," *ACS Nano*, vol. 5, no. 12, pp. 9703–9709, 2011, pMID: 22087740. [Online]. Available: https://doi.org/10.1021/nn203879f

[285] K. He, C. Poole, K. F. Mak, and J. Shan, "Experimental Demonstration of Continuous Electronic Structure Tuning via Strain in Atomically Thin MoS2," *Nano Letters*, vol. 13, no. 6, pp. 2931–2936, 2013, pMID: 23675872. [Online]. Available: https://doi.org/10.1021/nl4013166

[286] H. J. Conley, B. Wang, J. I. Ziegler, R. F. Haglund, S. T. Pantelides, and K. I. Bolotin, "Bandgap Engineering of Strained Monolayer and Bilayer MoS2," *Nano Letters*, vol. 13, no. 8, pp. 3626–3630, 2013, pMID: 23819588. [Online]. Available: https://doi.org/10.1021/nl4014748

[287] C. Rice, R. J. Young, R. Zan, U. Bangert, D. Wolverson, T. Georgiou, R. Jalil, and K. S. Novoselov, "Raman-scattering measurements and first-principles calculations of strain-induced phonon shifts in monolayer MoS_2," *Phys. Rev. B*, vol. 87, p. 081307, Feb 2013. [Online]. Available: https://link.aps.org/doi/10.1103/PhysRevB.87.081307

[288] A. Castellanos-Gomez, R. Roldán, E. Cappelluti, M. Buscema, F. Guinea, H. S. J. van der Zant, and G. A. Steele, "Local Strain Engineering in Atomically Thin MoS2," *Nano Letters*, vol. 13, no. 11, pp. 5361–5366, 2013, pMID: 24083520. [Online]. Available: https://doi.org/10.1021/nl402875m

[289] L. Mennel, M. M. Furchi, S. Wachter, M. Paur, D. K. Polyushkin, and T. Mueller, "Optical imaging of strain in two-dimensional crystals," *Nature Communications*, vol. 9, no. 1, p. 516, 2018. [Online]. Available: https://doi.org/10.1038/s41467-018-02830-y

[290] M. G. Harats, J. N. Kirchhof, M. Qiao, K. Greben, and K. I. Bolotin, "Dynamics and efficient conversion of excitons to trions in non-uniformly strained monolayer WS2," *Nature Photonics*, 2020. [Online]. Available: https://doi.org/10.1038/s41566-019-0581-5

[291] H. Li, A. W. Contryman, X. Qian, S. M. Ardakani, Y. Gong, X. Wang, J. M. Weisse, C. H. Lee, J. Zhao, P. M. Ajayan, J. Li, H. C. Manoharan, and X. Zheng, "Optoelectronic crystal of artificial atoms in strain-textured molybdenum disulphide," *Nature Communications*, vol. 6, no. 1, p. 7381, 2015. [Online]. Available: https://doi.org/10.1038/ncomms8381

[292] A. Branny, S. Kumar, R. Proux, and B. D. Gerardot, "Deterministic strain-induced arrays of quantum emitters in a two-dimensional semiconductor," *Nature Communications*, vol. 8, no. 1, p. 15053, May 2017. [Online]. Available: https://doi.org/10.1038/ncomms15053

[293] E. Khestanova, F. Guinea, L. Fumagalli, A. K. Geim, and I. V. Grigorieva, "Universal shape and pressure inside bubbles appearing in van der Waals heterostructures," *Nature Communications*, vol. 7, no. 1, p. 12587, 2016. [Online]. Available: https://doi.org/10.1038/ncomms12587

[294] J. H. Warner, M. H. Rümmeli, T. Gemming, B. Büchner, and G. A. D. Briggs, "Direct Imaging of Rotational Stacking Faults in Few Layer Graphene," *Nano Letters*, vol. 9, no. 1, pp. 102–106, 2009, pMID: 19072722. [Online]. Available: https://doi.org/10.1021/nl8025949

[295] G. Li, A. Luican, J. M. B. Lopes dos Santos, A. H. Castro Neto, A. Reina, J. Kong, and E. Y. Andrei, "Observation of Van Hove singularities in twisted graphene layers," *Nature Physics*, vol. 6, no. 2, pp. 109–113, 2010. [Online]. Available: https://doi.org/10.1038/nphys1463

[296] L. Brown, R. Hovden, P. Huang, M. Wojcik, D. A. Muller, and J. Park, "Twinning and Twisting of Tri- and Bilayer Graphene," *Nano Letters*, vol. 12, no. 3, pp. 1609–1615, 2012, pMID: 22329410. [Online]. Available: https://doi.org/10.1021/nl204547v

[297] R. W. Havener, H. Zhuang, L. Brown, R. G. Hennig, and J. Park, "Angle-Resolved Raman Imaging of Interlayer Rotations and Interactions in Twisted Bilayer Graphene," *Nano Letters*, vol. 12, no. 6, pp. 3162–3167, 2012, pMID: 22612855. [Online]. Available: https://doi.org/10.1021/nl301137k

[298] K. Kim, S. Coh, L. Z. Tan, W. Regan, J. M. Yuk, E. Chatterjee, M. F. Crommie, M. L. Cohen, S. G. Louie, and A. Zettl, "Raman Spectroscopy Study of Rotated Double-Layer Graphene: Misorientation-Angle Dependence of Electronic Structure," *Phys. Rev. Lett.*, vol. 108, p. 246103, Jun 2012. [Online]. Available: https://link.aps.org/doi/10.1103/PhysRevLett.108.246103

[299] I. Brihuega, P. Mallet, H. González-Herrero, G. Trambly de Laissardière, M. M. Ugeda, L. Magaud, J. M. Gómez-Rodríguez, F. Ynduráin, and J.-Y. Veuillen, "Unraveling the Intrinsic and Robust Nature of van Hove Singularities in Twisted Bilayer Graphene by Scanning Tunneling Microscopy and Theoretical Analysis," *Phys. Rev. Lett.*, vol. 109, p. 196802, Nov 2012. [Online]. Available: https://link.aps.org/doi/10.1103/PhysRevLett.109.196802

[300] W. Yan, M. Liu, R.-F. Dou, L. Meng, L. Feng, Z.-D. Chu, Y. Zhang, Z. Liu, J.-C. Nie, and L. He, "Angle-Dependent van Hove Singularities in a Slightly Twisted Graphene Bilayer," *Phys. Rev. Lett.*, vol. 109, p. 126801, Sep 2012. [Online]. Available: https://link.aps.org/doi/10.1103/PhysRevLett.109.126801

[301] J. S. Alden, A. W. Tsen, P. Y. Huang, R. Hovden, L. Brown, J. Park, D. A. Muller, and P. L. McEuen, "Strain solitons and topological defects in bilayer graphene," *Proceedings of the National Academy of Sciences*, vol. 110, no. 28, pp. 11 256–11 260, 2013. [Online]. Available: https://www.pnas.org/content/110/28/11256

[302] Y. Kim, P. Herlinger, P. Moon, M. Koshino, T. Taniguchi, K. Watanabe, and J. H. Smet, "Charge Inversion and Topological Phase Transition at a Twist Angle Induced van Hove Singularity of Bilayer Graphene," *Nano Letters*, vol. 16, no. 8, pp. 5053–5059, 2016, pMID: 27387484. [Online]. Available: https://doi.org/10.1021/acs.nanolett.6b01906

[303] D. I. Indolese, R. Delagrange, P. Makk, J. R. Wallbank, K. Wanatabe, T. Taniguchi, and C. Schönenberger, "Signatures of van Hove Singularities Probed by the Supercurrent in a Graphene-hBN Superlattice," *Phys. Rev. Lett.*, vol. 121, p. 137701, Sep 2018. [Online]. Available: https://link.aps.org/doi/10.1103/PhysRevLett.121.137701

[304] H. Yoo, R. Engelke, S. Carr, S. Fang, K. Zhang, P. Cazeaux, S. H. Sung, R. Hovden, A. W. Tsen, T. Taniguchi, K. Watanabe, G.-C. Yi, M. Kim, M. Luskin, E. B. Tadmor, E. Kaxiras, and P. Kim, "Atomic and electronic reconstruction at the van der Waals interface in twisted bilayer graphene," *Nature Materials*, vol. 18, no. 5, pp. 448–453, 2019. [Online]. Available: https://doi.org/10.1038/s41563-019-0346-z

[305] J. Xue, J. Sanchez-Yamagishi, D. Bulmash, P. Jacquod, A. Deshpande, K. Watanabe, T. Taniguchi, P. Jarillo-Herrero, and B. J. LeRoy, "Scanning tunnelling microscopy and spectroscopy of ultra-flat graphene on hexagonal boron nitride," *Nature Materials*, vol. 10, no. 4, pp. 282–285, 2011. [Online]. Available: https://doi.org/10.1038/nmat2968

[306] R. Decker, Y. Wang, V. W. Brar, W. Regan, H.-Z. Tsai, Q. Wu, W. Gannett, A. Zettl, and M. F. Crommie, "Local Electronic Properties of Graphene on a BN Substrate via Scanning Tunneling Microscopy," *Nano Letters*, vol. 11, no. 6, pp. 2291–2295, 2011, pMID: 21553853. [Online]. Available: https://doi.org/10.1021/nl2005115

[307] M. Yankowitz, J. Xue, D. Cormode, J. D. Sanchez-Yamagishi, K. Watanabe, T. Taniguchi, P. Jarillo-Herrero, P. Jacquod, and B. J. LeRoy, "Emergence of superlattice Dirac points in graphene on hexagonal boron nitride," *Nature Physics*, vol. 8, no. 5, pp. 382–386, 2012. [Online]. Available: https://doi.org/10.1038/nphys2272

[308] C. R. Dean, L. Wang, P. Maher, C. Forsythe, F. Ghahari, Y. Gao, J. Katoch, M. Ishigami, P. Moon, M. Koshino, T. Taniguchi, K. Watanabe, K. L. Shepard, J. Hone, and P. Kim, "Hofstadter's butterfly and the fractal quantum Hall effect in moiré superlattices," *Nature*, vol. 497, no. 7451, pp. 598–602, 2013. [Online]. Available: https://doi.org/10.1038/nature12186

[309] C. R. Woods, L. Britnell, A. Eckmann, R. S. Ma, J. C. Lu, H. M. Guo, X. Lin, G. L. Yu, Y. Cao, R. . V. Gorbachev, A. V. Kretinin, J. Park, L. A. Ponomarenko, M. I. Katsnelson, Y. N. Gornostyrev, K. Watanabe, T. Taniguchi, C. Casiraghi, H.-J. Gao, A. K. Geim, and K. . S. Novoselov, "Commensurate-incommensurate transition in graphene on hexagonal boron nitride," *Nature Physics*, vol. 10, no. 6, pp. 451–456, 2014. [Online]. Available: https://doi.org/10.1038/nphys2954

[310] Z. Shi, C. Jin, W. Yang, L. Ju, J. Horng, X. Lu, H. A. Bechtel, M. C. Martin, D. Fu, J. Wu, K. Watanabe, T. Taniguchi, Y. Zhang, X. Bai, E. Wang, G. Zhang, and F. Wang, "Gate-dependent pseudospin mixing in graphene/boron nitride moiré superlattices," *Nature Physics*, vol. 10, no. 10, pp. 743–747, 2014. [Online]. Available: https://doi.org/10.1038/nphys3075

[311] M. Yankowitz, J. Jung, E. Laksono, N. Leconte, B. L. Chittari, K. Watanabe, T. Taniguchi, S. Adam, D. Graf, and C. R. Dean, "Dynamic band-structure tuning of graphene moiré superlattices with pressure," *Nature*, vol. 557, no. 7705, pp. 404–408, 2018. [Online]. Available: https://doi.org/10.1038/s41586-018-0107-1

[312] R. Ribeiro-Palau, C. Zhang, K. Watanabe, T. Taniguchi, J. Hone, and C. R. Dean, "Twistable electronics with dynamically rotatable heterostructures," *Science*, vol. 361, no. 6403, pp. 690–693, 2018. [Online]. Available: https://science.sciencemag.org/content/361/6403/690

[313] R. V. Gorbachev, J. C. W. Song, G. L. Yu, A. V. Kretinin, F. Withers, Y. Cao, A. Mishchenko, I. V. Grigorieva, K. S. Novoselov, L. S. Levitov, and A. K. Geim, "Detecting topological currents in graphene superlattices," *Science*, vol. 346, no. 6208, pp. 448–451, 2014. [Online]. Available: https://science.sciencemag.org/content/346/6208/448

[314] L. Wang, Y. Gao, B. Wen, Z. Han, T. Taniguchi, K. Watanabe, M. Koshino, J. Hone, and C. R. Dean, "Evidence for a fractional fractal quantum Hall effect in graphene superlattices," *Science*, vol. 350, no. 6265, pp. 1231–1234, 2015. [Online]. Available: https://science.sciencemag.org/content/350/6265/1231

[315] C. Forsythe, X. Zhou, K. Watanabe, T. Taniguchi, A. Pasupathy, P. Moon, M. Koshino, P. Kim, and C. R. Dean, "Band structure engineering of 2D materials using patterned dielectric superlattices," *Nature Nanotechnology*, vol. 13, no. 7, pp. 566–571, 2018. [Online]. Available: https://doi.org/10.1038/s41565-018-0138-7

[316] E. M. Spanton, A. A. Zibrov, H. Zhou, T. Taniguchi, K. Watanabe, M. P. Zaletel, and A. F. Young, "Observation of fractional Chern insulators in a van der Waals heterostructure," *Science*, vol. 360, no. 6384, pp. 62–66, 2018. [Online]. Available: https://science.sciencemag.org/content/360/6384/62

[317] G. X. Ni, H. Wang, J. S. Wu, Z. Fei, M. D. Goldflam, F. Keilmann, B. Özyilmaz, A. H. Castro Neto, X. M. Xie, M. M. Fogler, and D. N. Basov, "Plasmons in graphene moiré superlattices," *Nature Materials*, vol. 14, no. 12, pp. 1217–1222, 2015. [Online]. Available: https://doi.org/10.1038/nmat4425

[318] A. M. van der Zande, J. Kunstmann, A. Chernikov, D. A. Chenet, Y. You, X. Zhang, P. Y. Huang, T. C. Berkelbach, L. Wang, F. Zhang, M. S. Hybertsen, D. A. Muller, D. R. Reichman, T. F. Heinz, and J. C. Hone, "Tailoring the Electronic Structure in Bilayer Molybdenum Disulfide via Interlayer Twist," *Nano Letters*, vol. 14, no. 7, pp. 3869–3875, 2014, pMID: 24933687. [Online]. Available: https://doi.org/10.1021/nl501077m

[319] K. Liu, L. Zhang, T. Cao, C. Jin, D. Qiu, Q. Zhou, A. Zettl, P. Yang, S. G. Louie, and F. Wang, "Evolution of interlayer coupling in twisted molybdenum disulfide bilayers," *Nature Communications*, vol. 5, no. 1, p. 4966, 2014. [Online]. Available: https://doi.org/10.1038/ncomms5966

[320] S. Huang, X. Ling, L. Liang, J. Kong, H. Terrones, V. Meunier, and M. S. Dresselhaus, "Probing the Interlayer Coupling of Twisted Bilayer MoS2 Using Photoluminescence Spectroscopy," *Nano Letters*, vol. 14, no. 10, pp. 5500–5508, 2014, pMID: 25171263. [Online]. Available: https://doi.org/10.1021/nl5014597

[321] P.-C. Yeh, W. Jin, N. Zaki, J. Kunstmann, D. Chenet, G. Arefe, J. T. Sadowski, J. I. Dadap, P. Sutter, J. Hone, and R. M. Osgood, "Direct Measurement of the Tunable Electronic Structure of Bilayer MoS2 by Interlayer Twist," *Nano Letters*, vol. 16, no. 2, pp. 953–959, 2016, pMID: 26760447. [Online]. Available: https://doi.org/10.1021/acs.nanolett.5b03883

[322] S. Huang, L. Liang, X. Ling, A. A. Puretzky, D. B. Geohegan, B. G. Sumpter, J. Kong, V. Meunier, and M. S. Dresselhaus, "Low-Frequency Interlayer Raman Modes to Probe Interface of Twisted Bilayer MoS2," *Nano Letters*, vol. 16, no. 2, pp. 1435–1444, 2016, pMID: 26797083. [Online]. Available: https://doi.org/10.1021/acs.nanolett.5b05015

[323] J. Kunstmann, F. Mooshammer, P. Nagler, A. Chaves, F. Stein, N. Paradiso, G. Plechinger, C. Strunk, C. Schüller, G. Seifert, D. R. Reichman, and T. Korn, "Momentum-space indirect interlayer excitons in transition-metal dichalcogenide van der Waals heterostructures," *Nature Physics*, vol. 14, no. 8, pp. 801–805, 2018. [Online]. Available: https://doi.org/10.1038/s41567-018-0123-y

[324] K. Tran, G. Moody, F. Wu, X. Lu, J. Choi, K. Kim, A. Rai, D. A. Sanchez, J. Quan, A. Singh, J. Embley, A. Zepeda, M. Campbell, T. Autry, T. Taniguchi, K. Watanabe, N. Lu, S. K. Banerjee, K. L. Silverman, S. Kim, E. Tutuc, L. Yang, A. H. MacDonald, and X. Li, "Evidence for moiré excitons in van der Waals heterostructures," *Nature*, vol. 567, no. 7746, pp. 71–75, 2019. [Online]. Available: https://doi.org/10.1038/s41586-019-0975-z

[325] K. L. Seyler, P. Rivera, H. Yu, N. P. Wilson, E. L. Ray, D. G. Mandrus, J. Yan, W. Yao, and X. Xu, "Signatures of moiré-trapped valley excitons in MoSe2/WSe2 heterobilayers," *Nature*, vol. 567, no. 7746, pp. 66–70, 2019. [Online]. Available: https://doi.org/10.1038/s41586-019-0957-1

[326] C. Jin, E. C. Regan, A. Yan, M. Iqbal Bakti Utama, D. Wang, S. Zhao, Y. Qin, S. Yang, Z. Zheng, S. Shi, K. Watanabe, T. Taniguchi, S. Tongay, A. Zettl, and F. Wang, "Observation of moiré excitons in WSe2/WS2 heterostructure superlattices," *Nature*, vol. 567, no. 7746, pp. 76–80, 2019. [Online]. Available: https://doi.org/10.1038/s41586-019-0976-y

[327] E. M. Alexeev, D. A. Ruiz-Tijerina, M. Danovich, M. J. Hamer, D. J. Terry, P. K. Nayak, S. Ahn, S. Pak, J. Lee, J. I. Sohn, M. R. Molas, M. Koperski, K. Watanabe, T. Taniguchi, K. S. Novoselov, R. V. Gorbachev, H. S. Shin, V. I. Fal'ko, and A. I. Tartakovskii, "Resonantly hybridized excitons in moiré superlattices in van der Waals heterostructures," *Nature*, vol. 567, no. 7746, pp. 81–86, 2019. [Online]. Available: https://doi.org/10.1038/s41586-019-0986-9

[328] Y. Cao, V. Fatemi, A. Demir, S. Fang, S. L. Tomarken, J. Y. Luo, J. D. Sanchez-Yamagishi, K. Watanabe, T. Taniguchi, E. Kaxiras, R. C. Ashoori, and P. Jarillo-Herrero, "Correlated insulator behaviour at half-filling in magic-angle graphene superlattices," *Nature*, vol. 556, no. 7699, pp. 80–84, 2018. [Online]. Available: https://doi.org/10.1038/nature26154

[329] Y. Cao, V. Fatemi, S. Fang, K. Watanabe, T. Taniguchi, E. Kaxiras, and P. Jarillo-Herrero, "Unconventional superconductivity in magic-angle graphene superlattices," *Nature*, vol. 556, no. 7699, pp. 43–50, 2018. [Online]. Available: https://doi.org/10.1038/nature26160

[330] M. Yankowitz, S. Chen, H. Polshyn, Y. Zhang, K. Watanabe, T. Taniguchi, D. Graf, A. F. Young, and C. R. Dean, "Tuning superconductivity in twisted bilayer graphene," *Science*, vol. 363, no. 6431, pp. 1059–1064, 2019. [Online]. Available: https://science.sciencemag.org/content/363/6431/1059

[331] Y. Tang, L. Li, T. Li, Y. Xu, S. Liu, K. Barmak, K. Watanabe, T. Taniguchi, A. H. MacDonald, J. Shan, and K. F. Mak, "Simulation of Hubbard model physics in WSe2/WS2 moiré superlattices," *Nature*, vol. 579, no. 7799, pp. 353–358, 2020. [Online]. Available: https://doi.org/10.1038/s41586-020-2085-3

[332] E. C. Regan, D. Wang, C. Jin, M. I. Bakti Utama, B. Gao, X. Wei, S. Zhao, W. Zhao, Z. Zhang, K. Yumigeta, M. Blei, J. D. Carlström, K. Watanabe, T. Taniguchi, S. Tongay, M. Crommie, A. Zettl, and F. Wang, "Mott and generalized Wigner crystal states in WSe2/WS2 moiré superlattices," *Nature*, vol. 579, no. 7799, pp. 359–363, 2020. [Online]. Available: https://doi.org/10.1038/s41586-020-2092-4

[333] S. C. de la Barrera, M. R. Sinko, D. P. Gopalan, N. Sivadas, K. L. Seyler, K. Watanabe, T. Taniguchi, A. W. Tsen, X. Xu, D. Xiao, and B. M. Hunt, "Tuning Ising superconductivity with layer and spin-orbit coupling in two-dimensional transition-metal dichalcogenides," *Nature Communications*, vol. 9, no. 1, p. 1427, 2018. [Online]. Available: https://doi.org/10.1038/s41467-018-03888-4

[334] X. Xi, Z. Wang, W. Zhao, J.-H. Park, K. T. Law, H. Berger, L. Forró, J. Shan, and K. F. Mak, "Ising pairing in superconducting NbSe2 atomic layers," *Nature Physics*, vol. 12, no. 2, pp. 139–143, 2016. [Online]. Available: https://doi.org/10.1038/nphys3538

[335] J. T. Ye, Y. J. Zhang, R. Akashi, M. S. Bahramy, R. Arita, and Y. Iwasa, "Superconducting Dome in a Gate-Tuned Band Insulator," *Science*, vol. 338, no. 6111, pp. 1193–1196, 2012. [Online]. Available: https://science.sciencemag.org/content/338/6111/1193

[336] Y. Saito, Y. Nakamura, M. S. Bahramy, Y. Kohama, J. Ye, Y. Kasahara, Y. Nakagawa, M. Onga, M. Tokunaga, T. Nojima, Y. Yanase, and Y. Iwasa, "Superconductivity protected by spin-valley locking in ion-gated MoS2," *Nature Physics*, vol. 12, no. 2, pp. 144–149, 2016. [Online]. Available: https://doi.org/10.1038/nphys3580

[337] J. M. Lu, O. Zheliuk, I. Leermakers, N. F. Q. Yuan, U. Zeitler, K. T. Law, and J. T. Ye, "Evidence for two-dimensional Ising superconductivity in gated MoS2," *Science*, vol. 350, no. 6266, pp. 1353–1357, 2015. [Online]. Available: https://science.sciencemag.org/content/350/6266/1353

[338] D. Costanzo, H. Zhang, B. A. Reddy, H. Berger, and A. F. Morpurgo, "Tunnelling spectroscopy of gate-induced superconductivity in MoS2," *Nature Nanotechnology*, vol. 13, no. 6, pp. 483–488, 2018. [Online]. Available: https://doi.org/10.1038/s41565-018-0122-2

[339] J. Lu, O. Zheliuk, Q. Chen, I. Leermakers, N. E. Hussey, U. Zeitler, and J. Ye, "Full superconducting dome of strong Ising protection in gated monolayer WS2," *Proceedings of the National Academy of Sciences*, vol. 115, no. 14, pp. 3551–3556, 2018. [Online]. Available: https://www.pnas.org/content/115/14/3551

[340] O. Zheliuk, J. M. Lu, Q. H. Chen, A. A. E. Yumin, S. Golightly, and J. T. Ye, "Josephson coupled Ising pairing induced in suspended MoS2 bilayers by double-side ionic gating," *Nature Nanotechnology*, vol. 14, no. 12, pp. 1123–1128, 2019. [Online]. Available: https://doi.org/10.1038/s41565-019-0564-1

[341] J. Bardeen, L. N. Cooper, and J. R. Schrieffer, "Theory of Superconductivity," *Phys. Rev.*, vol. 108, pp. 1175–1204, Dec 1957. [Online]. Available: https://link.aps.org/doi/10.1103/PhysRev.108.1175

[342] R. Roldán, E. Cappelluti, and F. Guinea, "Interactions and superconductivity in heavily doped MoS_2," *Phys. Rev. B*, vol. 88, p. 054515, Aug 2013. [Online]. Available: https://link.aps.org/doi/10.1103/PhysRevB.88.054515

[343] N. F. Q. Yuan, K. F. Mak, and K. T. Law, "Possible Topological Superconducting Phases of MoS_2," *Phys. Rev. Lett.*, vol. 113, p. 097001, Aug 2014. [Online]. Available: https://link.aps.org/doi/10.1103/PhysRevLett.113.097001

[344] Y.-T. Hsu, A. Vaezi, M. H. Fischer, and E.-A. Kim, "Topological superconductivity in monolayer transition metal dichalcogenides," *Nature Communications*, vol. 8, no. 1, p. 14985, 2017. [Online]. Available: https://doi.org/10.1038/ncomms14985

[345] S. Nakosai, Y. Tanaka, and N. Nagaosa, "Topological Superconductivity in Bilayer Rashba System," *Phys. Rev. Lett.*, vol. 108, p. 147003, Apr 2012. [Online]. Available: https://link.aps.org/doi/10.1103/PhysRevLett.108.147003

[346] C.-X. Liu, "Unconventional Superconductivity in Bilayer Transition Metal Dichalcogenides," *Phys. Rev. Lett.*, vol. 118, p. 087001, Feb 2017. [Online]. Available: https://link.aps.org/doi/10.1103/PhysRevLett.118.087001

[347] Y. Ge and A. Y. Liu, "Phonon-mediated superconductivity in electron-doped single-layer MoS_2: A first-principles prediction," *Phys. Rev. B*, vol. 87, p. 241408, Jun 2013. [Online]. Available: https://link.aps.org/doi/10.1103/PhysRevB.87.241408

[348] T. Sohier, E. Ponomarev, M. Gibertini, H. Berger, N. Marzari, N. Ubrig, and A. F. Morpurgo, "Enhanced Electron-Phonon Interaction in Multivalley Materials," *Phys. Rev. X*, vol. 9, p. 031019, Aug 2019. [Online]. Available: https://link.aps.org/doi/10.1103/PhysRevX.9.031019

[349] E. Piatti, D. De Fazio, D. Daghero, S. R. Tamalampudi, D. Yoon, A. C. Ferrari, and R. S. Gonnelli, "Multi-Valley Superconductivity in Ion-Gated MoS2 Layers," *Nano Letters*, vol. 18, no. 8, pp. 4821–4830, 2018, pMID: 29949374. [Online]. Available: https://doi.org/10.1021/acs.nanolett.8b01390

[350] E. Piatti, D. Romanin, and R. S. Gonnelli, "Mapping multi-valley Lifshitz transitions induced by field-effect doping in strained MoS2 nanolayers," *Journal of Physics: Condensed Matter*, vol. 31, no. 11, p. 114002, jan 2019. [Online]. Available: https://doi.org/10.1088%2F1361-648x%2Faaf981

[351] V. Fatemi, S. Wu, Y. Cao, L. Bretheau, Q. D. Gibson, K. Watanabe, T. Taniguchi, R. J. Cava, and P. Jarillo-Herrero, "Electrically tunable low-density superconductivity in a monolayer topological insulator," *Science*, vol. 362, no. 6417, pp. 926–929, 2018. [Online]. Available: https://science.sciencemag.org/content/362/6417/926

[352] F. Lüpke, D. Waters, S. C. de la Barrera, M. Widom, D. G. Mandrus, J. Yan, R. M. Feenstra, and B. M. Hunt, "Proximity-induced superconducting gap in the quantum spin Hall edge state of monolayer WTe2," *Nature Physics*, 2020. [Online]. Available: https://doi.org/10.1038/s41567-020-0816-x

[353] L. F. Mattheiss, "Band Structures of Transition-Metal-Dichalcogenide Layer Compounds," *Phys. Rev. B*, vol. 8, pp. 3719–3740, Oct 1973. [Online]. Available: https://link.aps.org/doi/10.1103/PhysRevB.8.3719

[354] R. Coehoorn, C. Haas, J. Dijkstra, C. J. F. Flipse, R. A. de Groot, and A. Wold, "Electronic structure of $MoSe_2$, MoS_2, and WSe_2. I. Band-structure calculations and photoelectron spectroscopy," *Phys. Rev. B*, vol. 35, pp. 6195–6202, Apr 1987. [Online]. Available: https://link.aps.org/doi/10.1103/PhysRevB.35.6195

[355] K. Kobayashi and J. Yamauchi, "Electronic structure and scanning-tunneling-microscopy image of molybdenum dichalcogenide surfaces," *Phys. Rev. B*, vol. 51, pp. 17 085–17 095, Jun 1995. [Online]. Available: https://link.aps.org/doi/10.1103/PhysRevB.51.17085

[356] C. M. Fang, R. A. de Groot, and C. Haas, "Bulk and surface electronic structure of $1T - TiS_2$ and $1T - TiSe_2$," *Phys. Rev. B*, vol. 56, pp. 4455–4463, Aug 1997. [Online]. Available: https://link.aps.org/doi/10.1103/PhysRevB.56.4455

[357] M. Traving, M. Boehme, L. Kipp, M. Skibowski, F. Starrost, E. E. Krasovskii, A. Perlov, and W. Schattke, "Electronic structure of WSe_2: A combined photoemission and inverse photoemission study," *Phys. Rev. B*, vol. 55, pp. 10 392–10 399, Apr 1997. [Online]. Available: https://link.aps.org/doi/10.1103/PhysRevB.55.10392

[358] T. Finteis, M. Hengsberger, T. Straub, K. Fauth, R. Claessen, P. Auer, P. Steiner, S. Hüfner, P. Blaha, M. Vögt, M. Lux-Steiner, and E. Bucher, "Erratum: Occupied and unoccupied electronic band structure of WSe_2 [Phys. Rev. B 55, 10 400 (1997)]," *Phys. Rev. B*, vol. 59, pp. 2461–2461, Jan 1999. [Online]. Available: https://link.aps.org/doi/10.1103/PhysRevB.59.2461

[359] A. Klein, S. Tiefenbacher, V. Eyert, C. Pettenkofer, and W. Jaegermann, "Electronic band structure of single-crystal and single-layer WS_2 : Influence of interlayer van der Waals interactions," *Phys. Rev. B*, vol. 64, p. 205416, Nov 2001. [Online]. Available: https://link.aps.org/doi/10.1103/PhysRevB.64.205416

[360] A. Kuc, N. Zibouche, and T. Heine, "Influence of quantum confinement on the electronic structure of the transition metal sulfide TS_2," *Phys. Rev. B*, vol. 83, p. 245213, Jun 2011. [Online]. Available: https://link.aps.org/doi/10.1103/PhysRevB.83.245213

[361] R. V. Coleman, B. Drake, P. K. Hansma, and G. Slough, "Charge-density waves observed with a tunneling microscope," *Phys. Rev. Lett.*, vol. 55, pp. 394–397, Jul 1985. [Online]. Available: https://link.aps.org/doi/10.1103/PhysRevLett.55.394

[362] G. W. Stupian and M. S. Leung, "Imaging of MoS2 by scanning tunneling microscopy," *Applied Physics Letters*, vol. 51, no. 19, pp. 1560–1562, 1987. [Online]. Available: https://doi.org/10.1063/1.98635

[363] D. Sarid, T. D. Henson, N. R. Armstrong, and L. S. Bell, "Probing of basal planes of MoS2 by scanning tunneling microscopy," *Applied Physics Letters*, vol. 52, no. 26, pp. 2252–2254, 1988. [Online]. Available: https://doi.org/10.1063/1.99769

[364] W. M. Heckl, F. Ohnesorge, G. Binnig, M. Specht, and M. Hashmi, "Ring structures on natural molybdenum disulfide investigated by scanning tunneling and scanning force microscopy," *Journal of Vacuum Science & Technology B: Microelectronics and Nanometer Structures Processing, Measurement, and Phenomena*, vol. 9, no. 2, pp. 1072–1078, 1991. [Online]. Available: https://avs.scitation.org/doi/abs/10.1116/1.585263

[365] D. Vanderbilt, "Soft self-consistent pseudopotentials in a generalized eigenvalue formalism," *Phys. Rev. B*, vol. 41, pp. 7892–7895, Apr 1990. [Online]. Available: https://link.aps.org/doi/10.1103/PhysRevB.41.7892

[366] J. C. Caulfield and A. J. Fisher, "Ab initiostudy of STM-induced vacancy formation on the surface," *Journal of Physics: Condensed Matter*, vol. 10, no. 21, pp. 4533–4551, jun 1998. [Online]. Available: https://doi.org/10.1088%2F0953-8984%2F10%2F21%2F011

[367] G. L. Frey, R. Tenne, M. J. Matthews, M. S. Dresselhaus, and G. Dresselhaus, "Optical Properties of MS2 (M = Mo, W) Inorganic Fullerenelike and Nanotube Material Optical Absorption and Resonance Raman Measurements," *Journal of Materials Research*, vol. 13, no. 9, p. 2412–2417, 1998.

[368] G. Seifert, H. Terrones, M. Terrones, G. Jungnickel, and T. Frauenheim, "Structure and Electronic Properties of MoS_2 Nanotubes," *Phys. Rev. Lett.*, vol. 85, pp. 146–149, Jul 2000. [Online]. Available: https://link.aps.org/doi/10.1103/PhysRevLett.85.146

[369] ——, "On the electronic structure of WS2 nanotubes," *Solid State Communications*, vol. 114, no. 5, pp. 245 – 248, 2000. [Online]. Available: http://www.sciencedirect.com/science/article/pii/S0038109800000478

[370] S. Helveg, J. V. Lauritsen, E. Lægsgaard, I. Stensgaard, J. K. Nørskov, B. S. Clausen, H. Topsøe, and F. Besenbacher, "Atomic-Scale Structure of Single-Layer MoS_2 Nanoclusters," *Phys. Rev. Lett.*, vol. 84, pp. 951–954, Jan 2000. [Online]. Available: https://link.aps.org/doi/10.1103/PhysRevLett.84.951

[371] M. V. Bollinger, K. W. Jacobsen, and J. K. Nørskov, "Atomic and electronic structure of MoS_2 nanoparticles," *Phys. Rev. B*, vol. 67, p. 085410, Feb 2003. [Online]. Available: https://link.aps.org/doi/10.1103/PhysRevB.67.085410

[372] T. Li and G. Galli, "Electronic Properties of MoS2 Nanoparticles," *The Journal of Physical Chemistry C*, vol. 111, no. 44, pp. 16 192–16 196, 2007. [Online]. Available: https://doi.org/10.1021/jp075424v

[373] M. V. Bollinger, J. V. Lauritsen, K. W. Jacobsen, J. K. Nørskov, S. Helveg, and F. Besenbacher, "One-Dimensional Metallic Edge States in MoS_2," *Phys. Rev. Lett.*, vol. 87, p. 196803, Oct 2001. [Online]. Available: https://link.aps.org/doi/10.1103/PhysRevLett.87.196803

[374] K. Dolui, C. D. Pemmaraju, and S. Sanvito, "Electric Field Effects on Armchair MoS2 Nanoribbons," *ACS Nano*, vol. 6, no. 6, pp. 4823–4834, 2012, pMID: 22546015. [Online]. Available: https://doi.org/10.1021/nn301505x

[375] S. Lebègue and O. Eriksson, "Electronic structure of two-dimensional crystals from ab initio theory," *Phys. Rev. B*, vol. 79, p. 115409, Mar 2009. [Online]. Available: https://link.aps.org/doi/10.1103/PhysRevB.79.115409

[376] Y. Ding, Y. Wang, J. Ni, L. Shi, S. Shi, and W. Tang, "First principles study of structural, vibrational and electronic properties of graphene-like MX2 (M=Mo, Nb, W, Ta; X=S, Se, Te) monolayers," *Physica B: Condensed Matter*, vol. 406, no. 11, pp. 2254 – 2260, 2011. [Online]. Available: http://www.sciencedirect.com/science/article/pii/S0921452611002651

[377] J. Heyd, G. E. Scuseria, and M. Ernzerhof, "Hybrid functionals based on a screened Coulomb potential," *The Journal of Chemical Physics*, vol. 118, no. 18, pp. 8207–8215, 2003. [Online]. Available: https://doi.org/10.1063/1.1564060

[378] L. Hedin, "New Method for Calculating the One-Particle Green's Function with Application to the Electron-Gas Problem," *Phys. Rev.*, vol. 139, pp. A796–A823, Aug 1965. [Online]. Available: https://link.aps.org/doi/10.1103/PhysRev.139.A796

[379] A. Kumar and P. K. Ahluwalia, "Electronic structure of transition metal dichalcogenides monolayers 1H-MX2 (M = Mo, W; X = S, Se, Te) from ab-initio theory: new direct band gap semiconductors," *The European Physical Journal B*, vol. 85, no. 6, p. 186, 2012. [Online]. Available: https://doi.org/10.1140/epjb/e2012-30070-x

[380] F. Aryasetiawan and O. Gunnarsson, "The GW method," *Reports on Progress in Physics*, vol. 61, no. 3, pp. 237–312, mar 1998. [Online]. Available: https://doi.org/10.1088%2F0034-4885%2F61%2F3%2F002

[381] W. G. Aulbur, L. Jönsson, and J. W. Wilkins, "Quasiparticle Calculations in Solids," in *Solid State Physics*, ser. Solid State Physics, H. Ehrenreich and F. Spaepen, Eds. Academic Press, 2000, vol. 54, pp. 1 – 218. [Online]. Available: http://www.sciencedirect.com/science/article/pii/S0081194708602489

[382] F. Hüser, T. Olsen, and K. S. Thygesen, "Quasiparticle GW calculations for solids, molecules, and two-dimensional materials," *Phys. Rev. B*, vol. 87, p. 235132, Jun 2013. [Online]. Available: https://link.aps.org/doi/10.1103/PhysRevB.87.235132

[383] P. Scherpelz, M. Govoni, I. Hamada, and G. Galli, "Implementation and Validation of Fully Relativistic GW Calculations: Spin–Orbit Coupling in Molecules, Nanocrystals, and Solids," *Journal of Chemical Theory and Computation*, vol. 12, no. 8, pp. 3523–3544, 2016, pMID: 27331614. [Online]. Available: https://doi.org/10.1021/acs.jctc.6b00114

[384] D. Golze, M. Dvorak, and P. Rinke, "The GW Compendium: A Practical Guide to Theoretical Photoemission Spectroscopy," *Frontiers in Chemistry*, vol. 7, p. 377, 2019. [Online]. Available: https://www.frontiersin.org/article/10.3389/fchem.2019.00377

[385] M. Del Ben, F. H. da Jornada, G. Antonius, T. Rangel, S. G. Louie, J. Deslippe, and A. Canning, "Static subspace approximation for the evaluation of G_0W_0 quasiparticle energies within a sum-over-bands approach," *Phys. Rev. B*, vol. 99, p. 125128, Mar 2019. [Online]. Available: https://link.aps.org/doi/10.1103/PhysRevB.99.125128

[386] T. Cheiwchanchamnangij and W. R. L. Lambrecht, "Quasiparticle band structure calculation of monolayer, bilayer, and bulk MoS_2," *Phys. Rev. B*, vol. 85, p. 205302, May 2012. [Online]. Available: https://link.aps.org/doi/10.1103/PhysRevB.85.205302

[387] D. Y. Qiu, T. Cao, and S. G. Louie, "Nonanalyticity, Valley Quantum Phases, and Lightlike Exciton Dispersion in Monolayer Transition Metal Dichalcogenides: Theory and First-Principles Calculations," *Phys. Rev. Lett.*, vol. 115, p. 176801, Oct 2015. [Online]. Available: https://link.aps.org/doi/10.1103/PhysRevLett.115.176801

[388] D. Y. Qiu, F. H. da Jornada, and S. G. Louie, "Erratum: Optical Spectrum of MoS_2: Many-Body Effects and Diversity of Exciton States [Phys. Rev. Lett. 111, 216805 (2013)]," *Phys. Rev. Lett.*, vol. 115, p. 119901, Sep 2015. [Online]. Available: https://link.aps.org/doi/10.1103/PhysRevLett.115.119901

[389] F. A. Rasmussen, P. S. Schmidt, K. T. Winther, and K. S. Thygesen, "Efficient many-body calculations for two-dimensional materials using exact limits for the screened potential: Band gaps of $\mathbf{MoS_2}$, h-BN, and phosphorene," *Phys. Rev. B*, vol. 94, p. 155406, Oct 2016. [Online]. Available: https://link.aps.org/doi/10.1103/PhysRevB.94.155406

[390] R. Roldán, J. A. Silva-Guillén, M. P. López-Sancho, F. Guinea, E. Cappelluti, and P. Ordejón, "Electronic properties of single-layer and multilayer transition metal dichalcogenides MX2 (M = Mo, W and X = S, Se)," *Annalen der Physik*, vol. 526, no. 9-10, pp. 347–357, 2014. [Online]. Available: https://onlinelibrary.wiley.com/doi/abs/10.1002/andp.201400128

[391] A. Grüneis, G. Kresse, Y. Hinuma, and F. Oba, "Ionization Potentials of Solids: The Importance of Vertex Corrections," *Phys. Rev. Lett.*, vol. 112, p. 096401, Mar 2014. [Online]. Available: https://link.aps.org/doi/10.1103/PhysRevLett.112.096401

[392] P. S. Schmidt, C. E. Patrick, and K. S. Thygesen, "Simple vertex correction improves *GW* band energies of bulk and two-dimensional crystals," *Phys. Rev. B*, vol. 96, p. 205206, Nov 2017. [Online]. Available: https://link.aps.org/doi/10.1103/PhysRevB.96.205206

[393] J. McClain, Q. Sun, G. K.-L. Chan, and T. C. Berkelbach, "Gaussian-Based Coupled-Cluster Theory for the Ground-State and Band Structure of Solids," *Journal of Chemical Theory and Computation*, vol. 13, no. 3, pp. 1209–1218, 2017, pMID: 28218843. [Online]. Available: https://doi.org/10.1021/acs.jctc.7b00049

[394] M. F. Lange and T. C. Berkelbach, "On the Relation between Equation of Motion Coupled Cluster Theory and the GW Approximation," *Journal of Chemical Theory and Computation*, vol. 14, no. 8, pp. 4224–4236, 2018, pMID: 30028614. [Online]. Available: https://doi.org/10.1021/acs.jctc.8b00455

[395] A. Dittmer, R. Izsák, F. Neese, and D. Maganas, "Accurate Band Gap Predictions of Semiconductors in the Framework of the Similarity Transformed Equation of Motion Coupled Cluster Theory," *Inorganic Chemistry*, vol. 58, no. 14, pp. 9303–9315, 2019, pMID: 31240911. [Online]. Available: https://doi.org/10.1021/acs.inorgchem.9b00994

[396] W. M. C. Foulkes, L. Mitas, R. J. Needs, and G. Rajagopal, "Quantum Monte Carlo simulations of solids," *Rev. Mod. Phys.*, vol. 73, pp. 33–83, Jan 2001. [Online]. Available: https://link.aps.org/doi/10.1103/RevModPhys.73.33

[397] R. J. Hunt, M. Szyniszewski, G. I. Prayogo, R. Maezono, and N. D. Drummond, "Quantum Monte Carlo calculations of energy gaps from first principles," *Phys. Rev. B*, vol. 98, p. 075122, Aug 2018. [Online]. Available: https://link.aps.org/doi/10.1103/PhysRevB.98.075122

[398] T. Frank, R. Derian, K. Tokár, L. Mitas, J. Fabian, and I. Štich, "Many-Body Quantum Monte Carlo Study of 2D Materials: Cohesion and Band Gap in Single-Layer Phosphorene," *Phys. Rev. X*, vol. 9, p. 011018, Jan 2019. [Online]. Available: https://link.aps.org/doi/10.1103/PhysRevX.9.011018

[399] Y. Yang, V. Gorelov, C. Pierleoni, D. M. Ceperley, and M. Holzmann, "Electronic band gaps from quantum Monte Carlo methods," *Phys. Rev. B*, vol. 101, p. 085115, Feb 2020. [Online]. Available: https://link.aps.org/doi/10.1103/PhysRevB.101.085115

[400] A. Seidl, A. Görling, P. Vogl, J. A. Majewski, and M. Levy, "Generalized Kohn-Sham schemes and the band-gap problem," *Phys. Rev. B*, vol. 53, pp. 3764–3774, Feb 1996. [Online]. Available: https://link.aps.org/doi/10.1103/PhysRevB.53.3764

[401] M. Städele, J. A. Majewski, P. Vogl, and A. Görling, "Exact Kohn-Sham Exchange Potential in Semiconductors," *Phys. Rev. Lett.*, vol. 79, pp. 2089–2092, Sep 1997. [Online]. Available: https://link.aps.org/doi/10.1103/PhysRevLett.79.2089

[402] M. Städele, M. Moukara, J. A. Majewski, P. Vogl, and A. Görling, "Exact exchange Kohn-Sham formalism applied to semiconductors," *Phys. Rev. B*, vol. 59, pp. 10 031–10 043, Apr 1999. [Online]. Available: https://link.aps.org/doi/10.1103/PhysRevB.59.10031

[403] H. Shi, H. Pan, Y.-W. Zhang, and B. I. Yakobson, "Quasiparticle band structures and optical properties of strained monolayer MoS_2 and WS_2," *Phys. Rev. B*, vol. 87, p. 155304, Apr 2013. [Online]. Available: https://link.aps.org/doi/10.1103/PhysRevB.87.155304

[404] D. Y. Qiu, F. H. da Jornada, and S. G. Louie, "Screening and many-body effects in two-dimensional crystals: Monolayer MoS_2," *Phys. Rev. B*, vol. 93, p. 235435, Jun 2016. [Online]. Available: https://link.aps.org/doi/10.1103/PhysRevB.93.235435

[405] K. Zollner, P. E. F. Junior, and J. Fabian, "Strain-tunable orbital, spin-orbit, and optical properties of monolayer transition-metal dichalcogenides," *Phys. Rev. B*, vol. 100, p. 195126, Nov 2019. [Online]. Available: https://link.aps.org/doi/10.1103/PhysRevB.100.195126

[406] M. H. Naik and M. Jain, "Substrate screening effects on the quasiparticle band gap and defect charge transition levels in MoS_2," *Phys. Rev. Materials*, vol. 2, p. 084002, Aug 2018. [Online]. Available: https://link.aps.org/doi/10.1103/PhysRevMaterials.2.084002

[407] I. C. Gerber and X. Marie, "Dependence of band structure and exciton properties of encapsulated WSe_2 monolayers on the hBN-layer thickness," *Phys. Rev. B*, vol. 98, p. 245126, Dec 2018. [Online]. Available: https://link.aps.org/doi/10.1103/PhysRevB.98.245126

[408] W.-T. Hsu, J. Quan, C.-Y. Wang, L.-S. Lu, M. Campbell, W.-H. Chang, L.-J. Li, X. Li, and C.-K. Shih, "Dielectric impact on exciton binding energy and quasiparticle bandgap in monolayer WS2 and WSe2," *2D Materials*, vol. 6, no. 2, p. 025028, mar 2019. [Online]. Available: https://doi.org/10.1088%2F2053-1583%2Fab072a

[409] Y. Uchiyama, A. Kutana, K. Watanabe, T. Taniguchi, K. Kojima, T. Endo, Y. Miyata, H. Shinohara, and R. Kitaura, "Momentum-forbidden dark excitons in hBN-encapsulated monolayer MoS2," *npj 2D Materials and Applications*, vol. 3, no. 1, p. 26, 2019. [Online]. Available: https://doi.org/10.1038/s41699-019-0108-4

[410] P. Johari and V. B. Shenoy, "Tuning the Electronic Properties of Semiconducting Transition Metal Dichalcogenides by Applying Mechanical Strains," *ACS Nano*, vol. 6, no. 6, pp. 5449–5456, 2012, pMID: 22591011. [Online]. Available: https://doi.org/10.1021/nn301320r

[411] Q. Zhang, Y. Cheng, L.-Y. Gan, and U. Schwingenschlögl, "Giant valley drifts in uniaxially strained monolayer MoS_2," *Phys. Rev. B*, vol. 88, p. 245447, Dec 2013. [Online]. Available: https://link.aps.org/doi/10.1103/PhysRevB.88.245447

[412] S. Horzum, H. Sahin, S. Cahangirov, P. Cudazzo, A. Rubio, T. Serin, and F. M. Peeters, "Phonon softening and direct to indirect band gap crossover in strained single-layer $MoSe_2$," *Phys. Rev. B*, vol. 87, p. 125415, Mar 2013. [Online]. Available: https://link.aps.org/doi/10.1103/PhysRevB.87.125415

[413] C.-H. Chang, X. Fan, S.-H. Lin, and J.-L. Kuo, "Orbital analysis of electronic structure and phonon dispersion in MoS_2, $MoSe_2$, WS_2, and WSe_2 monolayers under strain," *Phys. Rev. B*, vol. 88, p. 195420, Nov 2013. [Online]. Available: https://link.aps.org/doi/10.1103/PhysRevB.88.195420

[414] L. Wang, A. Kutana, and B. I. Yakobson, "Many-body and spin-orbit effects on direct-indirect band gap transition of strained monolayer MoS2 and WS2," *Annalen der Physik*, vol. 526, no. 9-10, pp. L7–L12, 2014. [Online]. Available: https://onlinelibrary.wiley.com/doi/abs/10.1002/andp.201400098

[415] L. Ortenzi, L. Pietronero, and E. Cappelluti, "Zero-point motion and direct-indirect band-gap crossover in layered transition-metal dichalcogenides," *Phys. Rev. B*, vol. 98, p. 195313, Nov 2018. [Online]. Available: https://link.aps.org/doi/10.1103/PhysRevB.98.195313

[416] J. Peto, G. Dobrik, G. Kukucska, P. Vancsó, A. A. Koós, J. Koltai, P. Nemes-Incze, C. Hwang, and L. Tapasztó, "Moderate strain induced indirect bandgap and conduction electrons in MoS2 single layers," *npj 2D Materials and Applications*, vol. 3, no. 1, p. 39, 2019. [Online]. Available: https://doi.org/10.1038/s41699-019-0123-5

[417] E. Blundo, M. Felici, T. Yildirim, G. Pettinari, D. Tedeschi, A. Miriametro, B. Liu, W. Ma, Y. Lu, and A. Polimeni, "Evidence of the direct-to-indirect band gap transition in strained two-dimensional WS_2, MoS_2, and WSe_2," *Phys. Rev. Research*, vol. 2, p. 012024, Jan 2020. [Online]. Available: https://link.aps.org/doi/10.1103/PhysRevResearch.2.012024

[418] L. Debbichi, O. Eriksson, and S. Lebègue, "Electronic structure of two-dimensional transition metal dichalcogenide bilayers from ab initio theory," *Phys. Rev. B*, vol. 89, p. 205311, May 2014. [Online]. Available: https://link.aps.org/doi/10.1103/PhysRevB.89.205311

[419] Z. Y. Zhu, Y. C. Cheng, and U. Schwingenschlögl, "Giant spin-orbit-induced spin splitting in two-dimensional transition-metal dichalcogenide semiconductors," *Phys. Rev. B*, vol. 84, p. 153402, Oct 2011. [Online]. Available: https://link.aps.org/doi/10.1103/PhysRevB.84.153402

[420] W. Yao, D. Xiao, and Q. Niu, "Valley-dependent optoelectronics from inversion symmetry breaking," *Phys. Rev. B*, vol. 77, p. 235406, Jun 2008. [Online]. Available: https://link.aps.org/doi/10.1103/PhysRevB.77.235406

[421] A. Kormányos, G. Burkard, M. Gmitra, J. Fabian, V. Zólyomi, N. D. Drummond, and V. Fal'ko, "kp theory for two-dimensional transition metal dichalcogenide semiconductors," *2D Materials*, vol. 2, no. 2, p. 022001, 2015. [Online]. Available: http://dx.doi.org/10.1088/2053-1583/2/2/022001

[422] Y. Ferreiros and A. Cortijo, "Large conduction band and Fermi velocity spin splitting due to Coulomb interactions in single-layer MoS_2," *Phys. Rev. B*, vol. 90, p. 195426, Nov 2014. [Online]. Available: https://link.aps.org/doi/10.1103/PhysRevB.90.195426

[423] F. Liu, M. E. Ziffer, K. R. Hansen, J. Wang, and X. Zhu, "Direct Determination of Band-Gap Renormalization in the Photoexcited Monolayer MoS_2," *Phys. Rev. Lett.*, vol. 122, p. 246803, Jun 2019. [Online]. Available: https://link.aps.org/doi/10.1103/PhysRevLett.122.246803

[424] M. M. Glazov, M. A. Semina, C. Robert, B. Urbaszek, T. Amand, and X. Marie, "Intervalley polaron in atomically thin transition metal dichalcogenides," *Phys. Rev. B*, vol. 100, p. 041301, Jul 2019. [Online]. Available: https://link.aps.org/doi/10.1103/PhysRevB.100.041301

[425] D. Lloyd, X. Liu, J. W. Christopher, L. Cantley, A. Wadehra, B. L. Kim, B. B. Goldberg, A. K. Swan, and J. S. Bunch, "Band Gap Engineering with Ultralarge Biaxial Strains in Suspended Monolayer MoS2," *Nano Letters*, vol. 16, no. 9, pp. 5836–5841, 2016, pMID: 27509768. [Online]. Available: https://doi.org/10.1021/acs.nanolett.6b02615

[426] O. B. Aslan, I. M. Datye, M. J. Mleczko, K. Sze Cheung, S. Krylyuk, A. Bruma, I. Kalish, A. V. Davydov, E. Pop, and T. F. Heinz, "Probing the Optical Properties and Strain-Tuning of Ultrathin Mo1–xWxTe2," *Nano Letters*, vol. 18, no. 4, pp. 2485–2491, 2018, pMID: 29561623. [Online]. Available: https://doi.org/10.1021/acs.nanolett.8b00049

[427] O. B. Aslan, M. Deng, and T. F. Heinz, "Strain tuning of excitons in monolayer WSe_2," *Phys. Rev. B*, vol. 98, p. 115308, Sep 2018. [Online]. Available: https://link.aps.org/doi/10.1103/PhysRevB.98.115308

[428] S. Kumar, A. Kaczmarczyk, and B. D. Gerardot, "Strain-Induced Spatial and Spectral Isolation of Quantum Emitters in Mono- and Bilayer WSe2," *Nano Letters*, vol. 15, no. 11, pp. 7567–7573, 2015, pMID: 26480237. [Online]. Available: https://doi.org/10.1021/acs.nanolett.5b03312

[429] Y.-M. He, G. Clark, J. R. Schaibley, Y. He, M.-C. Chen, Y.-J. Wei, X. Ding, Q. Zhang, W. Yao, X. Xu, C.-Y. Lu, and J.-W. Pan, "Single quantum emitters in monolayer semiconductors," *Nature Nanotechnology*, vol. 10, no. 6, pp. 497–502, Jun 2015. [Online]. Available: https://doi.org/10.1038/nnano.2015.75

[430] A. Srivastava, M. Sidler, A. V. Allain, D. S. Lembke, A. Kis, and A. Imamoğlu, "Optically active quantum dots in monolayer WSe2," *Nature Nanotechnology*, vol. 10, no. 6, pp. 491–496, Jun 2015. [Online]. Available: https://doi.org/10.1038/nnano.2015.60

[431] M. Koperski, K. Nogajewski, A. Arora, V. Cherkez, P. Mallet, J.-Y. Veuillen, J. Marcus, P. Kossacki, and M. Potemski, "Single photon emitters in exfoliated WSe2 structures," *Nature Nanotechnology*, vol. 10, no. 6, pp. 503–506, Jun 2015. [Online]. Available: https://doi.org/10.1038/nnano.2015.67

[432] C. Chakraborty, L. Kinnischtzke, K. M. Goodfellow, R. Beams, and A. N. Vamivakas, "Voltage-controlled quantum light from an atomically thin semiconductor," *Nature Nanotechnology*, vol. 10, no. 6, pp. 507–511, Jun 2015. [Online]. Available: https://doi.org/10.1038/nnano.2015.79

[433] O. Iff, D. Tedeschi, J. Martín-Sánchez, M. Moczała-Dusanowska, S. Tongay, K. Yumigeta, J. Taboada-Gutiérrez, M. Savaresi, A. Rastelli, P. Alonso-González, S. Höfling, R. Trotta, and C. Schneider, "Strain-Tunable Single Photon Sources in WSe2 Monolayers," *Nano Letters*, vol. 19, no. 10, pp. 6931–6936, 2019, pMID: 31486648. [Online]. Available: https://doi.org/10.1021/acs.nanolett.9b02221

[434] A. Kormányos, V. Zólyomi, N. D. Drummond, and G. Burkard, "Spin-Orbit Coupling, Quantum Dots, and Qubits in Monolayer Transition Metal Dichalcogenides," *Phys. Rev. X*, vol. 4, p. 011034, Mar 2014. [Online]. Available: https://link.aps.org/doi/10.1103/PhysRevX.4.011034

[435] S. Gao and L. Yang, "Renormalization of the quasiparticle band gap in doped two-dimensional materials from many-body calculations," *Phys. Rev. B*, vol. 96, p. 155410, Oct 2017. [Online]. Available: https://link.aps.org/doi/10.1103/PhysRevB.96.155410

[436] L. Meckbach, T. Stroucken, and S. W. Koch, "Giant excitation induced bandgap renormalization in TMDC monolayers," *Applied Physics Letters*, vol. 112, no. 6, p. 061104, 2018. [Online]. Available: https://doi.org/10.1063/1.5017069

[437] A. Chernikov, C. Ruppert, H. M. Hill, A. F. Rigosi, and T. F. Heinz, "Population inversion and giant bandgap renormalization in atomically thin WS2 layers," *Nature Photonics*, vol. 9, no. 7, pp. 466–470, Jul 2015. [Online]. Available: https://doi.org/10.1038/nphoton.2015.104

[438] S. Ulstrup, A. G. Čabo, J. A. Miwa, J. M. Riley, S. S. Grønborg, J. C. Johannsen, C. Cacho, O. Alexander, R. T. Chapman, E. Springate, M. Bianchi, M. Dendzik, J. V. Lauritsen, P. D. C. King, and P. Hofmann, "Ultrafast Band Structure Control of a Two-Dimensional Heterostructure," *ACS Nano*, vol. 10, no. 6, pp. 6315–6322, 2016, pMID: 27267820. [Online]. Available: https://doi.org/10.1021/acsnano.6b02622

[439] A. Steinhoff, J.-H. Kim, F. Jahnke, M. Rösner, D.-S. Kim, C. Lee, G. H. Han, M. S. Jeong, T. O. Wehling, and C. Gies, "Efficient Excitonic Photoluminescence in Direct and Indirect Band Gap Monolayer MoS2," *Nano Letters*, vol. 15, no. 10, pp. 6841–6847, 2015, pMID: 26322814. [Online]. Available: https://doi.org/10.1021/acs.nanolett.5b02719

[440] A. Steinhoff, M. Rösner, F. Jahnke, T. O. Wehling, and C. Gies, "Influence of Excited Carriers on the Optical and Electronic Properties of MoS2," *Nano Letters*, vol. 14, no. 7, pp. 3743–3748, 2014, pMID: 24956358. [Online]. Available: https://doi.org/10.1021/nl500595u

[441] D. Erben, A. Steinhoff, C. Gies, G. Schönhoff, T. O. Wehling, and F. Jahnke, "Excitation-induced transition to indirect band gaps in atomically thin transition-metal dichalcogenide semiconductors," *Phys. Rev. B*, vol. 98, p. 035434, Jul 2018. [Online]. Available: https://link.aps.org/doi/10.1103/PhysRevB.98.035434

[442] C. Ataca and S. Ciraci, "Functionalization of Single-Layer MoS2 Honeycomb Structures," *The Journal of Physical Chemistry C*, vol. 115, no. 27, pp. 13 303–13 311, 2011. [Online]. Available: https://doi.org/10.1021/jp2000442

[443] H.-P. Komsa, J. Kotakoski, S. Kurasch, O. Lehtinen, U. Kaiser, and A. V. Krasheninnikov, "Two-Dimensional Transition Metal Dichalcogenides under Electron Irradiation: Defect Production and Doping," *Phys. Rev. Lett.*, vol. 109, p. 035503, Jul 2012. [Online]. Available: https://link.aps.org/doi/10.1103/PhysRevLett.109.035503

[444] W. Zhou, X. Zou, S. Najmaei, Z. Liu, Y. Shi, J. Kong, J. Lou, P. M. Ajayan, B. I. Yakobson, and J.-C. Idrobo, "Intrinsic Structural Defects in Monolayer Molybdenum Disulfide," *Nano Letters*, vol. 13, no. 6, pp. 2615–2622, 2013, pMID: 23659662. [Online]. Available: https://doi.org/10.1021/nl4007479

[445] S. Haldar, H. Vovusha, M. K. Yadav, O. Eriksson, and B. Sanyal, "Systematic study of structural, electronic, and optical properties of atomic-scale defects in the two-dimensional transition metal dichalcogenides MX_2 (M = Mo, W; X = S, Se, Te)," *Phys. Rev. B*, vol. 92, p. 235408, Dec 2015. [Online]. Available: https://link.aps.org/doi/10.1103/PhysRevB.92.235408

[446] M. Bahmani, M. Faghihnasiri, M. Lorke, A.-B. Kuc, and T. Frauenheim, "Electronic Properties of Defective MoS2 Monolayers Subject to Mechanical Deformations: A First-Principles Approach," *physica status solidi (b)*, vol. 257, no. 5, p. 1900541, 2020. [Online]. Available: https://onlinelibrary.wiley.com/doi/abs/10.1002/pssb.201900541

[447] Y.-C. Lin, T. Björkman, H.-P. Komsa, P.-Y. Teng, C.-H. Yeh, F.-S. Huang, K.-H. Lin, J. Jadczak, Y.-S. Huang, P.-W. Chiu, A. V. Krasheninnikov, and K. Suenaga, "Three-fold rotational defects in two-dimensional transition metal dichalcogenides," *Nature Communications*, vol. 6, no. 1, p. 6736, Apr 2015. [Online]. Available: https://doi.org/10.1038/ncomms7736

[448] J. Hong, Z. Hu, M. Probert, K. Li, D. Lv, X. Yang, L. Gu, N. Mao, Q. Feng, L. Xie, J. Zhang, D. Wu, Z. Zhang, C. Jin, W. Ji, X. Zhang, J. Yuan, and Z. Zhang, "Exploring atomic defects in molybdenum disulphide monolayers," *Nature Communications*, vol. 6, no. 1, p. 6293, Feb 2015. [Online]. Available: https://doi.org/10.1038/ncomms7293

[449] S. Zhang, C.-G. Wang, M.-Y. Li, D. Huang, L.-J. Li, W. Ji, and S. Wu, "Defect Structure of Localized Excitons in a WSe_2 Monolayer," *Phys. Rev. Lett.*, vol. 119, p. 046101, Jul 2017. [Online]. Available: https://link.aps.org/doi/10.1103/PhysRevLett.119.046101

[450] M. Ghorbani-Asl, S. Kretschmer, D. E. Spearot, and A. V. Krasheninnikov, "Two-dimensional MoS2 under ion irradiation: from controlled defect production to electronic structure engineering," *2D Materials*, vol. 4, no. 2, p. 025078, apr 2017. [Online]. Available: https://doi.org/10.1088%2F2053-1583%2Faa6b17

[451] B. Schuler, J.-H. Lee, C. Kastl, K. A. Cochrane, C. T. Chen, S. Refaely-Abramson, S. Yuan, E. van Veen, R. Roldán, N. J. Borys, R. J. Koch, S. Aloni, A. M. Schwartzberg, D. F. Ogletree, J. B. Neaton, and A. Weber-Bargioni, "How Substitutional Point Defects in Two-Dimensional WS2 Induce Charge Localization, Spin–Orbit Splitting, and Strain," *ACS Nano*, vol. 13, no. 9, pp. 10 520–10 534, 2019, pMID: 31393700. [Online]. Available: https://doi.org/10.1021/acsnano.9b04611

[452] S. Barja, S. Refaely-Abramson, B. Schuler, D. Y. Qiu, A. Pulkin, S. Wickenburg, H. Ryu, M. M. Ugeda, C. Kastl, C. Chen, C. Hwang, A. Schwartzberg, S. Aloni, S.-K. Mo, D. Frank Ogletree, M. F. Crommie, O. V. Yazyev, S. G. Louie, J. B. Neaton, and A. Weber-Bargioni, "Identifying substitutional oxygen as a prolific point defect in monolayer transition metal dichalcogenides," *Nature Communications*, vol. 10, no. 1, p. 3382, Jul 2019. [Online]. Available: https://doi.org/10.1038/s41467-019-11342-2

[453] B. Schuler, D. Y. Qiu, S. Refaely-Abramson, C. Kastl, C. T. Chen, S. Barja, R. J. Koch, D. F. Ogletree, S. Aloni, A. M. Schwartzberg, J. B. Neaton, S. G. Louie, and A. Weber-Bargioni, "Large Spin-Orbit Splitting of Deep In-Gap Defect States of Engineered Sulfur Vacancies in Monolayer WS_2," *Phys. Rev. Lett.*, vol. 123, p. 076801, Aug 2019. [Online]. Available: https://link.aps.org/doi/10.1103/PhysRevLett.123.076801

[454] T. Y. Jeong, H. Kim, S.-J. Choi, K. Watanabe, T. Taniguchi, K. J. Yee, Y.-S. Kim, and S. Jung, "Spectroscopic studies of atomic defects and bandgap renormalization in semiconducting monolayer transition metal dichalcogenides," *Nature Communications*, vol. 10, no. 1, p. 3825, Aug 2019. [Online]. Available: https://doi.org/10.1038/s41467-019-11751-3

[455] L. Yin, P. He, R. Cheng, F. Wang, F. Wang, Z. Wang, Y. Wen, and J. He, "Robust trap effect in transition metal dichalcogenides for advanced multifunctional devices," *Nature Communications*, vol. 10, no. 1, p. 4133, Sep 2019. [Online]. Available: https://doi.org/10.1038/s41467-019-12200-x

[456] M. Aghajanian, B. Schuler, K. A. Cochrane, J.-H. Lee, C. Kastl, J. B. Neaton, A. Weber-Bargioni, A. A. Mostofi, and J. Lischner, "Resonant and bound states of charged defects in two-dimensional semiconductors," *Phys. Rev. B*, vol. 101, p. 081201, Feb 2020. [Online]. Available: https://link.aps.org/doi/10.1103/PhysRevB.101.081201

[457] Y. Wang, L. Deng, Q. Wei, Y. Wan, Z. Liu, X. Lu, Y. Li, L. Bi, L. Zhang, H. Lu, H. Chen, P. Zhou, L. Zhang, Y. Cheng, X. Zhao, Y. Ye, W. Huang, S. J. Pennycook, K. P. Loh, and B. Peng, "Spin-Valley Locking Effect in Defect States of Monolayer MoS2," *Nano Letters*, vol. 20, no. 3, pp. 2129–2136, 2020, pMID: 32078769. [Online]. Available: https://doi.org/10.1021/acs.nanolett.0c00138

[458] Z. Lin, B. R. Carvalho, E. Kahn, R. Lv, R. Rao, H. Terrones, M. A. Pimenta, and M. Terrones, "Defect engineering of two-dimensional transition metal dichalcogenides," *2D Materials*, vol. 3, no. 2, p. 022002, apr 2016. [Online]. Available: https://doi.org/10.1088%2F2053-1583%2F3%2F2%2F022002

[459] Z. Hu, Z. Wu, C. Han, J. He, Z. Ni, and W. Chen, "Two-dimensional transition metal dichalcogenides: interface and defect engineering," *Chem. Soc. Rev.*, vol. 47, pp. 3100–3128, 2018. [Online]. Available: http://dx.doi.org/10.1039/C8CS00024G

[460] R. B. Murray and A. D. Yoffe, "The band structures of some transition metal dichalcogenides: band structures of the titanium dichalcogenides," *Journal of Physics C: Solid State Physics*, vol. 5, no. 21, pp. 3038–3046, oct 1972. [Online]. Available: https://doi.org/10.1088%2F0022-3719%2F5%2F21%2F009

[461] R. B. Murray, R. A. Bromley, and A. D. Yoffe, "The band structures of some transition metal dichalcogenides. II. Group IVA octahedral coordination," *Journal of Physics C: Solid State Physics*, vol. 5, no. 7, pp. 746–758, apr 1972. [Online]. Available: https://doi.org/10.1088%2F0022-3719%2F5%2F7%2F006

[462] G.-B. Liu, W.-Y. Shan, Y. Yao, W. Yao, and D. Xiao, "Three-band tight-binding model for monolayers of group-vib transition metal dichalcogenides," *Phys. Rev. B*, vol. 88, p. 085433, Aug 2013. [Online]. Available: https://link.aps.org/doi/10.1103/PhysRevB.88.085433

[463] H. Rostami, A. G. Moghaddam, and R. Asgari, "Effective lattice hamiltonian for monolayer mos2: Tailoring electronic structure with perpendicular electric and magnetic fields," *Phys. Rev. B*, vol. 88, p. 085440, Aug 2013. [Online]. Available: https://link.aps.org/doi/10.1103/PhysRevB.88.085440

[464] E. Cappelluti, R. Roldan, J. A. Silva-Guillen, P. Ordejon, and F. Guinea, "Tight-binding model and direct-gap/indirect-gap transition in single-layer and multilayer mos2," *Phys. Rev. B*, vol. 88, p. 075409, Aug 2013. [Online]. Available: https://link.aps.org/doi/10.1103/PhysRevB.88.075409

[465] F. Zahid, L. Liu, Y. Zhu, J. Wang, and H. Guo, "A generic tight-binding model for monolayer, bilayer and bulk mos2," *AIP Advances*, vol. 3, no. 5, p. 052111, 2013. [Online]. Available: http://dx.doi.org/10.1063/1.4804936

[466] S. Fang, R. Kuate Defo, S. N. Shirodkar, S. Lieu, G. A. Tritsaris, and E. Kaxiras, "Ab initio tight-binding hamiltonian for transition metal dichalcogenides," *Phys. Rev. B*, vol. 92, p. 205108, Nov 2015. [Online]. Available: https://link.aps.org/doi/10.1103/PhysRevB.92.205108

[467] Y.-H. Ho, Y.-H. Wang, and H.-Y. Chen, "Magnetoelectronic and optical properties of a mos2 monolayer," *Phys. Rev. B*, vol. 89, p. 155316, Apr 2014. [Online]. Available: https://link.aps.org/doi/10.1103/PhysRevB.89.155316

[468] G.-B. Liu, D. Xiao, Y. Yao, X. Xu, and W. Yao, "Electronic structures and theoretical modelling of two-dimensional group-vib transition metal dichalcogenides," *Chem. Soc. Rev.*, vol. 44, pp. 2643–2663, 2015. [Online]. Available: http://dx.doi.org/10.1039/C4CS00301B

[469] E. Ridolfi, D. Le, T. S. Rahman, E. R. Mucciolo, and C. H. Lewenkopf, "A tight-binding model for mos 2 monolayers," *Journal of Physics: Condensed Matter*, vol. 27, no. 36, p. 365501, 2015. [Online]. Available: http://dx.doi.org/10.1088/0953-8984/27/36/365501

[470] K. V. Shanavas and S. Satpathy, "Effective tight-binding model for mx2 under electric and magnetic fields," *Phys. Rev. B*, vol. 91, p. 235145, Jun 2015. [Online]. Available: https://link.aps.org/doi/10.1103/PhysRevB.91.235145

[471] J. A. Silva-Guillen, P. San-Jose, and R. Roldan, "Electronic band structure of transition metal dichalcogenides from ab initio and slater - koster tight-binding model," *Applied Sciences*, vol. 6, p. 284, 2016. [Online]. Available: http://dx.doi.org/10.3390/app6100284

[472] A. J. Pearce, E. Mariani, and G. Burkard, "Tight-binding approach to strain and curvature in monolayer transition-metal dichalcogenides," *Phys. Rev. B*, vol. 94, p. 155416, Oct 2016. [Online]. Available: https://link.aps.org/doi/10.1103/PhysRevB.94.155416

[473] A. C. Dias, F. Qu, D. L. Azevedo, and J. Fu, "Band structure of monolayer transition-metal dichalcogenides and topological properties of their nanoribbons: Next-nearest-neighbor hopping," *Phys. Rev. B*, vol. 98, p. 075202, Aug 2018. [Online]. Available: https://link.aps.org/doi/10.1103/PhysRevB.98.075202

[474] A. Kormányos, V. Zólyomi, N. D. Drummond, P. Rakyta, G. Burkard, and V. I. Fal'ko, "Monolayer MoS_2: Trigonal warping, the Γ valley, and spin-orbit coupling effects," *Phys. Rev. B*, vol. 88, p. 045416, Jul 2013. [Online]. Available: https://link.aps.org/doi/10.1103/PhysRevB.88.045416

[475] A. Kormányos, P. Rakyta, and G. Burkard, "Landau levels and shubnikov–de haas oscillations in monolayer transition metal dichalcogenide semiconductors," *New J. Phys.*, vol. 17, p. 103006, 2015. [Online]. Available: http://dx.doi.org/10.1088/1367-2630/17/10/103006

[476] D. V. Rybkovskiy, I. C. Gerber, and M. V. Durnev, "Atomically inspired $k \cdot p$ approach and valley zeeman effect in transition metal dichalcogenide monolayers," *Phys. Rev. B*, vol. 95, p. 155406, Apr 2017. [Online]. Available: https://link.aps.org/doi/10.1103/PhysRevB.95.155406

[477] R. Pisoni, A. Kormányos, M. Brooks, Z. Lei, P. Back, M. Eich, H. Overweg, Y. Lee, P. Rickhaus, K. Watanabe, T. Taniguchi, A. Imamoglu, G. Burkard, T. Ihn, and K. Ensslin, "Interactions and Magnetotransport through Spin-Valley Coupled Landau Levels in Monolayer MoS_2," *Phys. Rev. Lett.*, vol. 121, p. 247701, Dec 2018. [Online]. Available: https://link.aps.org/doi/10.1103/PhysRevLett.121.247701

[478] X. Qian, J. Liu, L. Fu, and J. Li, "Quantum spin Hall effect in two-dimensional transition metal dichalcogenides," *Science*, vol. 346, no. 6215, pp. 1344–1347, 2014. [Online]. Available: https://science.sciencemag.org/content/346/6215/1344

[479] M. M. Ugeda, A. Pulkin, S. Tang, H. Ryu, Q. Wu, Y. Zhang, D. Wong, Z. Pedramrazi, A. Martín-Recio, Y. Chen, F. Wang, Z.-X. Shen, S.-K. Mo, O. V. Yazyev, and M. F. Crommie, "Observation of topologically protected states at crystalline phase boundaries in single-layer WSe2," *Nature Communications*, vol. 9, no. 1, p. 3401, Aug 2018. [Online]. Available: https://doi.org/10.1038/s41467-018-05672-w

[480] Y.-H. Song, Z.-Y. Jia, D. Zhang, X.-Y. Zhu, Z.-Q. Shi, H. Wang, L. Zhu, Q.-Q. Yuan, H. Zhang, D.-Y. Xing, and S.-C. Li, "Observation of Coulomb gap in the quantum spin Hall candidate single-layer 1T'-WTe2," *Nature Communications*, vol. 9, no. 1, p. 4071, Oct 2018. [Online]. Available: https://doi.org/10.1038/s41467-018-06635-x

[481] L. Muechler, A. Alexandradinata, T. Neupert, and R. Car, "Topological Nonsymmorphic Metals from Band Inversion," *Phys. Rev. X*, vol. 6, p. 041069, Dec 2016. [Online]. Available: https://link.aps.org/doi/10.1103/PhysRevX.6.041069

[482] S. Ok, L. Muechler, D. Di Sante, G. Sangiovanni, R. Thomale, and T. Neupert, "Custodial glide symmetry of quantum spin Hall edge modes in monolayer WTe_2," *Phys. Rev. B*, vol. 99, p. 121105, Mar 2019. [Online]. Available: https://link.aps.org/doi/10.1103/PhysRevB.99.121105

[483] A. Lau, R. Ray, D. Varjas, and A. R. Akhmerov, "Influence of lattice termination on the edge states of the quantum spin Hall insulator monolayer $1T^{'}-WTe_2$," *Phys. Rev. Materials*, vol. 3, p. 054206, May 2019. [Online]. Available: https://link.aps.org/doi/10.1103/PhysRevMaterials.3.054206

[484] Q. Tong, H. Yu, Q. Zhu, Y. Wang, X. Xu, and W. Yao, "Topological mosaics in moiré superlattices of van der Waals heterobilayers," *Nature Physics*, vol. 13, no. 4, pp. 356–362, 2017. [Online]. Available: https://doi.org/10.1038/nphys3968

[485] F. Wu, T. Lovorn, E. Tutuc, I. Martin, and A. H. MacDonald, "Topological Insulators in Twisted Transition Metal Dichalcogenide Homobilayers," *Phys. Rev. Lett.*, vol. 122, p. 086402, Feb 2019. [Online]. Available: https://link.aps.org/doi/10.1103/PhysRevLett.122.086402

[486] P. K. Das, D. D. Sante, F. Cilento, C. Bigi, D. Kopic, D. Soranzio, A. Sterzi, J. A. Krieger, I. Vobornik, J. Fujii, T. Okuda, V. N. Strocov, M. B. H. Breese, F. Parmigiani, G. Rossi, S. Picozzi, R. Thomale, G. Sangiovanni, R. J. Cava, and G. Panaccione, "Electronic properties of candidate type-II Weyl semimetal WTe2. A review perspective," *Electronic Structure*, vol. 1, no. 1, p. 014003, mar 2019. [Online]. Available: https://doi.org/10.1088%2F2516-1075%2Fab0835

[487] M. Gmitra, S. Konschuh, C. Ertler, C. Ambrosch-Draxl, and J. Fabian, "Band-structure topologies of graphene: Spin-orbit coupling effects from first principles," *Phys. Rev. B*, vol. 80, p. 235431, Dec 2009. [Online]. Available: https://link.aps.org/doi/10.1103/PhysRevB.80.235431

[488] S. Konschuh, M. Gmitra, and J. Fabian, "Tight-binding theory of the spin-orbit coupling in graphene," *Phys. Rev. B*, vol. 82, p. 245412, Dec 2010. [Online]. Available: https://link.aps.org/doi/10.1103/PhysRevB.82.245412

[489] J. Sichau, M. Prada, T. Anlauf, T. J. Lyon, B. Bosnjak, L. Tiemann, and R. H. Blick, "Resonance Microwave Measurements of an Intrinsic Spin-Orbit Coupling Gap in Graphene: A Possible Indication of a Topological State," *Phys. Rev. Lett.*, vol. 122, p. 046403, Feb 2019. [Online]. Available: https://link.aps.org/doi/10.1103/PhysRevLett.122.046403

[490] M. G. Vergniory, L. Elcoro, C. Felser, N. Regnault, B. A. Bernevig, and Z. Wang, "A complete catalogue of high-quality topological materials," *Nature*, vol. 566, no. 7745, pp. 480–485, Feb 2019. [Online]. Available: https://doi.org/10.1038/s41586-019-0954-4

[491] T. Zhang, Y. Jiang, Z. Song, H. Huang, Y. He, Z. Fang, H. Weng, and C. Fang, "Catalogue of topological electronic materials," *Nature*, vol. 566, no. 7745, pp. 475–479, Feb 2019. [Online]. Available: https://doi.org/10.1038/s41586-019-0944-6

[492] F. Tang, H. C. Po, A. Vishwanath, and X. Wan, "Comprehensive search for topological materials using symmetry indicators," *Nature*, vol. 566, no. 7745, pp. 486–489, Feb 2019. [Online]. Available: https://doi.org/10.1038/s41586-019-0937-5

[493] ——, "Efficient topological materials discovery using symmetry indicators," *Nature Physics*, vol. 15, no. 5, pp. 470–476, May 2019. [Online]. Available: https://doi.org/10.1038/s41567-019-0418-7

[494] T. Olsen, E. Andersen, T. Okugawa, D. Torelli, T. Deilmann, and K. S. Thygesen, "Discovering two-dimensional topological insulators from high-throughput computations," *Phys. Rev. Materials*, vol. 3, p. 024005, Feb 2019. [Online]. Available: https://link.aps.org/doi/10.1103/PhysRevMaterials.3.024005

[495] A. Marrazzo, M. Gibertini, D. Campi, N. Mounet, and N. Marzari, "Relative Abundance of Z2 Topological Order in Exfoliable Two-Dimensional Insulators," *Nano Letters*, vol. 19, no. 12, pp. 8431–8440, 2019, pMID: 31658415. [Online]. Available: https://doi.org/10.1021/acs.nanolett.9b02689

[496] S. Murakami, "Quantum Spin Hall Effect and Enhanced Magnetic Response by Spin-Orbit Coupling," *Phys. Rev. Lett.*, vol. 97, p. 236805, Dec 2006. [Online]. Available: https://link.aps.org/doi/10.1103/PhysRevLett.97.236805

[497] K. Hricovini, M. C. Richter, O. Heckmann, L. Nicolaï, J.-M. Mariot, and J. Minár, "Topological electronic structure and Rashba effect in Bi thin layers: theoretical predictions and experiments," *Journal of Physics: Condensed Matter*, vol. 31, no. 28, p. 283001, apr 2019. [Online]. Available: https://doi.org/10.1088%2F1361-648x%2Fab1529

[498] J. L. Collins, A. Tadich, W. Wu, L. C. Gomes, J. N. B. Rodrigues, C. Liu, J. Hellerstedt, H. Ryu, S. Tang, S.-K. Mo, S. Adam, S. A. Yang, M. S. Fuhrer, and M. T. Edmonds, "Electric-field-tuned topological phase transition in ultrathin Na3Bi," *Nature*, vol. 564, no. 7736, pp. 390–394, Dec 2018. [Online]. Available: https://doi.org/10.1038/s41586-018-0788-5

[499] R. Stühler, F. Reis, T. Müller, T. Helbig, T. Schwemmer, R. Thomale, J. Schäfer, and R. Claessen, "Tomonaga–Luttinger liquid in the edge channels of a quantum spin Hall insulator," *Nature Physics*, vol. 16, no. 1, pp. 47–51, Jan 2020. [Online]. Available: https://doi.org/10.1038/s41567-019-0697-z

[500] M. Bieniek, T. Woźniak, and P. Potasz, "Stability of topological properties of bismuth (1 1 1) bilayer," *Journal of Physics: Condensed Matter*, vol. 29, no. 15, p. 155501, mar 2017. [Online]. Available: https://doi.org/10.1088%2F1361-648x%2Faa5e79

[501] M. Brzezińska, M. Bieniek, T. Woźniak, P. Potasz, and A. Wójs, "Entanglement entropy and entanglement spectrum of Bi1-xSbx(1 1 1) bilayers," *Journal of Physics: Condensed Matter*, vol. 30, no. 12, p. 125501, feb 2018. [Online]. Available: https://doi.org/10.1088%2F1361-648x%2Faaaf54

[502] N. Nouri, M. Bieniek, M. Brzezińska, M. Modarresi, S. Zia Borujeni, G. Rashedi, A. Wójs, and P. Potasz, "Topological phases in Bi/Sb planar and buckled honeycomb monolayers," *Physics Letters A*, vol. 382, no. 40, pp. 2952 – 2958, 2018. [Online]. Available: http://www.sciencedirect.com/science/article/pii/S0375960118307096

[503] G. Onida, L. Reining, and A. Rubio, "Electronic excitations: density-functional versus many-body Green's-function approaches," *Rev. Mod. Phys.*, vol. 74, pp. 601–659, Jun 2002. [Online]. Available: https://link.aps.org/doi/10.1103/RevModPhys.74.601

[504] E. E. Salpeter and H. A. Bethe, "A Relativistic Equation for Bound-State Problems," *Phys. Rev.*, vol. 84, pp. 1232–1242, Dec 1951. [Online]. Available: https://link.aps.org/doi/10.1103/PhysRev.84.1232

[505] L. J. Sham and T. M. Rice, "Many-Particle Derivation of the Effective-Mass Equation for the Wannier Exciton," *Phys. Rev.*, vol. 144, pp. 708–714, Apr 1966. [Online]. Available: https://link.aps.org/doi/10.1103/PhysRev.144.708

[506] G. Strinati, "Dynamical Shift and Broadening of Core Excitons in Semiconductors," *Phys. Rev. Lett.*, vol. 49, pp. 1519–1522, Nov 1982. [Online]. Available: https://link.aps.org/doi/10.1103/PhysRevLett.49.1519

[507] ——, "Effects of dynamical screening on resonances at inner-shell thresholds in semiconductors," *Phys. Rev. B*, vol. 29, pp. 5718–5726, May 1984. [Online]. Available: https://link.aps.org/doi/10.1103/PhysRevB.29.5718

[508] W. Hanke and L. J. Sham, "Many-Particle Effects in the Optical Excitations of a Semiconductor," *Phys. Rev. Lett.*, vol. 43, pp. 387–390, Jul 1979. [Online]. Available: https://link.aps.org/doi/10.1103/PhysRevLett.43.387

[509] S. Albrecht, G. Onida, and L. Reining, "Ab initio calculation of the quasiparticle spectrum and excitonic effects in Li_2O," *Phys. Rev. B*, vol. 55, pp. 10 278–10 281, Apr 1997. [Online]. Available: https://link.aps.org/doi/10.1103/PhysRevB.55.10278

[510] S. Albrecht, L. Reining, R. Del Sole, and G. Onida, "Ab Initio Calculation of Excitonic Effects in the Optical Spectra of Semiconductors," *Phys. Rev. Lett.*, vol. 80, pp. 4510–4513, May 1998. [Online]. Available: https://link.aps.org/doi/10.1103/PhysRevLett.80.4510

[511] M. Rohlfing and S. G. Louie, "Electron-hole excitations and optical spectra from first principles," *Phys. Rev. B*, vol. 62, pp. 4927–4944, Aug 2000. [Online]. Available: https://link.aps.org/doi/10.1103/PhysRevB.62.4927

[512] J. Deslippe, G. Samsonidze, D. A. Strubbe, M. Jain, M. L. Cohen, and S. G. Louie, "BerkeleyGW: A massively parallel computer package for the calculation of the quasiparticle and optical properties of materials and nanostructures," *Computer Physics Communications*, vol. 183, no. 6, pp. 1269–1289, 2012. [Online]. Available: http://www.sciencedirect.com/science/article/pii/S0010465511003912

[513] Y. Gillet, M. Giantomassi, and X. Gonze, "Efficient on-the-fly interpolation technique for Bethe–Salpeter calculations of optical spectra," *Computer Physics Communications*, vol. 203, pp. 83 – 93, 2016. [Online]. Available: http://www.sciencedirect.com/science/article/pii/S0010465516300236

[514] D. Sangalli, A. Ferretti, H. Miranda, C. Attaccalite, I. Marri, E. Cannuccia, P. Melo, M. Marsili, F. Paleari, A. Marrazzo, G. Prandini, P. Bonfà, M. O. Atambo, F. Affinito, M. Palummo, A. Molina-Sánchez, C. Hogan, M. Grüning, D. Varsano, and A. Marini, "Many-body perturbation theory calculations using the yambo code," *Journal of Physics: Condensed Matter*, vol. 31, no. 32, p. 325902, may 2019. [Online]. Available: https://doi.org/10.1088%2F1361-648x%2Fab15d0

[515] S. Ono, Y. Noguchi, R. Sahara, Y. Kawazoe, and K. Ohno, "TOMBO: All-electron mixed-basis approach to condensed matter physics," *Computer Physics Communications*, vol. 189, pp. 20 – 30, 2015. [Online]. Available: http://www.sciencedirect.com/science/article/pii/S0010465514003956

[516] C. Vorwerk, B. Aurich, C. Cocchi, and C. Draxl, "Bethe–Salpeter equation for absorption and scattering spectroscopy: implementation in the exciting code," *Electronic Structure*, vol. 1, no. 3, p. 037001, aug 2019. [Online]. Available: https://doi.org/10.1088%2F2516-1075%2Fab3123

[517] T. Sander, E. Maggio, and G. Kresse, "Beyond the Tamm-Dancoff approximation for extended systems using exact diagonalization," *Phys. Rev. B*, vol. 92, p. 045209, Jul 2015. [Online]. Available: https://link.aps.org/doi/10.1103/PhysRevB.92.045209

[518] H.-P. Komsa and A. V. Krasheninnikov, "Effects of confinement and environment on the electronic structure and exciton binding energy of MoS_2 from first principles," *Phys. Rev. B*, vol. 86, p. 241201, Dec 2012. [Online]. Available: https://link.aps.org/doi/10.1103/PhysRevB.86.241201

[519] D. Y. Qiu, F. H. da Jornada, and S. G. Louie, "Optical Spectrum of MoS_2: Many-Body Effects and Diversity of Exciton States," *Phys. Rev. Lett.*, vol. 111, p. 216805, Nov 2013. [Online]. Available: https://link.aps.org/doi/10.1103/PhysRevLett.111.216805

[520] A. R. Klots, A. K. M. Newaz, B. Wang, D. Prasai, H. Krzyzanowska, J. Lin, D. Caudel, N. J. Ghimire, J. Yan, B. L. Ivanov, K. A. Velizhanin, A. Burger, D. G. Mandrus, N. H. Tolk, S. T. Pantelides, and K. I. Bolotin, "Probing excitonic states in suspended two-dimensional semiconductors byphotocurrent spectroscopy," *Scientific Reports*, no. 4, p. 6608, 2014. [Online]. Available: https://dx.doi.org/10.1038/srep06608

[521] R. Soklaski, Y. Liang, and L. Yang, "Temperature effect on optical spectra of monolayer molybdenum disulfide," *Applied Physics Letters*, vol. 104, no. 19, p. 193110, 2014. [Online]. Available: https://doi.org/10.1063/1.4878098

[522] H. Yu, G.-B. Liu, P. Gong, X. Xu, and W. Yao, "Dirac cones and Dirac saddle points of bright excitons in monolayer transition metal dichalcogenides," *Nature Communications*, p. 3876, 2014. [Online]. Available: https://doi.org/10.1038/ncomms4876

[523] S. Latini, T. Olsen, and K. S. Thygesen, "Excitons in van der Waals heterostructures: The important role of dielectric screening," *Phys. Rev. B*, vol. 92, p. 245123, Dec 2015. [Online]. Available: https://link.aps.org/doi/10.1103/PhysRevB.92.245123

[524] A. Molina-Sánchez, M. Palummo, A. Marini, and L. Wirtz, "Temperature-dependent excitonic effects in the optical properties of single-layer MoS_2," *Phys. Rev. B*, vol. 93, p. 155435, Apr 2016. [Online]. Available: https://link.aps.org/doi/10.1103/PhysRevB.93.155435

[525] C. Robert, R. Picard, D. Lagarde, G. Wang, J. P. Echeverry, F. Cadiz, P. Renucci, A. Högele, T. Amand, X. Marie, I. C. Gerber, and B. Urbaszek, "Excitonic properties of semiconducting monolayer and bilayer $MoTe_2$," *Phys. Rev. B*, vol. 94, p. 155425, Oct 2016. [Online]. Available: https://link.aps.org/doi/10.1103/PhysRevB.94.155425

[526] V. Despoja, Z. Rukelj, and L. Marušić, "Ab initio study of electronic excitations and the dielectric function in molybdenum disulfide monolayer," *Phys. Rev. B*, vol. 94, p. 165446, Oct 2016. [Online]. Available: https://link.aps.org/doi/10.1103/PhysRevB.94.165446

[527] L. Guo, M. Wu, T. Cao, D. M. Monahan, Y.-H. Lee, S. G. Louie, and G. R. Fleming, "Exchange-driven intravalley mixing of excitons in monolayer transition metal dichalcogenides," *Nature Physics*, vol. 15, no. 3, p. 228, MAR 2019. [Online]. Available: https://www.doi.org/10.1038/s41567-018-0362-y

[528] A. Molina-Sánchez, D. Sangalli, K. Hummer, A. Marini, and L. Wirtz, "Effect of spin-orbit interaction on the optical spectra of single-layer, double-layer, and bulk MoS_2," *Phys. Rev. B*, vol. 88, p. 045412, Jul 2013. [Online]. Available: https://link.aps.org/doi/10.1103/PhysRevB.88.045412

[529] J. P. Echeverry, B. Urbaszek, T. Amand, X. Marie, and I. C. Gerber, "Splitting between bright and dark excitons in transition metal dichalcogenide monolayers," *Phys. Rev. B*, vol. 93, p. 121107, Mar 2016. [Online]. Available: https://link.aps.org/doi/10.1103/PhysRevB.93.121107

[530] S. Latini, E. Ronca, U. De Giovannini, H. Hübener, and A. Rubio, "Cavity Control of Excitons in Two-Dimensional Materials," *Nano Letters*, vol. 19, no. 6, p. 3473, 2019. [Online]. Available: https://doi.org/10.1021/acs.nanolett.9b00183

[531] H. Yu, M. Laurien, Z. Hu, and O. Rubel, "Exploration of the bright and dark exciton landscape and fine structure of MoS_2 using G_0W_0-BSE," *Phys. Rev. B*, vol. 100, p. 125413, Sep 2019. [Online]. Available: https://link.aps.org/doi/10.1103/PhysRevB.100.125413

[532] M. Druppel, T. Deilmann, P. Kruger, and M. Rohlfing, "Diversity of trion states and substrate effects in the optical properties of an MoS2 monolayer," *Nature Communications*, p. 2117, 2017. [Online]. Available: https://doi:10.1038/s41467-017-02286-6

[533] A. Torche and G. Bester, "First-principles many-body theory for charged and neutral excitations: Trion fine structure splitting in transition metal dichalcogenides," *Phys. Rev. B*, vol. 100, p. 201403, Nov 2019. [Online]. Available: https://link.aps.org/doi/10.1103/PhysRevB.100.201403

[534] Y. V. Zhumagulov, A. Vagov, N. Y. Senkevich, D. R. Gulevich, and V. Perebeinos, "Three-particle states and brightening of intervalley excitons in a doped MoS_2 monolayer," *Phys. Rev. B*, vol. 101, p. 245433, Jun 2020. [Online]. Available: https://link.aps.org/doi/10.1103/PhysRevB.101.245433

[535] S. Haastrup, M. Strange, M. Pandey, T. Deilmann, P. S. Schmidt, N. F. Hinsche, M. N. Gjerding, D. Torelli, P. M. Larsen, A. C. Riis-Jensen, J. Gath, K. W. Jacobsen, J. J. Mortensen, T. Olsen, and K. S. Thygesen, "The Computational 2D Materials Database: high-throughput modeling and discovery of atomically thin crystals," *2D Materials*, vol. 5, no. 4, p. 042002, sep 2018. [Online]. Available: https://doi.org/10.1088%2F2053-1583%2Faacfc1

[536] N. Zibouche, M. Schlipf, and F. Giustino, "Effect of substrate screening on the electronic structure of monolayer MoS2," *arXiv e-prints*, p. arXiv:2008.03980, Aug. 2020.

[537] A. Steinhoff, M. Rösner, F. Jahnke, T. O. Wehling, and C. Gies, "Influence of Excited Carriers on the Optical and Electronic Properties of MoS2," *Nano Letters*, vol. 14, no. 7, pp. 3743–3748, 2014, pMID: 24956358. [Online]. Available: https://doi.org/10.1021/nl500595u

[538] A. Steinhoff, J.-H. Kim, F. Jahnke, M. Rösner, D.-S. Kim, C. Lee, G. H. Han, M. S. Jeong, T. O. Wehling, and C. Gies, "Efficient Excitonic Photoluminescence in Direct and Indirect Band Gap Monolayer MoS2," *Nano Letters*, vol. 15, no. 10, pp. 6841–6847, 2015, pMID: 26322814. [Online]. Available: https://doi.org/10.1021/acs.nanolett.5b02719

[539] G. Berghäuser and E. Malic, "Analytical approach to excitonic properties of MoS_2," *Phys. Rev. B*, vol. 89, p. 125309, Mar 2014. [Online]. Available: https://link.aps.org/doi/10.1103/PhysRevB.89.125309

[540] S. Konabe and S. Okada, "Effect of Coulomb interactions on optical properties of monolayer transition-metal dichalcogenides," *Phys. Rev. B*, vol. 90, p. 155304, Oct 2014. [Online]. Available: https://link.aps.org/doi/10.1103/PhysRevB.90.155304

[541] F. Wu, F. Qu, and A. H. MacDonald, "Exciton band structure of monolayer MoS_2," *Phys. Rev. B*, vol. 91, p. 075310, Feb 2015. [Online]. Available: https://link.aps.org/doi/10.1103/PhysRevB.91.075310

[542] B. Scharf, T. Frank, M. Gmitra, J. Fabian, I. Žutić, and V. Perebeinos, "Excitonic Stark effect in MoS_2 monolayers," *Phys. Rev. B*, vol. 94, p. 245434, Dec 2016. [Online]. Available: https://link.aps.org/doi/10.1103/PhysRevB.94.245434

[543] E. Ridolfi, C. H. Lewenkopf, and V. M. Pereira, "Excitonic structure of the optical conductivity in MoS_2 monolayers," *Phys. Rev. B*, vol. 97, p. 205409, May 2018. [Online]. Available: https://link.aps.org/doi/10.1103/PhysRevB.97.205409

[544] M. M. Glazov, T. Amand, X. Marie, D. Lagarde, L. Bouet, and B. Urbaszek, "Exciton fine structure and spin decoherence in monolayers of transition metal dichalcogenides," *Phys. Rev. B*, vol. 89, p. 201302, May 2014. [Online]. Available: https://link.aps.org/doi/10.1103/PhysRevB.89.201302

[545] J. Zhou, W.-Y. Shan, W. Yao, and D. Xiao, "Berry Phase Modification to the Energy Spectrum of Excitons," *Phys. Rev. Lett.*, vol. 115, p. 166803, Oct 2015. [Online]. Available: https://link.aps.org/doi/10.1103/PhysRevLett.115.166803

[546] M. M. Glazov, E. L. Ivchenko, G. Wang, T. Amand, X. Marie, B. Urbaszek, and B. L. Liu, "Spin and valley dynamics of excitons in transition metal dichalcogenide monolayers," *physica status solidi (b)*, vol. 252, no. 11, pp. 2349–2362, 2015. [Online]. Available: https://onlinelibrary.wiley.com/doi/abs/10.1002/pssb.201552211

[547] M. Van der Donck and F. M. Peeters, "Spectrum of exciton states in monolayer transition metal dichalcogenides: Angular momentum and Landau levels," *Phys. Rev. B*, vol. 99, p. 115439, Mar 2019. [Online]. Available: https://link.aps.org/doi/10.1103/PhysRevB.99.115439

[548] A. J. Chaves, R. M. Ribeiro, T. Frederico, and N. M. R. Peres, "Excitonic effects in the optical properties of 2D materials:an equation of motion approach," *2D Materials*, vol. 4, no. 2, p. 025086, apr 2017. [Online]. Available: https://doi.org/10.1088%2F2053-1583%2Faa6b72

[549] M. Trushin, M. O. Goerbig, and W. Belzig, "Optical absorption by Dirac excitons in single-layer transition-metal dichalcogenides," *Phys. Rev. B*, vol. 94, p. 041301, Jul 2016. [Online]. Available: https://link.aps.org/doi/10.1103/PhysRevB.94.041301

[550] M. M. Glazov, L. E. Golub, G. Wang, X. Marie, T. Amand, and B. Urbaszek, "Intrinsic exciton-state mixing and nonlinear optical properties in transition metal dichalcogenide monolayers," *Phys. Rev. B*, vol. 95, p. 035311, Jan 2017. [Online]. Available: https://link.aps.org/doi/10.1103/PhysRevB.95.035311

[551] M. Trushin, M. O. Goerbig, and W. Belzig, "Model Prediction of Self-Rotating Excitons in Two-Dimensional Transition-Metal Dichalcogenides," *Phys. Rev. Lett.*, vol. 120, p. 187401, May 2018. [Online]. Available: https://link.aps.org/doi/10.1103/PhysRevLett.120.187401

[552] T. C. Berkelbach, M. S. Hybertsen, and D. R. Reichman, "Theory of neutral and charged excitons in monolayer transition metal dichalcogenides," *Phys. Rev. B*, vol. 88, p. 045318, Jul 2013. [Online]. Available: https://link.aps.org/doi/10.1103/PhysRevB.88.045318

[553] I. Kylänpää and H.-P. Komsa, "Binding energies of exciton complexes in transition metal dichalcogenide monolayers and effect of dielectric environment," *Phys. Rev. B*, vol. 92, p. 205418, Nov 2015. [Online]. Available: https://link.aps.org/doi/10.1103/PhysRevB.92.205418

[554] M. Z. Mayers, T. C. Berkelbach, M. S. Hybertsen, and D. R. Reichman, "Binding energies and spatial structures of small carrier complexes in monolayer transition-metal dichalcogenides via diffusion Monte Carlo," *Phys. Rev. B*, vol. 92, p. 161404, Oct 2015. [Online]. Available: https://link.aps.org/doi/10.1103/PhysRevB.92.161404

[555] K. A. Velizhanin and A. Saxena, "Excitonic effects in two-dimensional semiconductors: Path integral Monte Carlo approach," *Phys. Rev. B*, vol. 92, p. 195305, Nov 2015. [Online]. Available: https://link.aps.org/doi/10.1103/PhysRevB.92.195305

[556] T. Olsen, S. Latini, F. Rasmussen, and K. S. Thygesen, "Simple Screened Hydrogen Model of Excitons in Two-Dimensional Materials," *Phys. Rev. Lett.*, vol. 116, p. 056401, Feb 2016. [Online]. Available: https://link.aps.org/doi/10.1103/PhysRevLett.116.056401

[557] D. W. Kidd, D. K. Zhang, and K. Varga, "Binding energies and structures of two-dimensional excitonic complexes in transition metal dichalcogenides," *Phys. Rev. B*, vol. 93, p. 125423, Mar 2016. [Online]. Available: https://link.aps.org/doi/10.1103/PhysRevB.93.125423

[558] T. G. Pedersen, "Exciton Stark shift and electroabsorption in monolayer transition-metal dichalcogenides," *Phys. Rev. B*, vol. 94, p. 125424, Sep 2016. [Online]. Available: https://link.aps.org/doi/10.1103/PhysRevB.94.125424

[559] Y. Cho and T. C. Berkelbach, "Environmentally sensitive theory of electronic and optical transitions in atomically thin semiconductors," *Phys. Rev. B*, vol. 97, p. 041409, Jan 2018. [Online]. Available: https://link.aps.org/doi/10.1103/PhysRevB.97.041409

[560] M. Selig, G. Berghäuser, M. Richter, R. Bratschitsch, A. Knorr, and E. Malic, "Dark and bright exciton formation, thermalization, and photoluminescence in monolayer transition metal dichalcogenides," *2D Materials*, vol. 5, no. 3, p. 035017, may 2018. [Online]. Available: https://doi.org/10.1088%2F2053-1583%2Faabea3

[561] L. S. R. Cavalcante, D. R. da Costa, G. A. Farias, D. R. Reichman, and A. Chaves, "Stark shift of excitons and trions in two-dimensional materials," *Phys. Rev. B*, vol. 98, p. 245309, Dec 2018. [Online]. Available: https://link.aps.org/doi/10.1103/PhysRevB.98.245309

[562] M. Feierabend, Z. Khatibi, G. Berghäuser, and E. Malic, "Dark exciton based strain sensing in tungsten-based transition metal dichalcogenides," *Phys. Rev. B*, vol. 99, p. 195454, May 2019. [Online]. Available: https://link.aps.org/doi/10.1103/PhysRevB.99.195454

[563] N. S. Rytova, "Screened potential of a point charge in a thin film," *Proc. MSU, Phys. Astron.*, vol. 3, p. 30, 1967.

[564] L. V. Keldysh, "Coulomb interaction in thin semiconduc-tor and semimetal films," *JETP Lett.*, vol. 29, p. 658, 1979.

[565] A. Szabo and N. S. Ostlund, *Modern Quantum Chemistry: Introduction to Advanced Electronic Structure Theory*, 1st ed. Dover Publications Inc., 1989.

[566] I. Shavitt and R. J. Bartlett, *Many-Body Methods in Chemistry and Physics: MBPT and Coupled-Cluster Theory*, ser. Cambridge Molecular Science. Cambridge University Press, 2009.

[567] P. Hawrylak, "Single-electron capacitance spectroscopy of few-electron artificial atoms in a magnetic field: Theory and experiment," *Phys. Rev. Lett.*, vol. 71, pp. 3347–3350, Nov 1993. [Online]. Available: https://link.aps.org/doi/10.1103/PhysRevLett.71.3347

[568] P. Hawrylak and D. Pfannkuche, "Magnetoluminescence from correlated electrons in quantum dots," *Phys. Rev. Lett.*, vol. 70, pp. 485–488, Jan 1993. [Online]. Available: https://link.aps.org/doi/10.1103/PhysRevLett.70.485

[569] A. Wojs and P. Hawrylak, "Negatively charged magnetoexcitons in quantum dots," *Phys. Rev. B*, vol. 51, pp. 10 880–10 885, Apr 1995. [Online]. Available: https://link.aps.org/doi/10.1103/PhysRevB.51.10880

[570] A. Wojs, P. Hawrylak, S. Fafard, and L. Jacak, "Electronic structure and magneto-optics of self-assembled quantum dots," *Phys. Rev. B*, vol. 54, pp. 5604–5608, Aug 1996. [Online]. Available: https://link.aps.org/doi/10.1103/PhysRevB.54.5604

[571] A. Wojs and P. Hawrylak, "Theory of photoluminescence from modulation-doped self-assembled quantum dots in a magnetic field," *Phys. Rev. B*, vol. 55, pp. 13 066–13 071, May 1997. [Online]. Available: https://link.aps.org/doi/10.1103/PhysRevB.55.13066

[572] P. Hawrylak, G. A. Narvaez, M. Bayer, and A. Forchel, "Excitonic Absorption in a Quantum Dot," *Phys. Rev. Lett.*, vol. 85, pp. 389–392, Jul 2000. [Online]. Available: https://link.aps.org/doi/10.1103/PhysRevLett.85.389

[573] A. D. Güçlü, P. Potasz, O. Voznyy, M. Korkusinski, and P. Hawrylak, "Magnetism and Correlations in Fractionally Filled Degenerate Shells of Graphene Quantum Dots," *Phys. Rev. Lett.*, vol. 103, p. 246805, Dec 2009. [Online]. Available: https://link.aps.org/doi/10.1103/PhysRevLett.103.246805

[574] M. Zieliński, M. Korkusiński, and P. Hawrylak, "Atomistic tight-binding theory of multiexciton complexes in a self-assembled InAs quantum dot," *Phys. Rev. B*, vol. 81, p. 085301, Feb 2010. [Online]. Available: https://link.aps.org/doi/10.1103/PhysRevB.81.085301

[575] A. D. Güçlü, P. Potasz, and P. Hawrylak, "Excitonic absorption in gate-controlled graphene quantum dots," *Phys. Rev. B*, vol. 82, p. 155445, Oct 2010. [Online]. Available: https://link.aps.org/doi/10.1103/PhysRevB.82.155445

[576] M. Bayer, O. Stern, P. Hawrylak, S. Fafard, and A. Forchel, "Hidden symmetries in the energy levels of excitonic 'artificial atoms'," *Nature*, vol. 405, no. 6789, pp. 923–926, Jun 2000. [Online]. Available: https://doi.org/10.1038/35016020

[577] M. Korkusinski, O. Voznyy, and P. Hawrylak, "Theory of highly excited semiconductor nanostructures including Auger coupling: Exciton-biexciton mixing in CdSe nanocrystals," *Phys. Rev. B*, vol. 84, p. 155327, Oct 2011. [Online]. Available: https://link.aps.org/doi/10.1103/PhysRevB.84.155327

[578] P. Potasz, A. D. Güçlü, A. Wójs, and P. Hawrylak, "Electronic properties of gated triangular graphene quantum dots: Magnetism, correlations, and geometrical effects," *Phys. Rev. B*, vol. 85, p. 075431, Feb 2012. [Online]. Available: https://link.aps.org/doi/10.1103/PhysRevB.85.075431

[579] M. Korkusinski and P. Hawrylak, "Atomistic theory of emission from dark excitons in self-assembled quantum dots," *Phys. Rev. B*, vol. 87, p. 115310, Mar 2013. [Online]. Available: https://link.aps.org/doi/10.1103/PhysRevB.87.115310

[580] I. Ozfidan, M. Korkusinski, and P. Hawrylak, "Theory of biexcitons and biexciton-exciton cascade in graphene quantum dots," *Phys. Rev. B*, vol. 91, p. 115314, Mar 2015. [Online]. Available: https://link.aps.org/doi/10.1103/PhysRevB.91.115314

[581] F. Fan, O. Voznyy, R. P. Sabatini, K. T. Bicanic, M. M. Adachi, J. R. McBride, K. R. Reid, Y.-S. Park, X. Li, A. Jain, R. Quintero-Bermudez, M. Saravanapavanantham, M. Liu, M. Korkusinski, P. Hawrylak, V. I. Klimov, S. J. Rosenthal, S. Hoogland, and E. H. Sargent, "Continuous-wave lasing in colloidal quantum dot solids enabled by facet-selective epitaxy," *Nature*, vol. 544, no. 7648, pp. 75–79, Apr 2017. [Online]. Available: https://doi.org/10.1038/nature21424

[582] M. Cygorek, M. Otten, M. Korkusinski, and P. Hawrylak, "Accurate and efficient description of interacting carriers in quantum nanostructures by selected configuration interaction and perturbation theory," *Phys. Rev. B*, vol. 101, p. 205308, May 2020. [Online]. Available: https://link.aps.org/doi/10.1103/PhysRevB.101.205308

[583] A. Wójs, J. J. Quinn, and P. Hawrylak, "Charged excitons in a dilute two-dimensional electron gas in a high magnetic field," *Phys. Rev. B*, vol. 62, pp. 4630–4637, Aug 2000. [Online]. Available: https://link.aps.org/doi/10.1103/PhysRevB.62.4630

[584] A. Wójs and J. J. Quinn, "Photoluminescence from fractional quantum Hall systems: Role of separation between electron and hole layers," *Phys. Rev. B*, vol. 63, p. 045304, Dec 2000. [Online]. Available: https://link.aps.org/doi/10.1103/PhysRevB.63.045304

[585] J. Cizek, "On the Correlation Problem in Atomic and Molecular Systems. Calculation of Wavefunction Components in Ursell-Type Expansion Using Quantum-Field Theoretical Methods," *The Journal of Chemical Physics*, vol. 45, no. 11, pp. 4256–4266, 1966. [Online]. Available: https://doi.org/10.1063/1.1727484

[586] R. J. Bartlett and M. Musiał, "Coupled-cluster theory in quantum chemistry," *Rev. Mod. Phys.*, vol. 79, pp. 291–352, Feb 2007. [Online]. Available: https://link.aps.org/doi/10.1103/RevModPhys.79.291

[587] Q. Ou and J. E. Subotnik, "Comparison between GW and Wave-Function-Based Approaches: Calculating the Ionization Potential and Electron Affinity for 1D Hubbard Chains," *The Journal of Physical Chemistry A*, vol. 120, no. 26, pp. 4514–4525, 2016, pMID: 27336177. [Online]. Available: https://doi.org/10.1021/acs.jpca.6b03294

[588] ——, "Comparison between the Bethe–Salpeter Equation and Configuration Interaction Approaches for Solving a Quantum Chemistry Problem: Calculating the Excitation Energy for Finite 1D Hubbard Chains," *Journal of Chemical Theory and Computation*, vol. 14, no. 2, pp. 527–542, 2018, pMID: 29183113. [Online]. Available: https://doi.org/10.1021/acs.jctc.7b00246

[589] M. G. Bayne, J. A. Scher, B. H. Ellis, and A. Chakraborty, "Linked-Cluster Formulation of Electron–Hole Interaction Kernel in Real-Space Representation without Using Unoccupied States," *Journal of Chemical Theory and Computation*, vol. 14, no. 7, pp. 3656–3666, 2018, pMID: 29782165. [Online]. Available: https://doi.org/10.1021/acs.jctc.8b00123

[590] C. H. Patterson, "Photoabsorption spectra of small Na clusters: TDHF and BSE versus CI and experiment," *Phys. Rev. Materials*, vol. 3, p. 043804, Apr 2019. [Online]. Available: https://link.aps.org/doi/10.1103/PhysRevMaterials.3.043804

[591] M. Dvorak, D. Golze, and P. Rinke, "Quantum embedding theory in the screened Coulomb interaction: Combining configuration interaction with *GW*/BSE," *Phys. Rev. Materials*, vol. 3, p. 070801, Jul 2019. [Online]. Available: https://link.aps.org/doi/10.1103/PhysRevMaterials.3.070801

[592] J. McClain, J. Lischner, T. Watson, D. A. Matthews, E. Ronca, S. G. Louie, T. C. Berkelbach, and G. K.-L. Chan, "Spectral functions of the uniform electron gas via coupled-cluster theory and comparison to the *GW* and related approximations," *Phys. Rev. B*, vol. 93, p. 235139, Jun 2016. [Online]. Available: https://link.aps.org/doi/10.1103/PhysRevB.93.235139

[593] M. Kira and S. Koch, "Many-body correlations and excitonic effects in semiconductor spectroscopy," *Progress in Quantum Electronics*, vol. 30, no. 5, pp. 155 – 296, 2006. [Online]. Available: http://www.sciencedirect.com/science/article/pii/S0079672706000280

[594] T. Stroucken, J. H. Grönqvist, and S. W. Koch, "Optical response and ground state of graphene," *Phys. Rev. B*, vol. 84, p. 205445, Nov 2011. [Online]. Available: https://link.aps.org/doi/10.1103/PhysRevB.84.205445

[595] T. Stroucken and S. W. Koch, "Optically brightp-excitons indicating strong Coulomb coupling in transition-metal dichalcogenides," *Journal of Physics: Condensed Matter*, vol. 27, no. 34, p. 345003, aug 2015. [Online]. Available: https://doi.org/10.1088%2F0953-8984%2F27%2F34%2F345003

[596] L. Meckbach, T. Stroucken, and S. W. Koch, "Giant excitation induced bandgap renormalization in TMDC monolayers," *Applied Physics Letters*, vol. 112, no. 6, p. 061104, 2018. [Online]. Available: https://doi.org/10.1063/1.5017069

[597] L. Meckbach, J. Hader, U. Huttner, J. Neuhaus, J. T. Steiner, T. Stroucken, J. V. Moloney, and S. W. Koch, "Ultrafast band-gap renormalization and build-up of optical gain in monolayer $MoTe_2$," *Phys. Rev. B*, vol. 101, p. 075401, Feb 2020. [Online]. Available: https://link.aps.org/doi/10.1103/PhysRevB.101.075401

[598] X. Wang and T. C. Berkelbach, "Excitons in Solids from Periodic Equation-of-Motion Coupled-Cluster Theory," *Journal of Chemical Theory and Computation*, vol. 16, no. 5, pp. 3095–3103, 2020, pMID: 32223151. [Online]. Available: https://doi.org/10.1021/acs.jctc.0c00101

[599] D. K. Zhang, D. W. Kidd, and K. Varga, "Excited Biexcitons in Transition Metal Dichalcogenides," *Nano Letters*, vol. 15, no. 10, pp. 7002–7005, 2015, pMID: 26422057. [Online]. Available: https://doi.org/10.1021/acs.nanolett.5b03009

[600] D. Van Tuan, M. Yang, and H. Dery, "Coulomb interaction in monolayer transition-metal dichalcogenides," *Phys. Rev. B*, vol. 98, p. 125308, Sep 2018. [Online]. Available: https://link.aps.org/doi/10.1103/PhysRevB.98.125308

[601] E. Mostaani, M. Szyniszewski, C. H. Price, R. Maezono, M. Danovich, R. J. Hunt, N. D. Drummond, and V. I. Fal'ko, "Diffusion quantum Monte Carlo study of excitonic complexes in two-dimensional transition-metal dichalcogenides," *Phys. Rev. B*, vol. 96, p. 075431, Aug 2017. [Online]. Available: https://link.aps.org/doi/10.1103/PhysRevB.96.075431

[602] M. Szyniszewski, E. Mostaani, N. D. Drummond, and V. I. Fal'ko, "Binding energies of trions and biexcitons in two-dimensional semiconductors from diffusion quantum Monte Carlo calculations," *Phys. Rev. B*, vol. 95, p. 081301, Feb 2017. [Online]. Available: https://link.aps.org/doi/10.1103/PhysRevB.95.081301

[603] S. C. Kuhn and M. Richter, "Combined tensor network/cluster expansion method using logic gates: Illustrated for (bi)excitons by a single-layer MoS_2 model system," *Phys. Rev. B*, vol. 99, p. 241301, Jun 2019. [Online]. Available: https://link.aps.org/doi/10.1103/PhysRevB.99.241301

[604] ——, "Tensor network strategies for calculating biexcitons and trions in monolayer two-dimensional materials beyond the ground state," *Phys. Rev. B*, vol. 101, p. 075302, Feb 2020. [Online]. Available: https://link.aps.org/doi/10.1103/PhysRevB.101.075302

[605] E. Runge and E. K. U. Gross, "Density-Functional Theory for Time-Dependent Systems," *Phys. Rev. Lett.*, vol. 52, pp. 997–1000, Mar 1984. [Online]. Available: https://link.aps.org/doi/10.1103/PhysRevLett.52.997

[606] R. Singh and B. Deb, "Developments in excited-state density functional theory," *Physics Reports*, vol. 311, no. 2, pp. 47 – 94, 1999. [Online]. Available: http://www.sciencedirect.com/science/article/pii/S0370157398000817

[607] I. V. Tokatly and O. Pankratov, "Many-Body Diagrammatic Expansion in a Kohn-Sham Basis: Implications for Time-Dependent Density Functional Theory of Excited States," *Phys. Rev. Lett.*, vol. 86, pp. 2078–2081, Mar 2001. [Online]. Available: https://link.aps.org/doi/10.1103/PhysRevLett.86.2078

[608] Y.-M. Byun, J. Sun, and C. A. Ullrich, "Time-dependent density-functional theory for periodic solids: assessment of excitonic exchange–correlation kernels," *Electronic Structure*, vol. 2, no. 2, p. 023002, apr 2020. [Online]. Available: https://doi.org/10.1088%2F2516-1075%2Fab7b12

[609] L. Reining, V. Olevano, A. Rubio, and G. Onida, "Excitonic Effects in Solids Described by Time-Dependent Density-Functional Theory," *Phys. Rev. Lett.*, vol. 88, p. 066404, Jan 2002. [Online]. Available: https://link.aps.org/doi/10.1103/PhysRevLett.88.066404

[610] Y.-H. Kim and A. Görling, "Excitonic Optical Spectrum of Semiconductors Obtained by Time-Dependent Density-Functional Theory with the Exact-Exchange Kernel," *Phys. Rev. Lett.*, vol. 89, p. 096402, Aug 2002. [Online]. Available: https://link.aps.org/doi/10.1103/PhysRevLett.89.096402

[611] A. Marini, R. Del Sole, and A. Rubio, "Bound Excitons in Time-Dependent Density-Functional Theory: Optical and Energy-Loss Spectra," *Phys. Rev. Lett.*, vol. 91, p. 256402, Dec 2003. [Online]. Available: https://link.aps.org/doi/10.1103/PhysRevLett.91.256402

[612] V. U. Nazarov and G. Vignale, "Optics of Semiconductors from Meta-Generalized-Gradient-Approximation-Based Time-Dependent Density-Functional Theory," *Phys. Rev. Lett.*, vol. 107, p. 216402, Nov 2011. [Online]. Available: https://link.aps.org/doi/10.1103/PhysRevLett.107.216402

[613] D. Wing, J. B. Haber, R. Noff, B. Barker, D. A. Egger, A. Ramasubramaniam, S. G. Louie, J. B. Neaton, and L. Kronik, "Comparing time-dependent density functional theory with many-body perturbation theory for semiconductors: Screened range-separated hybrids and the *GW* plus Bethe-Salpeter approach," *Phys. Rev. Materials*, vol. 3, p. 064603, Jun 2019. [Online]. Available: https://link.aps.org/doi/10.1103/PhysRevMaterials.3.064603

[614] J. Sun, J. Yang, and C. A. Ullrich, "Low-cost alternatives to the Bethe-Salpeter equation: Towards simple hybrid functionals for excitonic effects in solids," *Phys. Rev. Research*, vol. 2, p. 013091, Jan 2020. [Online]. Available: https://link.aps.org/doi/10.1103/PhysRevResearch.2.013091

[615] R. Gaudoin and K. Burke, "Lack of Hohenberg-Kohn Theorem for Excited States," *Phys. Rev. Lett.*, vol. 93, p. 173001, Oct 2004. [Online]. Available: https://link.aps.org/doi/10.1103/PhysRevLett.93.173001

[616] Z.-h. Yang and C. A. Ullrich, "Direct calculation of exciton binding energies with time-dependent density-functional theory," *Phys. Rev. B*, vol. 87, p. 195204, May 2013. [Online]. Available: https://link.aps.org/doi/10.1103/PhysRevB.87.195204

[617] A. Ramasubramaniam, D. Wing, and L. Kronik, "Transferable screened range-separated hybrids for layered materials: The cases of MoS_2 and h-BN," *Phys. Rev. Materials*, vol. 3, p. 084007, Aug 2019. [Online]. Available: https://link.aps.org/doi/10.1103/PhysRevMaterials.3.084007

[618] Y. Suzuki and K. Watanabe, "Excitons in two-dimensional atomic layer materials from time-dependent density functional theory: mono-layer and bi-layer hexagonal boron nitride and transition-metal dichalcogenides," *Phys. Chem. Chem. Phys.*, vol. 22, pp. 2908–2916, 2020. [Online]. Available: http://dx.doi.org/10.1039/C9CP06034K

[619] B. Ganchev, N. Drummond, I. Aleiner, and V. Fal'ko, "Three-Particle Complexes in Two-Dimensional Semiconductors," *Phys. Rev. Lett.*, vol. 114, p. 107401, Mar 2015. [Online]. Available: https://link.aps.org/doi/10.1103/PhysRevLett.114.107401

[620] I. Filikhin, R. Y. Kezerashvili, S. M. Tsiklauri, and B. Vlahovic, "Trions in bulk and monolayer materials: Faddeev equations and hyperspherical harmonics," *Nanotechnology*, vol. 29, no. 12, p. 124002, feb 2018. [Online]. Available: https://doi.org/10.1088%2F1361-6528%2Faaa94d

[621] S. Gao, Y. Liang, C. D. Spataru, and L. Yang, "Dynamical Excitonic Effects in Doped Two-Dimensional Semiconductors," *Nano Letters*, vol. 16, no. 9, pp. 5568–5573, 2016, pMID: 27479740. [Online]. Available: https://doi.org/10.1021/acs.nanolett.6b02118

[622] S. A. Brown, J. F. Young, J. A. Brum, P. Hawrylak, and Z. Wasilewski, "Evolution of the interband absorption threshold with the density of a two-dimensional electron gas," *Phys. Rev. B*, vol. 54, pp. R11 082–R11 085, Oct 1996. [Online]. Available: https://link.aps.org/doi/10.1103/PhysRevB.54.R11082

[623] R. , V. Kochereshko, G. Astakhov, D. Yakovlev, W. Ossau, J. Nürnberger, W. Faschinger, G. Landwehr, T. Wojtowicz, G. Karczewski, and J. Kossut, "Excitons and Trions Modified by Interaction with a Two-Dimensional Electron Gas," *physica status solidi (b)*, vol. 227, no. 2, pp. 343–352, 2001. [Online]. Available: https://onlinelibrary.wiley.com/doi/abs/10.1002/1521-3951%28200110%29227%3A2%3C343%3A%3AAID-PSSB343%3E3.0.CO%3B2-W

[624] M. Combescot and J. Tribollet, "Trion oscillator strength," *Solid State Communications*, vol. 128, no. 6, pp. 273 – 277, 2003. [Online]. Available: http://www.sciencedirect.com/science/article/pii/S0038109803006574

[625] M. R. Carbone, M. Z. Mayers, and D. R. Reichman, "Microscopic model of the doping dependence of linewidths in monolayer transition metal dichalcogenides," *The Journal of Chemical Physics*, vol. 152, no. 19, p. 194705, 2020. [Online]. Available: https://doi.org/10.1063/5.0008730

[626] D. K. Efimkin and A. H. MacDonald, "Many-body theory of trion absorption features in two-dimensional semiconductors," *Phys. Rev. B*, vol. 95, p. 035417, Jan 2017. [Online]. Available: https://link.aps.org/doi/10.1103/PhysRevB.95.035417

[627] Y.-W. Chang and D. R. Reichman, "Many-body theory of optical absorption in doped two-dimensional semiconductors," *Phys. Rev. B*, vol. 99, p. 125421, Mar 2019. [Online]. Available: https://link.aps.org/doi/10.1103/PhysRevB.99.125421

[628] M. M. Glazov, "Optical properties of charged excitons in two-dimensional semiconductors," *The Journal of Chemical Physics*, vol. 153, no. 3, p. 034703, 2020. [Online]. Available: https://doi.org/10.1063/5.0012475

[629] M. Van der Donck and F. M. Peeters, "Spectrum of exciton states in monolayer transition metal dichalcogenides: Angular momentum and Landau levels," *Phys. Rev. B*, vol. 99, p. 115439, Mar 2019. [Online]. Available: https://link.aps.org/doi/10.1103/PhysRevB.99.115439

[630] X. Zhang, W.-Y. Shan, and D. Xiao, "Optical Selection Rule of Excitons in Gapped Chiral Fermion Systems," *Phys. Rev. Lett.*, vol. 120, p. 077401, Feb 2018. [Online]. Available: https://link.aps.org/doi/10.1103/PhysRevLett.120.077401

[631] T. Cao, M. Wu, and S. G. Louie, "Unifying Optical Selection Rules for Excitons in Two Dimensions: Band Topology and Winding Numbers," *Phys. Rev. Lett.*, vol. 120, p. 087402, Feb 2018. [Online]. Available: https://link.aps.org/doi/10.1103/PhysRevLett.120.087402

[632] L. Chirolli, "Brightening odd-parity excitons in transition-metal dichalcogenides: Rashba spin-orbit interaction, skyrmions, and cavity polaritons," *Phys. Rev. B*, vol. 101, p. 075426, Feb 2020. [Online]. Available: https://link.aps.org/doi/10.1103/PhysRevB.101.075426

[633] A. Taghizadeh and T. G. Pedersen, "Nonlinear optical selection rules of excitons in monolayer transition metal dichalcogenides," *Phys. Rev. B*, vol. 99, p. 235433, Jun 2019. [Online]. Available: https://link.aps.org/doi/10.1103/PhysRevB.99.235433

[634] A. Hichri, S. Jaziri, and M. O. Goerbig, "Charged excitons in two-dimensional transition metal dichalcogenides: Semiclassical calculation of Berry curvature effects," *Phys. Rev. B*, vol. 100, p. 115426, Sep 2019. [Online]. Available: https://link.aps.org/doi/10.1103/PhysRevB.100.115426

[635] I. Garate and M. Franz, "Excitons and optical absorption on the surface of a strong topological insulator with a magnetic energy gap," *Phys. Rev. B*, vol. 84, p. 045403, Jul 2011. [Online]. Available: https://link.aps.org/doi/10.1103/PhysRevB.84.045403

[636] D. K. Efimkin and Y. E. Lozovik, "Resonant manifestations of chiral excitons in Faraday and Kerr effects in a topological insulator film," *Phys. Rev. B*, vol. 87, p. 245416, Jun 2013. [Online]. Available: https://link.aps.org/doi/10.1103/PhysRevB.87.245416

[637] A. A. Allocca, D. K. Efimkin, and V. M. Galitski, "Fingerprints of Berry phases in the bulk exciton spectrum of a topological insulator," *Phys. Rev. B*, vol. 98, p. 045430, Jul 2018. [Online]. Available: https://link.aps.org/doi/10.1103/PhysRevB.98.045430

[638] K. Wakabayashi, "Electronic transport properties of nanographite ribbon junctions," *Phys. Rev. B*, vol. 64, p. 125428, Sep 2001. [Online]. Available: https://link.aps.org/doi/10.1103/PhysRevB.64.125428

[639] L. Yang, C.-H. Park, Y.-W. Son, M. L. Cohen, and S. G. Louie, "Quasiparticle Energies and Band Gaps in Graphene Nanoribbons," *Phys. Rev. Lett.*, vol. 99, p. 186801, Nov 2007. [Online]. Available: https://link.aps.org/doi/10.1103/PhysRevLett.99.186801

[640] Y.-W. Son, M. L. Cohen, and S. G. Louie, "Half-metallic graphene nanoribbons," *Nature*, vol. 444, no. 7117, pp. 347–349, Nov 2006. [Online]. Available: https://doi.org/10.1038/nature05180

[641] J. Cai, P. Ruffieux, R. Jaafar, M. Bieri, T. Braun, S. Blankenburg, M. Muoth, A. P. Seitsonen, M. Saleh, X. Feng, K. Müllen, and R. Fasel, "Atomically precise bottom-up fabrication of graphene nanoribbons," *Nature*, vol. 466, no. 7305, pp. 470–473, Jul 2010. [Online]. Available: https://doi.org/10.1038/nature09211

[642] P. Ruffieux, S. Wang, B. Yang, C. Sánchez-Sánchez, J. Liu, T. Dienel, L. Talirz, P. Shinde, C. A. Pignedoli, D. Passerone, T. Dumslaff, X. Feng, K. Müllen, and R. Fasel, "On-surface synthesis of graphene nanoribbons with zigzag edge topology," *Nature*, vol. 531, no. 7595, pp. 489–492, Mar 2016. [Online]. Available: https://doi.org/10.1038/nature17151

[643] D. J. Rizzo, G. Veber, T. Cao, C. Bronner, T. Chen, F. Zhao, H. Rodriguez, S. G. Louie, M. F. Crommie, and F. R. Fischer, "Topological band engineering of graphene nanoribbons," *Nature*, vol. 560, no. 7717, pp. 204–208, Aug 2018. [Online]. Available: https://doi.org/10.1038/s41586-018-0376-8

[644] O. Gröning, S. Wang, X. Yao, C. A. Pignedoli, G. Borin Barin, C. Daniels, A. Cupo, V. Meunier, X. Feng, A. Narita, K. Müllen, P. Ruffieux, and R. Fasel, "Engineering of robust topological quantum phases in graphene nanoribbons," *Nature*, vol. 560, no. 7717, pp. 209–213, Aug 2018. [Online]. Available: https://doi.org/10.1038/s41586-018-0375-9

[645] M. Slota, A. Keerthi, W. K. Myers, E. Tretyakov, M. Baumgarten, A. Ardavan, H. Sadeghi, C. J. Lambert, A. Narita, K. Müllen, and L. Bogani, "Magnetic edge states and coherent manipulation of graphene nanoribbons," *Nature*, vol. 557, no. 7707, pp. 691–695, May 2018. [Online]. Available: https://doi.org/10.1038/s41586-018-0154-7

[646] L. Liu, Z. Ge, C. Yan, A. D. Moghadam, M. Weinert, and L. Li, "Termination-dependent edge states of MBE-grown WSe_2," *Phys. Rev. B*, vol. 98, p. 235304, Dec 2018. [Online]. Available: https://link.aps.org/doi/10.1103/PhysRevB.98.235304

[647] R. Addou, C. M. Smyth, J.-Y. Noh, Y.-C. Lin, Y. Pan, S. M. Eichfeld, S. Fölsch, J. A. Robinson, K. Cho, R. M. Feenstra, and R. M. Wallace, "One dimensional metallic edges in atomically thin WSe2 induced by air exposure," *2D Materials*, vol. 5, no. 2, p. 025017, mar 2018. [Online]. Available: https://doi.org/10.1088%2F2053-1583%2Faab0cd

[648] M. Gibertini and N. Marzari, "Emergence of One-Dimensional Wires of Free Carriers in Transition-Metal-Dichalcogenide Nanostructures," *Nano Letters*, vol. 15, no. 9, pp. 6229–6238, 2015, pMID: 26291826. [Online]. Available: https://doi.org/10.1021/acs.nanolett.5b02834

[649] F. Cheng, H. Xu, W. Xu, P. Zhou, J. Martin, and K. P. Loh, "Controlled Growth of 1D MoSe2 Nanoribbons with Spatially Modulated Edge States," *Nano Letters*, vol. 17, no. 2, pp. 1116–1120, 2017, pMID: 28090772. [Online]. Available: https://doi.org/10.1021/acs.nanolett.6b04715

[650] G. Yang, Y. Shao, J. Niu, X. Ma, C. Lu, W. Wei, X. Chuai, J. Wang, J. Cao, H. Huang, G. Xu, X. Shi, Z. Ji, N. Lu, D. Geng, J. Qi, Y. Cao, Z. Liu, L. Liu, Y. Huang, L. Liao, W. Dang, Z. Zhang, Y. Liu, X. Duan, J. Chen, Z. Fan, X. Jiang, Y. Wang, L. Li, H.-J. Gao, X. Duan, and M. Liu, "Possible Luttinger liquid behavior of edge transport in monolayer transition metal dichalcogenide crystals," *Nature Communications*, vol. 11, no. 1, p. 659, Jan 2020. [Online]. Available: https://doi.org/10.1038/s41467-020-14383-0

[651] Z. Hu, J. Avila, X. Wang, J. F. Leong, Q. Zhang, Y. Liu, M. C. Asensio, J. Lu, A. Carvalho, C. H. Sow, and A. H. Castro Neto, "The Role of Oxygen Atoms on Excitons at the Edges of Monolayer WS2," *Nano Letters*, vol. 19, no. 7, pp. 4641–4650, 2019, pMID: 31189314. [Online]. Available: https://doi.org/10.1021/acs.nanolett.9b01670

[652] P. D'Amico, M. Gibertini, D. Prezzi, D. Varsano, A. Ferretti, N. Marzari, and E. Molinari, "Intrinsic edge excitons in two-dimensional MoS_2," *Phys. Rev. B*, vol. 101, p. 161410, Apr 2020. [Online]. Available: https://link.aps.org/doi/10.1103/PhysRevB.101.161410

[653] Y. Li, Z. Zhou, S. Zhang, and Z. Chen, "MoS2 Nanoribbons," *J. Am. Chem. Soc.*, vol. 130, p. 16739, 2008. [Online]. Available: https://pubs.acs.org/doi/abs/10.1021/ja805545x

[654] A. R. Botello-Méndez, F. López-Urías, M. Terrones, and H. Terrones, "Metallic and ferromagnetic edges in molybdenum disulfide nanoribbons," *Nanotechnology*, vol. 20, no. 32, p. 325703, 2009. [Online]. Available: http://stacks.iop.org/0957-4484/20/i=32/a=325703

[655] C. Ataca, H. Şahin, E. Aktürk, and S. Ciraci, "Mechanical and Electronic Properties of MoS2 Nanoribbons and Their Defects," *The Journal of Physical Chemistry C*, vol. 115, no. 10, pp. 3934–3941, 2011. [Online]. Available: https://doi.org/10.1021/jp1115146

[656] F. Khoeini, K. Shakouri, and F. M. Peeters, "Peculiar half-metallic state in zigzag nanoribbons of MoS_2: Spin filtering," *Phys. Rev. B*, vol. 94, p. 125412, Sep 2016. [Online]. Available: https://link.aps.org/doi/10.1103/PhysRevB.94.125412

[657] A. Heshmati-Moulai, H. Simchi, M. Esmaeilzadeh, and F. M. Peeters, "Phase transition and spin-resolved transport in MoS_2 nanoribbons," *Phys. Rev. B*, vol. 94, p. 235424, Dec 2016. [Online]. Available: https://link.aps.org/doi/10.1103/PhysRevB.94.235424

[658] L. Li, E. V. Castro, and P. D. Sacramento, "Strain-induced topological phase transition at zigzag edges of monolayer transition-metal dichalcogenides," *Phys. Rev. B*, vol. 94, p. 195419, Nov 2016. [Online]. Available: https://link.aps.org/doi/10.1103/PhysRevB.94.195419

[659] G. Xu, J. Wang, B. Yan, and X.-L. Qi, "Topological superconductivity at the edge of transition-metal dichalcogenides," *Phys. Rev. B*, vol. 90, p. 100505, Sep 2014. [Online]. Available: https://link.aps.org/doi/10.1103/PhysRevB.90.100505

[660] R.-L. Chu, G.-B. Liu, W. Yao, X. Xu, D. Xiao, and C. Zhang, "Spin-orbit-coupled quantum wires and Majorana fermions on zigzag edges of monolayer transition-metal dichalcogenides," *Phys. Rev. B*, vol. 89, p. 155317, Apr 2014. [Online]. Available: https://link.aps.org/doi/10.1103/PhysRevB.89.155317

[661] S. B. Touski, R. Roldán, M. Pourfath, and M. Pilar López-Sancho, "Enhanced spin-flip scattering by surface roughness in WS_2 and MoS_2 armchair nanoribbons," *Phys. Rev. B*, vol. 95, p. 165301, Apr 2017. [Online]. Available: https://link.aps.org/doi/10.1103/PhysRevB.95.165301

[662] E. Ridolfi, L. R. F. Lima, E. R. Mucciolo, and C. H. Lewenkopf, "Electronic transport in disordered $\mathbf{MoS_2}$ nanoribbons," *Phys. Rev. B*, vol. 95, p. 035430, Jan 2017. [Online]. Available: https://link.aps.org/doi/10.1103/PhysRevB.95.035430

[663] D. Davelou, G. Kopidakis, E. Kaxiras, and I. N. Remediakis, "Nanoribbon edges of transition-metal dichalcogenides: Stability and electronic properties," *Phys. Rev. B*, vol. 96, p. 165436, Oct 2017. [Online]. Available: https://link.aps.org/doi/10.1103/PhysRevB.96.165436

[664] J. V. Lauritsen, M. Nyberg, R. T. Vang, M. V. Bollinger, B. S. Clausen, H. Topse, K. W. Jacobsen, E. Lægsgaard, J. K. Nørskov, and F. Besenbacher, "Chemistry of one-dimensional metallic edge states in MoS $_2$ nanoclusters," *Nanotechnology*, vol. 14, no. 3, pp. 385–389, Mar. 2003. [Online]. Available: http://stacks.iop.org/0957-4484/14/i=3/a=306?key=crossref.879e9bbee4c7e1206c604ac88d2a0fe3

[665] J. V. Lauritsen, J. Kibsgaard, S. Helveg, H. Topsøe, B. S. Clausen, E. Lægsgaard, and F. Besenbacher, "Size-dependent structure of MoS2 nanocrystals," *Nature Nanotechnology*, vol. 2, no. 1, pp. 53–58, Jan 2007. [Online]. Available: https://doi.org/10.1038/nnano.2006.171

[666] T. F. Jaramillo, K. P. Jørgensen, J. Bonde, J. H. Nielsen, S. Horch, and I. Chorkendorff, "Identification of Active Edge Sites for Electrochemical H2 Evolution from MoS2 Nanocatalysts," *Science*, vol. 317, no. 5834, pp. 100–102, 2007. [Online]. Available: https://science.sciencemag.org/content/317/5834/100

[667] L. Pei, S. Tao, S. Haibo, and X. Song, "Structural stability, electronic and magnetic properties of MoS2 quantum dots based on the first principles," *Solid State Communications*, vol. 218, pp. 25–30, Sep. 2015. [Online]. Available: https://linkinghub.elsevier.com/retrieve/pii/S0038109815002161

[668] M. Javaid, D. W. Drumm, S. P. Russo, and A. D. Greentree, "A study of size-dependent properties of MoS2 monolayer nanoflakes using density-functional theory," *Scientific Reports*, vol. 7, no. 1, dec 2017. [Online]. Available: http://www.nature.com/articles/s41598-017-09305-y

[669] P. P. Shinde, S. P. Adiga, S. Pandian, S. Ramachandran, K. S. Hariharan, and S. M. Kolake, "MoS2 Quantum Dots: Effect of Hydrogenation on Surface Stability and H2S Release," *The Journal of Physical Chemistry C*, vol. 123, no. 46, pp. 28 106–28 113, 2019. [Online]. Available: https://doi.org/10.1021/acs.jpcc.8b04198

[670] G. Wei, D. A. Czaplewski, E. J. Lenferink, T. K. Stanev, I. W. Jung, and N. P. Stern, "Size-tunable Lateral Confinement in Monolayer Semiconductors," *Scientific Reports*, vol. 7, no. 1, p. 3324, Jun 2017. [Online]. Available: https://doi.org/10.1038/s41598-017-03594-z

[671] J. Kang, J.-W. T. Seo, D. Alducin, A. Ponce, M. J. Yacaman, and M. C. Hersam, "Thickness sorting of two-dimensional transition metal dichalcogenides via copolymer-assisted density gradient ultracentrifugation," *Nature Communications*, vol. 5, no. 1, p. 5478, Nov 2014. [Online]. Available: https://doi.org/10.1038/ncomms6478

[672] Z. X. Gan, L. Z. Liu, H. Y. Wu, Y. L. Hao, Y. Shan, X. L. Wu, and P. K. Chu, "Quantum confinement effects across two-dimensional planes in MoS2 quantum dots," *Applied Physics Letters*, vol. 106, no. 23, p. 233113, 2015. [Online]. Available: https://doi.org/10.1063/1.4922551

[673] D. Gopalakrishnan, D. Damien, B. Li, H. Gullappalli, V. K. Pillai, P. M. Ajayan, and M. M. Shaijumon, "Electrochemical synthesis of luminescent MoS2 quantum dots," *Chem. Commun.*, vol. 51, pp. 6293–6296, 2015. [Online]. Available: http://dx.doi.org/10.1039/C4CC09826A

[674] A. Granados del Águila, S. Liu, T. T. H. Do, Z. Lai, T. H. Tran, S. R. Krupp, Z.-R. Gong, H. Zhang, W. Yao, and Q. Xiong, "Linearly Polarized Luminescence of Atomically Thin MoS2 Semiconductor Nanocrystals," *ACS Nano*, vol. 13, no. 11, pp. 13 006–13 014, 2019, pMID: 31577129. [Online]. Available: https://doi.org/10.1021/acsnano.9b05656

[675] H. Jin, M. Ahn, S. Jeong, J. H. Han, D. Yoo, D. H. Son, and J. Cheon, "Colloidal Single-Layer Quantum Dots with Lateral Confinement Effects on 2D Exciton," *Journal of the American Chemical Society*, vol. 138, no. 40, pp. 13 253–13 259, 2016. [Online]. Available: https://doi.org/10.1021/jacs.6b06972

[676] X. Zhang, H. Cheng, and H. Zhang, "Recent Progress in the Preparation, Assembly, Transformation, and Applications of Layer-Structured Nanodisks beyond Graphene," *Advanced Materials*, vol. 29, no. 35, p. 1701704, 2017. [Online]. Available: https://onlinelibrary.wiley.com/doi/abs/10.1002/adma.201701704

[677] H. Jin, B. Baek, D. Kim, F. Wu, J. D. Batteas, J. Cheon, and D. H. Son, "Effects of Direct Solvent-Quantum Dot Interaction on the Optical Properties of Colloidal Monolayer WS2 Quantum Dots," *Nano Letters*, vol. 17, no. 12, pp. 7471–7477, 2017, pMID: 29076338. [Online]. Available: https://doi.org/10.1021/acs.nanolett.7b03381

[678] X. Cao, C. Ding, C. Zhang, W. Gu, Y. Yan, X. Shi, and Y. Xian, "Transition metal dichalcogenide quantum dots: synthesis, photoluminescence and biological applications," *J. Mater. Chem. B*, vol. 6, pp. 8011–8036, 2018. [Online]. Available: http://dx.doi.org/10.1039/C8TB02519C

[679] A. Barenco, D. Deutsch, A. Ekert, and R. Jozsa, "Conditional Quantum Dynamics and Logic Gates," *Phys. Rev. Lett.*, vol. 74, pp. 4083–4086, May 1995. [Online]. Available: https://link.aps.org/doi/10.1103/PhysRevLett.74.4083

[680] J. A. Brum and P. Hawrylak, "Coupled quantum dots as quantum exclusive-OR gate," *Superlattices and Microstructures*, vol. 22, no. 3, pp. 431 – 436, 1997. [Online]. Available: https://linkinghub.elsevier.com/retrieve/pii/S0749603696902633

[681] D. Loss and D. P. DiVincenzo, "Quantum computation with quantum dots," *Physical Review A*, vol. 57, no. 1, pp. 120–126, Jan. 1998. [Online]. Available: https://link.aps.org/doi/10.1103/PhysRevA.57.120

[682] G. Burkard, D. Loss, and D. P. DiVincenzo, "Coupled quantum dots as quantum gates," *Phys. Rev. B*, vol. 59, pp. 2070–2078, Jan 1999. [Online]. Available: https://link.aps.org/doi/10.1103/PhysRevB.59.2070

[683] F. Meier, J. Levy, and D. Loss, "Quantum Computing with Spin Cluster Qubits," *Phys. Rev. Lett.*, vol. 90, p. 047901, Jan 2003. [Online]. Available: https://link.aps.org/doi/10.1103/PhysRevLett.90.047901

[684] R. Hanson, L. P. Kouwenhoven, J. R. Petta, S. Tarucha, and L. M. K. Vandersypen, "Spins in few-electron quantum dots," *Rev. Mod. Phys.*, vol. 79, pp. 1217–1265, Oct 2007. [Online]. Available: https://link.aps.org/doi/10.1103/RevModPhys.79.1217

[685] J. M. Elzerman, R. Hanson, L. H. Willems van Beveren, B. Witkamp, L. M. K. Vandersypen, and L. P. Kouwenhoven, "Single-shot read-out of an individual electron spin in a quantum dot," *Nature*, vol. 430, no. 6998, pp. 431–435, Jul. 2004. [Online]. Available: http://www.nature.com/articles/nature02693

[686] J. Kyriakidis, M. Pioro-Ladriere, M. Ciorga, A. S. Sachrajda, and P. Hawrylak, "Voltage-tunable singlet-triplet transition in lateral quantum dots," *Phys. Rev. B*, vol. 66, p. 035320, Jul 2002. [Online]. Available: https://link.aps.org/doi/10.1103/PhysRevB.66.035320

[687] M. Kroutvar, Y. Ducommun, D. Heiss, M. Bichler, D. Schuh, G. Abstreiter, and J. J. Finley, "Optically programmable electron spin memory using semiconductor quantum dots," *Nature*, vol. 432, no. 7013, pp. 81–84, Nov 2004. [Online]. Available: https://doi.org/10.1038/nature03008

[688] A. Morello, J. J. Pla, F. A. Zwanenburg, K. W. Chan, K. Y. Tan, H. Huebl, M. Möttönen, C. D. Nugroho, C. Yang, J. A. van Donkelaar, A. D. C. Alves, D. N. Jamieson, C. C. Escott, L. C. L. Hollenberg, R. G. Clark, and A. S. Dzurak, "Single-shot readout of an electron spin in silicon," *Nature*, vol. 467, no. 7316, pp. 687–691, Oct 2010. [Online]. Available: https://doi.org/10.1038/nature09392

[689] K. C. Nowack, M. Shafiei, M. Laforest, G. E. D. K. Prawiroatmodjo, L. R. Schreiber, C. Reichl, W. Wegscheider, and L. M. K. Vandersypen, "Single-Shot Correlations and Two-Qubit Gate of Solid-State Spins," *Science*, vol. 333, no. 6047, pp. 1269–1272, 2011. [Online]. Available: https://science.sciencemag.org/content/333/6047/1269

[690] L. Robledo, L. Childress, H. Bernien, B. Hensen, P. F. A. Alkemade, and R. Hanson, "High-fidelity projective read-out of a solid-state spin quantum register," *Nature*, vol. 477, no. 7366, pp. 574–578, Sep 2011. [Online]. Available: https://doi.org/10.1038/nature10401

[691] R. Maurand, X. Jehl, D. Kotekar-Patil, A. Corna, H. Bohuslavskyi, R. Laviéville, L. Hutin, S. Barraud, M. Vinet, M. Sanquer, and S. De Franceschi, "A CMOS silicon spin qubit," *Nature Communications*, vol. 7, no. 1, p. 13575, Nov 2016. [Online]. Available: https://doi.org/10.1038/ncomms13575

[692] T. F. Watson, S. G. J. Philips, E. Kawakami, D. R. Ward, P. Scarlino, M. Veldhorst, D. E. Savage, M. G. Lagally, M. Friesen, S. N. Coppersmith, M. A. Eriksson, and L. M. K. Vandersypen, "A programmable two-qubit quantum processor in silicon," *Nature*, vol. 555, no. 7698, pp. 633–637, Mar 2018. [Online]. Available: https://doi.org/10.1038/nature25766

[693] L. Petit, H. G. J. Eenink, M. Russ, W. I. L. Lawrie, N. W. Hendrickx, S. G. J. Philips, J. S. Clarke, L. M. K. Vandersypen, and M. Veldhorst, "Universal quantum logic in hot silicon qubits," *Nature*, vol. 580, no. 7803, pp. 355–359, Apr 2020. [Online]. Available: https://doi.org/10.1038/s41586-020-2170-7

[694] C. H. Yang, R. C. C. Leon, J. C. C. Hwang, A. Saraiva, T. Tanttu, W. Huang, J. Camirand Lemyre, K. W. Chan, K. Y. Tan, F. E. Hudson, K. M. Itoh, A. Morello, M. Pioro-Ladrière, A. Laucht, and A. S. Dzurak, "Operation of a silicon quantum processor unit cell above one kelvin," *Nature*, vol. 580, no. 7803, pp. 350–354, Apr 2020. [Online]. Available: https://doi.org/10.1038/s41586-020-2171-6

[695] G.-B. Liu, H. Pang, Y. Yao, and W. Yao, "Intervalley coupling by quantum dot confinement potentials in monolayer transition metal dichalcogenides," *New Journal of Physics*, vol. 16, no. 10, p. 105011, Oct. 2014. [Online]. Available: http://stacks.iop.org/1367-2630/16/i=10/a=105011?key=crossref.78919ce0bab510139f2d3c94cbf85795

[696] Y. Wu, Q. Tong, G.-B. Liu, H. Yu, and W. Yao, "Spin-valley qubit in nanostructures of monolayer semiconductors: Optical control and hyperfine interaction," *Phys. Rev. B*, vol. 93, p. 045313, Jan 2016. [Online]. Available: https://link.aps.org/doi/10.1103/PhysRevB.93.045313

[697] A. C. Dias, J. Fu, L. Villegas-Lelovsky, and F. Qu, "Robust effective Zeeman energy in monolayer MoS_2 quantum dots," *Journal of Physics: Condensed Matter*, vol. 28, no. 37, p. 375803, Sep. 2016. [Online]. Available: http://stacks.iop.org/0953-8984/28/i=37/a=375803?key=crossref.edb69a72c9fc54bdce61de9dd006db6f

[698] M. Brooks and G. Burkard, "Spin-degenerate regimes for single quantum dots in transition metal dichalcogenide monolayers," *Phys. Rev. B*, vol. 95, p. 245411, Jun 2017. [Online]. Available: https://link.aps.org/doi/10.1103/PhysRevB.95.245411

[699] F. Qu, A. C. Dias, J. Fu, L. Villegas-Lelovsky, and D. L. Azevedo, "Tunable spin and valley dependent magneto-optical absorption in molybdenum disulfide quantum dots," *Scientific Reports*, vol. 7, no. 1, p. 41044, 2017. [Online]. Available: http://www.nature.com/articles/srep41044

[700] G. Széchenyi, L. Chirolli, and A. Pályi, "Impurity-assisted electric control of spin-valley qubits in monolayer MoS $_2$," *2D Materials*, vol. 5, no. 3, p. 035004, Apr. 2018. [Online]. Available: http://stacks.iop.org/2053-1583/5/i=3/a=035004?key=crossref.2f6a930956dccd952d366469a7b3bfec

[701] A. David, G. Burkard, and A. Kormányos, "Effective theory of monolayer TMDC double quantum dots," *2D Materials*, vol. 5, no. 3, p. 035031, jun 2018. [Online]. Available: https://doi.org/10.1088%2F2053-1583%2Faac17f

[702] J. Pawłowski, "Spin-valley system in a gated MoS2-monolayer quantum dot," *New Journal of Physics*, vol. 21, no. 12, p. 123029, dec 2019. [Online]. Available: https://doi.org/10.1088%2F1367-2630%2Fab5ac9

[703] F.-W. Chen and Y.-S. G. Wu, "Theory of field-modulated spin valley orbital pseudospin physics," *Phys. Rev. Research*, vol. 2, p. 013076, Jan 2020. [Online]. Available: https://link.aps.org/doi/10.1103/PhysRevResearch.2.013076

[704] M. Brooks and G. Burkard, "Electric dipole spin resonance of two-dimensional semiconductor spin qubits," *Phys. Rev. B*, vol. 101, p. 035204, Jan 2020. [Online]. Available: https://link.aps.org/doi/10.1103/PhysRevB.101.035204

[705] E. A. Laird, F. Pei, and L. P. Kouwenhoven, "A valley-spin qubit in a carbon nanotube," *Nature Nanotechnology*, vol. 8, no. 8, pp. 565–568, Aug 2013. [Online]. Available: https://doi.org/10.1038/nnano.2013.140

[706] X. Mi, S. Kohler, and J. R. Petta, "Landau-Zener interferometry of valley-orbit states in Si/SiGe double quantum dots," *Phys. Rev. B*, vol. 98, p. 161404, Oct 2018. [Online]. Available: https://link.aps.org/doi/10.1103/PhysRevB.98.161404

[707] K. E. J. Goh, F. Bussolotti, C. S. Lau, D. Kotekar-Patil, Z. E. Ooi, and J. Y. Chee, "Toward Valley-Coupled Spin Qubits," *Advanced Quantum Technologies*, vol. 3, no. 6, p. 1900123, 2020. [Online]. Available: https://onlinelibrary.wiley.com/doi/abs/10.1002/qute.201900123

[708] L. Chirolli, E. Prada, F. Guinea, R. Roldán, and P. San-Jose, "Strain-induced bound states in transition-metal dichalcogenide bubbles," *2D Materials*, vol. 6, no. 2, p. 025010, Feb. 2019. [Online]. Available: http://stacks.iop.org/2053-1583/6/i=2/a=025010?key=crossref.469993516328d71c0765a4f1ec31a3a2

[709] C. Palacios-Berraquero, M. Barbone, D. M. Kara, X. Chen, I. Goykhman, D. Yoon, A. K. Ott, J. Beitner, K. Watanabe, T. Taniguchi, A. C. Ferrari, and M. Atatüre, "Atomically thin quantum light-emitting diodes," *Nature Communications*, vol. 7, no. 1, p. 12978, Sep 2016. [Online]. Available: https://doi.org/10.1038/ncomms12978

[710] A. Branny, G. Wang, S. Kumar, C. Robert, B. Lassagne, X. Marie, B. D. Gerardot, and B. Urbaszek, "Discrete quantum dot like emitters in monolayer MoSe2: Spatial mapping, magneto-optics, and charge tuning," *Applied Physics Letters*, vol. 108, no. 14, p. 142101, 2016. [Online]. Available: https://doi.org/10.1063/1.4945268

[711] G. D. Shepard, O. A. Ajayi, X. Li, X.-Y. Zhu, J. Hone, and S. Strauf, "Nanobubble induced formation of quantum emitters in monolayer semiconductors," *2D Materials*, vol. 4, no. 2, p. 021019, mar 2017. [Online]. Available: https://doi.org/10.1088%2F2053-1583%2Faa629d

[712] J. Chaste, A. Missaoui, S. Huang, H. Henck, Z. Ben Aziza, L. Ferlazzo, C. Naylor, A. Balan, A. T. C. Johnson, R. Braive, and A. Ouerghi, "Intrinsic Properties of Suspended MoS2 on SiO2/Si Pillar Arrays for Nanomechanics and Optics," *ACS Nano*, vol. 12, no. 4, pp. 3235–3242, 2018, pMID: 29553713. [Online]. Available: https://doi.org/10.1021/acsnano.7b07689

[713] L. N. Tripathi, O. Iff, S. Betzold, u. Dusanowski, M. Emmerling, K. Moon, Y. J. Lee, S.-H. Kwon, S. Höfling, and C. Schneider, "Spontaneous Emission Enhancement in Strain-Induced WSe2 Monolayer-Based Quantum Light Sources on Metallic Surfaces," *ACS Photonics*, vol. 5, no. 5, pp. 1919–1926, 2018. [Online]. Available: https://doi.org/10.1021/acsphotonics.7b01053

[714] J. J. Fonseca, A. L. Yeats, B. Blue, M. K. Zalalutdinov, T. Brintlinger, B. S. Simpkins, D. C. Ratchford, J. C. Culbertson, J. Q. Grim, S. G. Carter, M. Ishigami, R. M. Stroud, C. D. Cress, and J. T. Robinson, "Enabling remote quantum emission in 2D semiconductors via porous metallic networks," *Nature Communications*, vol. 11, no. 1, p. 5, Jan 2020. [Online]. Available: https://doi.org/10.1038/s41467-019-13857-0

[715] F. Peyskens, C. Chakraborty, M. Muneeb, D. Van Thourhout, and D. Englund, "Integration of single photon emitters in 2D layered materials with a silicon nitride photonic chip," *Nature Communications*, vol. 10, no. 1, p. 4435, Sep 2019. [Online]. Available: https://doi.org/10.1038/s41467-019-12421-0

[716] Y. Luo, G. D. Shepard, J. V. Ardelean, D. A. Rhodes, B. Kim, K. Barmak, J. C. Hone, and S. Strauf, "Deterministic coupling of site-controlled quantum emitters in monolayer WSe2 to plasmonic nanocavities," *Nature Nanotechnology*, vol. 13, no. 12, pp. 1137–1142, Dec 2018. [Online]. Available: https://doi.org/10.1038/s41565-018-0275-z

[717] M. Blauth, M. Jürgensen, G. Vest, O. Hartwig, M. Prechtl, J. Cerne, J. J. Finley, and M. Kaniber, "Coupling Single Photons from Discrete Quantum Emitters in WSe2 to Lithographically Defined Plasmonic Slot Waveguides," *Nano Letters*, vol. 18, no. 11, pp. 6812–6819, 2018, pMID: 30153417. [Online]. Available: https://doi.org/10.1021/acs.nanolett.8b02687

[718] W. Li, X. Lu, S. Dubey, L. Devenica, and A. Srivastava, "Dipolar interactions between localized interlayer excitons in van der Waals heterostructures," *Nature Materials*, vol. 19, no. 6, pp. 624–629, Jun 2020. [Online]. Available: https://doi.org/10.1038/s41563-020-0661-4

[719] M. Toth and I. Aharonovich, "Single Photon Sources in Atomically Thin Materials," *Annual Review of Physical Chemistry*, vol. 70, no. 1, pp. 123–142, 2019, pMID: 30735459. [Online]. Available: https://doi.org/10.1146/annurev-physchem-042018-052628

[720] X. Lu, X. Chen, S. Dubey, Q. Yao, W. Li, X. Wang, Q. Xiong, and A. Srivastava, "Optical initialization of a single spin-valley in charged WSe2 quantum dots," *Nature Nanotechnology*, vol. 14, no. 5, pp. 426–431, May 2019. [Online]. Available: http://www.nature.com/articles/s41565-019-0394-1

[721] M. Brotons-Gisbert, A. Branny, S. Kumar, R. Picard, R. Proux, M. Gray, K. S. Burch, K. Watanabe, T. Taniguchi, and B. D. Gerardot, "Coulomb blockade in an atomically thin quantum dot coupled to a tunable Fermi reservoir," *Nature Nanotechnology*, vol. 14, no. 5, pp. 442–446, May 2019. [Online]. Available: http://www.nature.com/articles/s41565-019-0402-5

[722] H. Yu, G.-B. Liu, J. Tang, X. Xu, and W. Yao, "Moiré excitons: From programmable quantum emitter arrays to spin-orbit–coupled artificial lattices," *Science Advances*, vol. 3, no. 11, 2017. [Online]. Available: https://advances.sciencemag.org/content/3/11/e1701696

[723] F. Wu, T. Lovorn, and A. H. MacDonald, "Theory of optical absorption by interlayer excitons in transition metal dichalcogenide heterobilayers," *Phys. Rev. B*, vol. 97, p. 035306, Jan 2018. [Online]. Available: https://link.aps.org/doi/10.1103/PhysRevB.97.035306

[724] Y. Shimazaki, I. Schwartz, K. Watanabe, T. Taniguchi, M. Kroner, and A. Imamoğlu, "Strongly correlated electrons and hybrid excitons in a moiré heterostructure," *Nature*, vol. 580, no. 7804, pp. 472–477, Apr 2020. [Online]. Available: https://doi.org/10.1038/s41586-020-2191-2

[725] F. Wu, T. Lovorn, and A. H. MacDonald, "Topological Exciton Bands in Moiré Heterojunctions," *Phys. Rev. Lett.*, vol. 118, p. 147401, Apr 2017. [Online]. Available: https://link.aps.org/doi/10.1103/PhysRevLett.118.147401

[726] J. M. Pereira, P. Vasilopoulos, and F. M. Peeters, "Tunable Quantum Dots in Bilayer Graphene," *Nano Letters*, vol. 7, no. 4, pp. 946–949, 2007, pMID: 17352503. [Online]. Available: https://doi.org/10.1021/nl062967s

[727] M. Eich, R. Pisoni, H. Overweg, A. Kurzmann, Y. Lee, P. Rickhaus, T. Ihn, K. Ensslin, F. c. v. Herman, M. Sigrist, K. Watanabe, and T. Taniguchi, "Spin and Valley States in Gate-Defined Bilayer Graphene Quantum Dots," *Phys. Rev. X*, vol. 8, p. 031023, Jul 2018. [Online]. Available: https://link.aps.org/doi/10.1103/PhysRevX.8.031023

[728] A. Kurzmann, M. Eich, H. Overweg, M. Mangold, F. Herman, P. Rickhaus, R. Pisoni, Y. Lee, R. Garreis, C. Tong, K. Watanabe, T. Taniguchi, K. Ensslin, and T. Ihn, "Excited States in Bilayer Graphene Quantum Dots," *Phys. Rev. Lett.*, vol. 123, p. 026803, Jul 2019. [Online]. Available: https://link.aps.org/doi/10.1103/PhysRevLett.123.026803

[729] A. Kurzmann, H. Overweg, M. Eich, A. Pally, P. Rickhaus, R. Pisoni, Y. Lee, K. Watanabe, T. Taniguchi, T. Ihn, and K. Ensslin, "Charge Detection in Gate-Defined Bilayer Graphene Quantum Dots," *Nano Letters*, vol. 19, no. 8, pp. 5216–5221, 2019, pMID: 31311270. [Online]. Available: https://doi.org/10.1021/acs.nanolett.9b01617

[730] M. Eich, R. Pisoni, C. Tong, R. Garreis, P. Rickhaus, K. Watanabe, T. Taniguchi, T. Ihn, K. Ensslin, and A. Kurzmann, "Coulomb dominated cavities in bilayer graphene," *Phys. Rev. Research*, vol. 2, p. 022038, May 2020. [Online]. Available: https://link.aps.org/doi/10.1103/PhysRevResearch.2.022038

[731] J. Xue, Y. Chen, D. Pan, J.-Y. Wang, J. Zhao, S. Huang, and H. Q. Xu, "Gate defined quantum dot realized in a single crystalline InSb nanosheet," *Applied Physics Letters*, vol. 114, no. 2, p. 023108, 2019. [Online]. Available: https://doi.org/10.1063/1.5064368

[732] I. Kulesh, C. T. Ke, C. Thomas, S. Karwal, C. M. Moehle, S. Metti, R. Kallaher, G. C. Gardner, M. J. Manfra, and S. Goswami, "Quantum Dots in an InSb Two-Dimensional Electron Gas," *Phys. Rev. Applied*, vol. 13, p. 041003, Apr 2020. [Online]. Available: https://link.aps.org/doi/10.1103/PhysRevApplied.13.041003

[733] X.-X. Song, D. Liu, V. Mosallanejad, J. You, T.-Y. Han, D.-T. Chen, H.-O. Li, G. Cao, M. Xiao, G.-C. Guo, and G.-P. Guo, "A gate defined quantum dot on the two-dimensional transition metal dichalcogenide semiconductor WSe $_2$," *Nanoscale*, vol. 7, no. 40, pp. 16 867–16 873, 2015. [Online]. Available: http://xlink.rsc.org/?DOI=C5NR04961J

[734] Z.-Z. Zhang, X.-X. Song, G. Luo, G.-W. Deng, V. Mosallanejad, T. Taniguchi, K. Watanabe, H.-O. Li, G. Cao, G.-C. Guo, F. Nori, and G.-P. Guo, "Electrotunable artificial molecules based on van der Waals heterostructures," *Science Advances*, vol. 3, no. 10, p. e1701699, Oct. 2017. [Online]. Available: http://advances.sciencemag.org/lookup/doi/10.1126/sciadv.1701699

[735] R. Pisoni, Z. Lei, P. Back, M. Eich, H. Overweg, Y. Lee, K. Watanabe, T. Taniguchi, T. Ihn, and K. Ensslin, "Gate-tunable quantum dot in a high quality single layer MoS2 van der Waals heterostructure," *Applied Physics Letters*, vol. 112, no. 12, p. 123101, 2018. [Online]. Available: https://doi.org/10.1063/1.5021113

[736] K. Wang, K. De Greve, L. A. Jauregui, A. Sushko, A. High, Y. Zhou, G. Scuri, T. Taniguchi, K. Watanabe, M. D. Lukin, H. Park, and P. Kim, "Electrical control of charged carriers and excitons in atomically thin materials," *Nature Nanotechnology*, vol. 13, no. 2, pp. 128–132, Feb. 2018. [Online]. Available: http://www.nature.com/articles/s41565-017-0030-x

[737] C. S. Lau, J. Y. Chee, D. Thian, H. Kawai, J. Deng, S. L. Wong, Z. E. Ooi, Y.-F. Lim, and K. E. J. Goh, "Carrier control in 2D transition metal dichalcogenides with Al2O3 dielectric," *Scientific Reports*, vol. 9, no. 1, p. 8769, Jun 2019. [Online]. Available: https://doi.org/10.1038/s41598-019-45392-9

[738] S. Davari, J. Stacy, A. Mercado, J. Tull, R. Basnet, K. Pandey, K. Watanabe, T. Taniguchi, J. Hu, and H. Churchill, "Gate-Defined Accumulation-Mode Quantum Dots in Monolayer and Bilayer WSe_2," *Phys. Rev. Applied*, vol. 13, p. 054058, May 2020. [Online]. Available: https://link.aps.org/doi/10.1103/PhysRevApplied.13.054058

[739] P. Hawrylak, "Excitonic artificial atoms: Engineering optical properties of quantum dots," *Phys. Rev. B*, vol. 60, pp. 5597–5608, Aug 1999. [Online]. Available: https://link.aps.org/doi/10.1103/PhysRevB.60.5597

[740] S. A. Mikhailov, "Quantum-dot lithium in zero magnetic field: Electronic properties, thermodynamics, and Fermi liquid–Wigner solid crossover in the ground state," *Phys. Rev. B*, vol. 65, p. 115312, Feb 2002. [Online]. Available: https://link.aps.org/doi/10.1103/PhysRevB.65.115312

[741] M. Ciorga, A. Wensauer, M. Pioro-Ladriere, M. Korkusinski, J. Kyriakidis, A. S. Sachrajda, and P. Hawrylak, "Collapse of the Spin-Singlet Phase in Quantum Dots," *Phys. Rev. Lett.*, vol. 88, p. 256804, Jun 2002. [Online]. Available: https://link.aps.org/doi/10.1103/PhysRevLett.88.256804

[742] M. Bayer, P. Hawrylak, K. Hinzer, S. Fafard, M. Korkusinski, Z. R. Wasilewski, O. Stern, and A. Forchel, "Coupling and Entangling of Quantum States in Quantum Dot Molecules," *Science*, vol. 291, no. 5503, pp. 451–453, 2001. [Online]. Available: https://science.sciencemag.org/content/291/5503/451

[743] M. Van der Donck and F. M. Peeters, "Rich many-body phase diagram of electrons and holes in doped monolayer transition metal dichalcogenides," *Phys. Rev. B*, vol. 98, p. 115432, Sep 2018. [Online]. Available: https://link.aps.org/doi/10.1103/PhysRevB.98.115432

[744] E. Clementi and D. L. Raimondi, "Atomic Screening Constants from SCF Functions," *The Journal of Chemical Physics*, vol. 38, no. 11, p. 2686, 1963. [Online]. Available: https://doi.org/10.1063/1.1733573

[745] E. Clementi, D. L. Raimondi, and W. P. Reinhardt, "Atomic Screening Constants from SCF Functions. II. Atoms with 37 to 86 Electrons," *The Journal of Chemical Physics*, vol. 47, no. 4, p. 1300, 1967. [Online]. Available: https://doi.org/10.1063/1.1712084

[746] A. Urban, M. Reese, M. Mrovec, C. Elsässer, and B. Meyer, "Parameterization of tight-binding models from density functional theory calculations," *Phys. Rev. B*, vol. 84, p. 155119, Oct 2011. [Online]. Available: https://link.aps.org/doi/10.1103/PhysRevB.84.155119

[747] A. Carvalho, R. M. Ribeiro, and A. H. Castro Neto, "Band nesting and the optical response of two-dimensional semiconducting transition metal dichalcogenides," *Phys. Rev. B*, vol. 88, p. 115205, Sep 2013. [Online]. Available: https://link.aps.org/doi/10.1103/PhysRevB.88.115205

[748] X. Xu, W. Yao, D. Xiao, and T. F. Heinz, "Spin and pseudospins in layered transition metal dichalcogenides," *Nature Physics*, vol. 10, no. 5, p. 343, 2014. [Online]. Available: https://doi.org/10.1038/nphys2942

[749] A. H. Castro Neto, F. Guinea, N. M. R. Peres, K. S. Novoselov, and A. K. Geim, "The electronic properties of graphene," *Rev. Mod. Phys.*, vol. 81, pp. 109–162, Jan 2009. [Online]. Available: https://link.aps.org/doi/10.1103/RevModPhys.81.109

[750] T. G. Pedersen, K. Pedersen, and T. Brun Kriestensen, "Optical matrix elements in tight-binding calculations," *Phys. Rev. B*, vol. 63, p. 201101, May 2001. [Online]. Available: https://link.aps.org/doi/10.1103/PhysRevB.63.201101

[751] R. Sundararaman and T. A. Arias, "Regularization of the Coulomb singularity in exact exchange by Wigner-Seitz truncated interactions: Towards chemical accuracy in nontrivial systems," *Phys. Rev. B*, vol. 87, p. 165122, Apr 2013. [Online]. Available: https://link.aps.org/doi/10.1103/PhysRevB.87.165122

[752] P. Cudazzo, I. V. Tokatly, and A. Rubio, "Dielectric screening in two-dimensional insulators: Implications for excitonic and impurity states in graphane," *Phys. Rev. B*, vol. 84, p. 085406, Aug 2011. [Online]. Available: https://link.aps.org/doi/10.1103/PhysRevB.84.085406

[753] M. Tamulewicz, J. Kutrowska-Girzycka, K. Gajewski, J. Serafińczuk, A. Sierakowski, J. Jadczak, L. Bryja, and T. P. Gotszalk, "Layer number dependence of the work function and optical properties of single and few layers MoS2: effect of substrate," *Nanotechnology*, vol. 30, no. 24, p. 245708, apr 2019. [Online]. Available: https://doi.org/10.1088%2F1361-6528%2Fab0caf

[754] T. C. Berkelbach and D. R. Reichman, "Optical and Excitonic Properties of Atomically Thin Transition-Metal Dichalcogenides," *Annual Review of Condensed Matter Physics*, vol. 9, no. 1, p. 379, 2018. [Online]. Available: https://doi.org/10.1146/annurev-conmatphys-033117-054009

[755] M. L. Trolle, G. Seifert, and T. G. Pedersen, "Theory of excitonic second-harmonic generation in monolayer MoS_2," *Phys. Rev. B*, vol. 89, p. 235410, Jun 2014. [Online]. Available: https://link.aps.org/doi/10.1103/PhysRevB.89.235410

[756] F. Wilczek and A. Zee, "Appearance of Gauge Structure in Simple Dynamical Systems," *Phys. Rev. Lett.*, vol. 52, pp. 2111–2114, Jun 1984. [Online]. Available: https://link.aps.org/doi/10.1103/PhysRevLett.52.2111

[757] M.-C. Chang and Q. Niu, "Berry curvature, orbital moment, and effective quantum theory of electrons in electromagnetic fields," *Journal of Physics: Condensed Matter*, vol. 20, no. 19, p. 193202, apr 2008. [Online]. Available: https://doi.org/10.1088%2F0953-8984%2F20%2F19%2F193202

[758] L. X. Benedict, "Screening in the exchange term of the electron-hole interaction of the Bethe-Salpeter equation," *Phys. Rev. B*, vol. 66, p. 193105, Nov 2002. [Online]. Available: https://link.aps.org/doi/10.1103/PhysRevB.66.193105

[759] R. Tempelaar and T. C. Berkelbach, "Many-body simulation of two-dimensional electronic spectroscopy of excitons and trions in monolayer transition metal dichalcogenides," *Nature Communications*, vol. 10, no. 1, p. 3419, Jul 2019. [Online]. Available: https://doi.org/10.1038/s41467-019-11497-y

[760] M. Korkusinski and P. Hawrylak, "Quantum strain sensor with a topological insulator hgte quantum dot," *Scientific reports*, vol. 4, p. 4903, 2014. [Online]. Available: https://doi.org/10.1038/srep04903

[761] J. Klein, J. Wierzbowski, A. Regler, J. Becker, F. Heimbach, K. Müller, M. Kaniber, and J. J. Finley, "Stark Effect Spectroscopy of Mono- and Few-Layer MoS2," *Nano Letters*, vol. 16, no. 3, pp. 1554–1559, 2016, pMID: 26845085. [Online]. Available: https://doi.org/10.1021/acs.nanolett.5b03954

[762] E. Polizzi, "Density-matrix-based algorithm for solving eigenvalue problems," *Phys. Rev. B*, vol. 79, p. 115112, Mar 2009. [Online]. Available: https://link.aps.org/doi/10.1103/PhysRevB.79.115112

[763] S. Raymond, S. Studenikin, A. Sachrajda, Z. Wasilewski, S. J. Cheng, W. Sheng, P. Hawrylak, A. Babinski, M. Potemski, G. Ortner, and M. Bayer, "Excitonic Energy Shell Structure of Self-Assembled InGaAs/GaAs Quantum Dots," *Physical Review Letters*, vol. 92, no. 18, p. 187402, May 2004. [Online]. Available: https://link.aps.org/doi/10.1103/PhysRevLett.92.187402

[764] Z.-q. Bao, P. Cheung, and F. Zhang, "Flavor Quantum Dots and Artificial Quark Model in Transition Metal Dichalcogenides," *arXiv:1903.01967 [cond-mat]*, Mar. 2019, arXiv: 1903.01967. [Online]. Available: http://arxiv.org/abs/1903.01967

[765] M. Gell-Mann, "Symmetries of Baryons and Mesons," *Phys. Rev.*, vol. 125, pp. 1067–1084, Feb 1962. [Online]. Available: https://link.aps.org/doi/10.1103/PhysRev.125.1067

[766] H. Georgi, "Flavor SU(3) Symmetries in Particle Physics," *Physics Today*, vol. 41, no. 4, p. 29, 1988. [Online]. Available: https://doi.org/10.1063/1.881148

[767] M. Ciorga, A. S. Sachrajda, P. Hawrylak, C. Gould, P. Zawadzki, S. Jullian, Y. Feng, and Z. Wasilewski, "Addition spectrum of a lateral dot from Coulomb and spin-blockade spectroscopy," *Physical Review B*, vol. 61, no. 24, pp. R16 315–R16 318, Jun. 2000. [Online]. Available: https://link.aps.org/doi/10.1103/PhysRevB.61.R16315

[768] X. Gonze, J.-M. Beuken, R. Caracas, F. Detraux, M. Fuchs, G.-M. Rignanese, L. Sindic, M. Verstraete, G. Zerah, F. Jollet, M. Torrent, A. Roy, M. Mikami, P. Ghosez, J.-Y. Raty, and D. Allan, "First-principles computation of material properties: the ABINIT software project," *Computational Materials Science*, vol. 25, no. 3, pp. 478 – 492, 2002. [Online]. Available: http://www.sciencedirect.com/science/article/pii/S0927025602003257

[769] X. G. et al., "A brief introduction to the ABINIT software package," *Zeitschrift für Kristallographie - Crystalline Materials*, vol. 220, no. 5-6, pp. 558 – 562, 2005. [Online]. Available: https://www.degruyter.com/view/journals/zkri/220/5-6/article-p558.xml

[770] X. Gonze, B. Amadon, P.-M. Anglade, J.-M. Beuken, F. Bottin, P. Boulanger, F. Bruneval, D. Caliste, R. Caracas, M. Côté, T. Deutsch, L. Genovese, P. Ghosez, M. Giantomassi, S. Goedecker, D. Hamann, P. Hermet, F. Jollet, G. Jomard, S. Leroux, M. Mancini, S. Mazevet, M. Oliveira, G. Onida, Y. Pouillon, T. Rangel, G.-M. Rignanese, D. Sangalli, R. Shaltaf, M. Torrent, M. Verstraete, G. Zerah, and J. Zwanziger, "ABINIT: First-principles approach to material and nanosystem properties," *Computer Physics Communications*, vol. 180, no. 12, pp. 2582 – 2615, 2009, 40 YEARS OF CPC: A celebratory issue focused on quality software for high performance, grid and novel computing architectures. [Online]. Available: http://www.sciencedirect.com/science/article/pii/S0010465509002276

[771] X. Gonze, F. Jollet, F. Abreu Araujo, D. Adams, B. Amadon, T. Applencourt, C. Audouze, J.-M. Beuken, J. Bieder, A. Bokhanchuk, E. Bousquet, F. Bruneval, D. Caliste, M. Côté, F. Dahm, F. Da Pieve, M. Delaveau, M. Di Gennaro, B. Dorado, C. Espejo, G. Geneste, L. Genovese, A. Gerossier, M. Giantomassi, Y. Gillet, D. Hamann, L. He, G. Jomard, J. Laflamme Janssen, S. Le Roux, A. Levitt, A. Lherbier, F. Liu, I. Lukačević, A. Martin, C. Martins, M. Oliveira, S. Poncé, Y. Pouillon, T. Rangel, G.-M. Rignanese, A. Romero, B. Rousseau, O. Rubel, A. Shukri, M. Stankovski, M. Torrent, M. Van Setten, B. Van Troeye, M. Verstraete, D. Waroquiers, J. Wiktor, B. Xu, A. Zhou, and J. Zwanziger, "Recent developments in the ABINIT software package," *Computer Physics Communications*, vol. 205, pp. 106 – 131, 2016. [Online]. Available: http://www.sciencedirect.com/science/article/pii/S0010465516300923

[772] A. H. Romero, D. C. Allan, B. Amadon, G. Antonius, T. Applencourt, L. Baguet, J. Bieder, F. Bottin, J. Bouchet, E. Bousquet, F. Bruneval, G. Brunin, D. Caliste, M. Côté, J. Denier, C. Dreyer, P. Ghosez, M. Giantomassi, Y. Gillet, O. Gingras, D. R. Hamann, G. Hautier, F. Jollet, G. Jomard, A. Martin, H. P. C. Miranda, F. Naccarato, G. Petretto, N. A. Pike, V. Planes, S. Prokhorenko, T. Rangel, F. Ricci, G.-M. Rignanese, M. Royo, M. Stengel, M. Torrent, M. J. van Setten, B. Van Troeye, M. J. Verstraete, J. Wiktor, J. W. Zwanziger, and X. Gonze, "ABINIT: Overview and focus on selected capabilities," *The Journal of Chemical Physics*, vol. 152, no. 12, p. 124102, 2020. [Online]. Available: https://doi.org/10.1063/1.5144261

[773] J. P. Perdew, K. Burke, and M. Ernzerhof, "Generalized Gradient Approximation Made Simple," *Phys. Rev. Lett.*, vol. 77, pp. 3865–3868, Oct 1996. [Online]. Available: https://link.aps.org/doi/10.1103/PhysRevLett.77.3865

[774] P. Hawrylak and M. Grabowski, "Hydrogenic impurity in a parabolic quantum wire in a magnetic field: Quantum chaos and optical properties," *Phys. Rev. B*, vol. 49, p. 8174, Mar 1994. [Online]. Available: https://link.aps.org/doi/10.1103/PhysRevB.49.8174

[775] D. G. W. Parfitt and M. E. Portnoi, "The two-dimensional hydrogen atom revisited," *Journal of Mathematical Physics*, vol. 43, no. 10, pp. 4681–4691, 2002. [Online]. Available: https://aip.scitation.org/doi/abs/10.1063/1.1503868

[776] A. R. Botello-Méndez, F. López-Urías, M. Terrones, and H. Terrones, "Metallic and ferromagnetic edges in molybdenum disulfide nanoribbons," *Nanotechnology*, vol. 20, no. 32, p. 325703, jul 2009. [Online]. Available: https://doi.org/10.1088%2F0957-4484%2F20%2F32%2F325703

[777] T. Wakamura, F. Reale, P. Palczynski, S. Guéron, C. Mattevi, and H. Bouchiat, "Strong anisotropic spin-orbit interaction induced in graphene by monolayer ws_2," *Phys. Rev. Lett.*, vol. 120, p. 106802, Mar 2018. [Online]. Available: https://link.aps.org/doi/10.1103/PhysRevLett.120.106802

[778] T. Wakamura, F. Reale, P. Palczynski, M. Q. Zhao, A. T. C. Johnson, S. Guéron, C. Mattevi, A. Ouerghi, and H. Bouchiat, "Spin-orbit interaction induced in graphene by transition metal dichalcogenides," *Phys. Rev. B*, vol. 99, p. 245402, Jun 2019. [Online]. Available: https://link.aps.org/doi/10.1103/PhysRevB.99.245402

[779] J. Island, X. Cui, C. Lewandowski, J. Khoo, E. Spanton, H. Zhou, D. Rhodes, J. Hone, T. Taniguchi, K. Watanabe *et al.*, "Spin–orbit-driven band inversion in bilayer graphene by the van der waals proximity effect," *Nature*, p. 1, 2019. [Online]. Available: https://doi.org/10.1038/s41586-019-1304-2

[780] A. Marrazzo, M. Gibertini, D. Campi, N. Mounet, and N. Marzari, "Prediction of a large-gap and switchable kane-mele quantum spin hall insulator," *Phys. Rev. Lett.*, vol. 120, p. 117701, Mar 2018. [Online]. Available: https://link.aps.org/doi/10.1103/PhysRevLett.120.117701